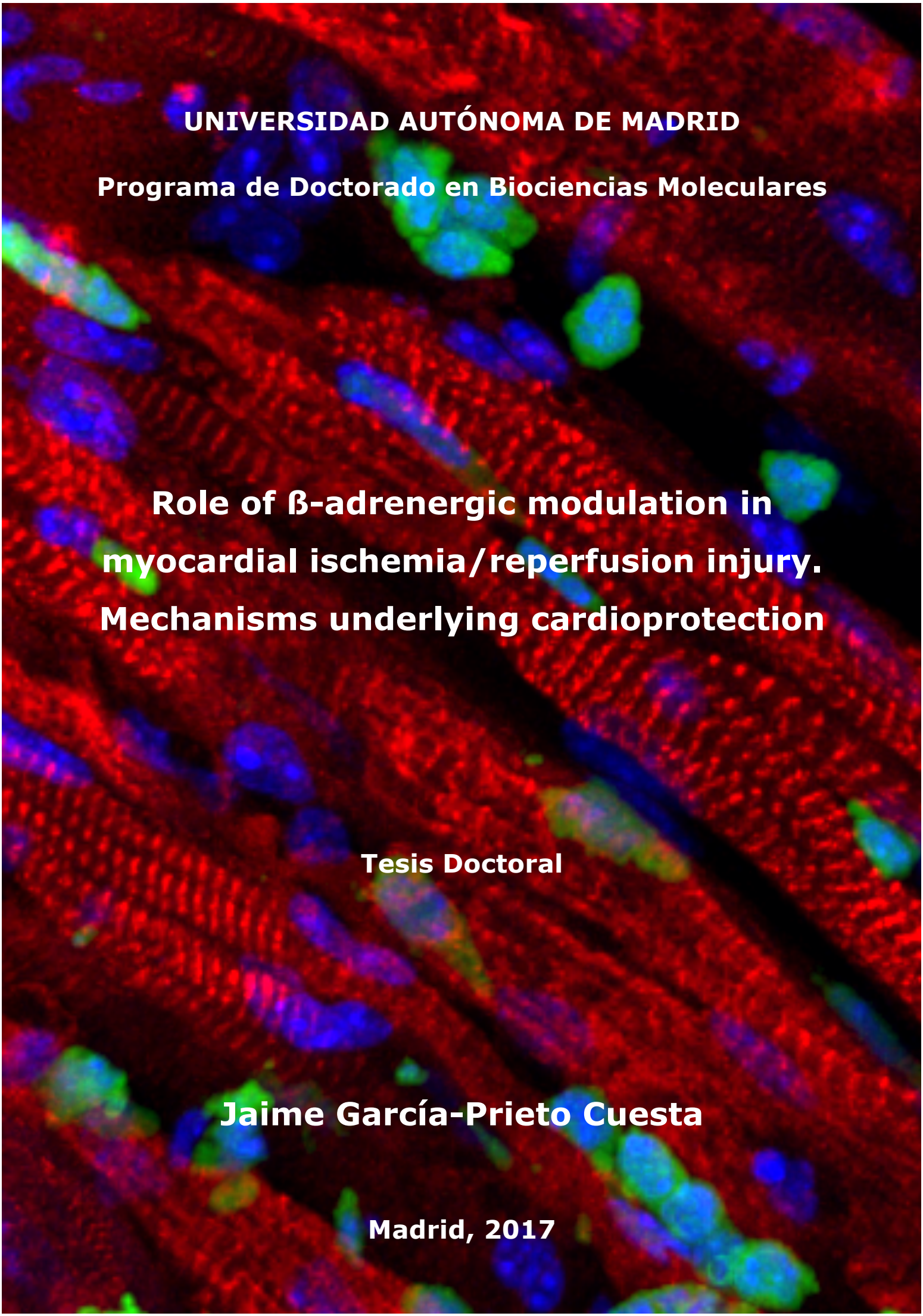

UNIVERSIDAD AUTÓNOMA DE MADRID

Programa de Doctorado en Biociencias Moleculares

Role of ß-adrenergic modulation in myocardial ischemia/reperfusion injury. Mechanisms underlying cardioprotection

Tesis Doctoral

Jaime García-Prieto Cuesta

Madrid, 2017

Departamento de Bioquímica
Facultad de Medicina
UNIVERSIDAD AUTÓNOMA DE MADRID

Role of ß-adrenergic modulation in myocardial ischemia/reperfusion injury. Mechanisms underlying cardioprotection

Memoria presentada para optar al grado de Doctor por:

Jaime García-Prieto Cuesta
Licenciado en Ciencias Biológicas y Máster en Biotecnología

Bajo la dirección de:
Borja Ibáñez Cabeza

Centro Nacional Investigaciones Cardiovasculares Carlos III

Madrid, 2017

Department of Biochemistry
School of Medicine
UNIVERSIDAD AUTÓNOMA DE MADRID

Role of ß-adrenergic modulation in myocardial ischemia/reperfusion injury. Mechanisms underlying cardioprotection

Doctoral thesis presented to earn the Doctor of Philosophy degree by:

Jaime García-Prieto Cuesta
BSc. in Biological Sciences & MSc. in Biotechnology

Under the guidance of:
Borja Ibáñez Cabeza

Spanish National Center for Cardiovascular Research (CNIC)

Madrid, 2017

A día 7 de noviembre del año 2017,

Don. BORJA IBÁÑEZ CABEZA, Doctor en Medicina y Cirugía y director del Departamento de Investigación Clínica del Centro Nacional Investigaciones Cardiovasculares Carlos III (CNIC) en Madrid, y

Dña. CARMEN VALENZUELA MIRANDA, Doctora en Biología e Investigadora Científica del Instituto de Investigaciones Biomédicas CSIC-UAM en Madrid,

CERTIFICAN:

Que durante los últimos 3 años Don. JAIME GARCÍA-PRIETO CUESTA ha realizado bajo su dirección y tutorización el trabajo de investigación titulado: *"Role of ß-adrenergic modulation in myocardial ischemia/reperfusion injury. Mechanisms underlying cardioprotection"* para alcanzar el Grado de Doctor. La presente memoria reúne los requisitos de originalidad y contenido exigidos y contribuye de manera significativa al ámbito de la investigación cardiovascular, por lo que autorizan su presentación para que pueda ser juzgada por el tribunal correspondiente.

Borja Ibáñez Cabeza

Director de Tesis

Carmen Valenzuela Miranda

Tutora de Tesis

This work was performed in the Translational Laboratory for Cardiovascular Imaging and Therapy led by Professor Borja Ibáñez Cabeza at the Spanish National Center for Cardiovascular Research Carlos III (CNIC) in Madrid.

This work was supported by a competitive grant from the Spanish Ministry of Economy and Competitiveness (MINECO) through the Carlos III Institute of Health-Fondo de Investigación Sanitaria FIS-ISCIII (PI13/01979) and FIS-ISCIII (PI10/02268), Fundacion Mutua Madrileña (AP8695-2011), from the competitive "CNIC translational 01/2009" and European Regional Development Fund (ERDF/FEDER) funds (PI10/02268 & PI13/01979). The CNIC is supported by the Spanish Ministry of Economy and Competitiveness (MINECO) and the Pro-CNIC Foundation, and is a Severo Ochoa Center of Excellence (MINECO award SEV-2015-0505).

To Blanca, for her love, company and unconditional support

It is only through labor and painful effort, by grim energy and resolute courage, that we move on to better things

Theodore Roosevelt

Acknowledgments

I would like to thank Dr. Borja Ibáñez for giving me the opportunity to be part of his exceptional team and for his guidance on my career, mentorship and personal development. I would like to very special thank Dr. Valentín Fuster for introducing me to the biomedical research back in 2006, his mentorship all these years and for transmitting me the sense of altruism and commitment with to society. I would like to thank my tutor Carmen Valenzuela for her help and guidance.

I would like to thank all my colleagues from the Translational Laboratory for Cardiovascular Imaging and Therapy at the CNIC, specially my friends Rodrigo J., David S-R, Rocío V., Mónica G., Andrés P., Gonzalo P., Javier S., Carlos G., Ana G., José M. G. and Jaume A., with whom I have been fortunate to share so many hours of hard work, for their inexhaustible enthusiasm and dedication, and the support they have given these years.

I would like to thank the old D.A.I.C. department and adjacent members specially María C., Laia T., María N., José R., Javier M., Cristina G., Pedro M., Raphael C., Mª Jesús A., Cristina R. Ricardo V-B, José M. G., Carlos S., Francisco C, Juan A. B., María V., Vicente A. and Andrés H. for their support and teachings. I would like to very special thank Eeva S. and Ana I. C for their unconditional help.

I would like to thank all the collaborators from UCL, Lyon and Max-Plank, and those from CNIC like Santiago R., Antonio M., Roisin D., Jose L., Antonio SB., Simon B., Ángel, Yolanda V., Fátima L. and many others who made my life easier throughout this amazing years.

Finally, I would like to thank my parents, my brothers and sister María and the pillar that holds my life Blanca, for their help and care during the difficult times.

Summary/Resumen

The β-adrenergic system plays an important role in the regulation of heart function. The early intravenous administration of ß1-adrenergic receptor (ADRB1)-antagonist, metoprolol, in patients with ST-segment elevation acute myocardial infarction (AMI) reduces the extent of infarct size. The prevailing view has been that metoprolol acts mainly on cardiomyocytes function, reducing cardiac output. This work presents evidence that metoprolol reduces ischemia/reperfusion injury by targeting the hematopoietic compartment, specifically by inhibiting neutrophil function through an ADRB1 signalling-dependent manner. Metoprolol acts during early phases of neutrophil recruitment, impairing structural and functional rearrangements necessary for effective interactions with circulating platelets to occur. Metoprolol, "stuns" neutrophils that cannot engage the structural conformation necessary to infiltrate tissues, triggering erratic intravascular dynamics and overall blunted inflammation. The in vitro functional assays confirm direct effect on neutrophils through an ADRB1-dependent mechanism. The depletion of circulating neutrophils, the lack of the *Adrb1* in hematopoietic cells and the blockade of P-selectin glycoprotein ligand-1, the receptor involved in neutrophil-platelet interactions, result in a complete abrogation of metoprolol´s infarct-limiting effect. Moreover, the association between neutrophil count and microvascular obstruction is abolished in early metoprolol-treated AMI patients. Metoprolol has no direct effect on platelet function, but inhibits neutrophil-platelet interactions in AMI patients by targeting neutrophils directly. Identification of the relevant role of ADRB1 in hematopoietic cells during acute injury and the protective role upon its modulation offers potential for developing new therapeutic strategies.

El sistema β-adrenérgico juega un papel importante en la regulación de la función cardíaca. La administración intravenosa y previa a la reperfusión del antagonista ß1-adrenérgico (ADRB1) específico metoprolol, en pacientes con infarto agudo de miocardio con elevación del segmento ST, reduce el tamaño final del infarto. Clásicamente se ha considerado que el metoprolol actúa principalmente sobre los miocardiocitos disminuyendo el gasto cardíaco. Este trabajo presenta por primera vez evidencia de que el metoprolol reduce el daño por isquemia/reperfusión cardiaco actuando directamente sobre el compartimento hematopoyético, inhibiendo de manera específica la cascada de señalización dependiente del ADRB1 en los neutrófilos. El metoprolol actúa durante las primeras etapas del reclutamiento de células inflamatorias al miocardio. Altera la conformación estructural y función neutrofílica, impidiendo que se establezcan interacciones eficientes entre los neutrófilos y las plaquetas circulantes. El metoprolol "aturde" los neutrófilos circulantes, provocando un comportamiento errático que termina abortando su infiltración y por tanto su acción inflamatoria general en los tejidos. Los ensayos funcionales in vitro realizados confirman un efecto directo del metoprolol sobre los neutrófilos dependiente de ADRB1. La depleción de neutrófilos circulantes, la falta de *Adrb1* en las células hematopoyéticas y el bloqueo del ligando-1 de la glucoproteína P-selectina, el cual está involucrado en las interacciones de neutrófilos con las plaquetas circulantes, inhiben el efecto limitante sobre el tamaño de infarto del metoprolol. Estos resultados indican que la presencia de ADRB1 en los neutrófilos es indispensable para que el metoprolol ejerza su acción protectora. Además, pacientes con infarto agudo de miocardio (IAM) tratados con metoprolol presentan abrogación de la asociación entre las cuentas de neutrófilos en sangre y la obstrucción microvascular. Por último, el metoprolol no tiene efecto directo sobre la función plaquetaria, e inhibe las interacciones de neutrófilos y plaquetas en pacientes con IAM ejerciendo su efecto directamente sobre los neutrófilos. La identificación del papel de ADRB1 en las células hematopoyéticas durante la lesión aguda y la función protectora de su modulación ofrece el potencial para desarrollar nuevas estrategias terapéuticas.

Table of contents

Abbreviations

Abbreviation	Meaning
CNIC	Spanish National Center for Cardiovascular Research
AMI	Acute myocardial infarction
IAM	Infarto agudo de miocardio
ADRB	ß-adrenergic-receptor
ADRB1	ß1-adrenergic-receptor
Adrb1	ß1-adrenergic-receptor gene
ADRB2	ß2-adrenergic-receptor
Adrb2	ß2-adrenergic-receptor gene
IR	Ischemia/reperfusion
MVO	Microvascular obstruction
i.v.	Intravenous
PCI	Percutaneous coronary intervention
IS	Infarct size
AAR	Area at risk
LAD	Left anterior descending
TTC	Triphenyl-tetrazolium chloride
BM	Bone marrow
CMR	Cardiac magnetic resonance
LV	Left ventricle
LVEF	Left ventricular ejection fraction
LysM	Lysozyme-M
PSGL1	P-selectin glycoprotein ligand-1
GFP	Green fluorescent protein
IVM	Intravascular microscopy
CXCL1	Chemokine (C-X-C motif) ligand 1
ROS	Reactive oxygen species
s.e.m.	Standard error of the mean
TNFα	Tumor necrosis factor alpha

Introduction

The topic of study covered in this doctoral thesis is the role of β-adrenergic (ADRB) system modulation with ADRB-antagonists (ß-blockers) in acute myocardial infarction (AMI), with special focus to the effect on ischemia/reperfusion (IR) injury-associated deleterious processes. Specifically, this work focuses on the study of the mechanisms underlying the benefits of early intravenous (i.v.) administration of the ß1-adrenergic receptor (ADRB1)-antagonist, metoprolol, as a cardioprotective strategy and evaluates its effect on neutrophil dynamics, tissue infiltration and neutrophil-platelet interactions and coaggregates formation. Further, the implications of these phenomena on myocardial microvascular obstruction (MVO) as a key factor for final myocardial infarct size (IS) and subsequent outcome in patients with ST-segment elevation AMI are evaluated.

Acute myocardial infarction

Cardiovascular disease is a growing healthcare problem. It is the leading cause of morbidity and mortality worldwide, and is projected to account for approximately 25 million deaths annually by 2030 (1). Heart attack is caused by intraluminal coronary artery occlusion, frequently due to a disrupted atherosclerotic plaque (2) (**Fig. 1**). Insufficient oxygen and nutrients supply into the capillaries (ischemia) limits both energy supply (mainly glucose and free-fatty acids) and energy production (adenosine triphosphate, ATP) essential for cellular viability. The heart, a high oxygen-demanding organ, can suffer irreversible damage if ischemia is maintained for several minutes (3). The amount of infarcted tissue, that is, the infarct size, is the main determinant of poor outcome and adverse events post AMI (4) and is mainly determined by the duration of the ischemic insult. Seminal studies performed three decades ago with animal models demonstrated that an early reperfusion (restoration of the blood flow) was able to limit myocardial IS (5) and improve prognosis. Several years later, pharmacological reperfusion with the administration of fibrinolytics was indisputably associated with a reduction in mortality in patients with AMI (6). A decade later, primary angioplasty (mechanical reperfusion by percutaneous coronary intervention (PCI) in the

cathlab) resulted to be superior to fibrinolysis (7) (8). Thereon, clinical practice guidelines, advocate to reduce the ischemia duration by re-establishing coronary artery blood flow, as the cornerstone of AMI management (9), in order to reduce myocardial damage and complications and improve survival (10). Despite these achievements, AMI is still one of the major clinical manifestations of cardiovascular disease (7) and a chief contributor to mortality and morbidity worldwide. Except for early reperfusion therapies, few additional therapies have shown mortality reduction or improved long-term prognosis of patients with AMI. The development of therapies able to reduce infarct size and to prevent cardiac dysfunction after myocardial infarction are, therefore, a matter of intense research (11) (12) (13) (14).

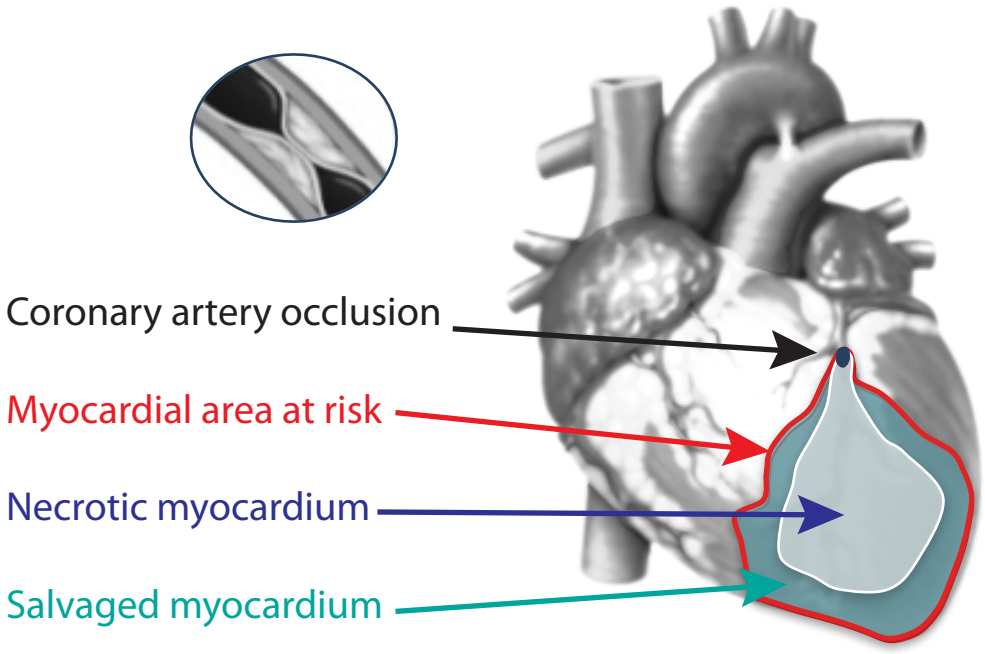

Figure 1.! Acute myocardial infarction concepts
Illustration of a heart defining different AMI-related concepts. Heart attack is caused by intraluminal coronary artery occlusion, frequently due to a disrupted atherosclerotic plaque. The myocardial zone irrigated by the occluded artery, the area at risk (AAR) is in jeopardy of becoming irreversibly injured if ischemia is not relieved. Most of the patients suffering from an AMI receive timely reperfusion therapy allowing part of the myocardial AAR to remain free of necrosis, i.e. to survive (salvaged myocardium). In white, the extent of infarcted myocardium.

Myocardial ischemia/reperfusion injury

Since the demonstration of the benefits of blood flow restoration to salvaged myocardium (15) (16), most of the patients suffering from AMI undergo reperfusion therapy allowing part of the myocardial area at risk (amount of tissue irrigated by the occluded artery in jeopardy of becoming necrotic due to the ischemic insult, AAR), to remain free of necrosis. Paradoxically, reperfusion of the occluded coronary artery, further contributes to myocardial injury (3), something known as reperfusion injury. Reperfusion-injury is defined as "the injury caused by the restoration of blood flow after an ischemic episode, leading to the death of cardiac cells that were reversibly injured at the time of blood flow restoration". The potential of reperfusion as a phenomenon able to induce subsequent injury following to ischemic damage is supported by strong evidence that interventions applied at the end of the ischemic period (i.e. coinciding with reperfusion) can significantly reduce infarct size (17) (18) (19) (20) (21). Clinical and experimental non-invasive cardiac magnetic resonance (CMR) recent studies have shown that shortly after myocardial reperfusion drastic myocardial tissue composition changes occur (22) (23) (24). Although experimental studies have shown reperfusion injury to contribute up to 50% of the total IS (25) (**Fig. 2**), the actual impact of reperfusion has not been fully determined. Ischemia duration (time that runs between onset of symptoms and reperfusion), brief episodes of spontaneous reperfusion, tissue temperature during ischemia and hemodynamic situation, as well as the area at risk, and the amount of residual blood flow through the collateral arteries and the extent of microvascular dysfunction, are all important reperfusion injury contributing factors (11). Overall, the injury inflicted to the myocardium during AMI is the result of both ischemia- and reperfusion-related phenomena, and is known as myocardial ischemia/reperfusion (IR) injury (8) (26) (27) (28) (29). The development of effective therapies to reduce myocardial IR injury is therefore an unmet clinical need (11).

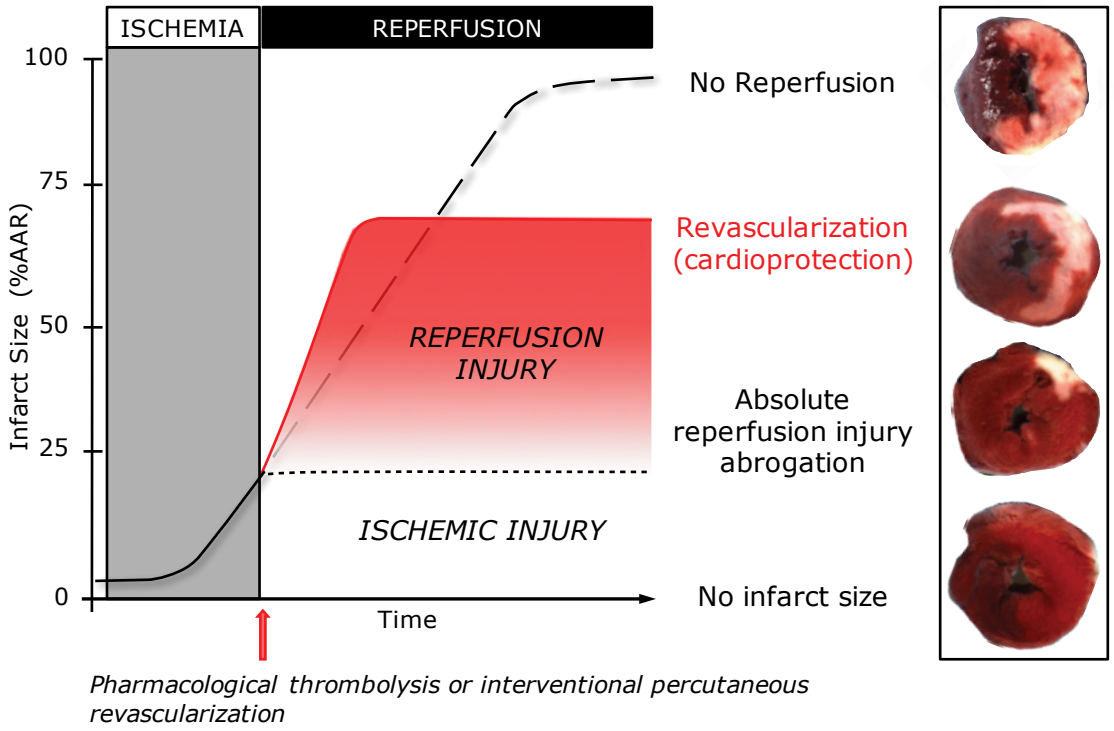

Figure 2.! Myocardial death during ischemia and reperfusion
When coronary artery occlusion occurs, myocardium is capable to maintain its performance for certain amount of time. Beyond this time, myocardial death grows exponentially due to ischemia. If there is no reperfusion, the entire myocardium irrigated by the occluded coronary artery myocardium (Area at risk, AAR) will become infarcted (striped line); If reperfusion occurs in a reasonable range of time, ischemia injury is reduced and therefore IS limited (dotted line). Paradoxically, reperfusion itself induces an additional damage (red line). Final infarct size (IS) is therefore dependent on two separate but related processes: ischemia and reperfusion. In an ideal situation (no reperfusion injury), IS will only be driven by ischemic injury. Pictures on the right panel show representative mouse hearts after myocardial temporal coronary occlusion. Triphenyl-tetrazolium chloride (TTC) staining depicts the viable myocardium (red), while necrotic myocardium is left uncoloured (white). Figure adapted from Sanz-Rosa *et al.* (30).

Inflammation as a contributor to reperfusion injury

Inflammation is a physiological process of self-protection in response to harmful stimuli, endogenous tissue damage, irritants or pathogen infection. Inflammation also promotes the healing process. Polimorphonuclear leukocytes, particularly neutrophils, constitute a great portion of circulating

leukocytes and are the primary effectors of the immune response against invading pathogens and the premier cellular mediators to acute injury (31). These two functions rely on their ability to migrate and patrol within the blood vessels and tissues. Selectins and chemokines trigger endothelial integrin's activation, allowing neutrophils to adhere, crawl and attach to the vessel wall (32) (33). Once recruited, neutrophils reorganize their 3D-structure disposing asymmetric polarization of membrane receptors (34) and subsequently direct a P-selectin glycoprotein ligand-1 (PSGL1) cluster-protruding domain into the lumen to scan for activated platelets present in the bloodstream. Only neutrophil-platelet PSGL1-dependent productive interactions thrive subsequent neutrophil inflammatory response and infiltration (35). When extravasated into the injured tissue, neutrophils enhance the release of pro-inflammatory cytokines and other inflammatory mediators causing deleterious effects to the tissue and inducing more recruitment (36) (37) (38). Consequently, those neutrophils unable to polarize or to transduce signals display aberrant inflammatory responses.

In the context of AMI, cardiac cytokine burst induces neutrophil activation and rapid recruitment to the injured myocardium leading to increase myocardial damage in several and sequential manners (36) (39) (40). Neutrophils cause direct injury to endothelial cells and cardiomyocytes via production of reactive oxygen species (ROS), proteases, cytokines and lipids (36). In addition, in an inflammatory milieu, neutrophils bind to activated platelets and red blood cells, forming PSGL1-dependent interaction coaggregates (39). Upon reperfusion, these coaggregates contribute to capillaries obliteration in the affected vessel, precluding tissue perfusion despite blood flow restoration in the proximal vessels. This phenomenon is known as MVO or "No Reflow phenomenon" (41) (42). MVO appears in 30 to 50% of the patients with efficient epicardial vessel recanalization, and is a major contributor to IR injury, infarct size, and an independent predictor of morbidity/mortality (8) (43). The microcirculatory network is the interface between the epicardial vessel and the cardiomyocytes. No matter how efficiently and rapidly the blood flow is restored to the epicardial artery, if there is MVO the myocardial tissue irrigated distally will remain without efficient perfusion. In summary,

neutrophils are clearly involved in reperfusion injury, and neutrophil cellular dynamics (including neutrophil-platelet interactions) are an attractive therapeutic target for the prevention of myocardial IR injury.

ß-Adrenergic system

The adrenergic (or sympathetic) neuro-hormonal axis is a main regulator of the cardiovascular system. It particularly regulates heart function. ß-adrenergic system activation results in and increase in heart rate and cardiac contractility, improvement of cardiac relaxation, decrease in venous capacitance, and constriction of resistance and cutaneous arteries (44) (**Fig. 3**). The relevance of ADRBs is depicted by the fact that two Nobel Prizes (Medicine 1988 and Chemistry 2012) were awarded for ADRBs-related discoveries (45) (46) (47) (48). ARDBs are non-sensory G-protein–coupled receptors, consisting of seven trans-membrane domains, expressed on the surface of a wide range of target cells which primarily signal through heterotrimeric G-proteins once in contact with adrenergic neurotransmitters norepinephrine and epinephrine (49) (50). There are 3 different ADRBs subtypes: ADRB1, ADRB2, and ADRB3 which differ in structure, function, affinity states and pharmacological properties (51) (52) (53) (54) (55) (56). From them, ADRB1 is the predominant subtype- in the (normal, healthy) myocardium, representing 75% to 80% of total ADRBs density, followed by ADRB2, which comprises ≈15% to 18% of total cardiomyocyte ADRBs, and the remaining 2% to 3% is ADRB3 (under normal conditions) (44) (50).

The ß-adrenergic system is critically involved in many inflammatory reactions and has been widely studied in immunity (57) (58). Particularly, both ADRB1 and ADRB2 in humans are expressed in a wide variety of tissues including immune cells, as lymphocytes, macrophages, and neutrophils (59) (60). During ischemia, catecholamine induced-stress alters neutrophil trafficking (60) (61) (62) and promotes formation of neutrophil-platelet coaggregates (63). Moreover, extra neuronal generation of epinephrine by neutrophils provides amplification of the catecholamine-mediated inflammation (57). Despite recent advances in understanding the role of catecholamines in the

inflammatory response, the precise mechanism by which infarction-induced catecholamine release has an impact on the leukocytic-dependent innate immune response and contributes to further increase myocardial infarct size is unclear. It is known that ß-blockers inhibit inflammatory cells' activity, mobilization and migration (64) (65) (66), however and besides promising experimental findings no clinical trial has shown positive results in the context of ischemia reperfusion injury.

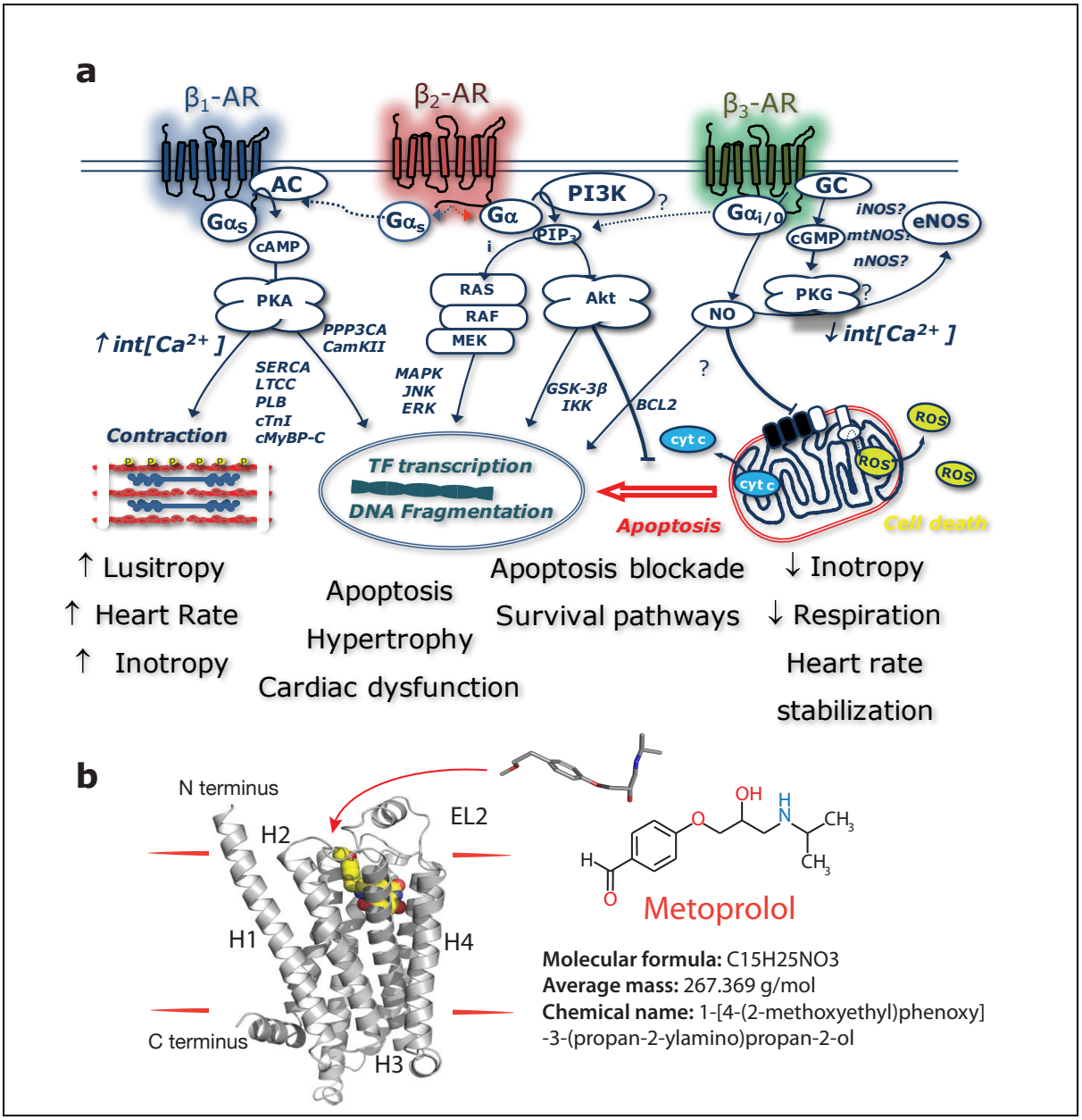

Figure 3. ß-adrenergic signalling & effector functions
(a) Fight-or-flight stress responses deliver catecholamines distally into the tissues through the blood and locally through the nerve fibres. Agonists occupy ß-adrenoceptors (β-ARs) which causes the dissociation of the heterotrimeric G-proteins into active Gα and free Gβγ subunits which can then transduce intracellular signals independently of each other. ADRB1 (β1AR) and ADRB2 (β2AR) activate Gs-protein signalling, stimulating the effector adenylate cyclase, which converts adenosine triphosphate (ATP) to adenosine 3',5'-monophosphate (cAMP), causing subsequent activation of the cAMP-dependent protein-kinase A (PKA). PKA is the major effector of cAMP and by phosphorylating a variety of substrates, ultimately induce a significant increase in free intracellular $Ca2^{+}$ concentration, which activates several biochemical effector and transcriptional effectors. Lower panel summarizes the functional consequences from βAR stimulation in the cardiovascular system. **(b)** Structure of the ß1-adrenergic receptor bound to ligand shown in cartoon representation with the intracellular side at the bottom of the figure. The ligand (in this case, carmoterol) is shown as a space filling model in yellow. The extracellular loop 2 (EL2), and transmembrane helices 1–4 (H1–H4) are labelled. Next, 2D and 3D illustrations of the ß1-adrenergic receptor antagonist, metoprolol. The oxygen (O, red), the nitrogen (N, blue). Adapted from Lymperopoulos *et al.* (44), Warne *et al.* (52) and Pubchem.

ß-blockers in AMI

In early stages of myocardial infarction, various types of stressors such as pain, anxiety and ischemia are activated resulting in intracellular catecholamine redistribution (67) and local and systemic release of catecholamines (68). Levels of circulating epinephrine can increase up to 10-fold in patients suffering from AMI. This hyper sympathetic systemic stimulation results in malignant arrhythmias and acceleration of cell damage in the injured myocardium (68). ß-adrenergic antagonists (ß-blockers) are therefore one of the oldest and most frequently prescribed drugs used by cardiologists in the treatment of cardiovascular diseases. In fact, current clinical guidelines in the management of AMI indicate the administration of oral β-blockers within the first 24 hours after AMI (69) because its use undoubtedly reduce mortality (70). However, the ability of β-blockers to reduce infarct size has been a matter of intense debate.

Several randomized clinical trials have contributed to understand whether early ß-blockers administration should be considered as a cardioprotective therapy against AMI. First, a subsequent analysis of the TEAHAT study revealed significant reduction in heart-enzyme-mediated infarction size in patients without ß-blockade contraindications (71). Later Van de Werf et al., designed a trial to study the effect of i.v. ß-blockers (atenolol) given concomitantly with thrombolytic therapy in patients with AMI, and found a neutral effect on infarct size (72). Next, in 2005, the COMMIT trial tested the value of adding early ß-blocker therapy in the emergency treatment of myocardial infarction to standard therapy against AMI. A total of 45,852 patients with AMI who were to be re-vascularized (aspirin and thrombolysis) were randomized to receive early metoprolol i.v. followed by oral metoprolol or placebo. Despite the lack of data on infarct size, authors found a significant reduction in rates of re-infarction and ventricular fibrillation in patients receiving metoprolol (73). A more recently randomized clinical trial included 96 patients who were randomized to receive the ultra-short-acting ADRB1-selective blocking agent, landiolol, or placebo, showing significant improvement in cardiac function (Left ventricular ejection fraction, LVEF) in landiolol-treated patients (74). In addition, evidence from retrospective studies performed while PCI being the treatment of choice for a AMI, suggests that β-blockade treated patients presented better short-term survival and better outcomes (75) (76) (77). Overall, the use of different ß-blockers (metoprolol or atenolol), the type (oral or i.v.) and timing (early or within the first hours) of administration, and the different contexts of AMI therapy under evaluation (non-reperfused, pharmacological thrombolysis or PCI) have contributed to the uncertain of this promising therapy.

Role of metoprolol on IR injury

Metoprolol is a moderately lipophilic, ADRB1-selective antagonist, that acts primarily on heart and blood vessels (54). It is one of the earliest ß-blocker accepted for clinical use (78) and given to its like short half-life, easy i.v. administration and potential pleiotropic effects, metoprolol is the leading drug

of its class (79). Our group has focused for the last 12 years, on the role of metoprolol-tartrate on myocardial IR injury. Specifically, evaluating the effect of its pre-reperfusion (i.e. during ongoing ischemia) administration on infarct size. Metoprolol, in experimental models of AMI demonstrated a significant reduction size only when administered prior to reperfusion (80) (81). Based on this experimental evidence, we conducted the METOCARD-CNIC clinical trial to test whether early metoprolol administration was cardioprotective in patients. A total of 270 patients with a first anterior ST-segment elevation AMI undergoing percutaneous coronary intervention within 6 hours of symptoms onset were randomized to or not to receive i.v. metoprolol tartrate during the transport by ambulance or at the hospital emergency room before PCI revascularization. Metoprolol-treated group presented a significant infarct size reduction measured by CMR at 5-7 days and improved long-term cardiac function by a follow up cardiac CMR at 6 months (82) (83). However, the mechanism underlying metoprolol's cardioprotective effect remains unclear (84) Identifying this mechanism could have significant implications for the understanding of IR injury and the development of novel infarct-limiting therapies. More recently, our group also participated in the EARLY BAMI trial, in which metoprolol administration was not associated with a significant infarct size reduction (85). However, the dose of metoprolol used in this trial was significantly less than in METOCARD-CNIC trial and it was not associated with a significant reduction in heart rate and blood pressure, suggesting an infradosing effect.

The mechanisms by which metoprolol reduces infarct size have not been demonstrated and this represented the main objective of the present thesis.

Objectives

Pre-reperfusion administration of i.v. ADRB1-blocker is a safe strategy that reduces infarct size and improves long-term cardiac function. Based on this evidence and the relevance of inflammation on IR injury, the main hypothesis tested on this work is that the mechanism responsible of the protective effect of early (pre-reperfusion) i.v. metoprolol administration is by altering neutrophil dynamics, which results in a dampened inflammatory response. This results in reduced myocardial IR injury and, in turn, in smaller infarct sizes.

The objectives set to test this working hypothesis are:

Objective 1: To set de myocardial IR murine model and confirm that pre-reperfusion administration of i.v. metoprolol-tartrate cardioprotective effect in a murine model of IR injury.

Objective 2: To assess the contribution of ADRB1 blockade on the different heart compartments (endothelium, myocardium (cardiomyocyte) and hematopoietic) to cardioprotection.

Objective 3: To study the effect of ADRB1-selective blockade with metoprolol on myeloid-derived leukocyte infiltration.

Objective 4: To assess the effect of ADRB1 blockade on neutrophil function, specifically evaluating its effect on neutrophil-platelet interactions and neutrophil migration.

Materials and methods

Human cardiac magnetic resonance imaging

The METOCARD-CNIC trial (NCT01311700) recruited patients suffering an AMI during hospital transit to undergo mechanical reperfusion by primary angioplasty. Patients were randomized to receive either i.v. metoprolol (up to 15 mg) or no drug (control). The study design can be revised in Ibanez et al. (86). Patients underwent two CMR studies: 1 week and 6 months after AMI. Images were acquired with a 3.0 Tesla magnet (Achieva Tx®, Philips Medical Systems) with vector-cardiographic gating and a dedicated cardiac 32-channel phased-array surface coil. The extent of MVO, was measured in the 1 week CMR study; to detect and quantify MVO, a delayed enhancement imaging was performed 10 minutes after gadolinium contrast injection, using a T1-weighted 2-D Inversion Recovery Turbo Field Echo (2D IR-TFE) sequence. Myocardial necrosis was defined by the extent of abnormal gadolinium enhancement, whereas MVO was defined as black hypo-enhanced areas within the bright-hyper-enhanced regions. CMR analysis was undertaken by operators blinded to treatment allocation at CNIC. Myocardial necrosis and MVO were quantified by semiautomatic delineation with dedicated software (QMass MR 7.6; Medis, Leiden, the Netherlands). Total MVO was quantified as grams of left ventricle (LV). To correct for infarct size, MVO was also expressed as a % of the infarcted area.

Mouse procedures

Experimental procedures were approved by the CNIC Animal Care and Ethics Committee and regional authorities. Myocardial IR, thioglycolate-induced peritonitis, and intravital microscopy (IVM) experiments were performed with 8-13-week-old wild-type male C57BL/6J mice. β1-adrenergic receptor (*Adrb1)* knockout (KO; *Adrb1*KO) mice were in a mixed background. β2-adrenergic receptor (*Adrb2*) knockout (KO; *Adrb2*KO) mice were in a C57BL/6J background. For the bone marrow (BM) transplant experiments, *Adrb1*KO mice were backcrossed with mice expressing DsRed under the control of the β-actin promoter to facilitate evaluation of BM engraftment. Male and female mice were used as donors in BM transplant procedures, but only males were

used in myocardial IR and thioglycolate-induced peritonitis experiments. All animals were randomized to receive a single i.v. injection (50 µL) of metoprolol-tartrate (10 mM) or vehicle (saline). Histological evaluation of injured myocardium in the myocardial IR model was performed in lysozyme M-GFP^{+} (LysM-GFP) (87) male mice. Intravascular neutrophil and neutrophil-platelet interactions were scored manually in the myocardium. Neutrophils were depleted in C57BL/6J male by i.v. injections of 50 µg anti-mouse Ly6G antibody 24 and 48 hours before the myocardial IR procedure (88). For in vivo blocking of PSGL1, 50 µg of anti-PSGL1 antibody (clone 4RA10) was i.v. injected 15 minutes after ischemia onset. Mice were maintained under pathogen-free conditions in a temperature-controlled room and a 12-hour light-dark cycle at the CNIC animal facilities. Chow and water were available ad libitum.

Reagents

Metoprolol-tartrate (M5391), Evans blue, triphenyltetrazolium chloride, DAPI (D8417-1MG), Mowiol mounting medium (81381), anti-laminin (L9393), anti-α-actinin (A7732), Dihydrorhodamine 123 (D1054) were obtained from Sigma-Aldrich. Dylight-650-conjugated anti-1A8 Ly6G (BE0075-1) and anti-*PSGL1* antibody (clone 4RA10) from BioXcell. Anti-CD41 (12-04-11-83) and anti-CD115 (12-1152-83) were obtained from ebioscience. O.C.T. was obtained from Tissue-Tek®. Qiagen RNeasy Plus Mini Kit (74136). Percoll Plus (17-5445-02) and Ready-to–go RT-PCR Beads (27-9259-01) from GE Healthcare. CXCL1 was obtained from (453-KC-010) from R&D Systems. W-peptide (WKYMVM, 1799) from Tocris. Thioglycolate (BD211716) and anti-GP IIb/IIIa from BD Biosciences. Anti-GR1 (ab2557) was obtained from Abcam and AF-647 (A-21472) from Molecular Probes. Anti CD45–FITC from Miltenyi Biotec, Germany. PC5-conjugated anti-CD14, anti-CD61 PC7 and Versalyse solution were obtained from Beckman Coulter. Cytokine tumor necrosis factor alpha (TNFα) was obtained from R&D Systems.

Mouse intra-carotid hemodynamic study

Animal preparation was identical to mouse model of myocardial IR injury in order to evaluate metoprolol dosage under similar conditions to that of myocardial IR model.

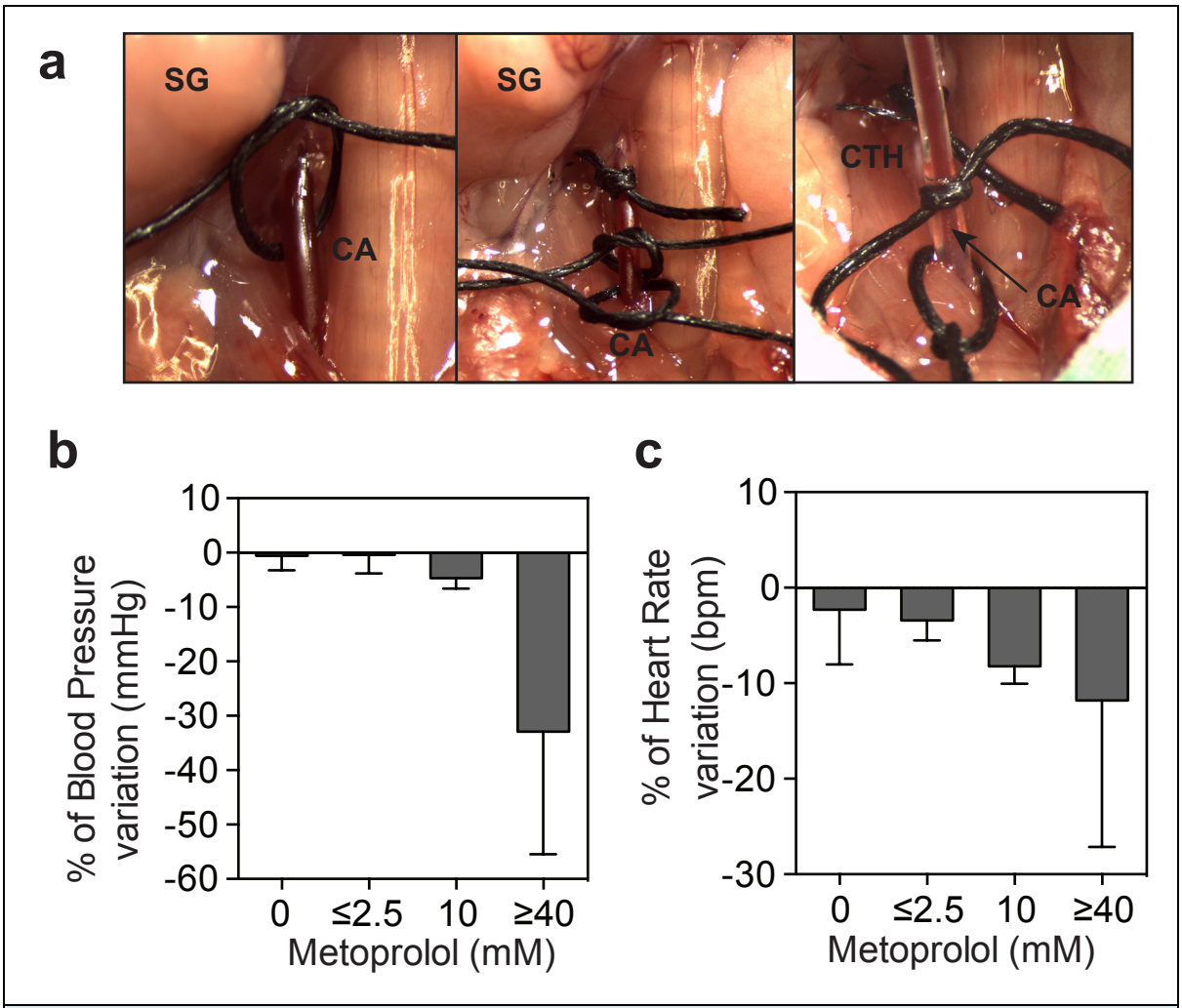

Figure 4. Hemodynamic effect of i.v. metoprolol on mouse
Hemodynamic effect of a single intravenous injection (50µL) of metoprolol-tartrate at different concentrations through the femoral vein. **(a)** Mean arterial blood pressure and **(b)** Heart rate (bpm) were registered through a left arterial carotid artery catheter. (n=3-4 per condition). Data are means ± s.e.m. SG, stands for salivary gland; CA, right carotid artery; CTH, catheter.

Once fully asleep, intubated and tempered in a heating pad, 5 mm of the right common carotid artery was dissected and exposed under aseptic conditions and using bluntly vessel-forceps and blood flow interrupted using several loose 6-0 silk sutures and knots. A small incision was made between the two

ligatures with a micro surgical scissor. Then a heparinized PE-tubing catheter connected to a pressure transducer was inserted in line with the vessel and then fixed with firm ligatures around the artery throughout the procedure (**Fig. 3**). Electrocardiogram, Systolic blood pressure (SBP), heart rate (HR) and temperature was monitored (MP36R, Biopac Systems Inc). Dose-response studies, consisted on 10 minutes of catheter stabilization record, followed by a single i.v. bolus of 50 µL of metoprolol-tartrate to each animal through the femoral vein (n=3/group), and 1 h continuous hemodynamic monitoring saved for posterior analysis of mean SBP and mean HR.

Mouse model of myocardial IR injury

Male 8-12-week-old mice were subjected to 45 minutes occlusion of the left anterior descending (LAD) coronary artery followed by 6 or 24 hours of reperfusion. For infarct size evaluation, reperfusion was maintained for 24 hours. For analysis of MVO, neutrophil infiltration, and neutrophil-platelet interactions, reperfusion was maintained for 6 or 24 hours as indicated. The IR procedure was performed as previously described (89). (**Fig. 5**) Briefly, fully asleep animals were intubated and temperature controlled throughout the experiment at 36.5 °C to prevent hypothermic cardioprotection. Thoracotomy was then performed and the LAD was ligated with a nylon 8/0 monofilament suture for 45 min. The electrocardiogram was monitored (MP36R, Biopac Systems Inc.) to confirm total coronary artery occlusion (ST-segment elevation) throughout the 45 minutes ischemia. Ten minutes before reperfusion onset, mice were randomized to receive a single i.v. injection (50 µL) of metoprolol-tartrate (10 mM) or vehicle (saline) through the femoral vein. Dose of metoprolol was chosen after a dose response study, which identified this dose as the highest dose inducing a moderate effect on heart rate and blood pressure (i.e. <10% variation in both parameters from pre-dose (**Fig. 4**). At the end of reperfusion, the chest was closed and animals were kept with 100% O_2 and analgesized with buprenorphine (S.C., 0.1 mg per kg) until the end of reperfusion.

Mouse infarct size quantification

At the end of follow up, mice were re-anesthetized and re-intubated, and the LAD coronary artery was re-occluded by ligating the suture in the same position as the original infarction (89).

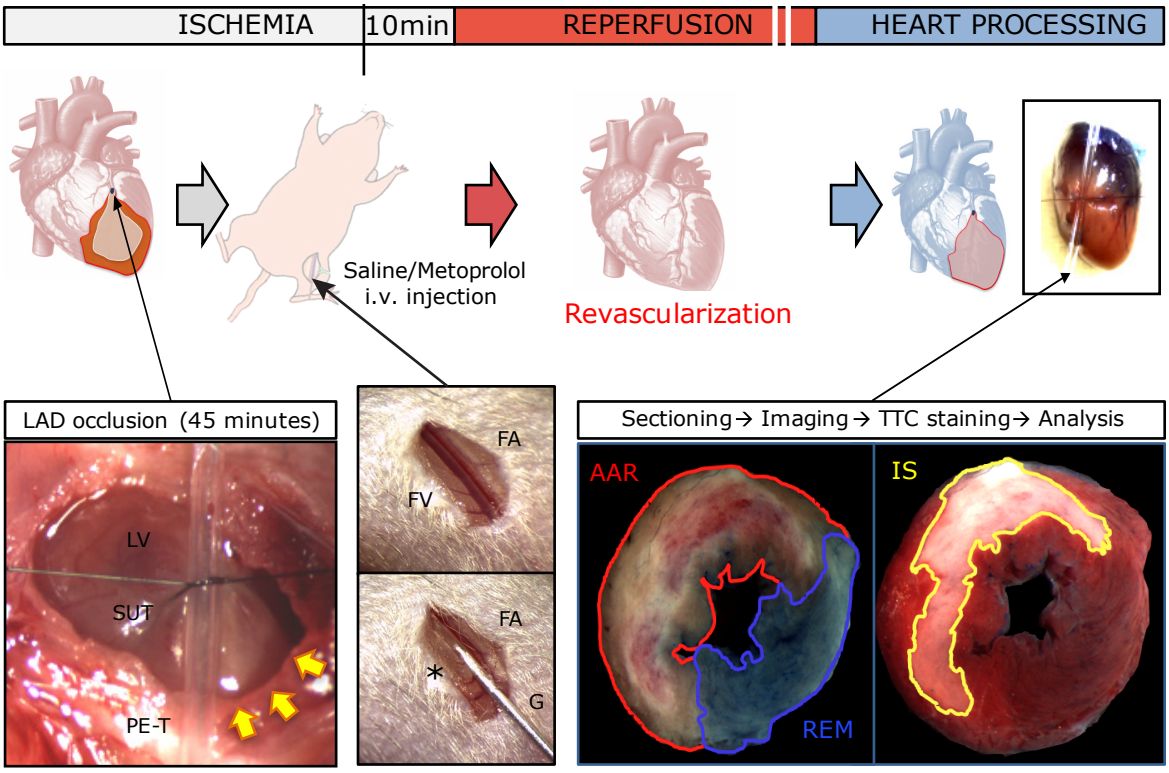

Figure 5. Mouse model of IR injury
Myocardial left ventricle (LV) regional ischemia is induced after stretching a simple knot of a ligature passed under the left anterior descending artery (LAD). A 2-cm piece of PE-tube (PE-T) is placed between the ligature and the myocardium to avoid heart sectioning and facilitate reperfusion when appropriate. Ten minutes before the onset of reperfusion 50 µL of metoprolol or saline is injected through the femoral vein with an insulin gauge. After 45 minutes of ischemia blood flow is re-established. At the end of reperfusion (6 or 24 hours) ligature is re-streched and coronary artery re-occluded. Heart is then perfused with Evans blue (EB) and processed. Short-axis sections are then stained, weighted, incubated in triphenyl-tetrazolium chloride (TTC) and imaged for following analysis. Red line delineates myocardium at risk (area at risk, AAR), determined as the myocardium negative to EB-perfusion (i.e. lack of blood flow or ischemic). Blue line delineates remote myocardium (REM, positive-EB perfused tissue). Yellow line delineates infarcted area, determined after TTC incubation as the myocardium negative to TTC staining (white area; i.e. dead myocardium). SUT, stands for suture; Yellow arrows indicate ischemic area; FA, stands for femoral artery; FV, stands for femoral vein; G, stands for insulin gauge.

Animals were then sacrificed and rapidly 1 mL of 1% (w per v) Evans Blue dye was infused i.v. to delineate AAR: myocardium lacking blood flow, i.e. negative for blue dye staining). The heart was then harvested, LV isolated, cut into transverse slices (5-7 1-mm thick slices per LV) and both sides imaged. Sections post-Evans blue staining present two different areas: one pale, negative for Evans blue perfusion, delineating AAR, and another blue, positive Evans blue, indicating remote tissue (**Fig. 5**). In order to differentiate infarcted from viable tissue, same slices were incubated in triphenyl-tetrazolium chloride (TTC, 1 % (w per v) diluted in PBS) at 37ºC for 15 minutes in constant shacking. The slices were then re-photographed and weighed. Post TTC incubation, Evans blue staining clears out and slices present two areas: one necrotic (pale negative to TTC staining) and one reddish alive (positive to TTC staining). Regions negative for Evans Blue staining (AAR) and for TTC (infarcted myocardium) were quantified using ImageJ (NIH, Bethesda, MD) by blinded observer (**Fig. 5**). Percentage values for AAR and infarcted myocardium were corrected to mg independently for each slice. Absolute AAR and infarct size were determined as the mg:mg ratio of AAR:LV and infarcted myocardium: AAR, respectively. Animals exceeding 80% of IS were excluded assuming absence of reperfusion.

Hearts processing for histology

At the end of reperfusion, LysM-GFP mice were re-anesthetized, placed in a supine position, their ventral thoracic regions wiped with 70% alcohol, and euthanized by cervical dislocation. Next, 10 mL of PBS with heparin (50 U per mL) was gently infused through the vena cava to avoid blood clots. Hearts were then removed and cut into 1-mm-thick transverse sections and fixed with 2% PFA in PBS for 24 hours at 4 ºC. Heart slices (1 mm) designated to histopathological analysis of capillary obliteration were dehydrated through an ethanol series, cleared in xylene, embedded in paraffin wax and consequently sectioned (4 µm) for staining with haematoxylin and eosin (H/E). All immunohistochemical procedures were performed with an automated autostainer (Autostainer Plus®, Dako) at the CNIC Histology Unit. Images

were digitally scanned (Nanozoomer-RS C110730®, Hamamatsu) and examined with image analysis software (Tissuemorph®, Visiopharm) by blinded observers. Once the lesion was identified, 10 to 12 images (20x) were taken at random, and capillary obliteration was scored from 0 to 2, with 0 indicating the absence of capillary obliteration and 2 indicating presence of obstruction in all capillaries.

Confocal microscopy

Sections designated for immunofluorescence staining and confocal microscopy were post-fixed overnight and placed in 30% sucrose for 24 hours and included in O.C.T. (Tissue-Tek®). Serial 4 µm coronal sections were cut on a freezing microtome (Leica CM1950) and stored in cryoprotective solution. Sections designated for evaluation of neutrophil infiltration of the injured area were washed in PBS for 15 minutes and incubated with DAPI (1:1000) at room temperature for 5 minutes, washed in PBS twice and mounted in Mowiol mounting medium. Images of full short-axis heart sections were acquired with an inverted confocal laser imaging system (Zeiss LSM7004 4-Laser) and reconstructed with Zeiss ZEN reprocessing software. Presence of Lysm-GFP+ cells analysis was performed with ImageJ (NIH, Bethesda, USA) by blinded observers. Values of total GFP+ surface were normalized to LV section surface. A second set of sections were stained with Dylight-650-conjugated anti-1A8 Ly6G and DAPI for quantification of specific neutrophil identification and temporal infiltration analysis. Eight independent 40x were evaluated from injured myocardium from each animal, and presence of myeloid derived cells (LysM+), neutrophils (*LysM*+*Ly6G*+) and monocytes (*LysM*+*Ly6G*neg) were identified and analysed using ImageJ by blinded observers. 4 animals were stained for basal quantification. Some sections were stained with anti-laminin to stain cell membranes (1:150) and anti-α-actinin to visualize sarcomeres in cardiac fibers (1:200) for detailed illustration of neutrophil infiltration in the injured myocardium. Images were post-processed and edited using the Imaris software (Bitplane AG, Switzerland) as indicated below.

Neutrophil-platelet interactions staining in infarcted mouse heart was adapted from Sreeramkumar et al. (35). Briefly, OCT-embedded heart slices were cut into 50 µm sections, washed in PBS for 15 minutes and incubated for 20 minutes at room temperature in blocking buffer (PBS containing 10% BSA and 2% goat serum). For detailed visualization and characterization of the injured zone, cell membranes were stained with anti-laminin (1:150) and platelets were stained with PE-conjugated anti-*CD41* (1:200). Primary and secondary antibodies were diluted 1:200 in blocking buffer, and incubations were conducted for 1 hour at room temperature. Nonspecific staining was assessed by omission of primary antibody. Samples were counterstained with DAPI and mounted in Mowiol. Images were acquired with a laser-scanning confocal imaging system (Leica SP8 or SP5) at the CNIC Microscopy Unit and post-processed with Leica Las AF and Imaris software (Bitplane AG, Switzerland). Independent vessels (7-9) were evaluated for each animal, and intravascular neutrophil and neutrophil-platelet interactions were scored manually.

Neutrophil purification and *Adrb1* expression

Adrb1 expression in circulating neutrophils was examined in blood drawn from wild-type or *Adrb1*KO mice 20 minute safter injection of heparin (50µL of 50U per mL). Whole blood was filtered and pooled, and polymorphonuclear leukocytes were purified by gradient-centrifugation (800xg, 20 min, 4 ºC) in 65% Percoll Plus in Hanks balanced salt solution (HBSS). Cells were washed in PBS and residual erythrocytes were lysed using hypotonic buffer. Neutrophils were washed and re-suspended in HBSS. Before RNA isolation, neutrophil identity was confirmed by flow cytometry (anti-1A8 Ly6G) and viability evaluated.

Total RNA from whole hearts, BM, and purified neutrophils samples was isolated with the Qiagen RNeasy Plus Mini Kit. RNA (1-2 µg) was reverse transcribed using Ready-to–go RT-PCR Beads (27-9259-01, GE Healthcare). PCR was performed with 40 cycles of 95°C for 12s and 60°C for 1 min. All PCR reactions were done in triplicate. Primers for Hprt and *Adrb1* were as follows: mHprt_fw:5'-GAGGAGTCCTGTTGATGTTGCCAG-3'; mHprt_rv:5'-

GGCTGGCCTATAGGCTCATAGTGC-3'; m*Adrb1*_fw:5'-GTGGGTAACGTGCTGGTGAT-3', m*Adrb1*_rv:5'-GAAGTCCAGAGCTCGCAGAA-3'. Amplicons generated in the qPCR were loaded on to an agarose gel to confirm single PCR products.

Migration transwell assay

The ability of leukocytes to migrate toward chemokine (C-X-C motif) ligand 1 (CXCL1) was assessed using a modification of the method of Villablanca et al. (90) Briefly, wild-type or *Adrb1*KO mice were heparinized (50 µL of 50 U per mL, IP) and 20 minutes later blood was collected and filtered, and residual erythrocytes were lysed with hypotonic buffer. PBS-washed leukocytes of the same genotype were pooled and resuspended in RPMI containing 10% FBS and the appropriate treatment: saline (vehicle control), 10 µM epinephrine (positive control), 10 µM metoprolol-tartrate, or a combination of epinephrine and metoprolol. Transwell inserts (6.5 mm, 5.0 µm pore size (3421; Corning Costar Corporation) were pretreated with 50 µL RPMI for 20 minutes and placed in 24-well-plates before seeding cells (100 µL; ~1 × 10^5; >90% viability). Lower compartments (wells) were filled with 600 µL DMEM medium containing 0.04 ng per µL CXCL1 to induce directional movement. Spontaneous migration was assessed in wells lacking CXCL1. After incubation at 37 °C for 1.5 h, cells in the lower compartment were collected and neutrophils (Ly6G+ cells) were evaluated by flow cytometry. Each independent experiment was conducted with leukocytes pooled from 9 animals, and each of the 5 conditions was run with 4 replicates. Mean spontaneous migration was subtracted from the migration value of each well, and neutrophil migration was expressed as a percentage of the total number of neutrophils seeded in the upper chamber at the start of the experiment. For comparison between experiments and genotypes, migration was normalized to the mean control (vehicle) value.

Neutrophil oxidative burst assay

Blood from wild-type or *Adrb1*KO mice was collected in heparinized tubes and distributed in 100 µL aliquots, erythrocytes were lysed with hypotonic buffer. After centrifugation leucocytes were first washed and then re-suspended in high glucose phenol red free DMEM. Cells were then incubated for 50 minuteswith or without metoprolol-tartrate 100 µM at 37ºC. As previously described (91) (92), Dihydrorhodamine 123 (DHR 123, 1 µM), which converts to the fluorescent product rhodamine 123 (Rho 123) upon oxidation was then added to the medium and cells were stimulated with the *chemotactic FPR activator-peptide,* w-peptide 1µM (WKYMVM, 1799 Tocris). After 20 minutesincubation at 37 ºC the reaction was stopped in ice and cells were washed in cold HBSS containing DAPI 0.1 µg per mL (D8417, Sigma). Mean fluorescent intensity (MFI) for Rho 123 was evaluated for neutrophils (*Ly6G*+ cells) alive (DAPIneg) by flow cytometry.

Model of thioglycolate-induced peritonitis

To assess the ability of metoprolol to inhibit neutrophil recruitment, we used a well-established thioglycolate-induced peritonitis model. Wild-type mice were intraperitoneally injected with 1 mL of thioglycolate and immediately randomized to receive a single 50 µL i.v. injection of vehicle or metoprolol-tartrate (10 mM). Sixteen hours later, 100µL of blood from each animal was collected into EDTA tubes for later haematological analysis in a haemocytometer (Pentra 80). Next, animals were sacrificed, 2 mL PBS was injected intraperitoneally and distributed manually for 30 seconds to detach infiltrated circulatory cells. Next, another 8 mL PBS was injected to facilitate collection of 6 mL peritoneal exudate. Exudates were gently centrifuged, and cells were washed twice with PBS and incubated for 1 hour with anti-GR1 (1:200) and PE-conjugated anti-CD115 (1:200). After washing with PBS, cells were incubated for 30 minutes with anti-rat 647 to detect GR1. Cell nuclei were stained with DAPI. All samples were analysed by flow cytometry for exactly 30 seconds of constant flow. Neutrophil recruitment efficiencies are presented as neutrophils per mL of exudate for each independent animal.

To evaluate the role of ADRB1 in different compartments, we performed the same experiments in *Adrb1*KO mice and generated cohorts of chimeric mice by transplantation with BM cells from wildtype and *Adrb1*KO donors. Four weeks after BM transplantation, chimerism was evaluated by flow cytometry as the % of donated cells. Animals with chimerism below 85% were discarded; those with chimerism above 85% underwent the thioglycolate-induced peritonitis protocol followed by randomization to receive either i.v. vehicle or metoprolol (10 mM). To compare between the different chimeric groups, the mean value for each metoprolol-treated group was normalized to the mean for the vehicle-treated group.

Bone marrow transplant

BM transplants protocols were adapted from Casanova et al. (88) Recipient mice from *Adrb1*KO or wild-type genotypes (DsRed+ or DsRed- as appropriate) were lethally irradiated (13Gy in 2 doses) before reconstitution with donor BM. Donor BM was harvested from mice of the appropriate genotype by flushing both tibiae and femurs into PBS containing 2 mM EDTA (PEB buffer). Contaminating erythrocytes were lysed with hypotonic buffer. Engraftment in recipient animals was assessed by flow cytometry 3-4 weeks after transplantation. Animals bled for engraftment evaluations were rested for one week before any other procedure.

Flow cytometry

Neutrophil purity for in vitro migration assay and *Adrb1* expression analysis was evaluated by incubating cells with Dylight-650-conjugated anti-1A8 *Ly6G* and with DAPI to assess viability. Mouse primary blood leukocytes from peritonitis experiments were incubated with anti-Gr1 conjugated with AF-647 and with PE-conjugated anti-CD115 and DAPI. Neutrophils were gated on the basis of Gr1-positive and CD115-negative staining in a FACS Canto-3L flow cytometer equipped with DIVA software (BD Biosciences). Doublet discrimination and viability (negative to DAPI) was assessed for every sample.

Data were analysed with FlowJo (Ashland) software by blinded observer. All experiments were conducted at the CNIC-Cellomics Unit.

Intravital microscopy

Intravital microscopy (IVM) of the cremaster muscle was performed after intrascrotal injection of TNFα (0.5 mg R&D Systems) (35), followed immediately by injection of a single i.v. bolus of metoprolol (10mM) or vehicle, and neutrophil behaviour was evaluated 3 hours after stimulus. In some experiments metoprolol was injected 3 h after treatment with TNFα and images immediately acquired for analysis. The IVM system was built by 3i (Intelligent Imaging Innovations, Denver, CO) on an Axio Examiner Z.1 workstation (Zeiss, Oberkochen, Germany) mounted on a 3-Dimensional Motorized Stage (Sutter Instrument, Novato, CA). This set up allows precise computer-controlled lateral movement between XY positions and a Z focusing drive for confocal acquisition. The microscope is equipped with a CoolLED pE widefield fluorescence LED light source system (CoolLED Ltd. UK) and a quad pass filter cube with a Semrock Di01-R405/488/561/635 dichroic and a FF01-446/523/600/677 emitter. We used a plan-Apochromat 40x W NA1.0 ∞/0 objective (Zeiss). Images were collected with a CoolSnap HQ2 camera (6.45 x 6.45-µm pixels, 1392 x 1040pixel format; Photometrics, Tucson, AZ). For confocal high-speed IVM, we used laser stacks for 488, 561 and 640nm beams coupled with a confocal scanner (Yokogawa CSUX-A1; Yokogawa, Japan); images were acquired at 0.5 µm Z-intervals. Image acquisition was coordinated and offline data analysis facilitated with SlideBook software (Intelligent Imaging Innovations), run on a Dell Precision T7500 computer (Dell Inc., Round Rock, TX. For 3-dimensional analysis we used the 3D surface view function to determine the position of the *CD62L*+ clusters relative to the cell body and the lumen. Six to ten venules per mouse were analysed 210 to 300 minutes after TNFα treatment by acquisition of fluorescence (Cy3/561 channels for phycoerythirn, FITC/488 channels for FITC, and Cy5/640 channels for allophycocianin) and bright-field images with 2×2 for 2 min. For double staining with PE- and FITC-conjugated antibodies, acquisition was

facilitated in single (FITC) and quad (PE) filters in order to avoid bleed-through of fluorescent signals between channels. For in vivo labeling of neutrophils and platelets surface molecules, fluorescently labeled antibodies were injected intravenously (anti-*CD62L*-FITC, anti-*Ly6G*-APC, and anti-*CD41*-PE; 0.5-1.25 µg per mouse). Images were post-processed and edited using the Imaris software (Bitplane AG, Switzerland) as indicated below.

Analysis of blood cell interactions

Platelets in the inflamed cremaster muscle were visualized as CD41-labelled cells and quantified as reported (35). Briefly, we defined the uropod of adherent neutrophils as the domain staining positive for CD62L, and the leading edge as the CD62L-negative pole forming multiple protrusions and showing guided movement. Six to ten venules per mouse were recorded, and platelet interactions with neutrophils were counted and analysed manually at the two distinct domains of the polarized neutrophil with the help of Slidebook software.

Analysis of tracking of crawling neutrophils

Time-lapse movies of crawling neutrophils were analysed with ImageJ, which includes the Manual Tracking and the Chemotaxis and Migration Tool plugins. For each movie, we first adjusted channel intensities and converted them into RGB format. Movies were rotated so that the vessels and the blood flow were positioned horizontally and oriented left-right. When necessary, the Background subtraction and Image stabilization pre-stablished plugins were applied to eliminate noise and reduce tissue twitching, respectively. Both plugins were set up with xy calibration values, which depend on the camera and microscope parameters, to convert pixels into linear measures, as well as the time interval value between movie frames (3s). Each polarized neutrophil (identified by a clear polarized morphology or uropod staining) was tracked manually for 1 minute using the Manual Tracking Plugin, which generated a dataset with the respective xy track coordinates. We then used the

Chemotaxis and Migration Tool to plot and the velocity (μm per s), accumulated distance (μm), euclidean distance (μm), and directionality of the tracks obtained. The euclidean distance is the length of the straight-line segment connecting the initial and finishing points, whereas the accumulated distance is the total length of the path covered by the cell. Directionality measures how straight the cell track is, and is calculated as the ratio of euclidean distance to accumulated distance.

Analysis of 3D reconstructions of polarized neutrophils

We measured the 3D features of intravascular neutrophils using Imaris Software (Bitplane, Oxford). From the parameters provided by the ImarisCell module, we selected prolate ellipticity by obtaining the lengths of the 3 semi-axes, which correspond with the Ellipsoid axis parameters. A prolate ellipsoid (cigar-like shape) is one for which the polar radius is greater than the equatorial radius. For 3D cell reconstructions, we used the ImarisCell module to define the cell body. We then segmented a region of interest to enclose an individual cell within this region, so that the subsequent reconstruction fitted the real cell structure. Afterwards, the respective source channel from which the cells had to be computed was selected. For reconstruction analysis, we chose the *Ly6G*-APC channel as it is a membrane-bound protein that yields a strong signal and allows a good rendering of the actual cell morphology. ImarisCell module determines the cell threshold by calculating voxel (3D pixel) intensities from the enclosed cell and comparing them with the background intensity in the enclosed sub-region. To obtain the height-to-length ratios, we visually established the cell orientation with respect to the vessel wall surface. Sections of each polarized neutrophil were analysed to manually measure the height of the cell and maximum length (from the top view) with respect to the vessel wall. For this purpose, we used Imaris Section View, which shows the coordinates in the 3 display areas (xy top view, zy lateral view, and xz front view), and the Extended Crosshairs of the Section View, which in turn allows selection of the z-stack planes to visualize the entire cell (not just one plane or section) in the 3 views. A snapshot of these 3 views from a single cell was

taken and imported into ImageJ, where height and maximum length were measured from the different views after setting the capture scale.

Human blood sampling

Functional tests were performed in blood samples from 20 volunteers (36±6 years, 15 men). Exclusion criteria were as follows: any antiplatelet, anticoagulant or anti-inflammatory drug taken within the 2 previous weeks; abnormal platelet or leukocyte count; or any history of abnormal bleeding, thrombosis, or active inflammatory disease. Written consent was obtained from all volunteers. Blood samples were collected into polypropylene tubes containing sodium citrate from an antecubital vein with a 21-gauge needle, discarding the first 2 mL to avoid platelet activation. Blood was collected between 8:00-10:00 a.m. after overnight fasting. Samples were processed immediately. Acute coronary syndrome (ACS) patients were recruited at our cathlab (both genders, age <80) from among those referred for coronary angiogram and subsequent percutaneous coronary intervention (PCI). Exclusion criteria were as follows: active treatment with β-blockers; any situation which might make it imprudent to administer an i.v. β-blocker; asthma or chronic obstructive lung disease; bradycardio (HR<55bpm); heart failure or valvular heart disease; atrial fibrillation requiring antiarrhythmic therapy; renal failure with creatinine ≥2 mg per mL; liver disease with bilirubin ≥2 mg per mL; acute illness of any malignancy; pregnancy or nursing; body mass index ≥27 kg per m^2; previous severe adverse reaction to β-blockers; concomitant use of other antithrombotic drugs such as anticoagulants, dypiridamol, ticlopidine, or cilostazol; treatment before the intervention with GP IIb/IIIa inhibitors, or need for nonsteroidal anti-inflammatory drugs. Written informed consent was obtained from all patients enrolled. Blood samples were collected from a femoral artery catheter into polypropylene tubes containing sodium citrate, discarding the first 2 mL. Samples were processed immediately.

Human neutrophil-platelet interactions evaluation

Human citrated blood was diluted 1:5 in HEPES-Tyrode´s* (5mM hydroxyethylpiperazineethane-sulfonic acid (HEPES), 137 mM NaCl, 2.7 mM $NaHCO_3$, 0.36mM NaH_2PO_4, 2 mM NaH_2PO_4, 2 mM $CaCl_2$, 5 mM glucose, bovine albumin 0.2%. pH=7.4) and incubated with 0, 2, or 5 μM metoprolol for 10 minutes. Then, 5 mL of diluted blood was incubated with 5 μM epinephrine for 10 minutes. Unstimulated and epinephrine-stimulated samples were stained with PC5-conjugated anti-*CD14* anti *CD45*–FITC and anti-*CD61* PC7 for 20 minutes at room temperature in the dark. Erythrocytes were lysed for 10 minutes using Versalyse solution. Appropriate mouse isotype controls were used for each antibody. Flow cytometry analysis was performed with a Gallios cytometer (Beckman Coulter, Miami, Florida). Leukocytes were by *CD45*-FITC staining. Neutrophils identification was adapted from (93) (94) and performed by morphological parameters (side scatter) and negative staining for *CD14*-PC5 but positive staining for *CD45*-FITC. Neutrophil-platelet conjugates were identified as bivariate histogram particles negative for *CD14*-PC5 and positive to *CD61*-PC7 (95) (96). The acquisition process was stopped after collection of 5000 monocytes. Data are expressed as the percentage of neutrophil-platelet aggregates. All experiments were conducted at the Hospital Universitario Clínico San Carlos, Madrid.

Human platelet aggregation assay

Platelet aggregation was assessed using light transmittance aggregometry (LTA) in platelet-rich plasma by the turbidimetric method in a four-channel aggregometer (Chrono-Log 490 Model, Chrono-Log Corp., Havertown, Pennsylvania) according to standard protocols. The platelet-rich plasma (PRP) was obtained from citrated blood at centrifuge (800 rpm) for 10 minutes and platelet-poor plasma (PPP) was obtained after a second centrifugation (2500 rpm) for 10 min. PRP will be adjusted to 250.000 per μL with autologous plasma. PRP was incubated with metoprolol 2 and 5 μM or saline buffer for 15 minutes and then stimulated using epinephrine (5 μM). Light transmission was adjusted to 0% with PRP and to 100% with PPP for each measurement. Curves

were recorded during 5 minutes. and platelet aggregation was determined as the maximal percent change in light transmittance.

Human platelet function evaluation

Platelet function was determined by assessing platelet activation as surface expression of activated GP IIb/IIIa (Becton Dickinson) and P-Selectin using flow cytometry. Whole blood from healthy donors were drawn into trisodium citrate tubes diluted with Hepes–tyrodes-buffer (0.2% BSA) to a final volume of 1:8:1 (blood: Hepes–tyrodes:citrate). Diluted blood was incubated with metoprolol 2 μM and 5 μM or saline for 15 minutes. Following activation with epinephrine (5 μM) samples were incubated for 20 minutes with polyclonal *PAC1*-FITC conjugated or PE-conjugated anti-*CD62P*. Appropriate isotype controls were used in each case. Platelet activation was expressed as the percentage of platelets positive for antibody binding. Platelets were gated on the basis of light scatter and *CD61* antibody expression. Activated platelets were defined as the percentage of expressing the activated confirmation of *PAC1* binding and P-selectin (*CD62P*). Data were expressed as the percentage of platelets positive for antibody binding. All experiments were conducted at the Hospital Universitario Clínico San Carlos, Madrid.

Statistics

Data are represented as mean ± standard error of the mean (s.e.m.), and analysed using Prism software (Graph pad, Inc.) and Stata (Stata 12.0; StataCorp LP, College Station, TX). Comparisons between two groups were performed by using the unpaired two-tailed Student´s t-test or the nonparametric Wilcoxon-Mann–Whitney test as appropriate. Comparisons between more than two groups were performed by using the one-way ANOVA. The P-value was adjusted with the Holm Sidak's multiple comparison test. Multiple linear regression analysis was used to study the influence of metoprolol on microvascular obstruction, adjusted for factors potentially affecting MVO such as sex, age, ischemia duration, diabetes, use of

thrombectomy or glycoprotein IIb/IIIa inhibitors. Test for linear trend after one-way ANOVA was used to study the relationship between LVEF at 6 months and MVO quartiles at one week. Power calculations were applied to obtain statistically significant at P-values below 0.05 significant. * $p<0.05$, ** $p<0.01$, *** $p<0.001$.

Study approval

All studies in patients and volunteers were approved by the ethics committee of Hospital Clínico San Carlos, Madrid. Written informed consent was received from all participants prior to inclusion in the study.

Results

I.v. metoprolol reduces MVO in AMI patients

The METOCARD-CNIC trial recruited patients with an ongoing acute ST-segment elevation AMI and randomized them to receive i.v. metoprolol or control before reperfusion (97). A total of 220 AMI patients underwent a CMR imaging exam 1 week after AMI to study the potential mechanisms underlying the infarct-limiting effect of metoprolol (82). MVO was defined as the absence of contrast wash-in inside the delayed gadolinium-enhanced area (43), and was quantified as grams of LV (**Fig. 6**). Patients treated with metoprolol during ongoing AMI had a 40% lower extent of MVO (**Fig. 7a**). This significant effect was maintained after adjusting for factors potentially affecting MVO by performing linear multiple regression analysis and including sex, age, ischemia duration, diabetes, and use of thrombectomy or glycoprotein IIb/IIIa inhibitors as covariates. To exclude the possibility that this effect simply reflected the reduction in total infarct size (82), MVO was further assessed as a percentage of the infarcted area (total late gadolinium enhanced area). Metoprolol-treated patients had 24% less infarct-normalized MVO than control patients (**Fig. 7b**). As expected, the extent of MVO was significantly associated with poor long-term outcome, evaluated as chronic ventricular performance (**Fig. 7c**). These data suggest that MVO reduction might be involved in the cardioprotective effect of metoprolol administration in patients during ongoing AMI.

Figure 6. Microvascular obstruction evaluation in patients
(a) METOCARD-CNIC trial scheme: patients with ongoing ST-segment elevation acute myocardial infarction (STEMI) were recruited and randomized to receive metoprolol (15mg i.v. doses) or control before reperfusion. A total of 220 patients were evaluated for microvascular obstruction (MVO) by cardiac magnetic resonance (CMR) imaging one week after AMI and 202 patients for an additional CMR at long-term left ventricle ejection fraction (LVEF) 6 months after AMI for ventricular function assessment. **(b)** Complete CMR exams (short-axis covering the entire LV from base to apex). **c)** Representative CMR images, showing significant differences in one-week MVO between a control patient (left) and a metoprolol-treated patient (right). Lower panels show detailed views of the boxed images, revealing MVO (blue area, automatic quantification), defined as the absence of contrast wash-in inside the delayed gadolinium-enhanced area (red, semiautomatic quantification). Yellow arrowheads indicate MVO in the LV wall.

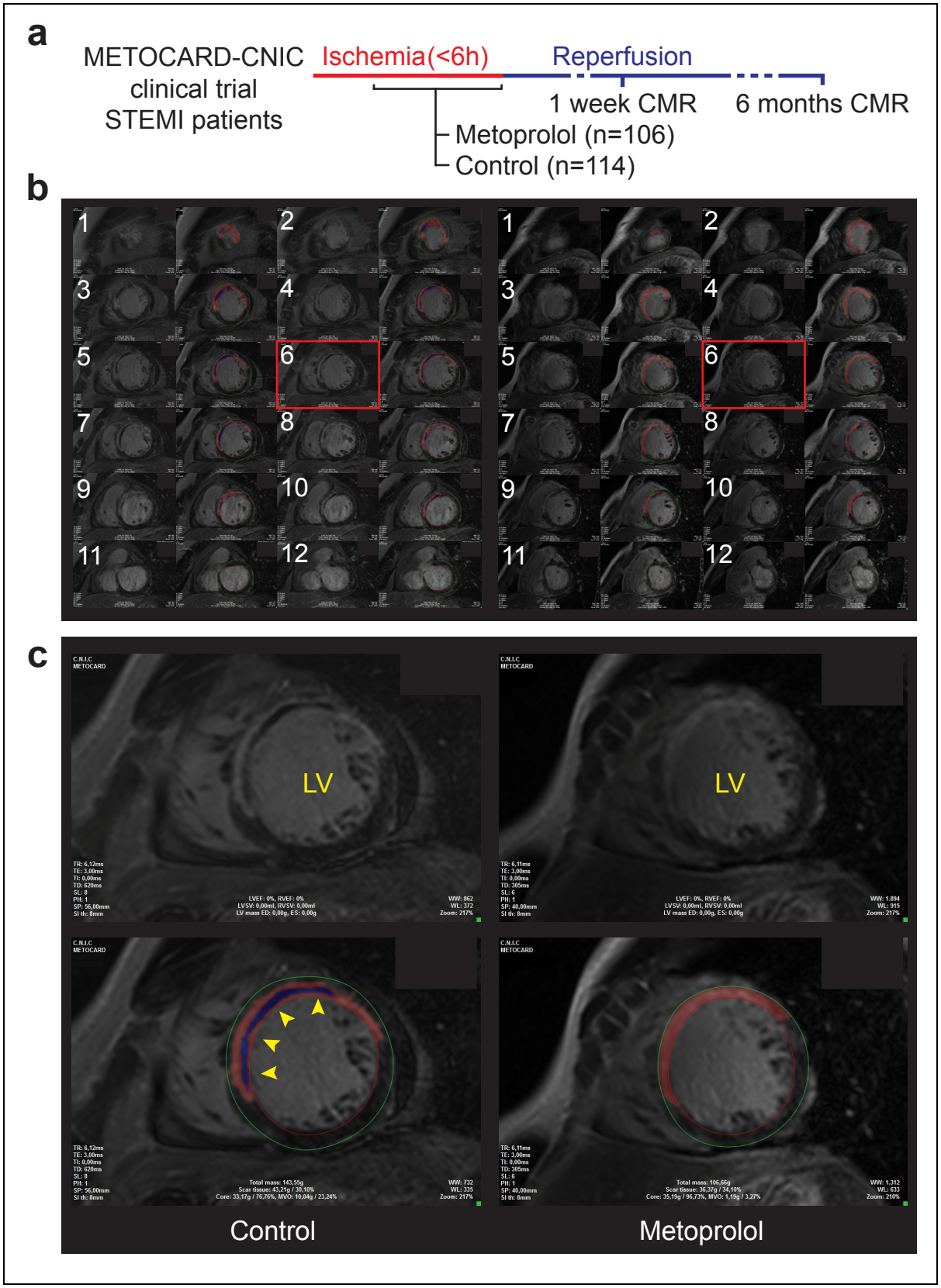
a
METOCARD-CNIC
clinical trial
STEMI patients
Ischemia(<6h)
Reperfusion
1 week CMR
6 months CMR
Metoprolol (n=106)
Control (n=114)
b
1
2
3
4
5
6
7
8
9
10
11
12
c
LV
LV
Control
Metoprolol

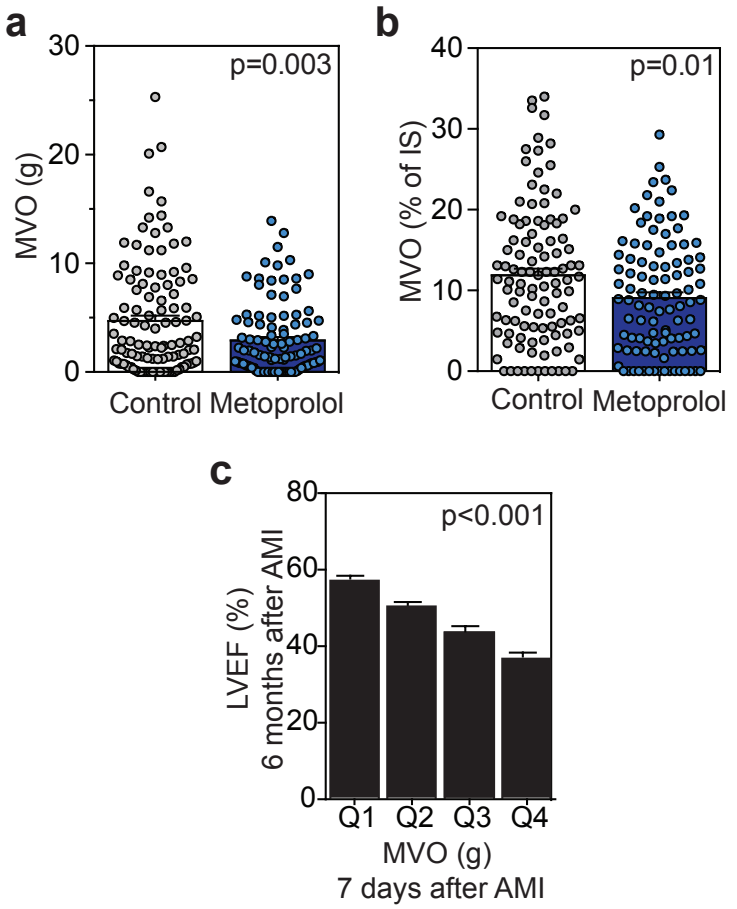

Figure 7. Early metoprolol reduces MVO in patients
(a) Quantification of microvascular obstruction (MVO) in grams of left ventricle. **(b)** Quantification of MVO relative to the infarcted area (%). Dots represent values for individual patients: 114 in the control group (gray) vs 106 in the metoprolol group (blue). P-value for linear trend is shown. **(c)** Long-term left ventricular ejection fraction (LVEF) evaluated by CMR 6 months after AMI (n=202) according to quartiles of MVO extent evaluated as in panel a. Cardiac function was significantly smaller in patients with larger extent of MVO. P-value for linear trend is shown. Data are means ± s.e.m compared by unpaired Student's *t*-test.

Intravenous metoprolol dampens neutrophilial–MVO association in patients

White blood cell (WBC) and neutrophil counts during an AMI are known to be associated with larger infarct sizes and extensive MVO (98) (99) (100). We

explored these associations in AMI patients from the METOCARD-CNIC trial. We found a significant positive correlation between absolute leukocyte count on admission and the extent of MVO on CMR: the higher the leukocyte count, the larger the extent of MVO (**Fig. 8a**). We further studied the association of the different WBC subpopulations and MVO. As expected, neutrophil count was significantly correlated with the extent of MVO (**Fig. 8b**). Conversely, there was no sign of association between other WBC subpopulations and MVO: lymphocyte, monocyte, eosinophil or platelet counts did not correlate with the extent of MVO (**Fig. 8e**). Next, we studied the effect of metoprolol on WBCs and on the association between these and MVO. Metoprolol treatment was not associated with any different in WBC count nor in any WBC subpopulation (**Table 1**). Of note, we found a significant interaction between metoprolol treatment and the correlation between leukocyte count and MVO: the significant positive correlation between neutrophil count and the extent of MVO was only present in control patients (that is, not receiving metoprolol); in patients receiving IV metoprolol before reperfusion there was no sign of association between total leukocyte or neutrophil counts and the extent of MVO (**Fig. 8c and 8d**). These results suggest that the administration of i.v. metoprolol during ongoing AMI do not affect the circulating levels of WBCs but modulates the impact of neutrophils on MVO.

Population	Control Median (IQR)	Metoprolol Median (IQR)	P-value
Leukocyte ($x10^3$)	12.3 (10.3 – 14.7)	11.9 (9.3 – 13.7)	0.183
Neutrophil ($x10^3$)	9.5 (7.7 – 12.4)	9.1 (6.4- 11.3)	0.098
Lymphocyte (Abs)	1574 (1171 - 2509)	1754 (1265 - 2344)	0.164
Monocyte (Abs)	629 (482 - 837)	632 (504 - 851)	0.5
Eosinophil (Abs)	56 (27 - 162)	78 (35 - 168)	0.156
Platelet ($x10^5$)	224.5 (194.5 - 259)	218 (186 – 283.5)	0.753

Table 1. White blood cell counts from METOCARD-CNIC patients
Treatment comparison of leukocyte and subpopulations (neutrophil, lymphocyte, monocyte, eosinophil and platelet) count on admission in METOCARD-CNIC trial patients. Abs, stands for absolute count. IQR, stands for Interquartile range.

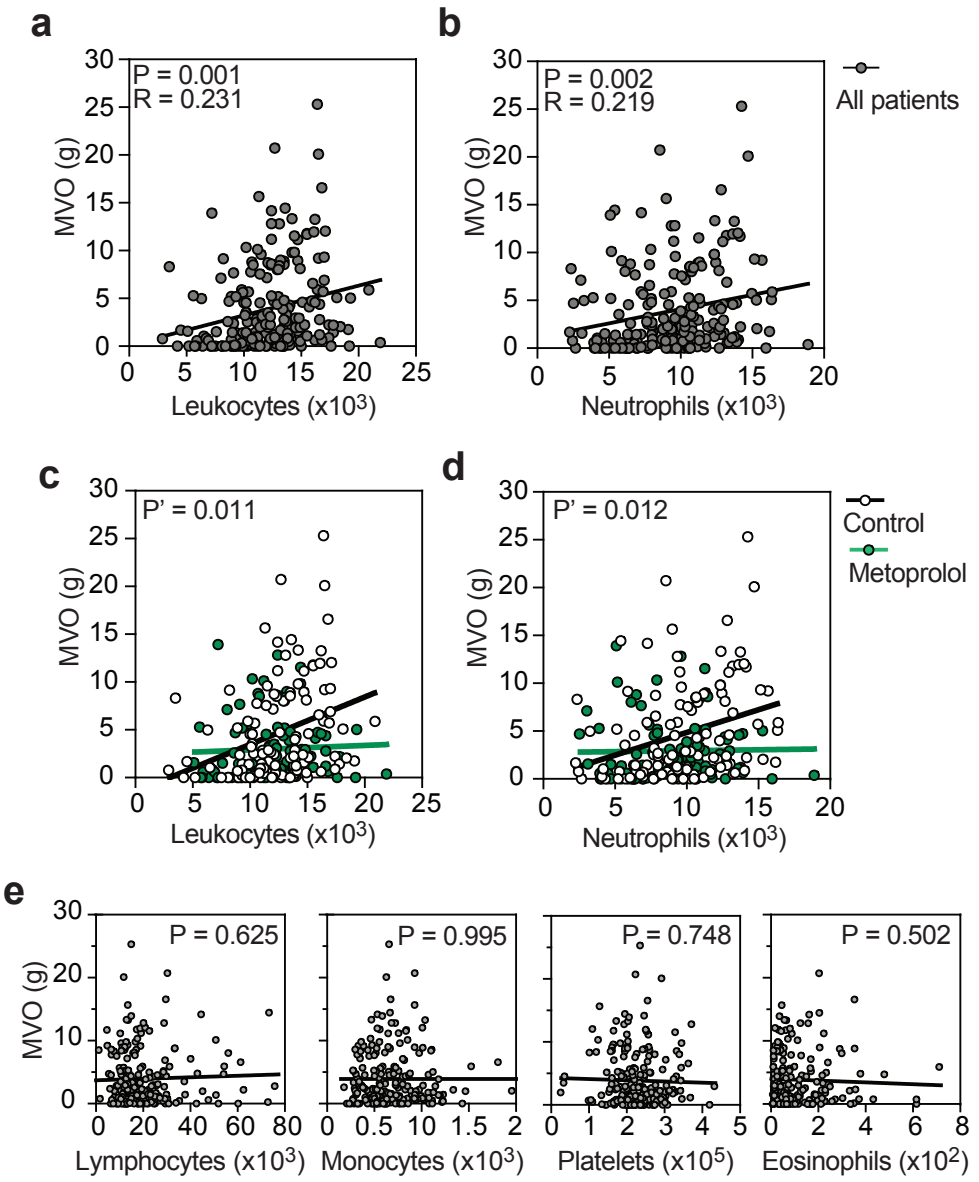

Figure 8. Metoprolol alters neutrophil counts - MVO association in patients

Sensitivity analysis of the association between MVO and leukocyte and subpopulations count on admission from METOCARD-CNIC trial patients. **(a,b)** Association between MVO and absolute leukocyte or neutrophil count on admission. Grey dots represent individual values and line linear relationship. **(c,d)** Linear regression comparison between MVO and leukocytes and neutrophils in the subsets of METOCARD-CNIC patients indicating loss of correlation in the metoprolol treated group (green) as compared to control group (white). P', stands for interaction P-value. **(e)** Association between MVO and rest of white blood cells subpopulations: Platelets, lymphocytes, eosinophils and monocytes showing no correlation in the extent of MVO. P stands for P-value and R, for Pearson's correlation coefficient.

Metoprolol blunts neutrophil infiltration and capillary obliteration

To identify the factors underlying the metoprolol-induced myocardial MVO reduction, we used the mouse model of in vivo myocardial IR injury (see **Fig. 5**). Given to the metoprolol's alteration of the association between neutrophil count and MVO observed in METOCARD-CNIC patients, we focused our attention into myeloid-derived cell population as main inflammatory players during in early phases of IR injury. First, we tested the infarct-limiting effect of metoprolol in wild-type mice. Mice were randomized to receive a single i.v. bolus (50 µL) of metoprolol (10 mM) or vehicle (saline) 35 minutes after ischemia onset (10 minutes before reperfusion) (**Fig. 9a**). Infarct size was evaluated at 24 hours reperfusion by TTC staining and normalized to area at risk (AAR, negative EB staining)**.** Metoprolol-treated mice had significantly smaller infarcts (% of AAR) than vehicle-treated mice (**Fig. 9b, 9c**).

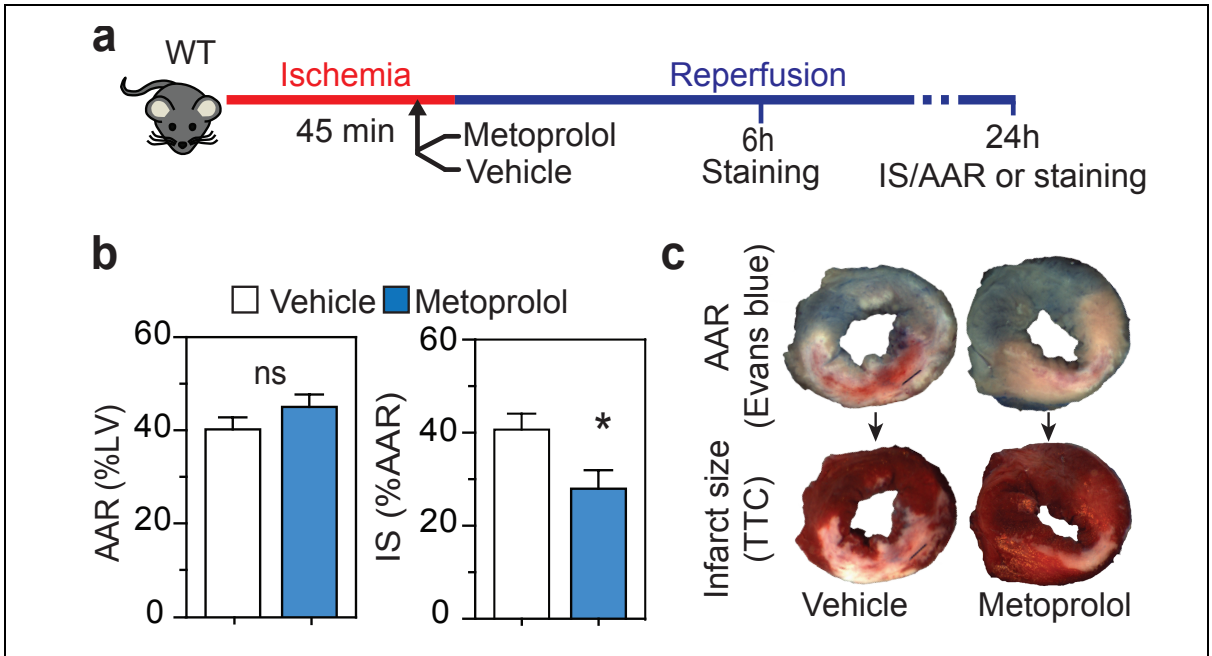

Figure 9. Metoprolol reduces infarct size in mouse
(a) Mouse model of myocardial IR. **(b)** Histological evaluation of left ventricle (LV) area at risk (AAR) and infarct size (IS) in mice subjected to IR and randomized to receive metoprolol (blue) or vehicle (white); NS stands for non-significant. n=8. **(c)** Representative images of LV slices showing AAR (negative for Evans Blue) in upper panels and extent of necrosis (triphenyl-tetrazolium chloride (TTC)-negative area in lower panels). Data are means ± s.e.m. *P<0.05; determined by the nonparametric Wilcoxon–Mann–Whitney test for each panel.

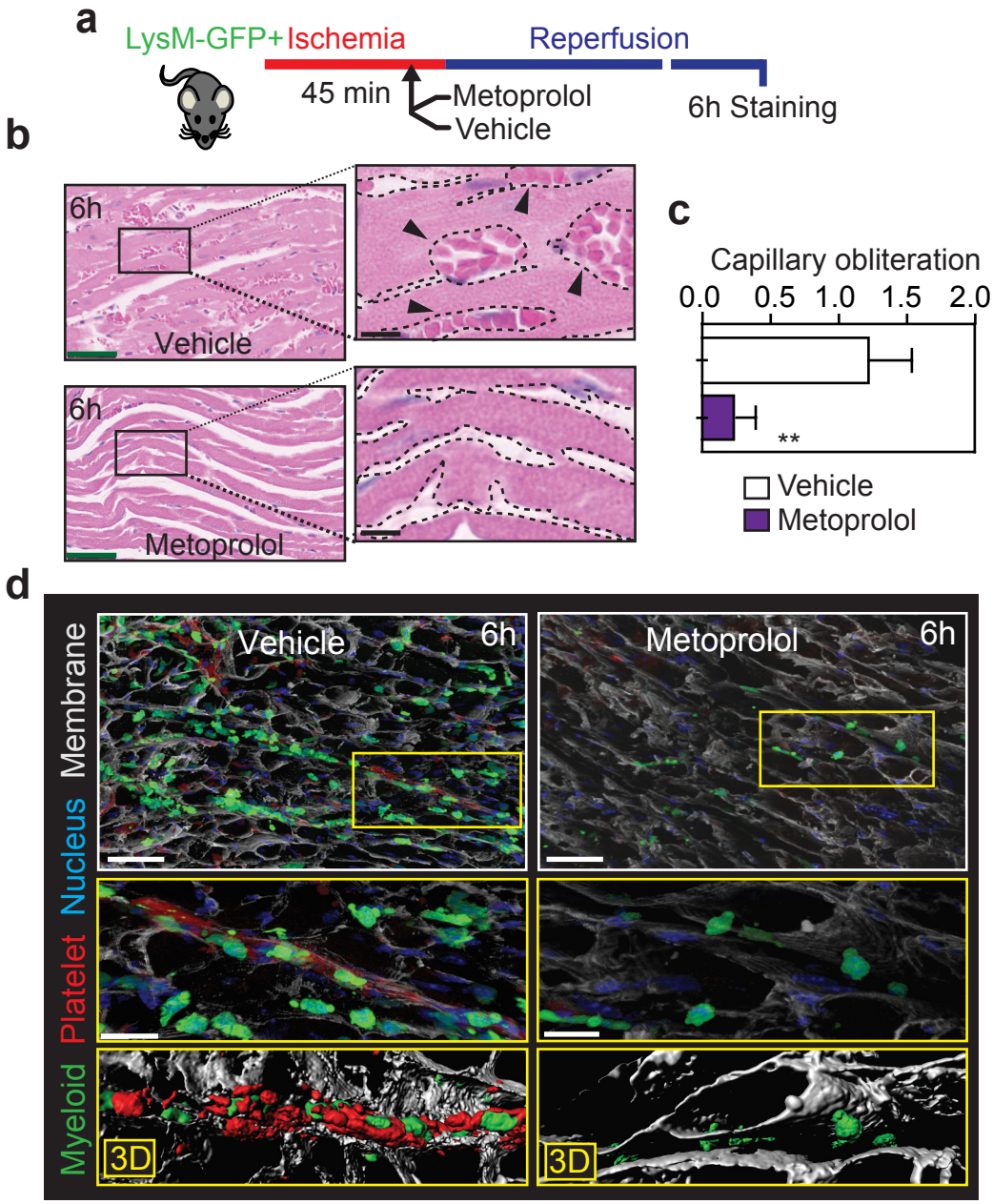

Figure 10. Metoprolol reduces capillary obliteration
(a) Mouse model of myocardial IR. **(b)** Representative H&E myocardial images at 6 h reperfusion showing disarrayed and abundant obstructed capillaries in the vehicle-treated sample; metoprolol-treated samples show cardiac injury, but no signs of MVO; scale bars, 50 μm. Amplification of the boxes shows obstructed capillaries indicated with black arrows; black scale bars, 10 μm. **(c)** Capillary obliteration quantification; n=5-6. **(d)** Confocal images from LV at 6h reperfusion onset showing massive vascular neutrophil migration (LysM-GFP, green) and co-aggregates with platelets (CD41, red) vehicle- but not in metoprolol-treated mice; scale bar, 25 μm. Below, amplified capillary obstruction region; scale bar, 10mm. Bottom, computed 3D reconstructions. Data are means + s.e.m. **P<0.01, determined by the nonparametric Wilcoxon–Mann–Whitney test for each panel.

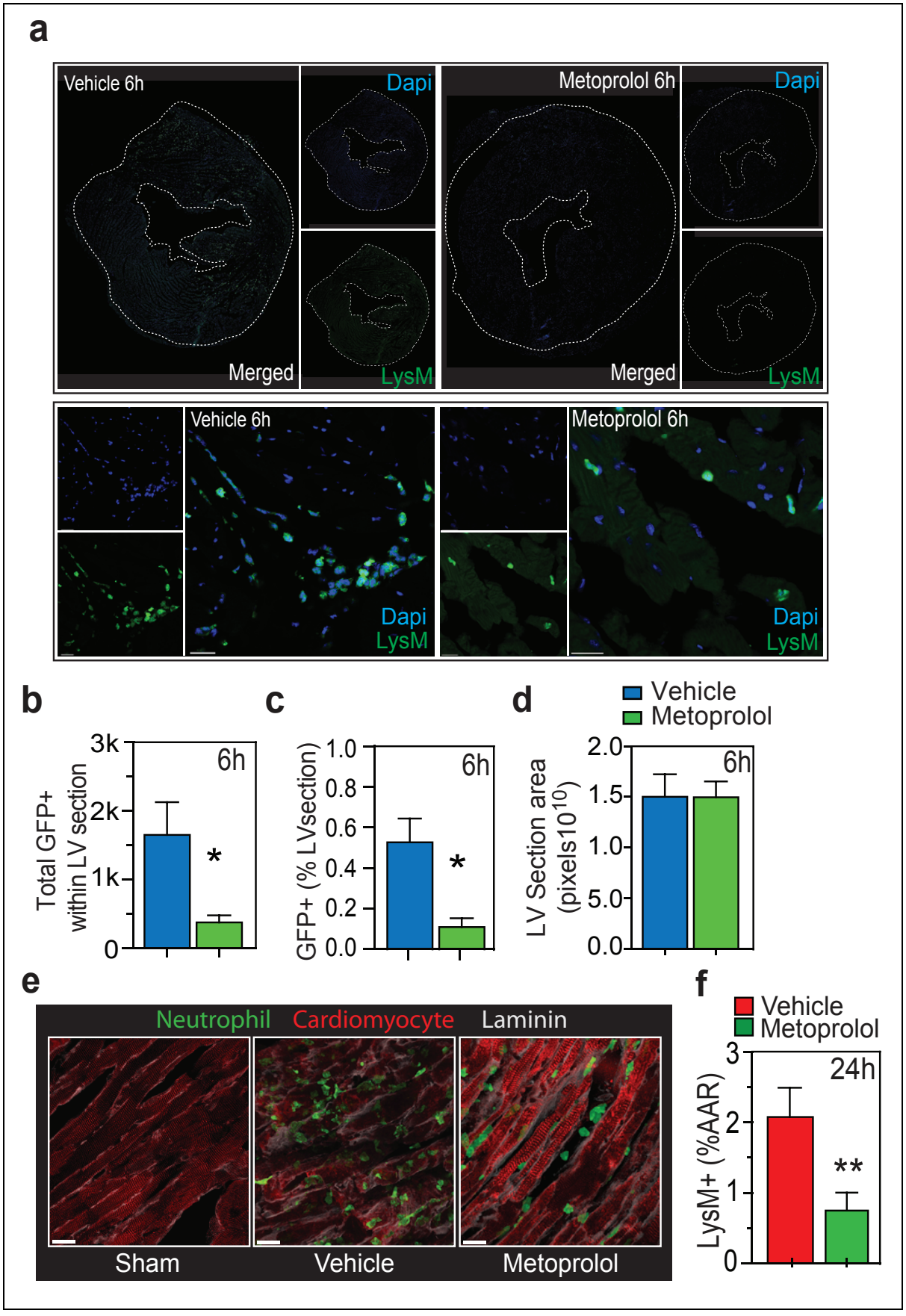
a
Vehicle 6h
Dapi
Merged
LysM
Metoprolol 6h
Dapi
Merged
LysM
Vehicle 6h
Dapi
LysM
Metoprolol 6h
Dapi
LysM
b
Total GFP+ within LV section
3k
2k
1k
0
6h
*
c
GFP+ (% LVsection)
1.0
0.8
0.6
0.4
0.2
0.0
6h
*
d
Vehicle
Metoprolol
LV Section area (pixels10^10)
2.0
1.5
1.0
5.0
0.0
6h
e
Neutrophil
Cardiomyocyte
Laminin
Sham
Vehicle
Metoprolol
f
Vehicle
Metoprolol
LysM+ (%AAR)
3
2
1
0
24h
**

Figure 11. Metoprolol abrogates myeloid infiltration
(a) Representative confocal microscopy images of complete left ventricle (LV) sections at 6 hours after reperfusion. Myeloid infiltration (LysM+, green) is massive within the injured myocardium of hearts from vehicle-treated mice as compared to those from metoprolol-treated mice. Lower panels represent magnifications illustrating the accumulation of myeloid cells in a vessel. **(b)** Average total positive LysM+ pixels within the complete LV section. **(c)** Average LysM+ as percentage of LV section area. **(d)** Mean complete LV sections area. **(e)** Representative confocal images of neutrophil infiltration 24 h after reperfusion onset. Vehicle-treated mice show massive myocardial myeloid derive-neutrophil infiltration (LysM-GFP+, green), with dispersed cells attached to the injured cardiac fibre membranes (α-actinin, red; laminin, grey). **(f)** LysM+ total area in the left ventricle (LV) section as a %AAR; scale bar, 20 mm; n=5–6. Data are means ± s.e.m. *P<0.05. **P<0.01. Comparison was determined by the nonparametric Wilcoxon-Mann–Whitney test.

Next, we examined mice carrying a GFP reporter in myeloid derived cells (LysM-GFP). LysM-GFP^{+} mice underwent the myocardial IR injury procedure and were randomized to receive i.v. metoprolol or vehicle. Capillary obliteration (a histological surrogate for MVO) and leukocyte infiltration were quantified at 6 hours post-reperfusion (**Fig. 10 to Fig 12).** Metoprolol administration during ongoing AMI resulted in a significant reduction of capillary obliteration by circulatory cell plugins when evaluated at 6 hours post-reperfusion (**Fig. 10a, 10b, 10c**). Confocal microscopy analyses revealed a significant reduction in the number of myeloid cells plugins (LysM-GFP+ particles) and percentage of LysM-GFP+ area within the LV sections, indicating rapid inhibition of leukocyte recruitment and protection of lumen vessel patency (**Fig. 10d**) (*See additional information,* **Movie 1**). Temporal (6 and 24 hours) evaluation of myeloid-derived cells infiltration into injured myocardium showed a maintained abrogation of neutrophil infiltration within the first 24 hours (**Fig. 11, Fig. 12**) (*See additional information* **Movie 2**) and a differential relative proportion of myeloid different cells (**Fig 12**). These mouse experiments confirm the clinical findings that pre-reperfusion metoprolol administration during ongoing AMI limits infarct size and reduces MVO, and further show that metoprolol reduces neutrophil infiltration, adding evidence to consider neutrophils as a potential target of this cardioprotective strategy.

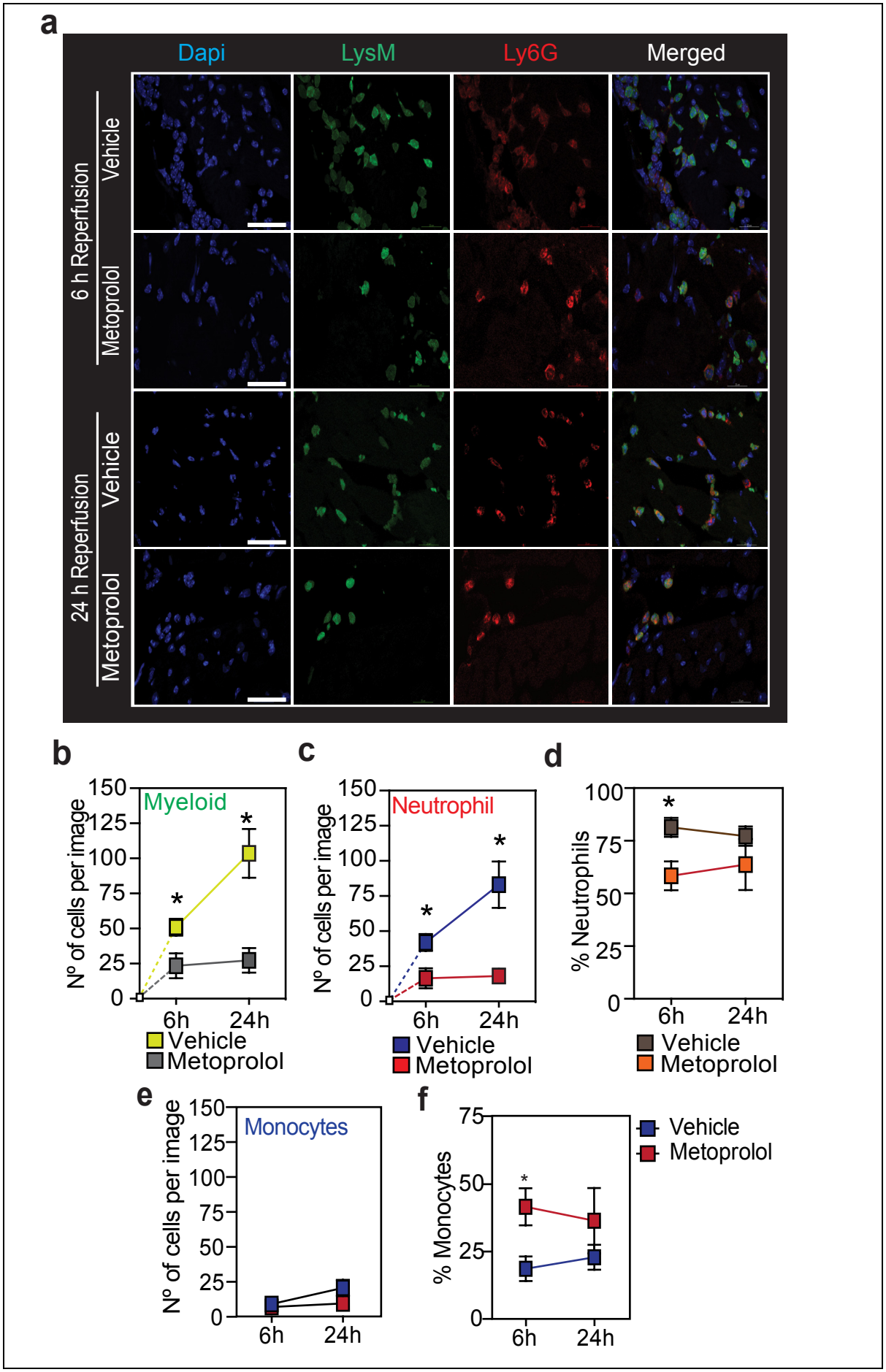
a
Dapi
LysM
Ly6G
Merged
6 h Reperfusion
Vehicle
Metoprolol
24 h Reperfusion
Vehicle
Metoprolol
b
Myeloid
N° of cells per image
150
125
100
75
50
25
0
6h
24h
Vehicle
Metoprolol
c
Neutrophil
N° of cells per image
d
% Neutrophils
100
75
50
25
0
e
Monocytes
N° of cells per image
f
% Monocytes
75
50
25
0
Vehicle
Metoprolol

Figure 12. Metoprolol abrogates neutrophil infiltration
(a) Representative confocal images of LV sections taken from injured mice after 6 and 24 h reperfusion onset. Myeloid infiltration (LysM-GFP+, green) most of which are neutrophil (Ly6G+, red) is evident in vehicle-treated mice and significantly attenuated in those from metoprolol treated mice; merged images show double positive cells (LysM+/Ly6G+, that is, neutrophils). Scale bar, 50 mm; n=3–5. **(b,c)** Myeloid-derived cell infiltration dynamics showing maintained attenuation in hearts from metoprolol-treated mice. n=5. **(d)** Neutrophilic proportions infiltrate dynamics. **(e)** Monocyte infiltration dynamics into the injured myocardium within the first 24 hours of reperfusion; n=5 animals per group. **(f)** Percentage of monocytes (LysM+/Ly6G-), within the myeloid–derived population. Data are means ± s.e.m. *P<0.05; determined by the nonparametric Wilcoxon–Mann–Whitney test for each panel.

Metoprolol does not protect from AMI in the absence of neutrophils

Catecholamine-stimulation of ADBRs alters neutrophil function, cytokine release, and neutrophil-platelet aggregate formation (63) (101) (102), processes associated with aggravated injury during AMI (103) (104) (105) (106). To decipher the role of neutrophils in the protection afforded by metoprolol during ongoing AMI, we evaluated the effect of the drug in the absence of neutrophils. Neutrohil depletion in mouse peripheral blood was achieved by administration of an anti-Ly6G monoclonal antibody (mAb) over 2 days (88) (35). After neutrophil depletion, animals were subjected to myocardial IR, and infarct size was evaluated at 24h post-reperfusion (**Fig. 13a**). Confirming earlier reports (106), neutrophil-depleted mice had smaller infarcts than controls. Administration of metoprolol to these mice during ongoing AMI did not reduce infarct size (**Fig. 13b, 13c 13d**). The abrogation of the cardioprotective effect of metoprolol confirms circulating neutrophils as a target of the beneficial effect associated with this pharmacological therapy.

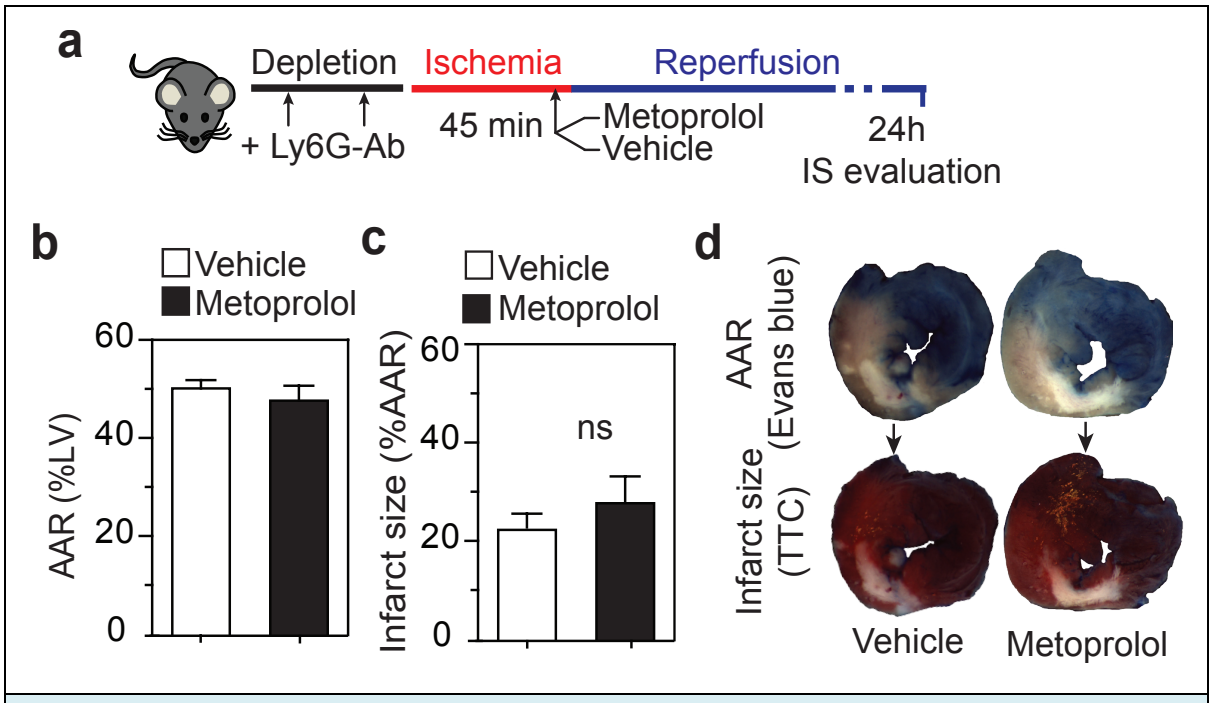

Figure 13. Neutrophil depletion abrogates metoprolol effect
(a) Mouse model of myocardial IR. **(b,c)** Histological evaluation of left ventricle (LV) area at risk (AAR) and infarct size (IS) in mice subjected to IR and randomized to receive metoprolol (blue) or vehicle (white); NS stands for non-significant. n=8. **(d)** Representative images of LV slices showing AAR (negative for Evans Blue) in upper panels and extent of necrosis TTC-negative area in lower panels). Data are means ± s.e.m.; ns, stands for non-significant, determined by the nonparametric Wilcoxon–Mann–Whitney test for each panel.

Metoprolol inhibits neutrophil migration by targeting ADRB1

The effect of metoprolol on primary neutrophils' function was evaluated in a chemokine-induced transwell migration assay and by evaluation of the chemotactic FPR activator-peptide, W-peptide (92), -induced ROS production assay (91). First, neutrophils were exposed across the transwell filter to the chemoattractant CXCL1 in the presence or absence of metoprolol for 1.5 hours, and level of migration through the transwell membrane was quantified by flow cytometry. Metoprolol inhibited baseline and epinephrine-stimulated neutrophil migration toward CXCL1, reducing migration to the same level in both cases (**Fig. 14a**). Second, ROS production in vitro was measured using DHR-123 and W-peptide activation. ROS production was tested in metoprolol-

treated and untreated neutrophils with and without W-peptide stimulation. Neutrophils incubated in metoprolol presented significant decreased oxidative burst compared to control group (**Fig. 14c, 14d**). Metoprolol alone had no effect on ROS endogenous production.

Metoprolol is a selective ADRB1-blocker, and ADRB1 signaling has been shown to mediate some of the pro-inflammatory response of monocytes (107). Neutrophils and monocytes are both myeloid derived cells, and we therefore reasoned that ADRB1 might be involved in the anti-migratory effect of metoprolol. *Adrb1* mRNA expression in fresh and viable isolated neutrophils was confirmed by PCR in wild-type mice and absence in neutrophils from *Adrb1*-knockout mice (*Adrb1*KO) (**Fig. 14e, 14f, 14g**). In vitro, the -epinephrine-mediated migration- and -W-peptide-mediated ROS production-inhibitory effect of metoprolol was lost in *Adrb1*KO neutrophils (**Fig. 14a, 14c**). In addition, β2-adrenergic receptor-knockout mice (*Adrb2*KO) was not involved in the effects observed after metoprolol administration (**Fig. 14b**).

Figure 14. Neutrophil function inhibition ADRB1-dependent
(a) Metoprolol inhibits neutrophil in vitro migration through a ADRB1-dependent signalling. Effect of metoprolol on CXCL1-induced migration of fresh primary isolated neutrophils (LysM+/Ly6G+/DAPIneg) from wild-type (WT) and in *Adrb1*KO (ß1KO) mice. CXCL1-stimulated neutrophils were incubated with vehicle, epinephrine (10mM), metoprolol (10mM) and epinephrine +metoprolol; n=4 independent experiments. ns, stands for non-significant. **(b)** Neutrophil migration inhibition is independent to ADRB2 signalling. CXCL1-induced migration fresh primary isolated neutrophils (LysM+/Ly6G+/DAPIneg) from WT and in *Adrb2*KO (ß2KO) mice, incubated with vehicle and metoprolol (10mM) n=5 independent experiments. ns, stands for non-significant. **(c,d)** Inhibitory effect of metoprolol on W-peptide-induced ROS production on fresh isolated primary neutrophils ($Ly6G^+$) from WT or ß1KO mice. On the left, flow cytometry plots illustrate reduced expression of Rho-123 in metoprolol-treated neutrophils. On the graph, mean fluorescent intensity of Rho123 in $Ly6G^+$ neutrophils after W-peptide stimulation. n=6 independent experiments; ns, stands for non-significant. **(e, f)** Purity and viability of mouse blood neutrophils (LysM+/Ly6G+/DAPIneg) evaluated by flow cytometry. **(g)** Agarose gel electrophoresis of PCR products, showing *Adrb1* expression in mouse left ventricle (LV), bone marrow (BM), and blood neutrophils ($Ly6G^+$) *Adrb1*KO (β1KO9 mice were used as a negative control Data are means ± s.e.m. * P<0.05; ** P<0.01 and *** P<0.001; Comparisons were performed using the one-way ANOVA and Holm Sidak's post-hoc multiple comparisons method.

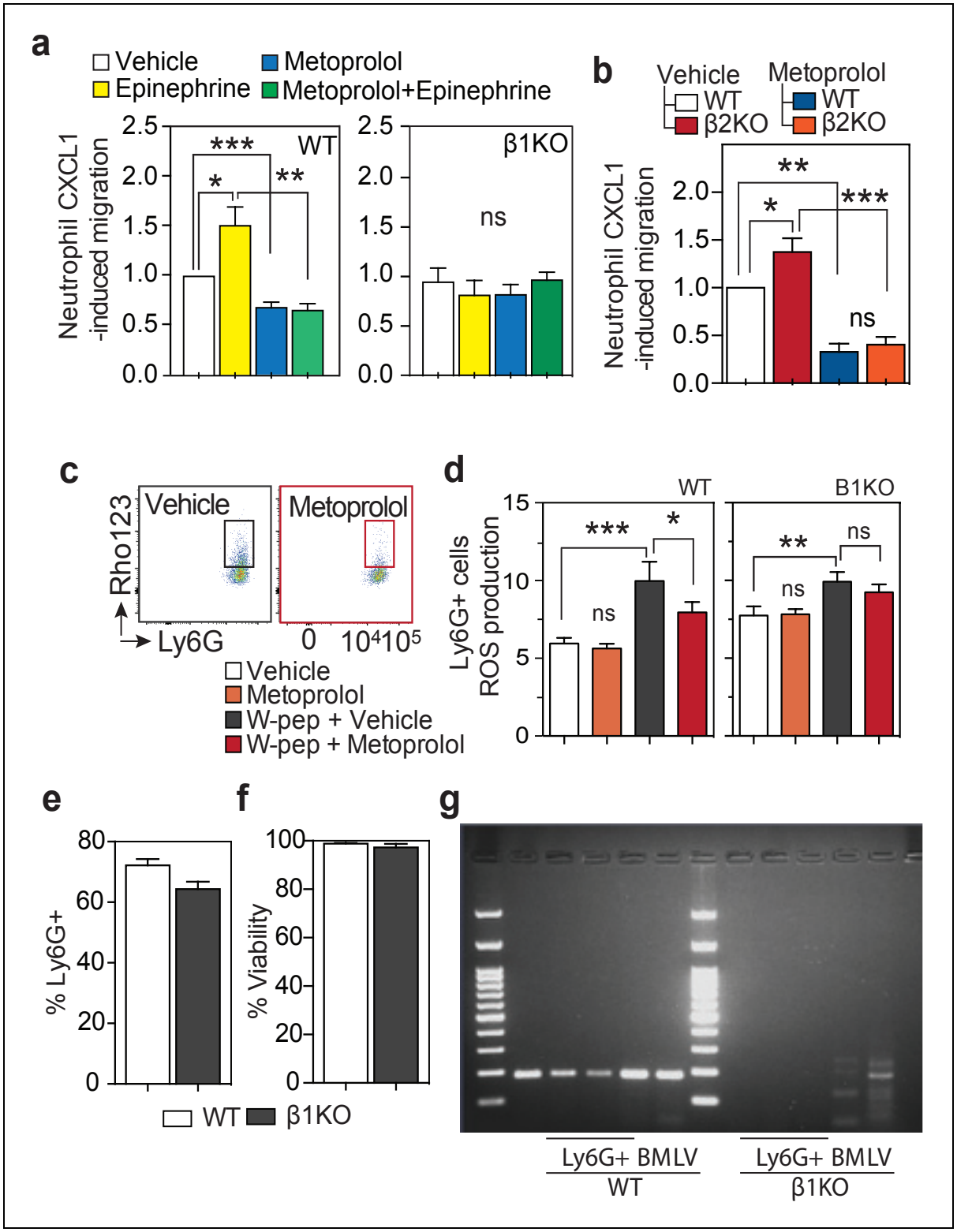

We next explored whether metoprolol directly inhibits the capacity of neutrophils to infiltrate tissues in vivo. For this, we first used a model of thioglycolate-induced peritonitis (**Fig. 15a**). Thioglycolate induces massive

leucocyte migration into the peritoneal cavity within the first 16 hours (**Fig. 15b**), with the majority of infiltrating cells being neutrophils (**Fig. 15d, 15e**)**.** Interestingly, a single bolus of 50 µL of Metoprolol (10 mM) sharply inhibited thioglycolate-induced neutrophil infiltration into the peritoneal cavity (after 16 hours injection) of wild-type mice (**Fig. 15c**), but the inhibitory effect of metoprolol was lost in *Adrb1*KO mice (**Fig. 15b, 15c, 15d**). To better define the cell compartment targeted by metoprolol, we lethally irradiated *Adrb1*KO mice and restored haematopoiesis with bone marrow transplanted from wild-type donors, generating chimeric mice expressing ADRB1 only in circulating cells (**Fig. 15e**). 4 weeks after the bone marrow procedure, transplanted animals presented >85% bone marrow engraftment (**Fig. 15g**) and were subjected to thioglycolate-induced peritonitis. Bone marrow transplant did not affect metoprolol's effect. However, the replenishment of ADRB1 only in hematopoietic cells was enough to rescue the anti–leucocyte-infiltration effect of metoprolol (**Fig. 16h**). Together, these data show a direct effect of metoprolol on neutrophil function and demonstrate that the presence of ADRB1 in circulating cells is essential for it to reduce neutrophil infiltration into injured tissue.

Figure 15. Metoprolol blocks neutrophil peritoneal infiltration
(a) Metoprolol effect on thioglycolate-induced peritoneal infiltration. **(b)** Absolute leucocyte number per mL of infiltrate 16 hours after intraperitoneal thioglycolate injection in wild-type (WT) mice (n= 7-9) or ADRB1-knockout (β1KO) mice (n=5) randomized to receive either i.v. metoprolol or vehicle. **(c)** Flowcytometry plots illustrating reduced infiltration of neutrophils (CD115neg; GR1+) in metoprolol-treated mice; and graphs representing absolute neutrophils detected per mL of infiltrate at 16 hours after thioglycolate injection in WT mice (n=7–9) or ß1KO mice (n=5). **(d)** Neutrophils as a percentage of the white blood cells evaluated in the infiltrate. **(e)** Peripheral blood neutrophil counts. Metoprolol's cardioprotective effect is dependent on the presence of ADRB1 on neutrophils. **(f)** Protocol scheme for thioglycolate-induced peritonitis assay after bone-marrow transplants (BMT) between WT and ß1KO mice, evaluating the influence of the presence or absence of ADRB1 in circulating cells. **(g)** Flow cytometry assessment of representative bone marrow transplant engraftment between 4 chimeric groups evaluated. n=10. **(h)** Effect of metoprolol on thioglycolate-induced neutrophil infiltration in the four BMT groups. Data are normalized to vehicle; n=4/9. and analysis determined by one-way ANOVA and Holm Sidak's post-hoc multiple comparisons method; Data are means ± s.e.m. *P<0.05** p<0.01; *** p<0.001, determined by the nonparametric Wilcoxon-Mann–Whitney test for each panel; ns, non-significant.

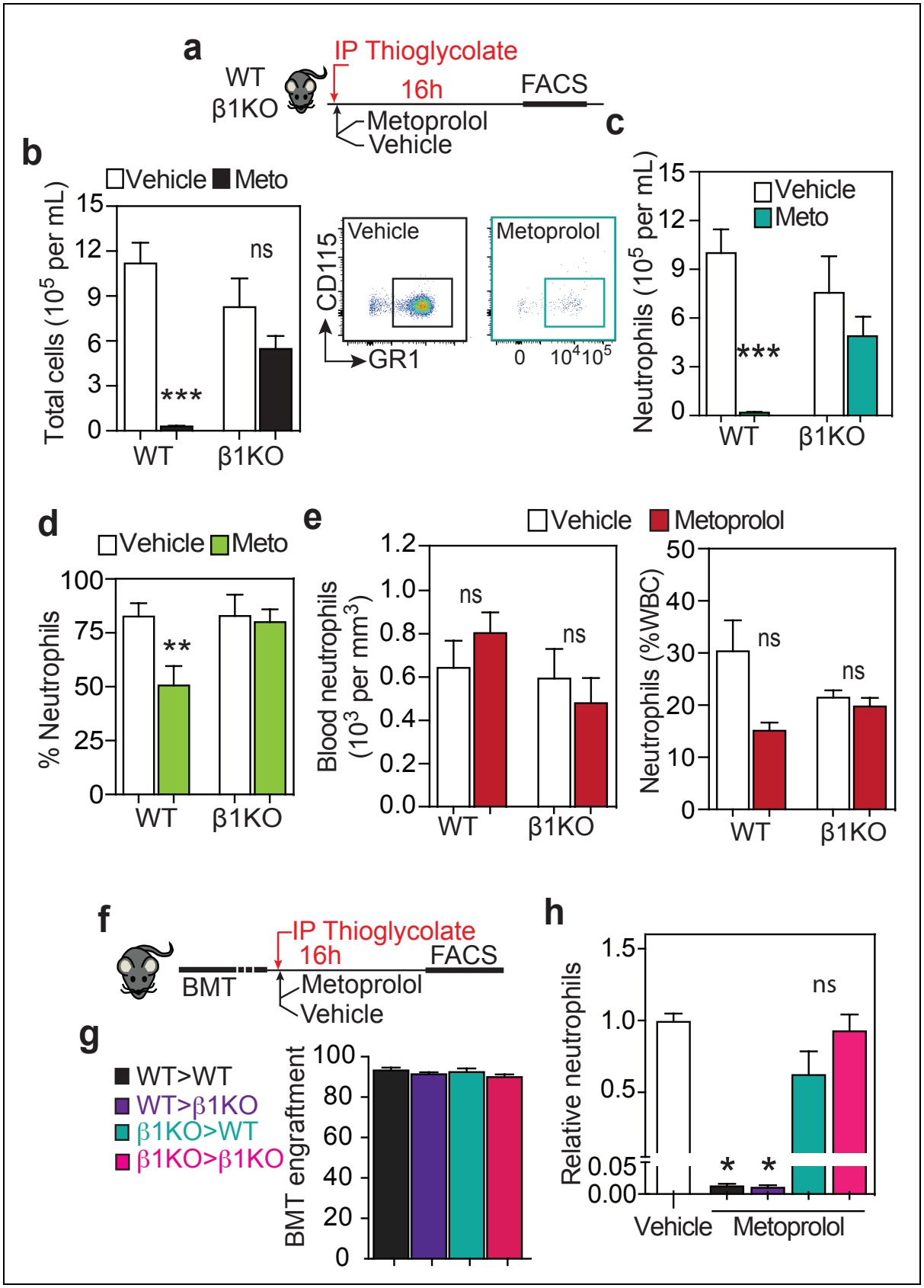
a
WT
β1KO
IP Thioglycolate
16h
FACS
Metoprolol
Vehicle
b
Vehicle
Meto
Total cells (10^5 per mL)
ns
***
WT
β1KO
Vehicle
Metoprolol
CD115
GR1
0
10^4
10^5
c
Vehicle
Meto
Neutrophils (10^5 per mL)
***
WT
β1KO
d
Vehicle
Meto
% Neutrophils
**
WT
β1KO
e
Vehicle
Metoprolol
Blood neutrophils (10^3 per mm^3)
ns
ns
WT
β1KO
Neutrophils (%WBC)
ns
ns
WT
β1KO
f
IP Thioglycolate
16h
FACS
BMT
Metoprolol
Vehicle
g
WT>WT
WT>β1KO
β1KO>WT
β1KO>β1KO
BMT engraftment
h
Relative neutrophils
ns
*
*
Vehicle
Metoprolol

Metoprolol cardioprotection involves hematopoietic cells´ *ADRB1*

We next investigated the involvement of ADRB1 blockade in hematopoietic circulating cells in the protective effect of metoprolol in the infarcted myocardium. *Adrb1*KO mice were subjected to myocardial IR and randomized to receive i.v. metoprolol or vehicle during ongoing AMI (**Fig. 16**). Unlike the situation in wild-type mice, metoprolol did not limit infarct size in *Adrb1*KO animals (**Fig. 16b, 16c, 16d**), demonstrating the critical role of ADRB1-blockade in the cardioprotective effect.

To demonstrate the role of ADRB1 expressed in hematopoietic circulating cells, we repeated the myocardial IR protocol in the chimeras described above (*Adrb1*KO mice transplanted with wild-type bone marrow). The presence of ADRB1 only in hematopoietic circulating cells was sufficient to restore susceptibility to the cardioprotective effect of metoprolol (**Fig. 16e, 16f, 16g**). Conversely, transplant of *Adrb1*KO bone marrow into irradiated wild-type mice abrogated the protective phenotype associated with metoprolol administration during IR (**Fig. 16h, 16i, 16j**). These data confirm the involvement of ADRB1-blockade in hematopoietic cells in the cardioprotection afforded by metoprolol administration during AMI.

Figure 16. Metoprolol inhibits neutrophil ADRB1 signaling
(a) Protocol scheme for IR experiments in chimeric animals after BM transplant, evaluating the infarct-limiting effect of metoprolol in the presence or absence of ADRB1 in circulating cells. (**b–j**) Histological evaluation of left ventricle (LV) area at risk (AAR) and infarct size in mice subjected to IR and randomized to receive metoprolol (coloured bars) or vehicle (white bars) for each of the groups under evaluation, plus the respectively representative images of evans blue and TTC staining in metoprolol-treated and vehicle-treated ß1KO and chimeras wild-type (WT) bone marrow transplanted into ß1KO mice and reverse transplants). Infarct size is reduced by metoprolol only when circulating cells express ß1-adrenergic receptor; n=9 (**b,c**), n=8 (**e,f**), n=5–6 (**h,i**). ns, stands for non-significant. Data are means ± s.e.m. *P<0.05; determined by the nonparametric Wilcoxon–Mann–Whitney test.

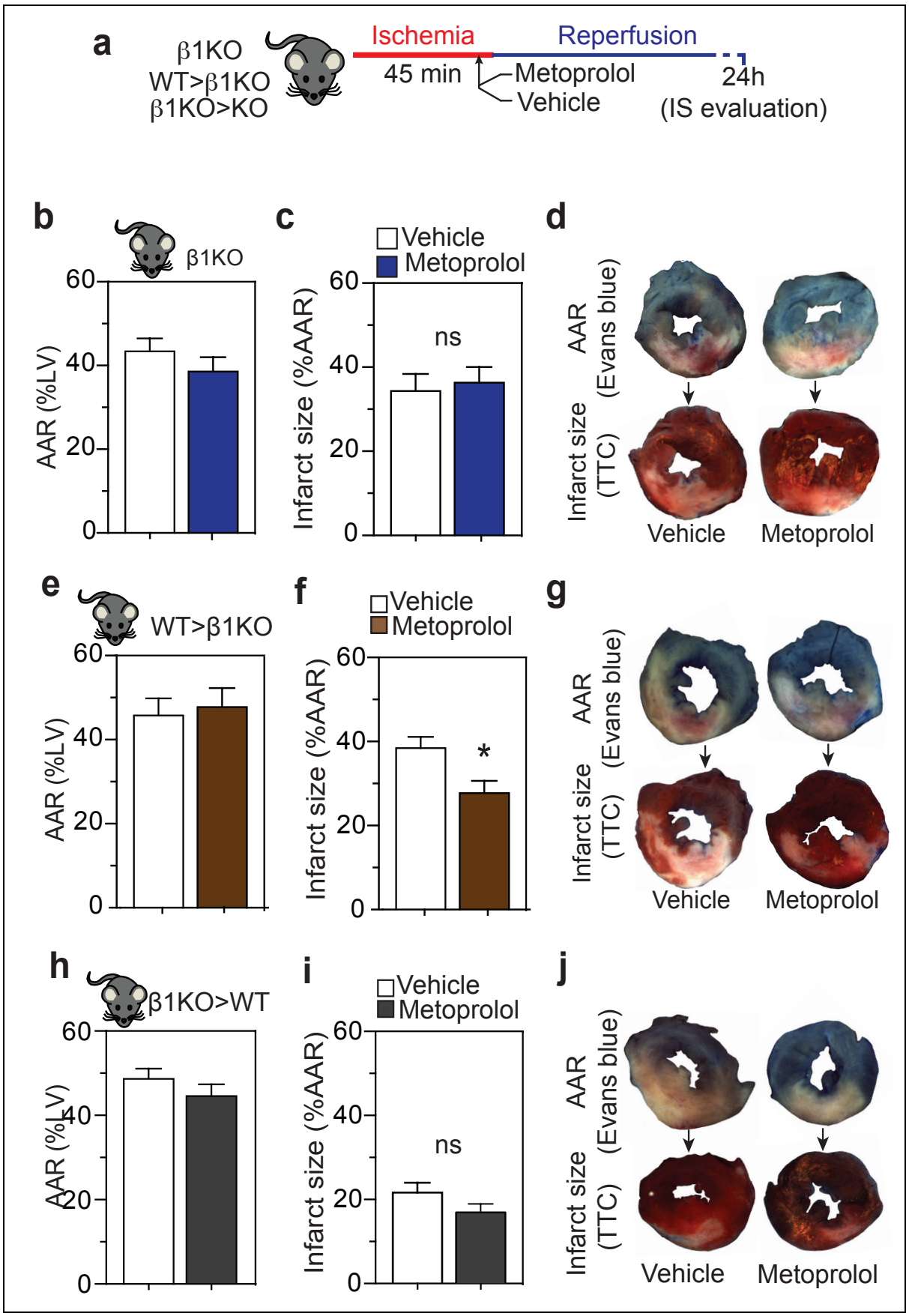
a
β1KO
WT>β1KO
β1KO>KO
Ischemia
45 min
Reperfusion
Metoprolol
Vehicle
24h
(IS evaluation)
b
β1KO
AAR (%LV)
c
Vehicle
Metoprolol
Infarct size (%AAR)
ns
d
AAR (Evans blue)
Infarct size (TTC)
Vehicle
Metoprolol
e
WT>β1KO
AAR (%LV)
f
Vehicle
Metoprolol
Infarct size (%AAR)
*
g
AAR (Evans blue)
Infarct size (TTC)
Vehicle
Metoprolol
h
β1KO>WT
AAR (%LV)
i
Vehicle
Metoprolol
Infarct size (%AAR)
ns
j
AAR (Evans blue)
Infarct size (TTC)
Vehicle
Metoprolol

Metoprolol alters neutrophil dynamics in vivo

During acute injury, neutrophils alter their morphology upon adhering to the activated endothelium. These shape change or polarization, permit intercellular interactions critical for the inflammatory response in several conditions, including myocardial IR (35) (108). Polarization of adhered neutrophils involves receptor redistribution and the assembly of a rearward protruding micro-domain called the uropod, and is essential for the integration of signals coming from the endothelium and activated platelets prior to infiltration (35). We were therefore interested in investigating whether metoprolol impaired neutrophil migration and infiltration through an effect on neutrophil dynamics. For this, we used bi-dimensional and 3D intravital microscopy (IVM) to image cremaster muscle vessels of mice treated with tumour necrosis factor-α (TNFα), an inflammatory model in which the vast majority of recruited leukocytes are neutrophils. Neutrophil behaviour was evaluated 3h after administration of metoprolol or vehicle (**Fig. 17a**). Notably, metoprolol reduced neutrophil migratory velocity, accumulated crawling distance, and directional movement (**Fig. 17b, 17c** and **Movie 3**).

Figure 17. Metoprolol stuns neutrophil function
(a) Experimental design: wild-type (WT) mice receiving TNFα were randomized to receive I.V. metoprolol or vehicle before analysis of cremaster muscle vessels by 2D and 3D intravital microscopy. **(b)** Quantification of parameters related to two-dimensional intravascular motility; N=54–141 cells from 3 to 4 mice. **(c)** Representative tracks of crawling neutrophils within inflamed vessels. **(d)** 3D reconstructions of representative neutrophils within live vessels of saline-treated and metoprolol-treated mice (red, uropod; green, cell body). **(e,f)** Quantification of 3D parameters, indicating reduced elongation (prolate ellipticity) and enhanced projection of recruited neutrophils into the luminal space (height-to-length ratio); N=68–105 cells from 3 to 4 mice. **(g,h)** Representative time-lapse images and percentage of interactions of platelets (CD41, red) with the polarized neutrophil uropod (CD62L, yellow) or leading edge (Ly6G, green); N=28–29 vessels from 3 to 4 mice. White arrowheads indicate interactions with the uropod and the dotted line the displacement of the cells during 30 s. Scale bar, 10 mm. Data are means ± s.e.m. *P<0.05; **P<0.01; ***P<0.001, determined by unpaired Student's t-test for each parameter.

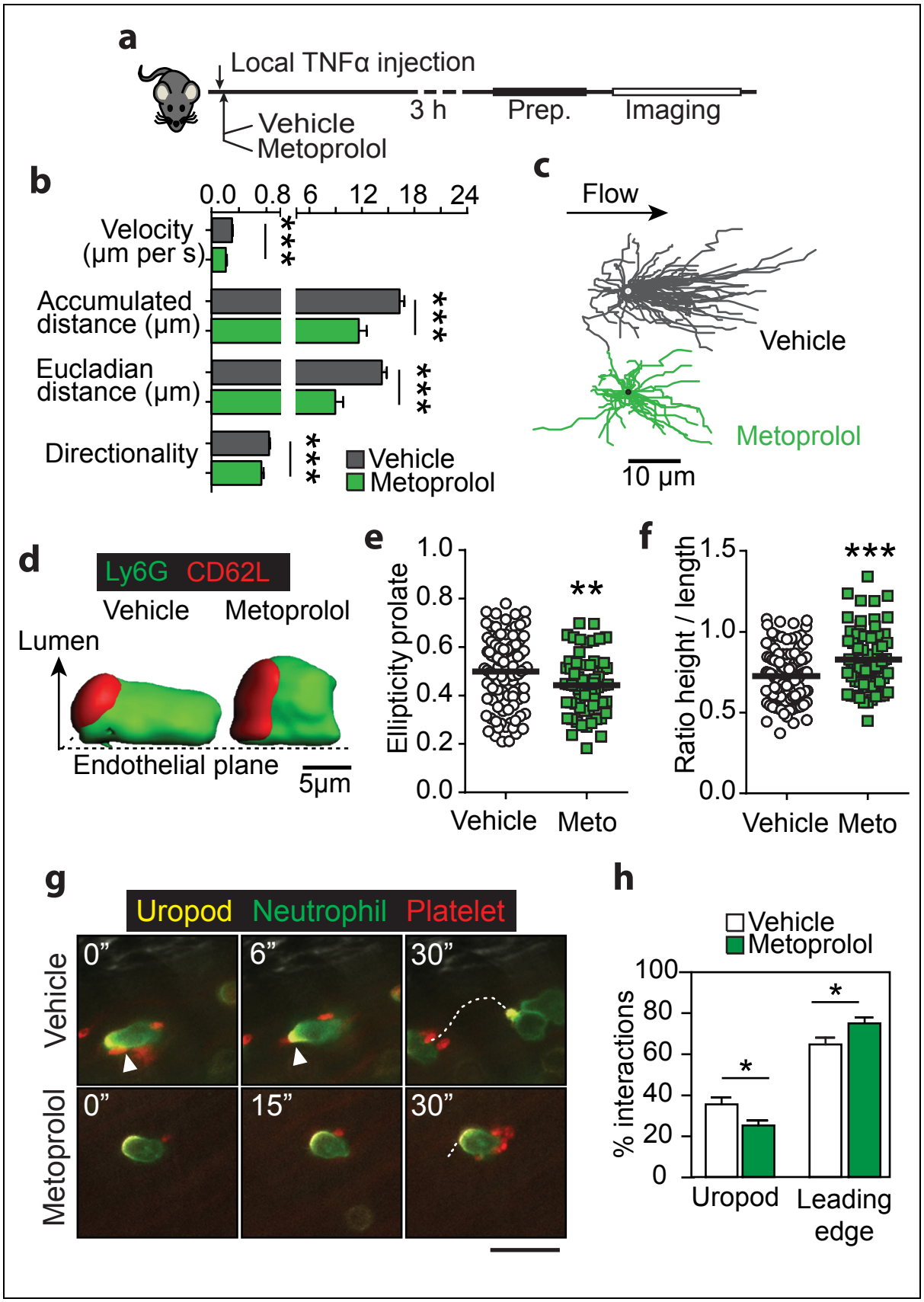
a
Local TNFα injection
3 h
Prep.
Imaging
Vehicle
Metoprolol
b
0.0 0.8 6 12 18 24
Velocity (μm per s)
Accumulated distance (μm)
Eucladian distance (μm)
Directionality
***
***
***
***
Vehicle
Metoprolol
c
Flow
Vehicle
Metoprolol
10 μm
d
Ly6G CD62L
Vehicle
Metoprolol
Lumen
Endothelial plane
5μm
e
Ellipticity prolate
1.0
0.8
0.6
0.4
0.2
0.0
**
Vehicle
Meto
f
Ratio height / length
1.5
1.0
0.5
0.0
***
Vehicle
Meto
g
Uropod Neutrophil Platelet
Vehicle
Metoprolol
0”
6”
30”
0”
15”
30”
h
Vehicle
Metoprolol
% interactions
100
80
60
40
20
0
*
*
Uropod
Leading edge

Independent-neutrophil 3D-reconstructions of live inflamed vessels showed that metoprolol consistently disabled the intravascular behavior of neutrophils without disrupting polarization within activated vessels, resulting in dramatic changes in cell morphology (**Fig. 17d, 17e, 17f**) that correlated with their abnormal crawling dynamics. These data show that metoprolol "stuns" neutrophils, resulting in altered dynamics and prevents the morphological changes needed to initiate intercellular interactions and subsequent tissue infiltration.

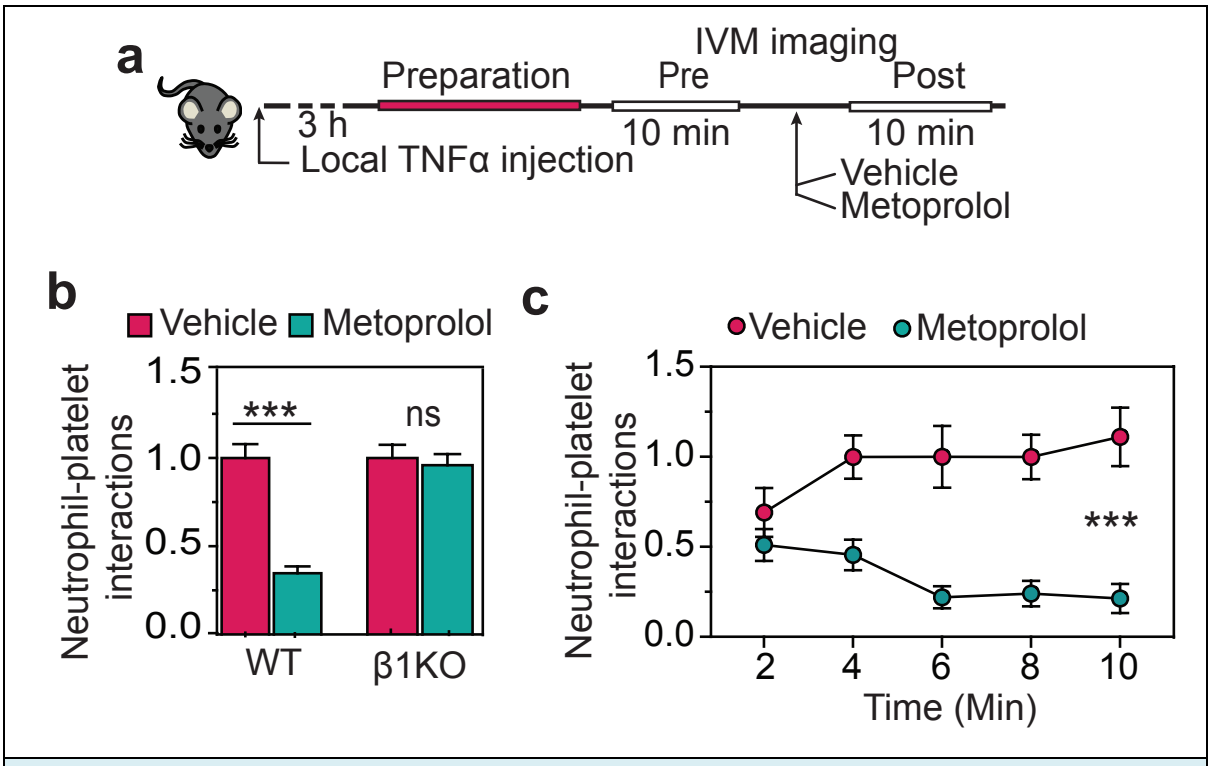

Figure 18. Metoprolol prevents neutrophil–platelet interactions
(a) Protocol scheme for evaluating the acute inhibitory effect of metoprolol on activated and polarized neutrophils on wild-type (WT) and AdrbB1-knockout (ß1KO) mice. **(b)** Absolute neutrophil–platelet intravascular interactions in WT and ß1KO mice. NS, stands for non-significant. **(c)** Temporal neutrophil–platelet interaction inhibition in WT mice afteradministration with i.v. metoprolol. Data are means±s.e.m. ***P<0.001, determined by unpaired Student's t-test for each parameter.

Metoprolol blocks *PSGL1*-dependent neutrophil-platelet interactions

Correct neutrophil polarization and organization of an extruding micro-domain that captures circulating platelets is required to initiate tissue-damaging inflammation (35). Indeed, plugs of neutrophil-platelet coaggregates in the microcirculation are a major contributor to MVO in AMI and in other models of injury (8) (35). We therefore explored the impact of metoprolol-induced neutrophil stunning on neutrophil-platelet interactions. Using the cremaster IVM model of TNFα-induced local inflammation, we evaluated the acute neutrophil-platelet inhibitory effect of metoprolol in polarized neutrophils (**Fig. 17** and **Fig. 18**) (*See additional information*, ***Movie 3***). Metoprolol i.v. administration effectively inhibited interactions with the uropod, but not the leading edge (**Fig. 17g, 17h**) and rapidly reduced total neutrophil-platelet interactions (**Fig. 18a, 18b, 18c**). IVM experiments in *Adrb*1KO mice revealed no differences between metoprolol-treated and vehicle-treated mice, implicating ADRB1 in the inhibitory effect of metoprolol on neutrophil-platelet interactions (**Fig. 18b**).

Figure 19. Metoprolol blocks neutrophil–platelet interactions
(a) Experimental scheme of IR model. **(b)** Representative confocal images evaluating the effect of metoprolol on the number of co-aggregates of neutrophils (LysM-GFP+, green) and platelets (CD41, red) in the post-reperfused mouse myocardium. **(c,d)** LysM-GFP+ cells (neutrophils) attached to coronary vessels; N=7–9) and the numbers of interacting platelets (CD41+) per neutrophil in reperfused myocardium. Scale bar, 20 mm. **(e)** Protocol scheme for the IR experiment evaluating the effect of neutrophil-platelet blockade with anti-PSGL1 Ab (administered 15 min after ischemia onset, that is, 30 min before reperfusion) on the infarct-limiting effect of metoprolol (administered 35 min after ischemia onset, that is, 10 min before reperfusion). **(f,g)** AAR, infarct size, and representative images of Evans blue and TTC staining in vehicle- and metoprolol-treated mice pre-treated with anti-PSGL1 Ab. N=5–7. ns, stands for non-significant. Data are means ± s.e.m. *P<0.05; **P<0.01. Comparison was determined by the nonparametric Wilcoxon–Mann–Whitney test.

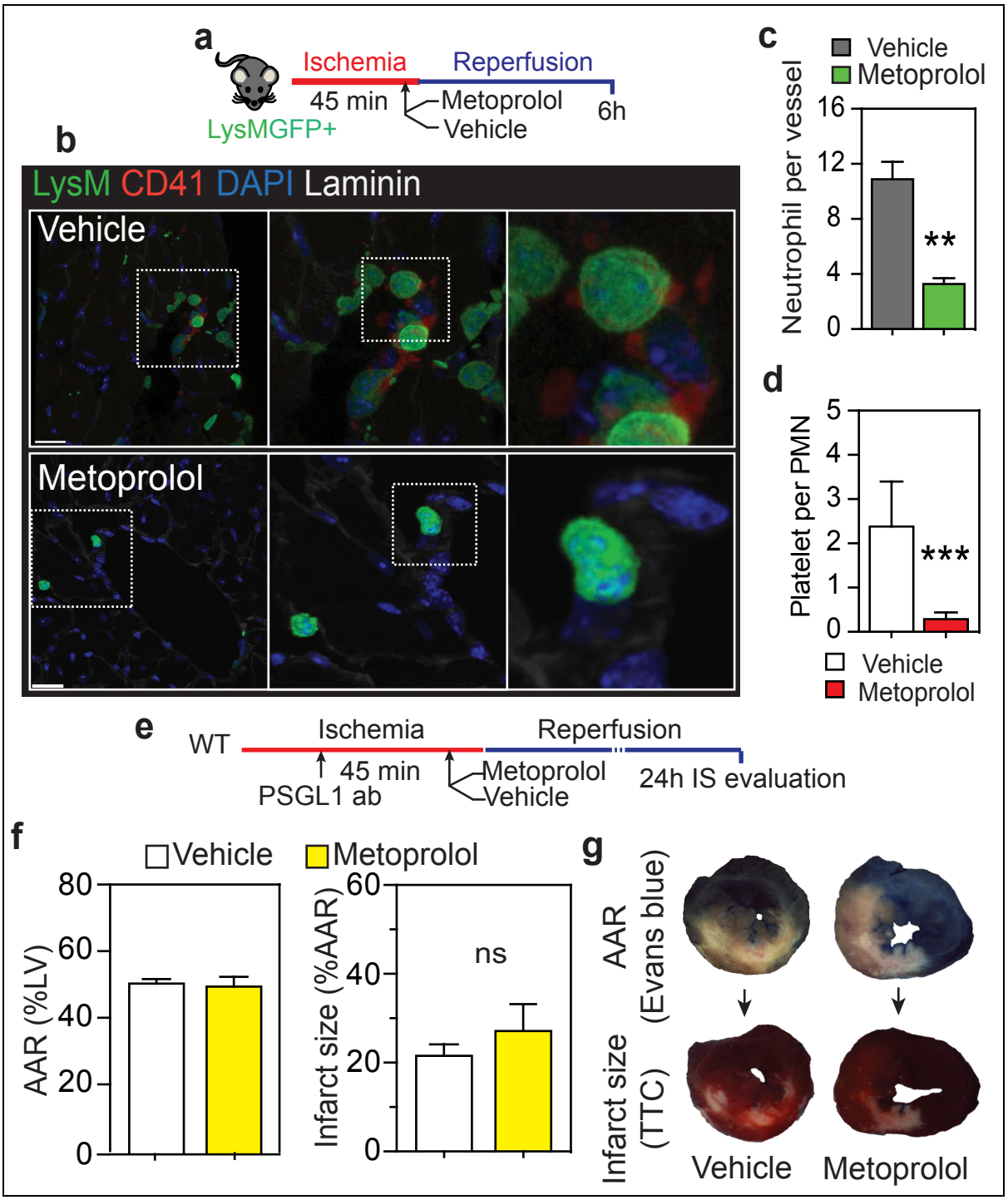

Based on these findings, we hypothesized that inhibition of neutrophil-platelet interactions underlies the inhibitory effect of metoprolol on MVO after myocardial IR. To test this, we first evaluated the effect of metoprolol on neutrophil-platelet coaggregate formation in mouse myocardial vessels after experimental IR. Administration of metoprolol to wild-type mice during ongoing AMI significantly reduced the number of neutrophils attached to the

vessel wall and the average number of interacting platelets per neutrophil (**Fig. 19a, 19b**, **19c, 19d**). Neutrophil-platelet interactions during acute injury are mediated by PSGL1 and signals delivered upon these contacts promote subsequent neutrophil extravasation and injury to the tissue (35). Blockade of PSGL1 by pretreatment with PSGL1-mAB (**Fig. 19e**) significantly reduced infarct size in the myocardial IR model, and administration of metoprolol during ongoing AMI did not yield any further infarct-size reductions (**Fig. 19f, 19g**). These data confirm that metoprolol protects the infarcted myocardium by uncoupling neutrophil recruitment and polarization, thereby disrupting neutrophil-platelet interactions and the downstream inflammatory response.

Metoprolol limits neutrophil-platelet aggregates in patients

To investigate whether metoprolol alters neutrophil dynamics and inhibits neutrophil-platelet interactions in humans, whole blood drawn from healthy donors was incubated ex-vivo with epinephrine (5 µM) and increasing concentrations of metoprolol (0, 2, 5 µM). Samples were then stained, and neutrophil-platelet coaggregate formation was evaluated by flow cytometry (94) (93) (95) (96) (morphological parameters, CD14neg, CD45+, CD61+). Metoprolol significantly inhibited epinephrine-stimulated neutrophil-platelet coaggregate formation (**Fig. 20a).** The effect of metoprolol in vivo was additionally studied in patients undergoing elective coronary angioplasty for acute coronary syndrome. Samples were collected before and after i.v. administration of metoprolol (15 mg) and circulating neutrophil-platelet coaggregates were assessed by flow cytometry. Metoprolol administration significantly reduced the number of neutrophil-platelet interactions (**Fig. 20b**).

To elucidate whether metoprolol was acting at the platelet level of action we evaluated effect of metoprolol on platelet function through platelet aggregation using light transmittance aggregometry (LTA) in platelet-rich plasma (**Fig. 20c**) or platelet activation surface markers expression assay using flow cytometry (**Fig. 20d, 20e**). Metoprolol did not show any effect on platelet aggregation/activation, which together with the aforementioned effects on

neutrophil migration and ROS-production suggest that the effect seen on neutrophil-platelet coaggregates was driven by a direct effect on neutrophils.

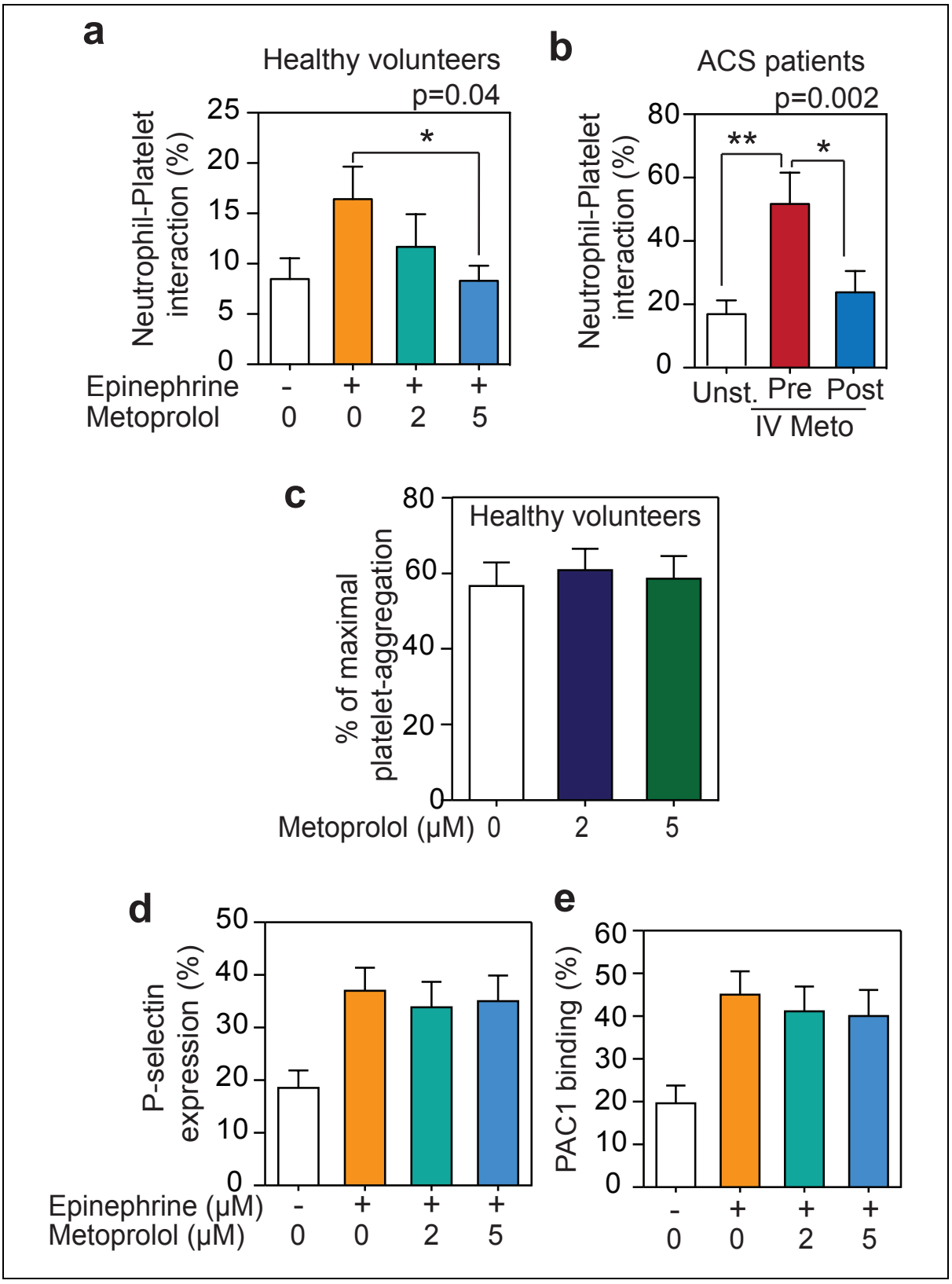

Figure 20. Metoprolol inhibits neutrophil function in patients
(a) Neutrophil–platelet formation in epinephrine-stimulated whole blood from healthy volunteers (n=20). Whole blood was incubated in vitro with epinephrine 5 mM and metoprolol (Meto) at different concentrations. **(b)** Metoprolol effect on the number of neutrophil i.v. platelet co-aggregates in acute coronary syndrome (ACS) patients scheduled for coronary angioplasty. Blood was drawn before and after metoprolol i.v. administration; n=6 ACS patients. Pre, before i.v. administration; Post, after i.v. administration. **(c-e)** Metoprolol on human platelet function. **(c)** Effect of metoprolol on maximal platelet aggregation on epinephrine-stimulated platelet rich plasma (PRP) from healthy volunteers (n=20). **(d,e)** Effect of metoprolol on platelet activation as determined by **(d)** surface expression of activated GP IIb/IIIa and **(e)** Surface expression of P-Selectin using flow cytometry from healthy donors (n=20). Data are means ± s.e.m.*P<0.05; **P<0.01, determined by one-way ANOVA and Holm Sidak's post-hoc multiple comparisons method.

Discussion

Early metoprolol intravenous administration given as an adjunct to mechanical reperfusion during ongoing AMI is a simple, inexpensive and save pharmacological therapy that reduces infarct size and ameliorates post-infarction severe cardiac dysfunction (84) (109) (110). To identify and to understand the mechanisms of action underlying this cardioprotective strategy is of great relevance since more efficient and specific protective strategies could be developed.

The ability of ß-blockers, specially ADRB1-selective antagonists, to reduce IS was tested decades ago in several clinical trials, under the hypothesis that ß-blockers reduce the extent of damage by a direct effect on cardiomyocytes via reducing oxygen consumption. However, results from early studies were inconclusive (8). This could be explained because most studies were performed in the context of non-reperfused AMI (that is, before pharmacological thrombolysis and primary PCI were developed). The advent of reperfusion as the treatment of choice for AMI changed the mode of myocardial death: from unrelieved ischemia to a combination of ischemic- and reperfusion-associated processes. This new scenario, suggested the potential cardioprotective effect of ß-blockers be revisited (8). A large animal study performed by our group in 2007, showed that metoprolol reduces IS only when administered before reperfusion (80) (81), suggesting that metoprolol might reduce infarct size by inhibiting reperfusion injury. Surprisingly, oxygen consumption was similar in metoprolol- and vehicle-treated pigs. Interestingly, IS reduction in metoprolol-treated pigs was associated with reduced myeloperoxidase activity in the post-ischemic myocardium 24 hours after reperfusion (81), which prompted us to investigate cellular mechanisms underlying this reperfusion-related injury-limiting effect of metoprolol on myocardial IR injury. Our group led the METOCARD-CNIC trial, which was the first trial to evaluate the ability of metoprolol to reduce IS in the context of angioplasty-mediated reperfused AMI (86). In this trial, early i.v. metoprolol administration during ongoing AMI resulted in a significant reduction of IS (82) (111) and of the incidence of severe ventricular dysfunction and heart failure readmissions (83). The mechanism of metoprolol´s protection remained unravelled and was the main purpose of the present dissertation.

Neutrophils are the most abundant inflammatory cells and ample evidence supports their critical implication in IR injury (27) (103) (104) (105) (106) (112) (113). Neutrophils exert two well described deleterious effects on the injured myocardium. On one side, activated neutrophils and neutrophil-platelet plugs contribute to microvessels occlusion preventing distal efficient tissue perfusion (MVO) (8). On the other, neutrophils migrate to the newly reperfused injured vessels, adhere to the injured endothelium and infiltrate the myocardium contributing to both endothelial and cardiomyocyte death (36) (38). This doctoral thesis confirms these associations in AMI patients: neutrophil count positively correlated with the extent of MVO at 7 days post-reperfusion in the METOCARD-CNIC trial. Although limited in number, some studies linked the action of metoprolol to neutrophils: reductions in post-IR myeloperoxidase activity in pig myocardium (81) and rat spinal cord (114), and inhibition of sepsis-induced inflammation in mice (115). The data obtained from METOCARD-CNIC trial patients MVO evaluation, is the first human evidence that links metoprolol with altered neutrophil behaviour in vivo and that shows that a positive correlation between neutrophil count and MVO can be altered in those patients receiving i.v. metoprolol before reperfusion. Although mechanism remained unknown, this result suggested altered neutrophil dynamics during acute injury.

The existence of ADRBs in human leukocytes was indirectly demonstrated (38) (116) (117) and extensively characterized in immune cell studies (103). This work confirms previous results in mouse (62). Furthermore, the studies here developed with *Adrb1*KO mice provide evidence for an important role of the ADRB1 axis in the cardioprotective effect of metoprolol. Metoprolol effect on migration was absent when evaluating *Adrb1*KO neutrophils, and in the peritonitis assay, the inhibitory effect of metoprolol on neutrophil infiltration was lost in *Adrb1*KO mice. The rescue of this inhibitory effect in chimeric animals in which *Adrb1* is expressed only in circulating cells (that is, in *Adrb1*KO animals transplanted with wild-type BM) demonstrates that the cellular target of metoprolol action to alter neutrophil dynamics is of hematopoietic origin, and rules out an involvement of other cellular compartments (vascular, nervous or muscular). More importantly, the

conclusion obtained from subjecting BM transplant mice to myocardial IR injury model, resulted to be in agreement: metoprolol exerts no cardioprotection in the absence of ADRB1 and this effect is rescued when ADRB1 is present only in the hematopoietic compartment. Finally, experiments developed in vitro on *Adrb2KO* mice with no significant effect exerted by metoprolol ruled out the involvement of ADRB2. Altogether, these results demonstrate the essential role of neutrophil ADRB1 blockade in the protective effect that metoprolol exerts against AMI, specially, against acute inflammatory-associated IR injury processes. In contrast to the data obtained and here presented, a prior study suggested that metoprolol abrogated neutrophil migration *in vitro* in an apparently ADRB1-independent manner (65), since metoprolol was able to inhibit neutrophil migration even in the presence of the β-adrenergic receptor agonist orciprenaline. The in vitro incubation conditions (pH, temperature and concentration) could have affected orciprenaline sensibility and affinity to other ADRBs and subsequently alter the related signalling pathways. In this doctoral thesis, genetically modified mice lacking ADRB1 receptor (*Adrb1*KO) were used to provide strong in vivo and in vitro data showing the indispensable role of ADRB1 in the modulation of neutrophil function. The absence of cardioprotective effect observed when using *Adrb1*KO, which ensures absence of ADRB1, helps clarify the essential role of ADRB1 in this cardioprotective therapy in vivo and *in vitro*.

IR injury-associated inflammation requires neutrophils to migrate and to subsequently infiltrate into the injured tissue. This complex process starts when endothelial stress signals favour neutrophil recruitment and attachment to the reperfused injured capillaries. This is followed by development of neutrophil structural changes, characterized by lumen-oriented PSGL1 polarized clusters protrusions, through which effective neutrophil-platelet interactions occur, and the consequent infiltration initiation (35). *In vitro* results presented in this dissertation confirmed previous data. First, the transwell migration assays confirmed the ability of metoprolol to inhibit migration on isolated neutrophils (65). Second, incubation of metoprolol inhibited endogenous, and deleterious to endothelial function, ROS production from neutrophils (65). This inhibitory effect on neutrophil function was

reinforced by the acute in vivo murine peritonitis experiments, in which a single metoprolol i.v. injection abrogates thioglycolate-induced neutrophil infiltration into the peritoneal cavity evaluated at 16 hours. Next, the IVM confocal imaging experiments revealed that metoprolol rapidly abrogates functional PSGL1 polarized clusters reducing essential neutrophil-platelet effective interactions. This correlated with the alteration of the essential-for-infiltration motile and structural properties, including migratory velocity and directionality. In agreement with these in vivo results, in the murine myocardial IR injury model, metoprolol reduced the number of neutrophil-platelet coaggregates that occlude myocardial vessels. In addition, metoprolol's inability to provide additional protection after blockade of neutrophil-platelet interactions with the anti-PSGL1 mAB is compelling evidence for interference in this interaction as the mechanism underlying the infarct-limiting action of metoprolol during myocardial IR injury. Finally, the demonstration that incubation of healthy volunteers and acute coronary syndrome patients' blood samples with metoprolol inhibited neutrophil-platelet interactions suggests that this mechanism also operates in humans. There is controversy on the direct effect of metoprolol on platelet aggregation. Old studies suggested that metoprolol was able to inhibit ADP- and epinephrine-mediated platelet aggregation (118). However, recent studies did not show any anti-platelet effect of metoprolol (119). In line with the latter evidence, this doctoral thesis shows metoprolol to have no effect on platelet aggregation or in platelet activation in humans again proving strong evidence that the inhibitory effect of metoprolol on neutrophil-platelet aggregates is driven by a direct effect on activated neutrophils. In the flow cytometry studies, we defined a positive neutrophil–platelet interaction as CD14neg, $CD45^{+}$, $CD61^{+}$ particles. It should be noted that there are more specific neutrophil markers and thus our selection is a limitation of these experiments. However, given that all data (human and mouse) point to the same direction, we think this limitation did not have an impact on the conclusions obtained in these experiments.

The role of neutrophils in experimental IR injury is well established; however, the negative results of clinical trials with anti-inflammatory therapies (e.g.

C5a, (120) (121) CD-18 (122)) dampened hopes for this pharmacological strategy (36), and suggested that parallel mechanisms driving myocardial injury were at play. The demonstration that neutrophil dynamics in general and neutrophil-platelet interactions in particular are the target for the protective actions of metoprolol administered to patients during AMI reinstates neutrophils as a potential target for the therapeutic reduction of infarct size.

Limitations

The main conclusion presented in this doctoral thesis is that metoprolol impedes neutrophils actions upon reperfusion. We show that these phenomena are ADRB1-mediated. However, how the metoprolol-ADRB1 binding occurs and how this influences the intracellular signaling cascade within the circulation neutrophils is still a matter of study. A better understanding of metoprolol-ADRBs binding and intracellular signaling would help to develop new pharmacological interventions directed to accurately modulate the inflammatory-associated processes, and thus improve prognosis of patients.

Despite this work include studies in human cells and MVO evaluation in patients, the extrapolation of the experimental results to the clinic should be done with caution. The differences between the mouse model IR developed in this doctoral thesis, where an open-heart surgery is performed to pass a ligature around the LAD coronary artery, with the AMI in humans are not trivial. Nevertheless, this model is based on temporal coronary occlusion and has important similarities with the sequentially orchestrated leukocyte migration courses described in the most accurate experimental AMI models (22) (23) making it the best of its class for AMI fundamental pathological processes study.

*Adrb1*KO mice and the BM transplant procedures contributed in an invaluable way to elucidate the involvement of ADRB1 in hematopoietic compartment as crucial for metoprolol's cardioprotective effect. However, it is worth mention that ADRB1 was absent in all the hematopoietic compartment, and not only in the circulating neutrophils. In these sense, having neutrophil-specific *Adrb1*KO

mice would have been a better tool, since it would have avoided having to perform BM transplants, and would have ruled out a possible indirect effect of other inflammatory cells.

Conclusions/Conclusiones

1. Pre-reperfusion administration of i.v. metoprolol to AMI patients is associated with a significant less microvascular obstruction incidence and extent

2. The positive association between neutrophil counts and the incidence/extent of microvascular obstruction in AMI patients is blunted by the pre-reperfusion administration of i.v. metoprolol

3. In a mouse model of myocardial ischemia/reperfusion, pre-reperfusion administration of i.v. metoprolol reduces infarct size and the extent of microvascular obstruction

4. The infarct-limiting effect of metoprolol is abolished in mice lacking *adrb1*, in neutrophil-depleted mice and when neutrophils are prevented from interacting with platelets

5. Pre-reperfusion administration of i.v. metoprolol inhibits deleterious neutrophil inflammatory responses

6. These results identify neutrophil dynamics as a target of the cardioprotective effect of metoprolol against myocardial IR injury

7. Identification of the essential role of ADRB1 in hematopoietic cells during acute injury and the protective role upon its modulation offers potential for new therapeutic strategies development

1. La administración previa a la reperfusión de metoprolol intravenoso en pacientes con IAM se asocia con una incidencia y extensión de obstrucción microvascular significativamente menor

2. La asociación positiva observada entre las cuentas de neutrófilos en sangre y la incidencia/extensión de la obstrucción microvascular en pacientes con IAM es mitigada por la administración previa a la reperfusión de metoprolol intravenoso

3. En un modelo isquemia/reperfusión miocárdica en ratón, el metoprolol intravenoso administrado previo a la reperfusión reduce el tamaño de infarto y la cantidad de la obstrucción microvascular

4. El efecto limitante del infarto que ejerce el metoprolol se ve abolido en ratones que carecen del gen *adrb1*, en ratones con depleción de neutrófilos y cuando se bloquea la interacción de los neutrófilos con las plaquetas

5. La administración previa a la reperfusión de metoprolol intravenoso inhibe las respuestas inflamatorias perjudiciales de los neutrófilos

6. Estos resultados identifican la dinámica y función de los neutrófilos como diana del efecto cardioprotector del metoprolol contra el daño por reperfusión miocárdico

7. La identificación del papel fundamental de ADRB1 en las células hematopoyéticas durante la lesión aguda y el papel protector sobre su modulación ofrece potencial para el desarrollo de nuevas estrategias terapéuticas

References

1. Department of Health Statistics and Informatics in the Information, Evidence and Research Cluster. *The global burden of disease 2004 (update).* WHO. 2004.

2. *Prevalence of total coronary occlusion during the early hours of transmural myocardial infarction.* DeWood MA, Spores J, Notske R, Mouser LT, Burroughs R, Golden MS, Lang HT. N Engl J Med, 1980, Vol. 303 (16), pp. 897-902.

3. *Myocardial reperfusion injury.* Yellon, DM and Hausenloy, DJ. N Engl J Med, 2007, Vol. 357(11), pp. 1121-35.

4. *The use of periinfarct contrast-enhanced cardiac magnetic resonance imaging for the prediction of late postmyocardial infarction ventricular dysfunction.* Rubenstein JC, Ortiz JT, Wu E, Kadish A, Passman R, Bonow RO, Goldberger JJ. American Heart Journal, Vol. 2008(156), pp. 498-505 .

5. *Factors involved in salvaging ischemic myocardium: effect of reperfusion of arterial blood.* Jennings, RB & Reimer, KA. Circulation, 1983, Vol. 68, pp. 25–36.

6. *Effectiveness of intravenous thrombolytic treatment in acute myocardial infarction. Gruppo Italiano per lo Studio della Streptochinasi nell'Infarto Miocardico (GISSI). .* Lancet, 1986, Vol. 1, pp. 397–402.

7. *Acute myocardial infarction.* GW, Reed and Rossi, JE and Cannon, CP. Lancet, 2017, Vol. 389, pp. 197-210.

8. *Evolving therapies for myocardial ischemia/reperfusion injury.* Ibanez B, Heusch G, Ovize M and Van de Werf F. J Am Coll Cardiol, 2015, Vol. 65, pp. 1454-1471.

9. *2017 ESC Guidelines for the management of acute myocardial infarction in patients presenting with ST-segment elevation: The Task Force for the management of acute myocardial infarction in patients presenting with ST-segment elevation of the European Society of Cardiology (ESC).* Borja Ibanez, Stefan James, Stefan Agewall, Manuel J Antunes, Chiara Bucciarelli-Ducci, Héctor Bueno, Alida L P Caforio, Filippo Crea, John A Goudevenos, Sigrun

Halvorsen, Gerhard Hindricks, Adnan Kastrati, Mattie J Lenzen, Eva Prescott, Marco Roffi, Marco Valgimigli, Christoph Varenhorst, Pascal Vranckx, Petr Widimský, ESC Scientific Document Group. Eur Heart J., 2017.

10. *Myocardial infarction and the open-artery hypothesis.* Hillis, LD and Lange, RA. N Engl J Med, 2006, Vol. 355(23), pp. 2475-7.

11. *The pathophysiology of acute myocardial infarction and strategies of protection beyond reperfusion: a continual challenge.* Heusch, G and Gersh, BJ. Eur Heart J, 2017, Vol. 38(11), pp. 774-784.

12. *Cardioprotection: chances and challenges of its translation to the clinic.* Heusch, G. Lancet, 2013, Vol. 381, pp. 166-175.

13. *Current state of clinical translation of cardioprotective agents for acute myocardial infarction.* Kloner, RA. Circ Res, 2013, Vol. 113, pp. 451-463.

14. *Novel targets and future strategies for acute cardioprotection: Position Paper of the European Society of Cardiology Working Group on Cellular Biology of the Heart.* Hausenloy DJ, Garcia-Dorado D, Botker HE, Davidson SM, Downey J, Engel FB, Jennings R, Lecour S, Leor J, Madonna R, Ovize M, Perrino C, Prunier F, Schulz R, Sluijter JPG, Van Laake LW, Vinten-Johansen J, Yellon DM, Ytrehus K, Heusch G and Ferdinandy P. Cardiovasc Res, 2017, Vol. 113, pp. 564-585.

15. *Coronary artery reperfusion. I. Early effects on local myocardial function and the extent of myocardial necrosis.* Maroko PR, Libby P, Ginks WR, Bloor CM, Shell WE, Sobel BE, Ross J Jr. J Clin Invest, 1972, Vol. 51(10), pp. 2710-6.

16. *Coronary artery reperfusion. II. Reduction of myocardial infarct size at 1 week after the coronary occlusion.* Ginks WR, Sybers HD, Maroko PR, Covell JW, Sobel BE, Ross J Jr. J Clin Invest, 1972, Vol. 51(10), pp. 2717-23.

17. *Reperfusion conditions: importance of ensuring gentle versus sudden reperfusion during relief of coronary occlusion.* Okamoto F, Allen BS, Buckberg

GD, Bugyi H, Leaf J. J Thorac Cardiovasc Surg, 1986, Vol. 92(3 Pt 2), pp. 613-20.

18. *Inhibition of myocardial injury by ischemic postconditioning during reperfusion: comparison with ischemic preconditioning.* Zhao ZQ, Corvera JS, Halkos ME, Kerendi F, Wang NP, Guyton RA, Vinten-Johansen J. Am J Physiol Heart Circ Physiol, 2003, Vol. 285(2), pp. H579-88.

19. *Postconditioning improves postischemic cardiac dysfunction independently of norepinephrine overflow after reperfusion in rat hearts: comparison with preconditioning.* Tawa M, Fukumoto T, Yamashita N, Ohkita M, Ayajiki K, Okamura T, Matsumura Y. J Cardiovasc Pharmacol, 2010, Vol. 55(1), pp. 6-13.

20. *Comparison of cardioprotective and anti-inflammatory effects of ischemia pre- and postconditioning in rats with myocardial ischemia-reperfusion injury.* Xiong J, Wang Q, Xue FS, Yuan YJ, Li S, Liu JH, Liao X, Zhang YM. Inflamm Res, 2011, Vol. 60(6), pp. 547-54.

21. *Effect of Ischemia Duration and Protective Interventions on the Temporal Dynamics of Tissue Composition After Myocardial Infarction.* Fernández-Jiménez R, Galán-Arriola C, Sánchez-González J, Agüero J, López-Martín GJ, Gomez-Talavera S, Garcia-Prieto J, Benn A, Molina-Iracheta A, Barreiro-Pérez M, Martin-García A, García-Lunar I, Pizarro G, Sanz J, Sánchez PL, Fuster V, Ibanez B. Circ Res, 2017, Vol. 121(4), pp. 439-450.

22. *Myocardial edema after ischemia/reperfusion is not stable and follows a bimodal pattern: imaging and histological tissue characterization.* Fernández-Jiménez R, Sánchez-González J, Agüero J, García-Prieto J, López-Martín GJ, García-Ruiz JM, Molina-Iracheta A, Rosselló X, Fernández-Friera L, Pizarro G, García-Álvarez A, Dall'Armellina E, Macaya C, Choudhury RP, Fuster V, Ibáñez B. J Am Coll Cardiol, 2015, Vol. 65(4), pp. 315-23.

23. *Pathophysiology Underlying the Bimodal Edema Phenomenon After Myocardial Ischemia/Reperfusion.* Fernández-Jiménez R, García-Prieto J, Sánchez-González J, Agüero J, López-Martín GJ, Galán-Arriola C, Molina-

Iracheta A, Doohan R, Fuster V, Ibáñez B. J Am Coll Cardiol, 2015, Vol. 66(7), pp. 816-28.

24. *Dynamic Edematous Response of the Human Heart to Myocardial Infarction: Implications for Assessing Myocardial Area at Risk and Salvage.* Fernández-Jiménez R, Barreiro-Pérez M, Martin-García A, Sánchez-González J, Agüero J, Galán-Arriola C, García-Prieto J, Díaz-Pelaez E, Vara P, Martinez I, Zamarro I, Garde B, Sanz J, Fuster V, Sánchez PL, Ibanez B. Circulation, 2017, Vol. 36(14), pp. 1288-1300.

25. *Lethal myocardial reperfusion injury: a necessary evil?* Ibanez B, Fuster V, Jimenez-Borreguero J and Badimon JJ. Int J Cardiol, 2011, Vol. 151, pp. 3-11.

26. *Lethal reperfusion injury in acute myocardial infarction: facts and unresolved issues.* Garcia-Dorado, D., M. Ruiz-Meana, and H.M. Piper, Cardiovasc Res, 2009, Vol. 83(2), pp. 165-8.

27. *Ischemia and reperfusion-from mechanism to translation.* Eltzschig, HK and Eckle, T. Nat Med, 2011, Vol. 17(11), pp. 1391-401.

28. *Factors influencing infarct size following experimental coronary artery occlusions.* Maroko PR, Kjekshus JK, Sobel BE, Watanabe T, Covell JW, Ross J Jr, Braunwald E. Circulation, 1971, Vol. 43(1), pp. 67-82.

29. *Impact of ischemia and reperfusion times on myocardial infarct size in mice in vivo.* Redel A, Jazbutyte V, Smul TM, Lange M, Eckle T, Eltzschig H, Roewer N, Kehl F. Exp Biol Med (Maywood), 2008, Vol. 233(1), pp. 84-93.

30. *The future: therapy of myocardial protection.* Sanz-Rosa D, García-Prieto J, Ibanez B. 2012, Vol. 1254, pp. 90-8.

31. *The neutrophil in vascular inflammation.* Phillipson M, Kubes P. Nat Med, 2011, Vol. 17(11), pp. 1381-90.

32. *Getting to the site of inflammation: the leukocyte adhesion cascade updated.* Ley K, Laudanna C, Cybulsky MI, Nourshargh S. Nat Rev Immunol, 2007, Vol. 7, pp. 678–689.

33. *Intraluminal crawling of neutrophils to emigration sites: a molecularly distinct process from adhesion in the recruitment cascade.* Phillipson M, Heit B, Colarusso P, Liu L, Ballantyne CM, Kubes P. J Exp Med, 2006, Vol. 203(12), pp. 2569–2575.

34. *Eukaryotic chemotaxis: a network of signaling pathways controls motility, directional sensing, and polarity.* Swaney KF, Huang CH, Devreotes PN. Annu Rev Biophys, 2010, Vol. 39, pp. 265–289.

35. *Neutrophils scan for activated platelets to initiate inflammation.* Sreeramkumar V, Adrover JM, Ballesteros I, Cuartero MI, Rossaint J, Bilbao I, Nácher M, Pitaval C, Radovanovic I, Fukui Y, McEver RP, Filippi MD, Lizasoain I, Ruiz-Cabello J, Zarbock A, Moro MA, Hidalgo A. 2014, Science, Vol. 346(6214), pp. 1234-8.

36. *Involvement of neutrophils in the pathogenesis of lethal myocardial reperfusion injury.* Vinten-Johansen, J. Cardiovasc Res, 2004, Vol. 61(3), pp. 481-97.

37. *The production of cytokines by polymorphonuclear neutrophils.* Cassatella, M.A. Immunol Today, 1995, Vol. 16, pp. 21-6.

38. *Leukocyte behavior in atherosclerosis, myocardial infarction, and heart failure.* Swirski FK and Nahrendorf M. 6116, Science, 2013, Vol. 339, pp. 161-6.

39. *Neutrophil AKT2 regulates heterotypic cell-cell interactions during vascular inflammation.* Li J, Kim K, Hahm E, Molokie R, Hay N, Gordeuk VR, Du X, Cho J. 4, J Clin Invest, 2014, Vol. 124, pp. 1483-96.

40. *The HMGB1/RAGE axis triggers neutrophil-mediated injury amplification following necrosis.* Huebener P, Pradere JP, Hernandez C, Gwak GY, Caviglia JM, Mu X, Loike JD, Jenkins RE, Antoine DJ, Schwabe RF. 2, J Clin Invest, 2015, Vol. 125, pp. 539-50.

41. *The no-reflow phenomenon: A basic mechanism of myocardial ischemia and reperfusion.* Reffelmann, T. and R.A. Kloner, Basic Res Cardiol, 2006, Vol. 101(5), pp. 359-72.

42. *An intense and short-lasting burst of neutrophil activation differentiates early acute myocardial infarction from systemic inflammatory syndromes.* Maugeri N, Rovere-Querini P, Evangelista V, Godino C, Demetrio M, Baldini M, Figini F, Coppi G, Slavich M, Camera M, Bartorelli A, Marenzi G, Campana L, Baldissera E, Sabbadini MG, Cianflone D, Tremoli E, D'Angelo A, Manfredi AA, Maseri A. PLoS One, 2012, Vol. 7(6), p. e39484.

43. *Comprehensive prognosis assessment by CMR imaging after ST-segment elevation myocardial infarction.* Eitel I, de Waha S, Wöhrle J, Fuernau G, Lurz P, Pauschinger M, Desch S, Schuler G, Thiele H. J Am Coll Cardiol, 2014, Vol. 64(12), pp. 1217-26.

44. *Adrenergic Nervous System in Heart Failure Pathophysiology and Therapy.* Lymperopoulos, et al. 6, Circ Res, 2013, Vol. 13, pp. 739-53.

45. *Evolution of β-blockers: from anti-anginal drugs to ligand-directed signalling.* Jillian G. Baker, Stephen J. Hill, Roger J. Summers. Trends Pharmacol Sci., 2011, Vols. 32(4-2), pp. 227–234.

46. *G-protein coupled receptors. Nobel Prize 2012 for chemistry to Robert J. Lefkowitz and Brian Kobilka.* Bockaert J. Med Sci (Paris), 2012, Vol. 28(12), pp. 1133-7.

47. *Activation and blockade of beta adrenoceptors in common cardiac disorders.* Black JW, Prichard BN. Br Med Bull, 1973, Vols. 9(2)2:163-7.

48. *James Black: Nobel prize winning pharmacologist who invented β blockers.* J., Lyall. Br. Med. J., 2010, Vol. 340:c1817.

49. *Beta-adrenergic receptors and their interacting proteins.* Hall, RA. Cell Dev. Biol., 2004, Vol. 15, pp. 281–288.

50. *THE CONCISE GUIDE TO PHARMACOLOGY 2017/18: G protein-coupled receptors.* Alexander SP, Christopoulos A, Davenport AP, Kelly E, Marrion NV,

Peters JA, Faccenda E, Harding SD, Pawson AJ, Sharman JL, Southan C, Davies JA and Collaborators., CGTP. Br J Pharmacol, 2017, Vol. 174 Suppl 1, pp. S17-S129.

51. *Structure of a β1-adrenergic G-protein-coupled receptor.* Warne T, Serrano-Vega MJ, Baker JG, Moukhametzianov R, Edwards PC, Henderson R, Leslie AG, Tate CG, Schertler GF. Nature, 2008, Vol. 454, pp. 486–491.

52. *The structural basis for agonist and partial agonist action on a β(1)-adrenergic receptor.* Warne T, Moukhametzianov R, Baker JG, Nehmé R, Edwards PC, Leslie AG, Schertler GF, Tate CG. Nature, 2011, Vol. 469(7329), pp. 241-4.

53. *Structural insights into adrenergic receptor function and pharmacology.* BK, Kobilka. Trends in Pharmacological Sciences, 2011, Vol. 32(4), pp. 213-218.

54. *The selectivity of beta-adrenoceptor antagonists at the human beta1, beta2 and beta3 adrenoceptors.* Baker JG. Br J Pharmacol., 2005, Vol. 144(3), pp. 317-22.

55. *Site of action of beta-ligands at the human beta1-adrenoceptor.* Baker JG. J Pharmacol Exp Ther., 2005, Vol. 313(3), pp. 1163-71.

56. *Evidence for a secondary state of the human beta3-adrenoceptor.* Baker JG. Mol Pharmacol., 2005, Vol. 68(6), pp. 1645-55.

57. *Phagocyte-derived catecholamines enhance acute inflammatory injury.* Flierl MA, Rittirsch D, Nadeau BA, Chen AJ, Sarma JV, Zetoune FS, McGuire SR, List RP, Day DE, Hoesel LM, Gao H, Van Rooijen N, Huber-Lang MS, Neubig RR, Ward PA. 7163, Nature, 2007, Vol. 449, pp. 721-5.

58. *Adrenergic modulation of immune cells: an update.* Marino, F. and M. Cosentino,. 1, Amino Acids, 2013, Vol. 45, pp. 55-71.

59. *Norepinephrine and beta 2-adrenergic receptor stimulation regulate CD4+ T and B lymphocyte function in vitro and in vivo.* Kohm, A.P. and V.M. Sanders,. Pharmacol Rev, 201, Vol. 53(4), pp. 487-525.

60. *Stress-induced effects, which inhibit host defenses, alter leukocyte trafficking.* Zieziulewicz TJ, Mondal TK, Gao D, Lawrence DA. Cell Stress Chaperones, 2013, Vol. 18(3), pp. 279-91.

61. *Catecholamine stress alters neutrophil trafficking and impairs wound healing by beta2-adrenergic receptor-mediated upregulation of IL-6.* Kim MH, Gorouhi F, Ramirez S, Granick JL, Byrne BA, Soulika AM, Simon SI, Rivkah Isseroff R. J Invest Dermatol, 2014, Vol. 134(3), pp. 809-17.

62. *Adrenergic modulation of migration, CD11b and CD18 expression, ROS and interleukin-8 production by human polymorphonuclear leukocytes.* Scanzano A, Schembri L, Rasini E, Luini A, Dallatorre J, Legnaro M, Bombelli R, Congiu T, Cosentino M, Marino F. Inflamm Res., 2015, Vol. 64(2), pp. 127-35.

63. *Epinephrine enhances platelet-neutrophil adhesion in whole blood in vitro.* Horn NA, Anastase DM, Hecker KE, Baumert JH, Robitzsch T, Rossaint R. 2, Anesth Analg, 2005, Vol. 100, pp. 520-6.

64. *Inhibition of neutrophil migration and oxygen free radical release by metipranolol and timolol.* Djanani A, Kaneider NC, Meierhofer C, Sturn D, Dunzendorfer S, Allmeier H, Wiedermann CJ. Pharmacology, 2003, Vol. 68(4), pp. 198-203.

65. *Modulation of neutrophil migration and superoxide anion release by metoprolol.* Dunzendorfer, S and Wiedermann, CJ. J Mol Cell Cardiol, 2000, Vol. 32(6), pp. 915-24.

66. *Effects of two antihypertensive agents, labetalol and metoprolol, on the production of reactive oxygen species by normal polymorphonuclear leukocytes in vitro.* Jaboureck-Bouttier R, Gressier B, Dine T, Brunet C, Luyckx M, Harfaut P, Ballester L, Cazin M, Cazin JC. Hypertens Pregnancy, 1999, Vol. 18(3), pp. 239-47.

67. *Externalization of beta-adrenergic receptors promoted by myocardial ischemia.* Maisel AS, Motulsky HJ, Insel PA,. Science, 1985, Vol. 230(4722), pp. 183-6.

68. *Catecholamines in myocardial ischemia. Systemic and cardiac release.* Schomig, A.,. Circulation, 1990, Vol. 82(3), pp. II13-22.

69. *2017 ESC Guidelines for themanagement of acutemyocardial infarction in patients presenting with ST-segment elevation.* Cardiology, The Task Force for the management of acute myocardial infarction in patients presenting with ST-segment elevation of the European Society of. European Heart Journal, 2017, Vol. 00, pp. 1-66.

70. *Expert consensus document on beta-adrenergic receptor blockers.* López-Sendón J, Swedberg K, McMurray J, Tamargo J, Maggioni AP, Dargie H, Tendera M, Waagstein F, Kjekshus J, Lechat P, Torp-Pedersen C and Cardiology., Task ForceOn Beta-Blockers of the European Society of. Eur Heart J, 2004, Vol. 25, pp. 1341-62.

71. *Effect of early intravenous rt-PA on infarct size estimated from serum enzyme activity: results from the TEAHAT Study.* Risenfors M HM, Dellborg M, Luepker R, Hjalmarsson A, Swedberg K, Holmberg S, Herlitz J, J Intern Med Suppl , 1991, Vol. 734, pp. 11-8.

72. *Short-term effects of early intravenous treatment with a beta-adrenergic blocking agent or a specific bradycardiac agent in patients with acute myocardial infarction receiving thrombolytic therapy.* Van de Werf F, Janssens L, Brzostek T, Mortelmans L, Wackers FJ, Willems GM, Heidbüchel H, Lesaffre E, Scheys I, Collen D, Hilaire De Geest MD. J Am Coll Cardiol, 1993, Vol. 22, pp. 407-16.

73. *Early intravenous then oral metoprolol in 45,852 patients with acute myocardial infarction: randomised placebo-controlled trial.* Chen ZM, Pan HC, Chen YP, Peto R, Collins R, Jiang LX, Xie JX, Liu LS and group, COMMIT (ClOpidogrel and Metoprolol in Myocardial Infarction Trial) collaborative. Lancet, 2005, Vol. 366, pp. 1622-32.

74. *Randomized study on the efficacy and safety of landiolol, an ultra-short-acting beta1-adrenergic blocker, in patients with acute myocardial infarction undergoing primary percutaneous coronary intervention.* Hanada K, Higuma T,

Nishizaki F, Sukekawa T, Yokota T, Yamada M, Saito S, Kushibiki M, Oikawa K, Abe N, Tomita H, Osanai T, Okumura K. Circulation journal: official journal of the Japanese Circulation Society , 2012, Vol. 76, pp. 439-45.

75. *Effects of prior beta-blocker therapy on clinical outcomes after primary coronary angioplasty for acute myocardial infarction.* Harjai KJ, Stone GW, Boura J, Grines L, Garcia E, Brodie B, Cox D, O'Neill WW, Grines C. Am J Cardiol, 2003, Vol. 91, pp. 655-60.

76. *Impact of intravenous beta-blockade before primary angioplasty on survival in patients undergoing mechanical reperfusion therapy for acute myocardial infarction.* Halkin A, Grines CL, Cox DA, Garcia E, Mehran R, Tcheng JE, Griffin JJ, Guagliumi G, Brodie B, Turco M, Rutherford BD, Aymong E, Lansky AJ, Stone GW. J Am Coll Cardiol, 2004, Vol. 43(10), pp. 1780-7.

77. *Impact of Pre-Procedural Beta Blockade on Inpatient Mortality in Patients Undergoing Primary Percutaneous Coronary Intervention for ST Elevation Myocardial Infarction.* Valle JA, Zhang M, Dixon S, Aronow HD, Share D, Naoum JB, Gurm HS. 12, Am J Cardiol, 2013, Vol. 111, pp. 1714-20.

78. *Drug therapy: metoprolol.* Koch-Weser, J,. N Engl J Med, 1979, Vol. 301(13), pp. 698-703.

79. *Health and cost benefits associated with the use of metoprolol in heart attack patients.* Fernandez-Jimenez, R, Ibanez B. Expert Rev Clin Pharmacol, 2014, Vol. 7(6), pp. 687-9.

80. *Early metoprolol administration before coronary reperfusion results in increased myocardial salvage: analysis of ischemic myocardium at risk using cardiac magnetic resonance.* Ibanez B, Prat-González S, Speidl WS, Vilahur G, Pinero A, Cimmino G, García MJ, Fuster V, Sanz J, Badimon JJ. Circulation, 2007, Vol. 115(23), pp. 2909-16.

81. *The cardioprotection granted by metoprolol is restricted to its administration prior to coronary reperfusion.* Ibanez B, Cimmino G, Prat-González S, Vilahur G, Hutter R, García MJ, Fuster V, Sanz J, Badimon L, Badimon JJ. Int. J. Cardiol, 2011, Vol. 147, pp. 428–432.

82. *Effect of early metoprolol on infarct size in ST-segment-elevation myocardial infarction patients undergoing primary percutaneous coronary intervention: the Effect of Metoprolol in Cardioprotection During an Acute Myocardial Infarction (METOCARD-CNIC) trial.* Ibanez B, Macaya C, Sánchez-Brunete V, Pizarro G, Fernández-Friera L, Mateos A, Fernández-Ortiz A, García-Ruiz JM, García-Álvarez A, Iñiguez A, Jiménez-Borreguero J, López-Romero P, Fernández-Jiménez R, Goicolea J, Ruiz-Mateos B, Bastante T, Arias M, Iglesias-Vázquez JA, Rodriguez MD, Escalera N, Acebal C, Cabrera JA, Valenciano J, Pérez de Prado A, Fernández-Campos MJ, Casado I, García-Rubira JC, García-Prieto J, Sanz-Rosa D, Cuellas C, Hernández-Antolín R, Albarrán A, Fernández-Vázquez F, de la Torre-Hernández JM, Pocock S, Sanz G, Fuster V. Circulation, 2013, Vol. 128(14), pp. 1495-503.

83. *Long-term benefit of early pre-reperfusion metoprolol administration in patients with acute myocardial infarction: results from the METOCARD-CNIC trial (Effect of Metoprolol in Cardioprotection During an Acute Myocardial Infarction).* Pizarro G, Fernandez-Friera L, Fuster V, Fernandez-Jimenez R, Garcia-Ruiz JM, Garcia-Alvarez A, Mateos A, Barreiro MV, Escalera N, Rodriguez MD, de MiguelA, Garcia-Lunar I, Parra-Fuertes JJ, Sanchez-Gonzalez J, Pardillos L, Nieto B, Jimenez A, Abejon R, Bastante T, Martinez de Vega V, Cabrera JA, Lopez-Melgar B, Guzman G, Garcia-Prieto J, Mirelis JG, Zamorano JL, Albarran A, Goicolea J, Escaned J, Pocock S, Iniguez A, Fernandez-Ortiz A, Sanchez-Brunete V, Macaya C and Ibanez B. J Am Coll Cardiol, 2014, Vol. 63(22), pp. 2356-62.

84. *Block the ischemia and reperfusion damage: an old adjunctive drug for a new reperfusion strategy.* Antoniucci D, J Am Coll Cardiol, 2014, Vol. 63(22), pp. 2363-4.

85. *Early Intravenous Beta-Blockers in Patients With ST-Segment Elevation Myocardial Infarction Before Primary Percutaneous Coronary Intervention.* Roolvink V, Ibáñez B, Ottervanger JP, Pizarro G, van Royen N, Mateos A, Dambrink JE, Escalera N, Lipsic E, Albarran A, Fernández-Ortiz A, Fernández-Avilés F, Goicolea J, Botas J, Remkes W, Hernandez-Jaras V, Kedhi E, Zamorano JL, Navarro F, Alfonso F, García-Lledó A, Alonso J, van Leeuwen M,

Nijveldt R, Postma S, Kolkman E, Gosselink M, de Smet B, Rasoul S, Piek JJ, Fuster V, van 't Hof AWJ and Investigators., EARLY-BAMI. J Am Coll Cardiol, 2016, Vol. 67(23), pp. 2705-2715.

86. *Study design for the "effect of METOprolol in CARDioproteCtioN during an acute myocardial InfarCtion" (METOCARD-CNIC): a randomized, controlled parallel-group, observer-blinded clinical trial of early pre-reperfusion metoprolol administration in ST-segment elevation myocardial infarction.* Ibanez B, Fuster V, Macaya C, Sánchez-Brunete V, Pizarro G, López-Romero P, Mateos A, Jiménez-Borreguero J, Fernández-Ortiz A, Sanz G, Fernández-Friera L, Corral E, Barreiro MV, Ruiz-Mateos B, Goicolea J, Hernández-Antolín R, Acebal C, García-Rubira JC, Albarrán A, Zamorano JL, Casado I, Valenciano J, Fernández-Vázquez F, de la Torre JM, Pérez de Prado A, Iglesias-Vázquez JA, Martínez-Tenorio P, Iñiguez A. 4, Am Heart J, 2012, Vol. 164, pp. 473-480 e5.

87. *Insertion of enhanced green fluorescent protein into the lysozyme gene creates mice with green fluorescent granulocytes and macrophages.* Faust N, Varas F, Kelly LM, Heck S, Graf T. Blood, 2000, Vol. 96(2), pp. 719-26.

88. *Rhythmic modulation of the hematopoietic niche through neutrophil clearance.* Casanova-Acebes M, Pitaval C, Weiss LA, Nombela-Arrieta C, Chèvre R, A-González N, Kunisaki Y, Zhang D, van Rooijen N, Silberstein LE, Weber C, Nagasawa T, Frenette PS, Castrillo A, Hidalgo A. Cell, 2013, Vol. 153(5), pp. 1025-35.

89. *beta3 adrenergic receptor selective stimulation during ischemia/reperfusion improves cardiac function in translational models through inhibition of mPTP opening in cardiomyocytes.* García-Prieto J, García-Ruiz JM, Sanz-Rosa D, Pun A, García-Alvarez A, Davidson SM, Fernández-Friera L, Nuno-Ayala M, Fernández-Jiménez R, Bernal JA, Izquierdo-Garcia JL, Jimenez-Borreguero J, Pizarro G, Ruiz-Cabello J, Macaya C, Fuster V, Yellon DM, Ibanez B. Basic Res Cardiol, 2014, Vol. 109(4), p. 422.

90. *Tumor-mediated liver X receptor-alpha activation inhibits CC chemokine receptor-7 expression on dendritic cells and dampens antitumor responses.* Villablanca EJ, Raccosta L, Zhou D, Fontana R, Maggioni D, Negro A, Sanvito F,

Ponzoni M, Valentinis B, Bregni M, Prinetti A, Steffensen KR, Sonnino S, Gustafsson JA, Doglioni C, Bordignon C, Traversari C, Russo V. Nat Med, 2010, Vol. 16(1), pp. 98-105.

91. *Measurement of oxidative burst in neutrophils.* Chen, Y. and W.G. Junger,. Methods Mol Biol, 2012, Vol. 844, pp. 115-24.

92. *A peptide with unique receptor specificity: stimulation of phosphoinositide hydrolysis and induction of superoxide generation in human neutrophils.* Seo JK, Choi SY, Kim Y, Baek SH, Kim KT, Chae CB, Lambeth JD, Suh PG, Ryu SH. J Immunol, 1997, Vol. 158(4), pp. 1895-901.

93. *Clopidogrel inhibits platelet-leukocyte interactions and thrombin receptor agonist peptide-induced platelet activation in patients with an acute coronary syndrome.* Xiao, Z. and P. Theroux,. J Am Coll Cardiol, 2004, Vol. 43(11), pp. 1982-8.

94. *An increased platelet-leukocytes interaction at the culprit site of coronary artery occlusion in acute myocardial infarction: a pathogenic role for "no-reflow" phenomenon?* Botto, N., Sbrana S, Trianni G, Andreassi MG, Ravani M, Rizza A, Al-Jabri A, Palmieri C, Berti S. Int J Cardiol,, 2007, Vol. 117(1), pp. 123-30.

95. *Antiplatelet Agents Inhibit the Generation of Platelet-Derived Microparticles.* Giacomazzi A, Degan M, Calabria S, Meneguzzi A, Minuz P. Front Pharmacol, 2016, Vol. 7, p. 314.

96. *Multicolor flow cytometry for evaluation of platelet surface antigens and activation markers.* van Velzen JF, Laros-van Gorkom BA, Pop GA, van Heerde WL. Thromb Res, 2012, Vol. 130(1), pp. 92-8.

97. *Study design for the "effect of METOprolol in CARDioproteCtioN during an acute myocardial InfarCtion" (METOCARD-CNIC): a randomized, controlled parallel-group, observer-blinded clinical trial of early pre-reperfusion metoprolol administration in ST-segment elevation myocardial infarction.* Ibanez B, Fuster V, Macaya C, Sánchez-Brunete V, Pizarro G, López-Romero P, Mateos A, Jiménez-Borreguero J, Fernández-Ortiz A, Sanz G, Fernández-Friera

L, Corral E, Barreiro MV, Ruiz-Mateos B, Goicolea J, Hernández-Antolín R, Acebal C, García-Rubira JC, Albarrán A, Zamorano JL, Casado I, Valenciano J, Fernández-Vázquez F, de la Torre JM, Pérez de Prado A, Iglesias-Vázquez JA, Martínez-Tenorio P, Iñiguez A. Am Heart J, 2012, Vol. 164(4), pp. 473-480 e5.

98. *Association between white blood cell count, epicardial blood flow, myocardial perfusion, and clinical outcomes in the setting of acute myocardial infarction: a thrombolysis in myocardial infarction 10 substudy.* Barron HV, Cannon CP, Murphy SA, Braunwald E, Gibson CM. Circulation, 2000, Vol. 102(19), pp. 2329-34.

99. *Association between baseline neutrophil count, clopidogrel therapy, and clinical and angiographic outcomes in patients with ST-elevation myocardial infarction receiving fibrinolytic therapy.* O'Donoghue M, Morrow DA, Cannon CP, Guo W, Murphy SA, Gibson CM, Sabatine MS. Eur Heart J,, 2008, Vol. 29(8), pp. 984-91.

100. *Impact of leukocyte count on mortality and bleeding in patients with myocardial infarction undergoing primary percutaneous coronary interventions: analysis from the Harmonizing Outcome with Revascularization and Stent in Acute Myocardial Infarction trial.* Palmerini T, Mehran R, Dangas G, Nikolsky E, Witzenbichler B, Guagliumi G, Dudek D, Genereux P, Caixeta A, Rabbani L, Weisz G, Parise H, Fahy M, Xu K, Brodie B, Lansky A, Stone GW. Circulation, 2011, Vol. 123(24), pp. 2829-37, 7 p following 2837.

101. *Cocaine and catecholamines enhance inflammatory cell retention in the coronary circulation of mice by upregulation of adhesion molecules.* Chen Y, Ke Q, Xiao YF, Wu G, Kaplan E, Hampton TG, Malek S, Min JY, Amende I, Morgan JP. Am J Physiol Heart Circ Physiol, 2005, Vol. 288 (5), pp. H2323-31.

102. *Stress-induced redistribution of immune cells--from barracks to boulevards to battlefields: a tale of three hormones-Curt Richter Award winner.* Chen Y, Ke Q, Xiao YF, Wu G, Kaplan E, Hampton TG, Malek S, Min JY, Amende I, Morgan JP. Psychoneuroendocrinology, 2012, Vol. 37 (9), pp. 1345-68.

103. *Role of innate and adaptive immune mechanisms in cardiac injury and repair.* Epelman, S., P.P. Liu, and D.L. Mann,. Nat Rev Immunol, 2015, Vol. 15(2), pp. 117-29.

104. *The role of neutrophils in myocardial ischemia-reperfusion injury.* Jordan, J.E., Z.Q. Zhao, and J. Vinten-Johansen,. 4, Cardiovasc Res, 1999, Vol. 43, pp. 860-78.

105. *Neutrophil sandwiches injure the microcirculation.* Looney, M.R. and M.A. Matthay,. 4, Nat Med, 2009, Vol. 15, pp. 364-6.

106. *Do neutrophils contribute to myocardial reperfusion injury? .* Lefer, DJ. 4, Basic Res Cardiol, 2002, Vol. 97, pp. 263-7.

107. *Pro-inflammatory responses in human monocytes are beta1-adrenergic receptor subtype dependent.* Grisanti LA, Evanson J, Marchus E, Jorissen H, Woster AP, DeKrey W, Sauter ER, Combs CK, Porter JE. Mol Immunol, 2010, Vol. 47(6), pp. 1244-54.

108. *Leukocyte behavior in atherosclerosis, myocardial infarction, and heart failure.* M, Swirski FK and Nahrendorf. 6116, Science, 2013, Vol. 339, pp. 161-6.

109. *Intravenous beta-blockers in primary percutaneous coronary intervention: new hope for an old therapy.* Ndrepepa, G. and A. Kastrati, I. 14, Circulation, 2013, Vol. 128, pp. 1487-9.

110. *The impact of pre-primary percutaneous coronary intervention β blocker use on the no-reflow phenomenon in patients with acute myocardial infarction.* Wang J, Chen Y, Wang C, Zhu X. 2014, Vol. 42(10), pp. 822-6.

111. *Efficacy and safety of out-of-hospital intravenous metoprolol administration in anterior ST-segment elevation acute myocardial infarction: insights from the METOCARD-CNIC trial.* Mateos A, García-Lunar I, García-Ruiz JM, Pizarro G, Fernández-Jiménez R, Huertas P, García-Álvarez A, Fernández-Friera L, Bravo J, Flores-Arias J, Barreiro MV, Chayán-Zas L, Corral E, Fuster

V, Sánchez-Brunete V, Ibáñez B and Investigators., METOCARD-CNIC. 3, Ann Emerg Med, 2015, Vol. 65, pp. 318-24.

112. *Neutrophil recruitment and function in health and inflammation.* Kolaczkowska, E. and P. Kubes,. 3, Nat Rev Immunol, 2013, Vol. 13, pp. 159-175.

113. *The neutrophil in vascular inflammation.* Phillipson, M. and P. Kubes. Nat Med, 2011, Vol. 17(11), pp. 1381-90.

114. *Metoprolol treatment decreases tissue myeloperoxidase activity after spinal cord injury in rats.* Beril Gok H, Solaroglu I, Okutan O, Cimen B, Kaptanoglu E, Palaoglu S. J Clin Neurosci, 2007, Vol. 14(2), pp. 138-42.

115. *Inhibition of sepsis-induced inflammatory response by beta1-adrenergic antagonists.* Ibrahim-Zada I, Rhee P, Gomez CT, Weller J, Friese RS. J Trauma Acute Care Surg, 2014, Vol. 76(2), pp. 320-7; discussion 327-8.

116. *Adenyl cyclase in human leukocytes: evidence for activation by separate beta adrenergic and prostaglandin receptors.* Bourne, H.R. and K.L. Melmon,. J Pharmacol Exp Ther, 1971, Vol. 178(1), pp. 1-7.

117. *Lymphocyte blast transformation. I. Demonstration of adrenergic receptors in human peripheral lymphocytes.* Hadden, JW, Hadden, EM and Middleton, EJr.,. Cell Immunol, 1970, Vol. 1(6), pp. 583-95.

118. *Influence of some beta blockers (pindolol, atenolol, timolol and metoprolol) on aggregation and arachidonic acid metabolism in human platelets.* KC, Srivastava. 1, Prostaglandins Leukot Med, 1987, Vol. 29, pp. 79-84.

119. *Effects of nebivolol on platelet activation in hypertensive patients: a comparative study with metoprolol.* Celik T, Yuksel UC, Iyisoy A, Kursaklioglu H, Ozcan O, Kilic S, Ozmen N, Isik E. Int J Cardiol, 2007, Vol. 116(2), pp. 206-11.

120. *Pexelizumab for acute ST-elevation myocardial infarction in patients undergoing primary percutaneous coronary intervention: a randomized*

controlled trial. APEX AMI Investigators, Armstrong PW, Granger CB, Adams PX, Hamm C, Holmes D Jr, O'Neill WW, Todaro TG, Vahanian A, Van de Werf F. JAMA, 2007, Vol. 297(1), pp. 43-51.

121. *Pexelizumab, an anti-C5 complement antibody, as adjunctive therapy to primary percutaneous coronary intervention in acute myocardial infarction: the COMplement inhibition in Myocardial infarction treated with Angioplasty (COMMA) trial.* Granger CB, Mahaffey KW, Weaver WD, Theroux P, Hochman JS, Filloon TG, Rollins S, Todaro TG, Nicolau JC, Ruzyllo W, Armstrong PW and Investigators., COMMA. Circulation, 2003, Vol. 108(10), pp. 1184-90.

122. *The effect of blockade of the CD11/CD18 integrin receptor on infarct size in patients with acute myocardial infarction treated with direct angioplasty: the results of the HALT-MI study.* Faxon DP, Gibbons RJ, Chronos NA, Gurbel PA, Sheehan F and Investigators., HALT-MI. J Am Coll Cardiol, 2002, Vol. 40(7), pp. 1199-204.

Appendix

Additional Information

The supplementary information that accompanies this work is available in the following link: https://www.nature.com/articles/ncomms14780 or in the attached CD-ROM.

Movie 1

MVO and neutrophil-platelet interactions in the post-reperfused myocardium. 3D navigation of confocal microscopy samples showing MVO and neutrophil-platelet interactions in the myocardial vessels at 6h in vehicle (top) and metoprolol-treated (low) mice.

Movie 2

Neutrophil infiltration in the post-reperfused myocardium. 3D navigation of confocal microscopy samples showing neutrophil infiltration and cardiac disarray in vehicle- (top) and metoprolol-treated (low) mice. Note the massive neutrophil infiltration in vehicle-treated mice (absent in metoprolol-treated mice) and the irregular shaped neutrophils in vehicle as opposed to stunned rounded neutrophils in metoprolol.

Movie 3

Metoprolol alters neutrophil dynamics in inflamed vessels. Intravital microscopy showing neutrophils (green) crawling by the vessel. Note the migratory velocity, accumulated crawling distance, and directional movement in vehicle-treated mice. Conversely stunned neutrophils from metoprolol-treated mice show an erratic behaviour with reduced motility and altered platelet (red) interactions.

The following section resumes the PhD candidate's scientific production during his enrolment in the Postgraduate Program in Molecular Biosciences at the UAM as well as that published during the CNIC-PhD program period. Articles relevant to this doctoral thesis and those published as first author have been attached at the end of this section.

Scientific production during UAM PhD program enrolment

1. Neutrophil stunning by metoprolol reduces infarct size. **García-Prieto J**, Villena-Gutiérrez R, Gómez M, Bernardo E, Pun-García A, García-Lunar I, Crainiciuc G, Fernández-Jiménez R, Sreeramkumar V, Bourio-Martínez R, García-Ruiz JM, Del Valle AS, Sanz-Rosa D, Pizarro G, Fernández-Ortiz A, Hidalgo A, Fuster V, Ibanez B. Nat Commun. 2017 Apr 18;8:14780. **(First Author) (Attached)**

2. Imbalanced OPA1 processing and mitochondrial fragmentation cause heart failure in mice. Wai T*, **García-Prieto J*,** Baker MJ, Merkwirth C, Benit P, Rustin P, Rupérez FJ, Barbas C, Ibañez B, Langer T. Science. 2015 Dec 4;350(6265):aad0116. **(* Co-first Authorship) (Attached)**

3. Pathophysiology Underlying the Bimodal Edema Phenomenon After Myocardial Ischemia/Reperfusion. Fernández-Jiménez R, **García-Prieto J**, Sánchez-González J, Agüero J, López-Martín GJ, Galán-Arriola C, Molina-Iracheta A, Doohan R, Fuster V, Ibáñez B. J Am Coll Cardiol. 2015 Aug 18;66(7):816-828.

4. Dynamic Edematous Response of the Human Heart to Myocardial Infarction: Implications for Assessing Myocardial Area at Risk and Salvage. Fernández-Jiménez R, Barreiro-Pérez M, Martin-García A, Sánchez-González J, Agüero J, Galán-Arriola C, **García-Prieto J**, Díaz-Pelaez E, Vara P, Martinez I, Zamarro I, Garde B, Sanz J, Fuster V, Sánchez PL, Ibanez B. Circulation. 2017 Oct 3;136(14):1288-1300.

5. Effect of Ischemia Duration and Protective Interventions on the Temporal Dynamics of Tissue Composition After Myocardial Infarction. Fernández-

Jiménez R, Galán-Arriola C, Sánchez-González J, Agüero J, López-Martín GJ, Gomez-Talavera S, **Garcia-Prieto J**, Benn A, Molina-Iracheta A, Barreiro-Pérez M, Martin-García A, García-Lunar I, Pizarro G, Sanz J, Sánchez PL, Fuster V, Ibanez B. Circ Res. 2017 Aug 4;121(4):439-450.

6. Exercise triggers ARVC phenotype in mice expressing a disease-causing mutated version of human plakophilin-2. Cruz FM, Sanz-Rosa D, Roche-Molina M, **García-Prieto J**, García-Ruiz JM, Pizarro G, Jiménez-Borreguero LJ, Torres M, Bernad A, Ruíz-Cabello J, Fuster V, Ibáñez B, Bernal JA. J Am Coll Cardiol.2015Apr14;65(14):1438-50.

7. Lung ultrasound as a translational approach for non-invasive assessment of heart failure with reduced or preserved ejection fraction in mice. Villalba-Orero M, López-Olañeta MM, González-López E, Padrón-Barthe L, Gómez-Salinero JM, **García-Prieto J**, Wai T, García-Pavía P, Ibáñez B, Jiménez-Borreguero LJ, Lara-Pezzi E. Cardiovasc Res. 2017 Aug 1;113(10):1113-1123.

8. Impact of the Timing of Metoprolol Administration During STEMI on Infarct Size and Ventricular Function. García-Ruiz JM, Fernández-Jiménez R, García-Alvarez A, Pizarro G, Galán-Arriola C, Fernández-Friera L, Mateos A, Nuno-Ayala M, Aguero J, Sánchez-González J, **García-Prieto J**, López-Melgar B, Martínez-Tenorio P, López-Martín GJ, Macías A, Pérez-Asenjo B, Cabrera JA, Fernández-Ortiz A, Fuster V, Ibáñez B. J Am Coll Cardiol. 2016 May 10;67(18):2093-2104.

9. Beta-3 adrenergic agonists reduce pulmonary vascular resistance and improve right ventricular performance in a porcine model of chronic pulmonary hypertension. García-Álvarez A, Pereda D, García-Lunar I, Sanz-Rosa D, Fernández-Jiménez R, **García-Prieto J**, Nuño-Ayala M, Sierra F, Santiago E, Sandoval E, Campelos P, Agüero J, Pizarro G, Peinado VI, Fernández-Friera L, García-Ruiz JM, Barberá JA, Castellá M, Sabaté M, Fuster V, Ibañez B. Basic Res Cardiol. 2016 Jul;111(4):49. doi: 10.1007/s00395-016-0567-0. Epub 2016 Jun 21.

Scientific production during CNIC-PhD program enrolment

10. β3 adrenergic receptor selective stimulation during ischemia/reperfusion improves cardiac function in translational models through inhibition of mPTP opening in cardiomyocytes. **García-Prieto J**, García-Ruiz JM, Sanz-Rosa D, Pun A, García-Alvarez A, Davidson SM, Fernández-Friera L, Nuno-Ayala M, Fernández-Jiménez R, Bernal JA, Izquierdo-Garcia JL, Jimenez-Borreguero J, Pizarro G, Ruiz-Cabello J, Macaya C, Fuster V, Yellon DM, Ibanez B. Basic Res Cardiol. 2014 Jul;109(4):422. (First Author) (Attached)

11. Long-term benefit of early pre-reperfusion metoprolol administration in patients with acute myocardial infarction: results from the METOCARD-CNIC trial (Effect of Metoprolol in Cardioprotection During an Acute Myocardial Infarction). Pizarro G, Fernández-Friera L, Fuster V, Fernández-Jiménez R, García-Ruiz JM, García-Álvarez A, Mateos A, Barreiro MV, Escalera N, Rodriguez MD, de Miguel A, García-Lunar I, Parra-Fuertes JJ, Sánchez-González J, Pardillos L, Nieto B, Jiménez A, Abejón R, Bastante T, Martínez de Vega V, Cabrera JA, López-Melgar B, Guzman G, **García-Prieto J**, Mirelis JG, Zamorano JL, Albarrán A, Goicolea J, Escaned J, Pocock S, Iñiguez A, Fernández-Ortiz A, Sánchez-Brunete V, Macaya C, Ibanez B. J Am Coll Cardiol. 2014 Jun 10;63(22):2356-62. (Attached)

12. Effect of early metoprolol on infarct size in ST-segment-elevation myocardial infarction patients undergoing primary percutaneous coronary intervention: the Effect of Metoprolol in Cardioprotection During an Acute Myocardial Infarction (METOCARD-CNIC) trial. Ibanez B, Macaya C, Sánchez-Brunete V, Pizarro G, Fernández-Friera L, Mateos A, Fernández-Ortiz A, García-Ruiz JM, García-Álvarez A, Iñiguez A, Jiménez-Borreguero J, López-Romero P, Fernández-Jiménez R, Goicolea J, Ruiz-Mateos B, Bastante T, Arias M, Iglesias-Vázquez JA, Rodriguez MD, Escalera N, Acebal C, Cabrera JA, Valenciano J, Pérez de Prado A, Fernández-Campos MJ, Casado I, García-Rubira JC, **García-Prieto J**, Sanz-Rosa D, Cuellas C, Hernández-Antolín R, Albarrán A, Fernández-Vázquez F, de la Torre-Hernández JM, Pocock S, Sanz G, Fuster V. Circulation. 2013 Oct 1;128(14):1495-503. (Attached)

13. Myocardial edema after ischemia/reperfusion is not stable and follows a bimodal pattern: imaging and histological tissue characterization. Fernández-Jiménez R, Sánchez-González J, Agüero J, **García-Prieto J**, López-Martín GJ, García-Ruiz JM, Molina-Iracheta A, Rosselló X, Fernández-Friera L, Pizarro G, García-Álvarez A, Dall'Armellina E, Macaya C, Choudhury RP, Fuster V, Ibáñez B. J Am Coll Cardiol. 2015 Feb 3;65(4):315-23.

14. Induction of sustained hypercholesterolemia by single adeno-associated virus-mediated gene transfer of mutant hPCSK9. Roche-Molina M, Sanz-Rosa D, Cruz FM, **García-Prieto J**, López S, Abia R, Muriana FJ, Fuster V, Ibáñez B, Bernal JA. Arterioscler Thromb Vasc Biol. 2015 Jan;35(1):50-9.

15. Local control of nuclear calcium signaling in cardiac myocytes by perinuclear microdomains of sarcolemmal insulin-like growth factor 1 receptors. Ibarra C, Vicencio JM, Estrada M, Lin Y, Rocco P, Rebellato P, Munoz JP, **Garcia-Prieto J**, Quest AF, Chiong M, Davidson SM, Bulatovic I, Grinnemo KH, Larsson O, Szabadkai G, Uhlén P, Jaimovich E, Lavandero S. Circ Res. 2013 Jan 18;112(2):236-45.

16. The future: therapy of myocardial protection. Sanz-Rosa D, **García-Prieto J**, Ibanez B. Ann N Y Acad Sci. 2012 Apr;1254:90-8.

17. Impact of left ventricular hypertrophy on troponin release during acute myocardial infarction: new insights from a comprehensive translational study. Fernández-Jiménez R, Silva J, Martínez-Martínez S, López-Maderuelo MD, Nuno-Ayala M, García-Ruiz JM, García-Álvarez A, Fernández-Friera L, Pizarro TG, **García-Prieto J**, Sanz-Rosa D, López-Martin G, Fernández-Ortiz A, Macaya C, Fuster V, Redondo JM, Ibanez B. J Am Heart Assoc. 2015 Jan 21;4(1):e001218.

18. Response to letter regarding article, "effect of early metoprolol on infarct size in ST-segment-elevation myocardial infarction patients undergoing primary percutaneous coronary intervention: the Effect of Metoprolol in Cardioprotection During an Acute Myocardial Infarction (METOCARD-CNIC) trial". Ibanez B, Macaya C, Sánchez-Brunete V, Pizarro G, Fernández-Friera

L, Mateos A, Fernández-Ortiz A, García-Ruiz JM, García-Álvarez A, Iñiguez A, Jiménez-Borreguero J, López-Romero P, Fernández-Jiménez R, Goicolea J, Ruiz-Mateos B, Bastante T, Arias M, Iglesias-Vázquez JA, Rodriguez MD, Escalera N, Acebal C, Cabrera JA, Valenciano J, de Prado AP, Fernández-Campos MJ, Casado I, García-Rubira JC, **García-Prieto J**, Sanz-Rosa D, Cuellas C, Hernández-Antolín R, Albarrán A, Fernández-Vázquez F, de la Torre-Hernández JM, Pocock S, Sanz G, Fuster V. Circulation. 2014 Jul 15;130(3):e19-20.

19. Noninvasive monitoring of serial changes in pulmonary vascular resistance and acute vasodilator testing using cardiac magnetic resonance. García-Álvarez A, Fernández-Friera L, García-Ruiz JM, Nuño-Ayala M, Pereda D, Fernández-Jiménez R, Guzmán G, Sanchez-Quintana D, Alberich-Bayarri A, Pastor-Escuredo D, Sanz-Rosa D, **García-Prieto J**, Gonzalez-Mirelis JG, Pizarro G, Jimenez-Borreguero LJ, Fuster V, Sanz J, Ibáñez B. J Am Coll Cardiol. 2013 Oct 22;62(17):1621-3.

20. Acute ApoA-I Milano administration induces plaque regression and stabilisation in the long term. Giannarelli C, Cimmino G, Ibanez B, Chiesa G, **Garcia-Prieto J**, Santos-Gallego CG, Alique-Aguilar M, Fuster V, Sirtori C, Badimon JJ. Thromb Haemost. 2012 Dec;108(6):1246-8.

nature COMMUNICATIONS

ARTICLE

Received 22 Mar 2016 | Accepted 30 Jan 2017 | Published 18 Apr 2017

DOI: 10.1038/ncomms14780 OPEN

Neutrophil stunning by metoprolol reduces infarct size

Jaime García-Prieto[1,2], Rocío Villena-Gutiérrez[1], Mónica Gómez[1], Esther Bernardo[3], Andrés Pun-García[1], Inés García-Lunar[1,2,4,5], Georgiana Crainiciuc[1], Rodrigo Fernández-Jiménez[1,2,3], Vinatha Sreeramkumar[1,4], Rafael Bourio-Martínez[1,6], José M. García-Ruiz[1,2,7], Alfonso Serrano del Valle[1], David Sanz-Rosa[1,2,4], Gonzalo Pizarro[1,2,4,8], Antonio Fernández-Ortiz[1,2,3], Andrés Hidalgo[1,9], Valentín Fuster[1,10] & Borja Ibanez[1,2,11]

The β1-adrenergic-receptor (ADRB1) antagonist metoprolol reduces infarct size in acute myocardial infarction (AMI) patients. The prevailing view has been that metoprolol acts mainly on cardiomyocytes. Here, we demonstrate that metoprolol reduces reperfusion injury by targeting the haematopoietic compartment. Metoprolol inhibits neutrophil migration in an ADRB1-dependent manner. Metoprolol acts during early phases of neutrophil recruitment by impairing structural and functional rearrangements needed for productive engagement of circulating platelets, resulting in erratic intravascular dynamics and blunted inflammation. Depletion of neutrophils, ablation of *Adrb1* in haematopoietic cells, or blockade of PSGL-1, the receptor involved in neutrophil–platelet interactions, fully abrogated metoprolol's infarct-limiting effects. The association between neutrophil count and microvascular obstruction is abolished in metoprolol-treated AMI patients. Metoprolol inhibits neutrophil–platelet interactions in AMI patients by targeting neutrophils. Identification of the relevant role of ADRB1 in haematopoietic cells during acute injury and the protective role upon its modulation offers potential for developing new therapeutic strategies.

[1] Centro Nacional de Investigaciones Cardiovasculares Carlos III (CNIC), 28029 Madrid, Spain. [2] CIBER de enfermedades CardioVasculares (CIBERCV), 28029 Madrid, Spain. [3] Hospital Clínico San Carlos, 28040 Madrid, Spain. [4] Clinical Department, School of Biomedical Sciences, Universidad Europea, 28670 Madrid, Spain. [5] Hospital Universitario Quirón, 28223 Madrid, Spain. [6] Hospital de Basurto, 48013 Bilbao, Spain. [7] Hospital Universitario Central de Asturias (HUCA), 33011 Oviedo, Spain. [8] Complejo Hospitalario Ruber Juan Bravo-UEM, 28006 Madrid, Spain. [9] Institute for Cardiovascular Prevention (IPEK), Ludwig-Maximilians University, 80336 Munich, Germany. [10] Zena and Michael A. Wiener Cardiovascular Institute, Icahn School of medicine at Mount Sinai, New York, New York 10029, USA. [11] Department of Cardiology, Instituto de Investigación Sanitaria (IIS)-Fundación Jiménez Díaz, 28040 Madrid, Spain. Correspondence and requests for materials should be addressed to B.I. (email: bibanez@cnic.es).

Heart attack (acute myocardial infarction, AMI) is one of the principal manifestations of cardiovascular disease and a chief contributor to mortality and morbidity worldwide. The main determinant of poor outcome post AMI is the extent of irreversible injury (infarct size). The mainstay of AMI treatment is rapid reperfusion to restore blood flow, which reduces complications and improves survival. However, reperfusion itself accelerates and exacerbates the inflammatory response associated with myocardial injury[1]. Thus, the injury inflicted on the myocardium during AMI is the result of ischaemia and reperfusion processes, and is known as ischaemia/reperfusion (IR) injury. The development of effective therapies to reduce myocardial IR injury is an unmet clinical need[2].

The injured myocardium is infiltrated by circulating neutrophils, and these cells are critically involved in myocardial IR injury[3–7]. In an inflammatory milieu, neutrophils bind to platelets and red blood cells, forming plugs[7]. Upon reperfusion, these plugs are dispersed into the microcirculation, where they form embolisms, precluding tissue perfusion despite blood flow restoration in the large coronary arteries. This phenomenon, known as microvascular obstruction (MVO), is a major contributor to IR injury and infarct size[1]. Moreover, neutrophil infiltration into acutely damaged organs is dependent on their interaction with platelets[8], and these interactions are critical to the formation of harmful co-aggregates and the initiation of inflammatory-like responses before tissue infiltration[3,8]. Overall, neutrophil dynamics (including neutrophil–platelet interactions) are an attractive therapeutic target for the prevention of IR injury.

The intravenous (i.v.) administration of the selective β1-adrenergic receptor (ADRB1) antagonist metoprolol has been shown to reduce infarct size and improve long-term cardiac function after AMI in the recent METOCARD-CNIC trial[9,10]. The mechanism underlying metoprolol's cardioprotective effect remains unclear[11]. Identifying this mechanism could have significant implications for the understanding of IR and the development of novel infarct-limiting therapies. The adrenergic system is critically involved in inflammatory reactions[12,13]. In particular, the inflammatory response of neutrophils involves the *de novo* production and release by these cells of catecholamines[12,13]. Induced catecholamine stress (as during ischaemia) alters neutrophil trafficking[14–16] and promotes formation of neutrophil–platelet co-aggregates[17].

We hypothesized that pre-reperfusion i.v. metoprolol administration alters neutrophil dynamics, resulting in a dampened inflammatory response, less severe reperfusion injury and smaller infarcts. Here we show that pre-reperfusion administration of i.v. metoprolol to AMI patients significantly reduces the incidence of MVO, and moreover that metoprolol inhibits deleterious neutrophil inflammatory responses both in patients and in animal models of IR. The infarct-limiting effect of metoprolol is abolished in neutrophil-depleted mice and when neutrophils are prevented from interacting with platelets. The beneficial effects of metoprolol are also abolished by genetic ablation of *Adrb1* and are rescued by restitution of *Adrb1* expression only in haematopoietic cells. These results identify the neutrophil dynamics as the target of the cardioprotective effect of metoprolol against myocardial IR injury.

Results

Intravenous metoprolol reduces MVO in AMI patients. The METOCARD-CNIC trial recruited patients with an ongoing acute ST-segment elevation AMI and randomized them to receive i.v. metoprolol (15 mg) or control before reperfusion[18]. A total of 220 AMI patients underwent a cardiac magnetic resonance (CMR) imaging exam 1 week after AMI. To study the potential mechanisms underlying the infarct-limiting effect of metoprolol[9], we analysed the 1-week CMR data to evaluate the extent of MVO. MVO was defined as the absence of contrast wash-in inside the delayed gadolinium-enhanced area[19], and was quantified as grams of left ventricle (LV) (Fig. 1a,b and Supplementary Fig 1a,b). Patients treated with metoprolol during ongoing AMI had a 40% lower extent of MVO (Fig. 1c). This significant effect was maintained after adjusting for factors potentially affecting MVO by performing linear multiple regression analysis and including sex, age, ischaemia duration, diabetes, and use of thrombectomy or glycoprotein IIb/IIIa inhibitors as covariates. To exclude the possibility that this effect simply reflected the reduction in total infarct size[9], MVO was further assessed as a percentage of the infarcted area (total late gadolinium enhanced area). Metoprolol-treated patients had 24% less infarct-normalized MVO than control patients (Fig. 1d). As expected, the extent of MVO was significantly associated with poor long-term outcome, evaluated as chronic ventricular performance (Supplementary Fig. 1c). These data suggest that MVO reduction might be involved in the cardioprotective effect of metoprolol administration in patients during ongoing AMI.

Intravenous metoprolol dampens neutrophilial–MVO association in AMI. White blood cell (WBC) and neutrophil counts during an AMI are known to be associated with larger infarct sizes and extensive MVO[20–22]. We explored these associations in AMI patients from the METOCARD-CNIC trial. We found a significant positive correlation between absolute leukocyte count on admission and the extent of MVO on CMR: the higher the leukocyte count, the larger the extent of MVO (Fig. 2a). We further studied the association of the different WBC subpopulations and MVO. As expected, neutrophil count was significantly correlated with the extent of MVO (Fig. 2b). Conversely, there was no sign of association between other WBC subpopulations and MVO: lymphocyte, monocyte, eosinophil or platelet counts did not correlate with the extent of MVO (Fig. 2e). Next, we studied the effect of metoprolol on WBCs and on the association between these and MVO. Metoprolol treatment was not associated with any different in WBC count nor in any WBC subpopulation (Supplementary Table 1). Of note, we found a significant interaction between metoprolol treatment and the correlation between leukocyte count and MVO: the significant positive correlation between neutrophil count and the extent of MVO was only present in control patients (that is, not receiving metoprolol); in patients receiving i.v. metoprolol before reperfusion there was no sign of association between total leukocyte or neutrophil counts and the extent of MVO (Fig. 2c,d). These results suggest that the administration of i.v. metoprolol during ongoing AMI do not affect the circulating levels of WBCs but modulates the impact of neutrophils on MVO.

Metoprolol blunts neutrophil infiltration in experimental IR. To identify the factors underlying the metoprolol-induced reduction in MVO within the reperfused myocardium, we examined a mouse model of *in vivo* myocardial IR injury (Fig. 3a). Given the observed modulator effect of i.v. metoprolol in the association between neutrophil count and MVO in patients suffering an AMI, we focused our attention into this cell population. We first tested the infarct-limiting effect of metoprolol in wild-type mice by occluding the left anterior descending (LAD) coronary artery for 45 min followed by reperfusion. Mice were randomized to receive a single i.v. bolus (50 µl) of metoprolol (10 mM) or vehicle (saline) 35 min after

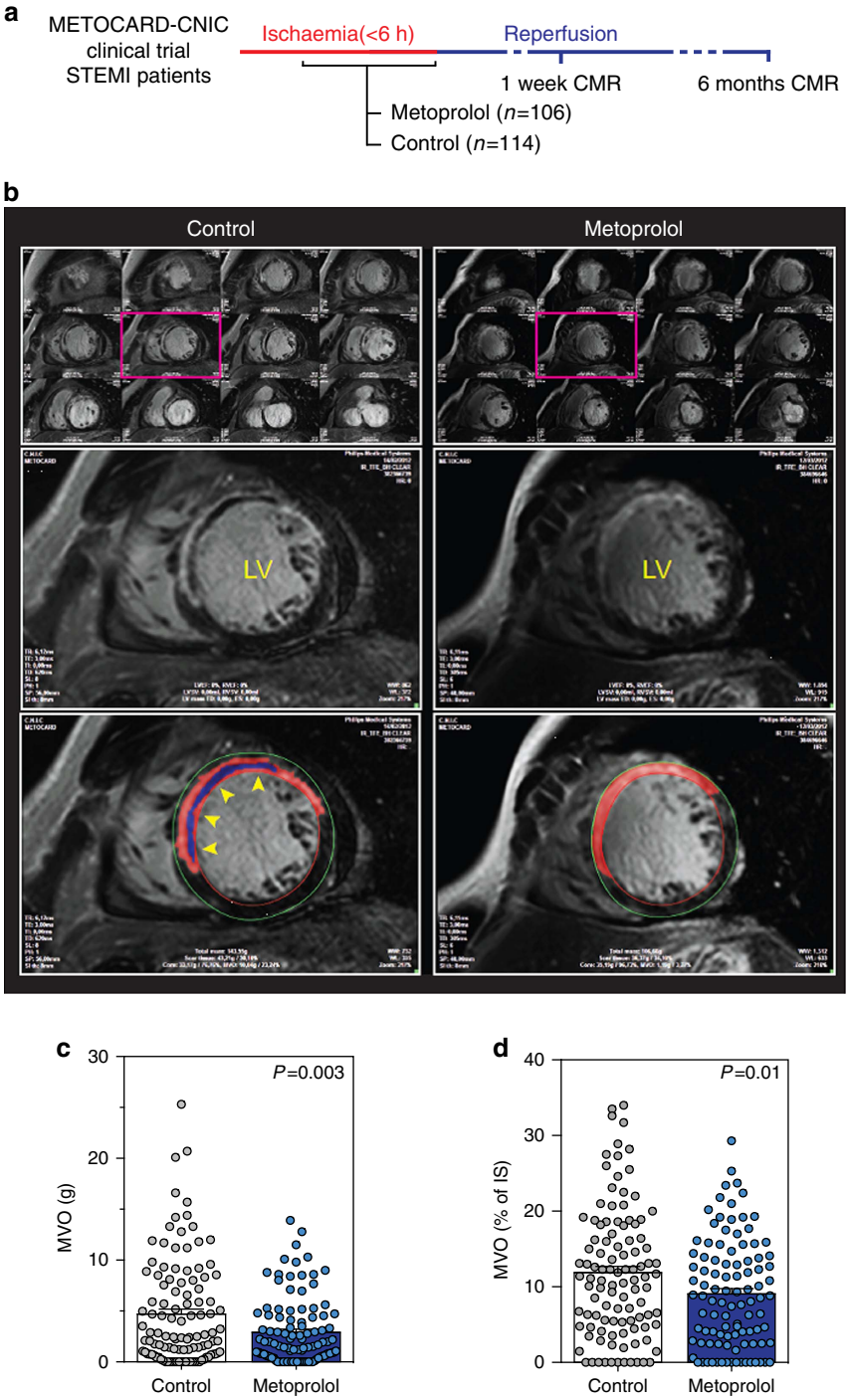

Figure 1 | Metoprolol administration during ongoing AMI reduces MVO in patients. (**a**) METOCARD-CNIC trial scheme: patients with ongoing ST-segment elevation myocardial infarction (STEMI) were recruited and randomized to receive metoprolol (15 mg i.v. doses) or control before reperfusion. A total of 220 patients were evaluated for MVO by cardiac magnetic resonance (CMR) imaging 1 week after AMI and 202 patients for an additional CMR at long-term LVEF 6 months after AMI for ventricular function assessment. (**b**) Representative CMR exams (short-axis covering the entire left ventricle (LV) from base to apex), showing significant differences in 1-week MVO between a control patient (left) and a metoprolol-treated patient (right). Lower panels show detailed views of the boxed images, revealing MVO (blue area, automatic quantification), defined as the absence of contrast wash-in inside the delayed gadolinium-enhanced area (red, semiautomatic quantification). Yellow arrowheads indicate MVO in the LV wall. (**c**) Quantification of MVO in grams of left ventricle. (**d**) Quantification of MVO relative to the infarcted area (%). Dots represent values for individual patients: 114 in the control group (grey) versus 106 in the metoprolol group (blue). Data are means ± s.e.m. and compared by unpaired Student's *t*-test.

ischaemia onset (10 min before reperfusion). Infarct size was evaluated at 24 h reperfusion by TTC staining and normalized to area at risk (AAR, negative Evans blue staining). Metoprolol-treated mice had significantly smaller infarcts (as % of AAR) than vehicle-treated mice (Fig. 3b–d). Next, we examined mice carrying a GFP reporter in myeloid derived cells (LysM-GFP). LysM-GFP mice underwent the myocardial IR procedure and were randomized to receive i.v. metoprolol or vehicle. Capillary

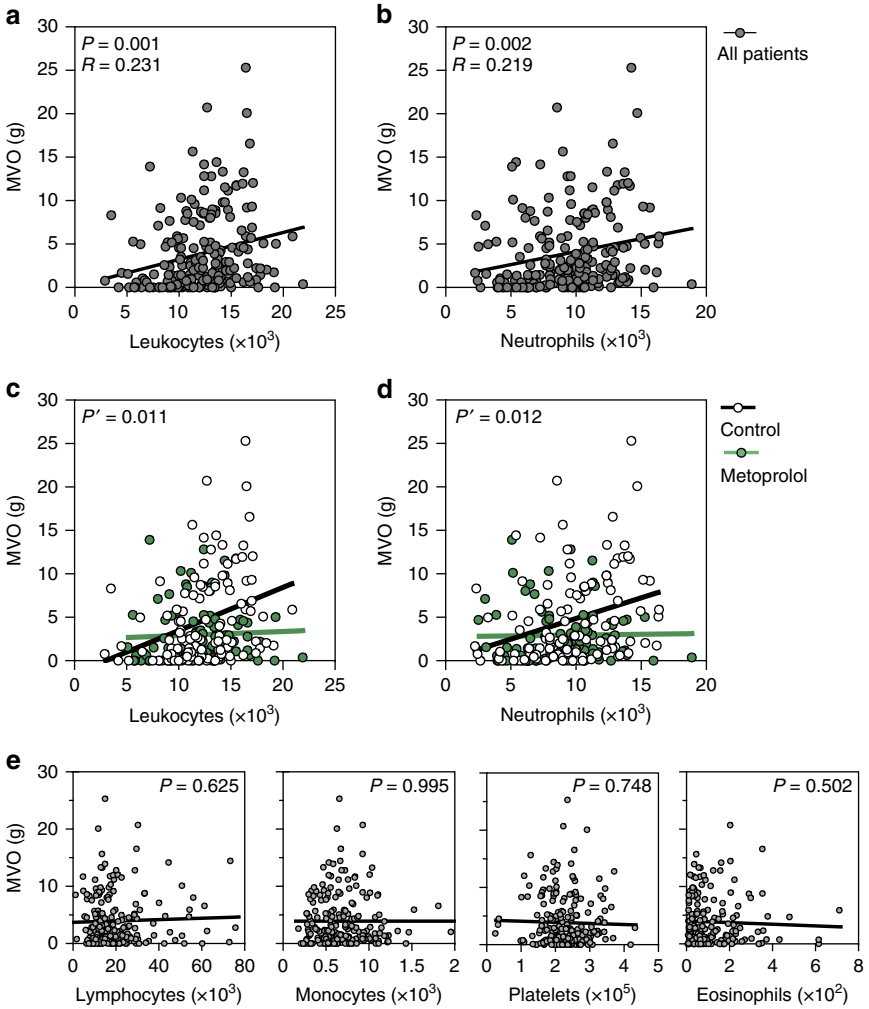

Figure 2 | Metoprolol abrogates neutrophil count positive association with extent of MVO. Sensitivity analysis of the association between MVO and leukocyte and subpopulations count on admission from METOCARD-CNIC trial patients. (**a**,**b**) Association between MVO and absolute leukocyte or neutrophil count on admission. Grey dots represent individual values and line linear relationship. (**c**,**d**) Linear regression comparison between MVO and leukocytes and neutrophils in the subsets of METOCARD patients indicating loss of correlation in the metoprolol treated group (green) as compared to control group (white). *P*′, stands for interaction *P* value. (**e**) Association between MVO and rest of white blood cells subpopulations: Platelets, lymphocytes, eosinophils and monocytes showing no correlation in the extent of MVO. *P* stands for *P* value and *R*, for Pearson's correlation coefficient.

obliteration (a histological surrogate for MVO) and leukocyte infiltration were quantified at 6 h post-reperfusion (Fig. 3e–m). Metoprolol administration during ongoing AMI resulted in a significant reduction of capillary obliteration by circulatory cell plugins when evaluated at 6 h post-reperfusion (Fig. 3e,f). Confocal microscopy analyses revealed a significant reduction in the number of myeloid cells plugins (LysM-GFP + particles) and percentage of LysM-GFP + area within the LV sections, indicating rapid inhibition of leukocyte recruitment and protection of lumen vessel patency (Fig. 3g, Supplementary Fig. 2a–d and Supplementary Movie 1). Temporal (6 and 24 h) evaluation of myeloid-derived cells infiltration into injured myocardium showed a persistent abrogation of neutrophil infiltration (Fig. 3h–m and Supplementary Movie 2) and a differential relative proportion of different myeloid cells in hearts from metoprolol and vehicle-treated mice (Fig. 3j and Supplementary Fig. 3). These mouse experiments confirm the clinical findings that pre-reperfusion metoprolol administration during ongoing AMI limits infarct size and reduces MVO, and further show that metoprolol reduces neutrophil infiltration, suggesting neutrophils as a potential target in this cardioprotective effect.

Metoprolol does not protect from AMI in the absence of neutrophils. Catecholamine-stimulation of βARs alters neutrophil function, cytokine release and neutrophil–platelet aggregate formation[17,23,24], processes associated with aggravated injury during AMI (refs 25–27). To decipher the role of neutrophils in the protection afforded by metoprolol during ongoing AMI, we evaluated the effect of the drug in the absence of neutrophils. Neutrophil depletion in mouse peripheral blood was achieved by administration of an anti-Ly6G mAb over 2 days[8,28]. After neutrophil depletion, animals were subjected to myocardial IR, and infarct size was evaluated at 24 h post-reperfusion (Fig. 3n). Confirming earlier reports[29], neutrophil-depleted mice had smaller infarcts than controls. Administration of metoprolol to these mice during ongoing AMI did not reduce infarct size (Fig. 3o–q). The abrogation of the cardioprotective effect of metoprolol confirms circulating neutrophils as a target of the beneficial effect associated with this pharmacological therapy.

Metoprolol inhibits neutrophil migration by targeting ADRB1. The effect of metoprolol on primary neutrophils' function was

evaluated in a chemokine-induced transwell migration assay and by evaluation of the chemotactic FPR activator-peptide, W-peptide[30], -induced reactive oxygen species (ROS) production assay[31]. First, neutrophils were exposed across the transwell filter to the chemoattractant CXCL1 in the presence or absence of metoprolol for 1.5 h, and migration through the transwell membrane was quantified by flow cytometry. Metoprolol inhibited baseline and epinephrine-stimulated neutrophil migration towards CXCL1, reducing migration to the same level in both cases (Fig. 4a). Second, ROS production *in vitro* was measured using DHR 123 and W-peptide activation. ROS production was tested in metoprolol-treated and untreated neutrophils with and without W-peptide stimulation. Metoprolol-treated neutrophils presented significant decreased oxidative burst compared to the non-treated cells after stimulation (Fig. 4b,c). Metoprolol alone had no effect on ROS endogenous production.

Metoprolol is a selective ADRB1-blocker, and ADRB1 signalling has been shown to mediate some of the pro-inflammatory response of monocytes[32]. Neutrophils and monocytes are both myeloid derived cells, and we therefore reasoned that ADRB1 might be involved in the anti-migratory effect of metoprolol. *Adrb1* mRNA expression in fresh and viable isolated neutrophils was confirmed by PCR in wild-type mice and absence in neutrophils from *Adrb1*-knockout mice (*Adrb1*KO) (Supplementary Fig. 4a–c). *In vitro*, the -epinephrine-mediated

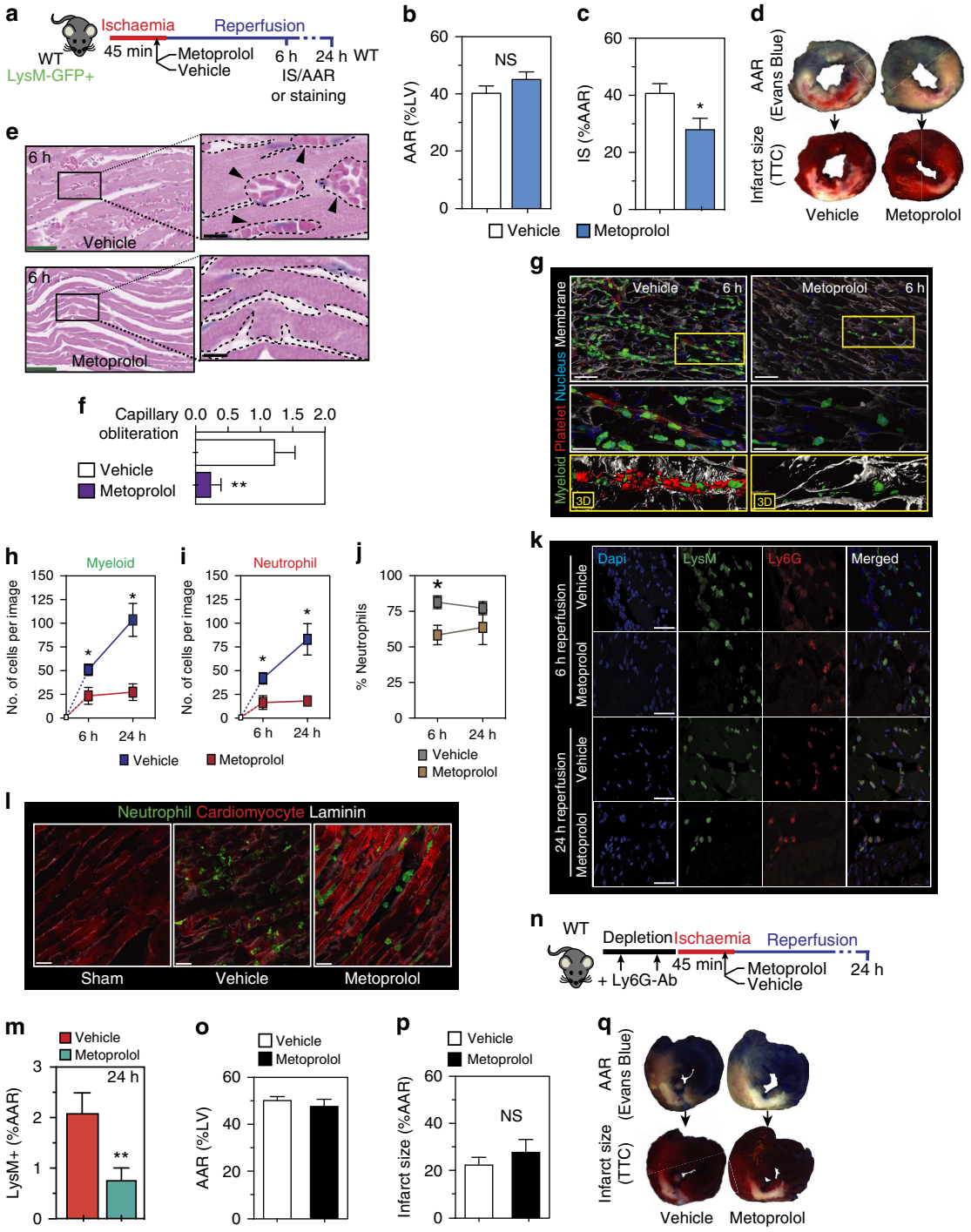

migration- and -W-peptide-mediated ROS production-inhibitory effect of metoprolol was lost in *Adrb1*KO neutrophils (Fig. 4a–c). β2-adrenergic receptor-knockout mice (*Adrb2*KO) was not involved in the effects observed after metoprolol administration (Supplementary Fig. 5).

We next explored whether metoprolol directly inhibits the capacity of neutrophils to infiltrate tissues *in vivo*. For this, we first used a model of thioglycolate-induced peritonitis (Fig. 4d). Thioglycolate induces massive leucocyte migration into the peritoneal cavity within the first 16 h (Supplementary Fig. 6a), with the majority of infiltrating cells being neutrophils (Supplementary Fig. 6b–d). Metoprolol i.v. administration sharply inhibited thioglycolate-induced neutrophil infiltration into the peritoneal cavity of wild-type mice (Fig. 4e,f), but the inhibitory effect of metoprolol was lost in *Adrb1*KO mice (Fig. 4f and Supplementary Fig. 6a,b).

To better define the cell compartment targeted by metoprolol, we lethally irradiated *Adrb1*KO mice and restored haematopoiesis with bone marrow (BM) transplanted from wild-type donors, generating chimeric mice expressing ADRB1 only in circulating cells. At 4 weeks after irradiation, transplanted animals presented >85% BM engraftment (Supplementary Fig. 7) and were subjected to thioglycolate-induced peritonitis. The replenishment of ADRB1 only in haematopoietic cells was enough to rescue the anti-leucocyte-infiltration effect of metoprolol (Fig. 4g). Together, these data show a direct effect of metoprolol on neutrophil function and demonstrate that the presence of ADRB1 in circulating cells is essential for the ability of metoprolol to reduce neutrophil infiltration into injured tissue.

IR reduction by metoprolol involves haematopoietic cells' *ADRB1*. We next investigated the involvement of ADRB1 blockade in haematopoietic circulating cells in the protective effect of metoprolol in the infarcted myocardium. *Adrb1*KO mice were subjected to myocardial IR and randomized to receive i.v. metoprolol or vehicle during ongoing AMI (Fig. 4h). Unlike the situation in wild-type mice, metoprolol did not limit infarct size in *Adrb1*KO animals (Fig. 4i–k), demonstrating the critical role of ADRB1 blockade in the cardioprotective effect. To demonstrate the role of ADRB1 expression in haematopoietic circulating cells, we repeated the myocardial IR protocol in the chimeras described above (*Adrb1*KO mice transplanted with wild-type BM). The presence of ADRB1 only in haematopoietic circulating cells was sufficient to restore susceptibility to the cardioprotective effect of metoprolol (Fig. 4l–n). Conversely, transplant of *Adrb1*KO BM into irradiated wild-type mice abrogated the protective phenotype associated with metoprolol administration during IR (Fig. 4o–q). These data confirm the involvement of ADRB1 blockade in haematopoietic cells in the cardioprotection afforded by metoprolol administration during AMI.

Metoprolol alters neutrophil dynamics *in vivo*. During acute injury, neutrophils alter their morphology upon adhering to the activated endothelium. These shape change or polarization, permit intercellular interactions critical for the inflammatory response in several conditions, including myocardial IR (refs 8,33). Polarization of adhered neutrophils involves receptor redistribution and the assembly of a rearward protruding microdomain called the uropod, and is essential for the integration of signals coming from the endothelium and activated platelets before infiltration[8]. We were therefore interested in investigating whether metoprolol impaired neutrophil migration and infiltration through an effect on neutrophil dynamics. For this, we used bi-dimensional and 3D intravital microscopy (IVM) to image cremaster muscle vessels of mice treated with tumour necrosis factor-α (TNFα), an inflammatory model in which the vast majority of recruited leukocytes are neutrophils. Neutrophil behaviour was evaluated 3 h after administration of metoprolol or vehicle (Fig. 5a). Notably, metoprolol reduced neutrophil migratory velocity, accumulated crawling distance and directional movement (Fig. 5b,c and online Supplementary Movie 3). Independent-neutrophil 3D-reconstructions of live inflamed vessels showed that metoprolol consistently disabled the intravascular behaviour of neutrophils without disrupting polarization within activated vessels, resulting in dramatic changes in cell morphology (Fig. 5d–f) that correlated with their abnormal crawling dynamics. These data show that metoprolol 'stuns' neutrophils, resulting in altered dynamics and prevents the morphological changes needed to initiate intercellular interactions and subsequent tissue infiltration.

Metoprolol blocks PSGL1-dependent neutrophil platelet interactions. Correct neutrophil polarization and organization of an extruding microdomain that captures circulating platelets is required to initiate tissue-damaging inflammation[8]. Indeed, plugs of neutrophil–platelet co-aggregates in the microcirculation are a major contributor to MVO in AMI and in other models of injury[1,8]. We therefore explored the impact of metoprolol-induced neutrophil stunning on neutrophil–platelet interactions.

Figure 3 | Metoprolol reduces neutrophil infiltration and capillary obliteration in murine IR. (**a**) Mouse model of myocardial IR. (**b**, **c**) Histological evaluation of left ventricle (LV) area at risk (AAR) and infarct size (IS) in mice subjected to IR and randomized to receive metoprolol (blue) or vehicle (white); NS stands for non-significant. $n=8$. (**d**) Representative images of LV slices showing AAR (negative for Evans Blue) in upper panels and extent of necrosis (triphenyltetrazoliumchloride (TTC)-negative area in lower panels). (**e**) Capillary oblliteration quantified in H&E ten random images; $n=5$–6. (**f**) Representative H&E myocardial images at 6 h reperfusion showing disarrayed and abundant obstructed capillaries in the vehicle-treated sample; metoprolol-treated samples show injury and nuclear condensation but no signs of MVO; green scale bars, 50 μm. Detailed amplification of the boxes show obstructed capillaries indicated with black arrows; black scale bars, 10 μm. (**g**) Confocal images from LV at 6 h after reperfusion onset showing massive vascular neutrophil migration (LysM-GFP, green) and co-aggregates with platelets (CD41, red) vehicle- but not in metoprolol-treated mice; scale bar, 25 μm. Next, amplified boxes indicating regions of capillary obstruction; scale bar, 10 μm. Bottom yellow panels show computed 3D reconstructions. (**h**,**i**) Myeloid-derived cell infiltration dynamics showing maintained attenuation in hearts from metoprolol-treated mice. $n=5$. (**j**) Neutrophilic proportions infiltrate dynamics. (**k**) Representative confocal images of LV sections taken from injured mice after 6 and 24 h reperfusion onset. Myeloid infiltration (LysM-GFP+, green) most of which are neutrophil (Ly6G+, red) is evident in vehicle-treated mice and significantly attenuated in those from metoprolol-treated mice; merged images show double positive cells (LysM+/Ly6G+, that is, neutrophils). Scale bar, 50 μm; $n=3$–5. (**l**) Representative confocal images of neutrophil infiltration 24 h after reperfusion onset. Vehicle-treated mice show massive myocardial neutrophil infiltration (LysM-GFP+, green), with dispersed cells attached to the injured cardiac fibre membranes (α-actinin, red; laminin, grey). (**m**) LysM+ total area in the LV section as a %AAR; scale bar, 20 μm; $n=5$–6. (**n**–**q**) Effect of metoprolol on limiting-infarct size in neutrophil-depleted mice. (**n**) Neutrophil depletion model. (**o**) Myocardial area at risk (AAR). (**p**) Infarct size. (**q**) Representative transverse ventricular slices showing AAR and infarct size Data are means ± s.e.m. $^{*}P<0.05$; $^{**}P<0.01$, determined by the nonparametric Wilcoxon–Mann–Whitney test for each panel.

Using the cremaster IVM model of TNFα-induced local inflammation, we evaluated the acute neutrophil–platelet inhibitory effect of metoprolol in polarized neutrophils (Fig. 5). Metoprolol i.v. administration effectively inhibited interactions with the uropod, but not the leading edge (Fig. 5g,h) and rapidly reduced total neutrophil–platelet interactions (Fig. 5i–k). IVM experiments in *Adrb*1KO mice revealed no differences between metoprolol-treated and vehicle-treated mice, implicating ADRB1 in the inhibitory effect of metoprolol on neutrophil–platelet interactions (Fig. 5j).

Based on these findings, we hypothesized that inhibition of neutrophil–platelet interactions underlies the inhibitory effect of metoprolol on MVO after myocardial IR. To test this, we first evaluated the effect of metoprolol on neutrophil–platelet

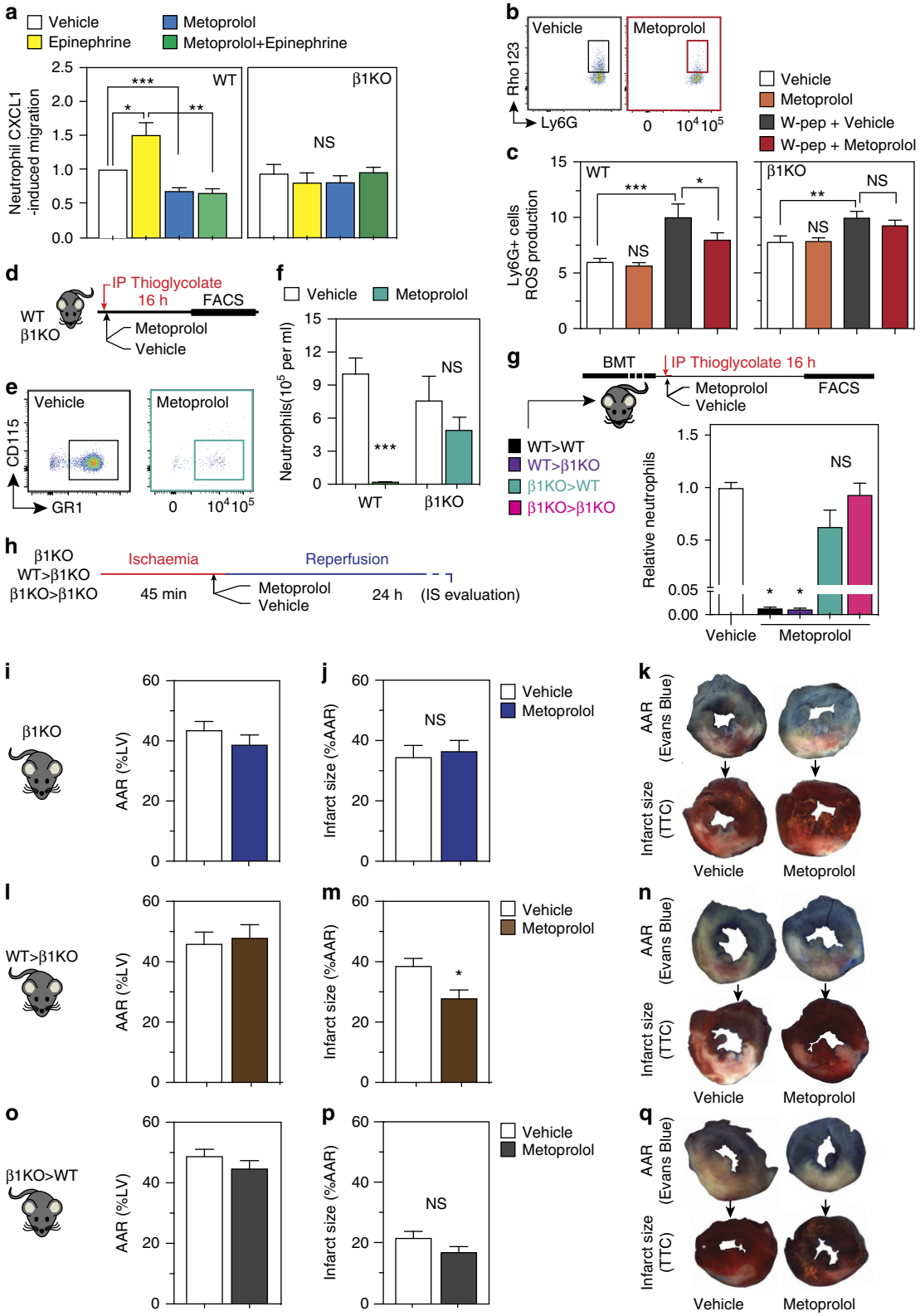

co-aggregate formation in mouse myocardial vessels after experimental IR. Administration of metoprolol to wild-type mice during ongoing AMI significantly reduced the number of neutrophils attached to the vessel wall (Fig. 6a,b) and the average number of interacting platelets per neutrophil (Fig. 6c).

Neutrophil–platelet interactions during acute injury are mediated by PSGL1 and signals delivered upon these contacts promote subsequent neutrophil extravasation and injury to the tissue[8]. Blockade of PSGL1 by pretreatment with PSGL1-mAB (Fig. 6e) significantly reduced infarct size in the myocardial IR model, and administration of metoprolol during ongoing AMI did not yield any further infarct-size reductions (Fig. 6f,g). These data confirm that metoprolol protects the infarcted myocardium by uncoupling neutrophil recruitment and polarization, thereby disrupting neutrophil–platelet interactions and the downstream inflammatory response.

Metoprolol limits neutrophil–platelet aggregates in patients. To investigate whether metoprolol alters neutrophil dynamics and inhibits neutrophil–platelet interactions in humans, whole blood drawn from healthy donors was incubated *ex vivo* with epinephrine (5 μM) and increasing concentrations of metoprolol (0, 2, 5 μM). Samples were then stained, and neutrophil–platelet co-aggregate formation was evaluated by flow cytometry[34–37] (morphological parameters, CD14neg, CD45+, CD61+). Metoprolol significantly inhibited epinephrine-stimulated neutrophil–platelet co-aggregate formation (Fig. 7a). The effect of metoprolol *in vivo* was additionally studied in patients undergoing elective coronary angioplasty for acute coronary syndrome (ACS). Samples were collected before and after i.v. administration of metoprolol (15 mg) and circulating neutrophil–platelet co-aggregates were assessed by flow cytometry. Metoprolol administration significantly reduced the number of neutrophil–platelet interactions (Fig. 7b). To elucidate whether metoprolol was acting at the platelet level of action we evaluated effect of metoprolol on platelet function through platelet aggregation using light transmittance aggregometry in platelet-rich plasma (PRP) (Supplementary Fig. 8a) or platelet activation surface markers expression assay using flow cytometry (Supplementary Fig. 8b,c). Metoprolol did not show any effect on platelet aggregation/activation, which together with the aforementioned effects on neutrophil migration and ROS-production suggests that the effect seen on neutrophil–platelet co-aggregates was driven by a direct effect on neutrophils.

Discussion

Early metoprolol administration during AMI, given as an adjunct to mechanical reperfusion has been shown to reduce infarct size and ameliorate post-infarction severe cardiac dysfunction[11,38]. Defining the mechanisms underlying this cardioprotection is therefore of great medical relevance since more efficient and specific protective strategies could be identified.

The ability of ADRB1 selective blockers to reduce infarct size was tested decades ago in several clinical trials, but the results were inconclusive[1]. However, most of these early studies were performed in the context of non-reperfused AMI. The advent of reperfusion as the treatment of choice for AMI changed the mode of myocardial death: from unrelieved ischaemia to a combination of ischaemia and reperfusion processes. Therefore the potential cardioprotective effects of ADRB1 selective blockers needed to be revisited in light of the current evidence of IR injury during AMI (ref. 1). The ability of metoprolol to reduce infarct size in the context of reperfused AMI was recently evaluated in the METOCARD-CNIC trial. In this trial, early i.v. metoprolol administration during ongoing AMI resulted in a significant reduction of infarct size[9,39], and also significantly reduced the incidence of severe ventricular dysfunction and heart failure readmissions[10]. Large animal studies conducted before the METOCARD-CNIC trial showed that metoprolol reduces infarct size only when administered before reperfusion[40,41], suggesting that metoprolol might reduce infarct size by inhibiting reperfusion injury. The early studies, testing the infarct-limiting properties of metoprolol in non-reperfused AMI, were undertaken under the hypothesis that ADRB1-blockers would reduce the extent of damage by a direct effect on cardiomyocytes via reducing oxygen consumption. Although our large animal study[40] did not investigate the mechanism of metoprolol-mediated protection, it did show that oxygen consumption was similar in metoprolol- and vehicle-treated pigs. In addition, the infarct-size reduction in metoprolol-treated pigs was associated with reduced myeloperoxidase activity in the post-ischaemic myocardium 24 h after reperfusion[41]. These findings challenged the idea that metoprolol could reduce cardiac damages simply by reducing myocardial oxygen consumption directly in the heart and prompted us to investigate the cellular mechanisms underlying the reperfusion-related injury-limiting effect of metoprolol during IR.

There is ample evidence supporting the critical implication of neutrophils in IR injury[4,25,27,29,42,43]. Neutrophils have two deleterious effects in this context. First, neutrophils and neutrophil–platelet plugs occlude microvessels, preventing efficient tissue perfusion: MVO. Second, neutrophils adhering to the newly reperfused injured vessels infiltrate the myocardium[1], prompting deleterious processes associated with reperfusion[25,33]. Our study confirms these associations in AMI patients: neutrophil count positively correlated with the extent of MVO as evaluated by state-of-the-art MRI 1 week after reperfusion. There exist weak pre-existing evidence linking the action of metoprolol to neutrophils, including reductions in

Figure 4 | Metoprolol directly inhibits neutrophil deleterious function through a *ADRB1*-blockade. (**a**) Effect of metoprolol on CXCL1-induced migration of fresh isolated primary neutrophils (Ly6G+) from WT or *Adrb1*-knockout (β1KO) mice. CXCL1-stimulated cells were incubated with vehicle, epinephrine (10 μM), metoprolol (10 μM) and epinephrine + metoprolol; $n=4$ independent experiments. NS, stands for non-significant. (**b**,**c**) Inhibitory effect of metoprolol on W-peptide-induced ROS production on fresh isolated primary neutrophils (Ly6G+) from WT or β1KO mice. Mean fluorescent intensity of Rho123 in Ly6G+ neutrophils after W-peptide stimulation. $n=6$ independent experiments; flow cytometry plots illustrate reduced expression of Rho123 in metoprolol-treated neutrophils. (**d**–**f**) Effect of metoprolol on limiting-thioglycolate-induced peritoneal infiltration on WT and β1KO mice. (**e**) Flow cytometry plots illustrating reduced infiltration of neutrophils (CD115neg; GR1+) in metoprolol-treated mice. Absolute neutrophils detected per ml of infiltrate at 16 h after thioglycolate injection in WT mice ($n=7$–9) or β1KO mice ($n=5$). (**g**) Effect of metoprolol on thioglycolate-induced neutrophil infiltration in the four BMT groups. Protocol scheme for thioglycolate-induced peritonitis assay after bone-marrow transplants (BMT) between WT and β1KO mice, evaluating the influence of the presence or absence of *ADRB1* in circulating cells. Data are normalized to vehicle; $n=4$–9. (**h**) Protocol scheme for IR experiments in chimeric animals after BMT, evaluating the infarct-limiting effect of metoprolol in the presence or absence of *ADRB1* in circulating cells. (**i**–**q**) Area at risk (AAR) and infarct size, as well as representative images of Evans blue and TTC staining in metoprolol-treated and vehicle-treated β1KO and chimeras (WT bone marrow transplanted into β1KO mice and reverse transplants). Infarct size is reduced by metoprolol only when circulating cells express β1-adrenergic receptor; $n=9$ (**i**,**j**), $n=8$ (**l**,**m**), $n=5$–6 (**o**,**p**). Data are means ± s.e.m. $^*P<0.05$; $^{**}P<0.01$; $^{***}P<0.001$, determined by the nonparametric Wilcoxon–Mann–Whitney test or using the one-way ANOVA and Holm Sidak's *post-hoc* multiple comparisons method.

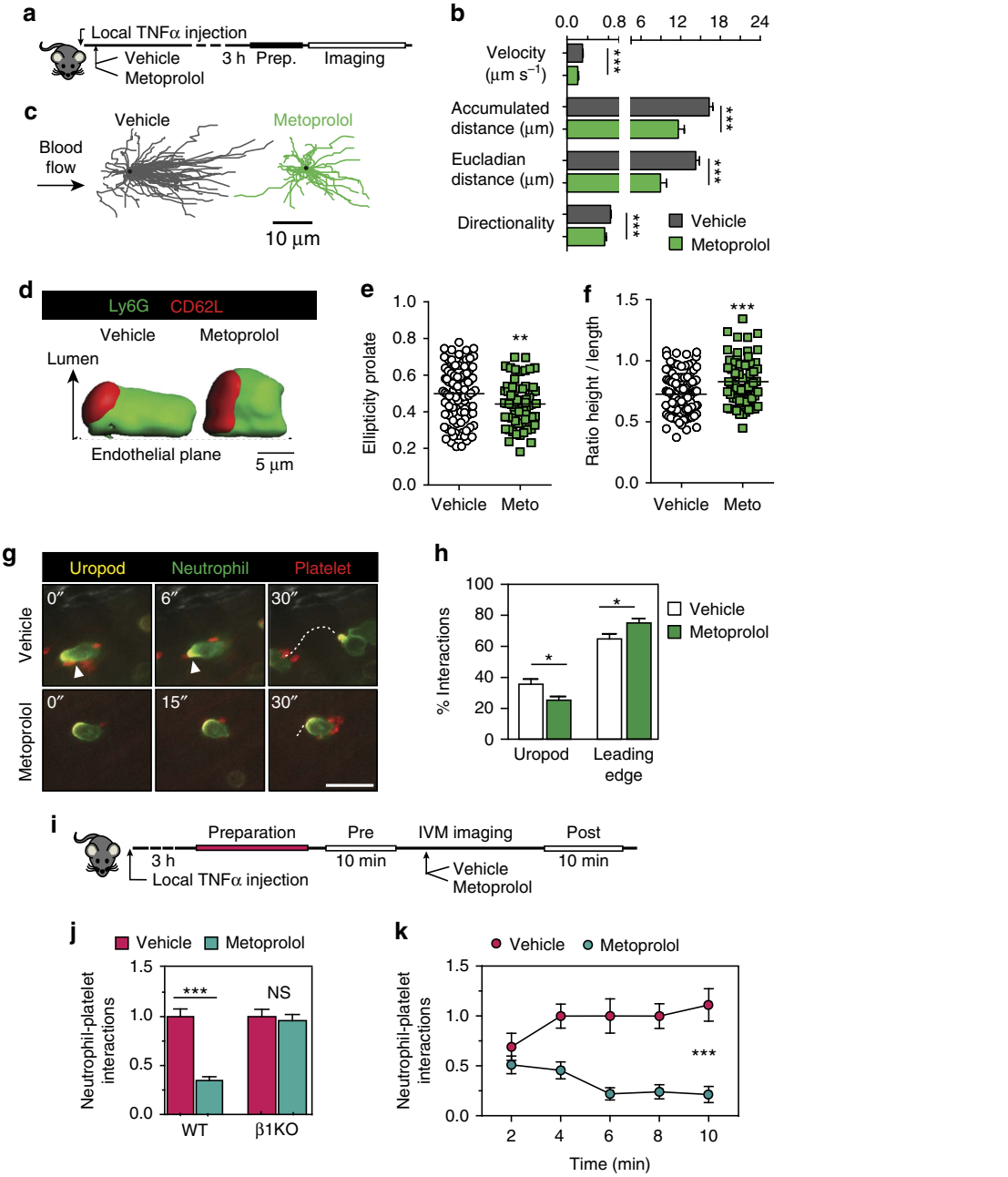

Figure 5 | Metoprolol stuns neutrophils and prevents interactions with platelets. (**a**) Experimental design: WT mice receiving TNFα were randomized to receive i.v. metoprolol or vehicle before analysis of cremaster muscle vessels by 2D and 3D intravital microscopy. (**b**) Quantification of parameters related to two-dimensional intravascular motility; $n = 54$–141 cells from 3 to 4 mice. (**c**) Representative tracks of crawling neutrophils within inflamed vessels. (**d**) 3D reconstructions of representative neutrophils within live vessels of saline-treated and metoprolol-treated mice (red, uropod; green, cell body). (**e**,**f**) Quantification of 3D parameters, indicating reduced elongation (prolate ellipticity) and enhanced projection of recruited neutrophils into the luminal space (height-to-length ratio); $n = 68$–105 cells from 3 to 4 mice. (**g**,**h**) Representative time-lapse images and percentage of interactions of platelets (CD41, red) with the polarized neutrophil uropod (CD62L, yellow) or leading edge (Ly6G, green); $n = 28$–29 vessels from 3 to 4 mice. White arrowheads indicate interactions with the uropod and the dotted line the displacement of the cells during 30 s. Scale bar, 10 μm. (**i**) Protocol scheme for evaluating the acute inhibitory effect of metoprolol on activated and polarized neutrophils on WT and *AdrbB1*-knockout (β1KO) mice. (**j**) Absolute neutrophil–platelet intravascular interactions in WT and β1KO mice. NS, stands for non-significant. (**k**) Temporal neutrophil–platelet interaction inhibition in WT mice after administration with i.v. metoprolol. Data are means ± s.e.m. $^*P < 0.05$; $^{**}P < 0.01$; $^{***}P < 0.001$, determined by unpaired Student's *t*-test for each parameter.

post-IR myeloperoxidase activity in pig myocardium[41] and rat spinal cord[44], and inhibition of sepsis-induced inflammation in mice[45]. The data here presented from patients randomized in a controlled clinical trial are the first human evidence linking metoprolol with altered neutrophil behaviour *in vivo*. We show that the strong positive correlation between neutrophil count and MVO was abolished in patients receiving i.v. metoprolol before reperfusion. The fact that metoprolol-treated patients' high neutrophil count was not associated with the extent of MVO suggests an altered neutrophil dynamics during acute injury.

Some preclinical studies have suggested an association between metoprolol exposure and altered neutrophil dynamics[41,44,45];

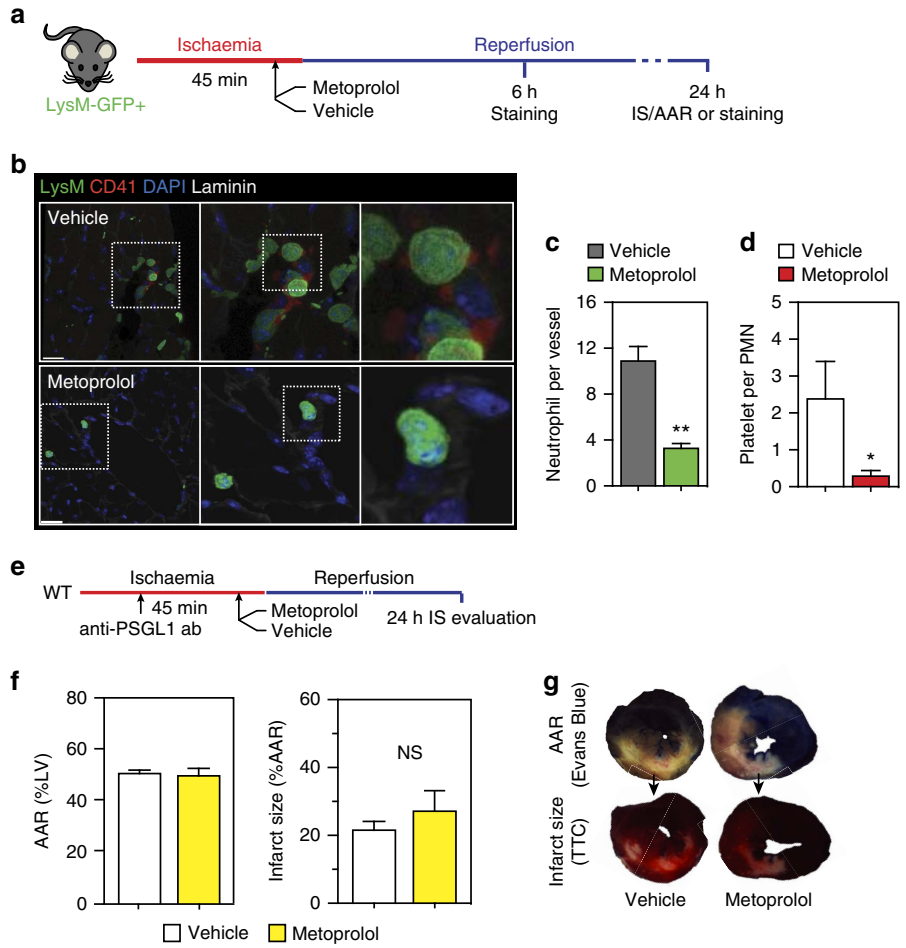

Figure 6 | Metoprolol inhibits neutrophil–platelet interactions. (**a**) Experimental scheme and representative confocal images evaluating the effect of metoprolol on the number of co-aggregates of neutrophils (LysM-GFP+, green) and platelets (CD41, red) in the post-reperfused mouse myocardium. (**b**,**c**) LysM-GFP+ cells (neutrophils) attached to coronary vessels ($n=7$–9) and the numbers of interacting platelets (CD41+) per neutrophil in reperfused myocardium. Scale bar, 20 μm. (**d**) Protocol scheme for the IR experiment evaluating the effect of neutrophil-platelet blockade with anti-*PSGL1* Ab (administered 15 min after ischaemia onset, that is, 30 min before reperfusion) on the infarct-limiting effect of metoprolol (administered 35 min after ischaemia onset, that is,10 min before reperfusion). (**e**–**g**) AAR, infarct size, and representative images of Evans blue and TTC staining in vehicle- and metoprolol-treated mice pretreated with anti-*PSGL1* Ab. $n=5$–7. NS, stands for non-significant. Data are means ± s.e.m. $^{*}P<0.05$; $^{**}P<0.01$. Comparison was determined by the nonparametric Wilcoxon–Mann–Whitney test.

however, the cellular mechanism responsible for this effect has remained unknown. Our results from the *in vitro* transwell migration assays confirm previous studies showing the ability of metoprolol to inhibit migration of isolated neutrophils[46]. Also, our *in vitro* data confirm previous studies showing that metoprolol was able to inhibit ROS production from neutrophils[47]. Our *in vitro* results showing migration inhibition by metoprolol are reinforced by the acute *in vivo* murine peritonitis model, in which a single metoprolol i.v. injection abrogates neutrophil infiltration into the peritoneal cavity. Furthermore, the studies with *Adrb1*KO mice provide evidence for a critical involvement of the ADRB1 axis in the effects of metoprolol. In the transwell assays, metoprolol had no effect on the migration of *Adrb1*KO neutrophils, and in the peritonitis assay, the inhibitory effect of metoprolol on neutrophil infiltration was lost in *Adrb1*KO mice. The rescue of this inhibitory effect in chimeric animals in which *Adrb1* is expressed only in circulating cells demonstrates that the cellular target of metoprolol action is of haematopoietic origin, and rules out an involvement of other compartments. Moreover, the findings in the peritonitis model were confirmed in the myocardial IR model, with metoprolol significantly reducing neutrophil infiltration into the injured myocardium of wild-type but not *Adrb1*KO mice, and rescue of the protective effect in the *Adrb1*KO after wild-type BM transplant. Finally, we ruled out any involvement of ADRB2 on the effect exerted by metoprolol. Altogether, these results demonstrate the essential role of neutrophil ADRB1 blockade in the protective effect of metoprolol against myocardial IR injury. Our data are in discrepancy with a prior study suggesting that metoprolol abrogated neutrophil migration *in vitro* in an apparently ADRB1-independent manner[46]. In that study authors reported that metoprolol was able to inhibit neutrophil migration even in the presence of the β-adrenergic receptor agonist orciprenaline, while in our study we have used a genetic ablation toll (that is, *Adrb1*KO mice), which ensures the absence of ADRB1.

Upon acute injury, neutrophils recruited to injured vessels initiate inflammation by scanning for activated platelets present in the circulation, establishing interactions with them through *PSGL1* exposed on neutrophil protrusions[8]. The IVM confocal imaging analysis demonstrated that metoprolol prevents the exposure of functional *PSGL1* clusters, which are essential for

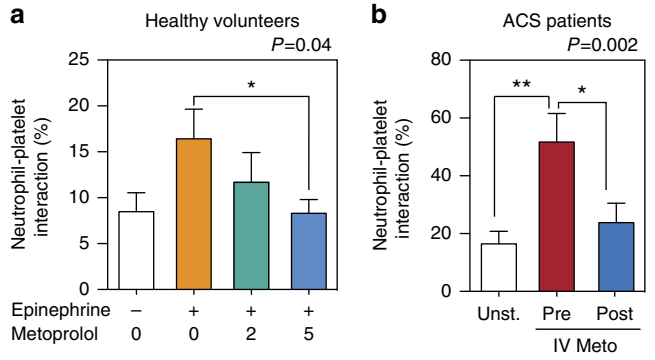

Figure 7 | Metoprolol inhibits neutrophil–platelet interactions in patients. (**a**) Effect of metoprolol on neutrophil–platelet co-aggregate formation in epinephrine-stimulated whole blood from healthy volunteers ($n=20$). Whole blood was incubated *in vitro* with epinephrine 5 μM and metroprolol (Meto, concentrations in μM). (**b**) *In vivo* effect of metoprolol (up to15 mg i.v.) on the number of neutrophil i.v.platelet co-aggregates in acute coronary syndrome (ACS) patients scheduled for coronary angioplasty. Blood was drawn before and after metoprolol i.v. administration; $n=6$ ACS patients. Pre, before i.v. administration; Post, after i.v. administration. Data are means ± s.e.m. $^{*}P<0.05$; $^{**}P<0.01$, determined by one-way ANOVA and Holm Sidak's *post-hoc* multiple comparisons method.

interaction with platelets. These events correlated with alterations in neutrophil properties essential for infiltration, including migratory velocity and directionality. In agreement with these data, in the mouse myocardial IR model, metoprolol altered neutrophil 3D structure and reduced the numbers of neutrophil–platelet co-aggregates that occluded myocardial vessels. The inability of metoprolol to provide additional protection after blockade of neutrophil–platelet interactions with the anti-PSGL1 mAB is compelling evidence for interference in this interaction as the mechanism underlying the infarct-limiting action of metoprolol during myocardial IR in mice. The demonstration that metoprolol inhibits neutrophil–platelet interactions in healthy volunteers and ACS patients suggests that this mechanism also operates in humans. There is controversy on the direct effect of metoprolol on platelet aggregation. Some studies suggested that metoprolol was able to inhibit ADP- and epinephrine-mediated platelet aggregation[48], but recent studies did not show any anti-platelet effect of metoprolol[49]. In line with the latter evidence, in our study we found that metoprolol had no effect on platelet aggregation or in platelet activation in healthy volunteers. These data strongly suggest that the inhibitory effect of metoprolol on neutrophil–platelet co-aggregates was driven by a direct effect on neutrophils. In our flow cytometry studies we defined a positive neutrophil–platelet interaction as CD14neg, CD45+, CD61+ particles. It should be noted that there are more specific neutrophil markers and thus our selection is a limitation of these experiments. However, given that all data (human and mouse) point to the same direction, we think this limitation did not have an impact on the conclusions obtained in these experiments.

The role of neutrophils in experimental IR injury is well established; however, the negative results of clinical trials with anti-inflammatory therapies (for example, C5a (refs 50,51), CD-18 (ref. 52)) dampened hopes for this pharmacological strategy[3], and suggested that parallel mechanisms driving myocardial injury were at play. The demonstration that neutrophil dynamics in general and neutrophil–platelet interactions in particular are the target for the protective actions of metoprolol administered to patients during AMI reinstates neutrophils as a potential target for the therapeutic reduction of infarct size.

Methods

Human cardiac magnetic resonance imaging. The METOCARD-CNIC trial (NCT01311700) recruited patients suffering an AMI during hospital transit to undergo mechanical reperfusion by primary angioplasty. Patients were randomized to receive i.v. metoprolol (up to 15 mg) or no drug (control). Patients underwent two CMR studies: 1 week and 6 months after AMI. Images were acquired with a 3.0 Tesla magnet (Achieva Tx, Philips Medical Systems) with vectorcardiographic gating and a dedicated cardiac 32-channel phased-array surface coil. The extent of MVO was measured in the 1-week CMR study; to detect and quantify MVO, a delayed enhancement imaging was performed 10 min after gadolinium contrast injection, using a T1-weighted 2-D Inversion Recovery Turbo Field Echo (2D IR-TFE) sequence. Myocardial necrosis was defined by the extent of abnormal gadolinium enhancement, whereas MVO was defined as black-hypoenhanced areas within the bright-hyperenhanced regions. CMR analysis was undertaken by operators blinded to treatment allocation at the Centro Nacional de Investigaciones Cardiovasculares Carlos III (CNIC). Myocardial necrosis and MVO were quantified by semiautomatic delineation with dedicated software (QMass MR 7.6; Medis, Leiden, the Netherlands). Total MVO was quantified as grams of LV. To correct for infarct size, MVO was also expressed as a percentage of the infarcted area.

Mouse procedures. Experimental procedures were approved by the CNIC Animal Care and Ethics Committee and regional authorities. IR, thioglycolate-induced peritonitis and IVM experiments were performed in 8–13-week-old wild-type male C57BL/6 mice. β1-adrenergic receptor (*Adrb1*) knockout (KO; *Adrb1*KO) mice were in a mixed background. β2-adrenergic receptor (*Adrb2*) knockout (KO; *Adrb2*KO) mice were in a C5BL/6 background. For the BM transplant experiments, *Adrb1*KO mice were backcrossed with mice expressing DsRed under the control of the β-actin promoter to facilitate evaluation of BM engraftment. Male and female mice were used as donors in BM transplant procedures, but only males were used in myocardial IR and thioglycolate-induced peritonitis experiments. All animals were randomized to receive a single i.v. injection (50 μl) of metoprolol-tartrate (10 mM) or vehicle (saline). Histological evaluation of injured myocardium in the myocardial IR model was performed in lysozyme M-GFP+ (LysM-GFP)[53] male mice. Intravascular neutrophil and neutrophil–platelet interactions were scored manually in the myocardium. Neutrophils were depleted in C57BL/6 male by i.v. injections of 50 μg anti-mouse Ly6G 24 and 48 h before the myocardial IR procedure[28]. For *in vivo* blocking of P-selectin glycoprotein ligand-1 (*PSGL1*), 50 μg of anti-*PSGL1* antibody (clone 4RA10) was i.v. injected 15 min after ischaemia onset. Mice were maintained under pathogen-free conditions in a temperature-controlled room and a 12-h light–dark cycle at the CNIC animal facilities. Chow and water were available *ad libitum*.

Reagents. Metoprolol-tartrate (M5391), Evans blue, triphenyltetrazolium chloride, DAPI (D8417-1MG), Mowiol mounting medium (81381), anti-laminin (L9393), anti-α-actinin (A7732), dihydrorhodamine 123 (D1054) were obtained from Sigma-Aldrich. Dylight-650-conjugated anti-1A8 Ly6G (BE0075-1) and anti-*PSGL1* antibody (clone 4RA10) from BioXcell. Anti-CD41 (12-04-11-83) and anti-CD115 (12-1152-83) were obtained from ebioscience. O.C.T. was obtained from Tissue-Tek. Qiagen RNeasy Plus Mini Kit (74136). Percoll Plus (17-5445-02) and Ready-to-go RT-PCR Beads (27-9259-01) from GE Healthcare. CXCL1 was obtained from (453-KC-010) from R&D Systems. W-peptide (WKYMVM, 1799) from Tocris. Thioglycolate (BD211716) and anti-GP IIb/IIIa from BD Biosciences. Anti-GR1 (ab2557) was obtained from Abcam and AF-647 (A-21472) from Molecular Probes. Anti-CD45-FITC from Miltenyi Biotec, Germany. PC5-conjugated anti-CD14, anti-CD61 PC7 and Versalyse solution were obtained from Beckman Coulter.

Mouse model of myocardial IR injury. Male 8–12-week-old mice were subjected to 45 min occlusion of the LAD coronary artery followed by 6 or 24 h of reperfusion. For infarct size evaluation, reperfusion was maintained for 24 h. For analysis of MVO, neutrophil infiltration and neutrophil–platelet interactions, reperfusion was maintained for 6 or 24 h as indicated. The IR procedure was performed as previously described[54]. Briefly, fully asleep animals were intubated and temperature controlled throughout the experiment at 36.5 °C to prevent hypothermic cardioprotection. Thoracotomy was then performed and the LAD was ligated with a nylon 8/0 monofilament suture for 45 min. The electrocardiogram was monitored (MP36R, Biopac Systems Inc.) to confirm total coronary artery occlusion (ST-segment elevation) throughout the 45 min ischaemia. Ten minutes before reperfusion onset, mice were randomized to receive a single i.v. injection (50 μl) of metoprolol-tartrate (10 mM) or vehicle (saline) through the femoral vein. Dose of metoprolol was chosen after a dose response study (Supplementary Fig. 9). At the end of reperfusion, the chest was closed and animals were kept with 100% O_2 and analgesized with buprenorphine (S.C., 0.1 mg per kg) until the end of reperfusion.

Mouse infarct size quantification. At the end of follow up, mice were re-anesthetized and re-intubated, and the LAD coronary artery was re-occluded by ligating the suture in the same position as the original infarction[54]. Animals were then killed and rapidly 1 ml of 1% (w per v) Evans Blue dye was infused i.v. to delineate AAR: myocardium lacking blood flow, that is, negative for blue dye staining. The heart was then harvested, LV was isolated, cut into transverse slices (5–7 1-mm thick slices per LV) and both sides were imaged. Sections post-Evans blue staining present two different areas: one palish negative for Evans blue perfusion, delineating AAR, and another blueish (positive Evans blue) area indicating remote tissue. In order to differentiate infarcted from viable tissue, same slices were incubated in triphenyltetrazolium chloride (TTC, 1% (w per v) diluted in PBS) at 37 °C for 15 min in constant shacking. The slices were then re-photographed and weighed. Post TTC incubation, Evans blue staining clears out and slices present two areas: one necrotic (palish negative to TTC staining) and one reddish alive (positive to TTC staining). Regions negative for Evans Blue staining (AAR) and for TTC (infarcted myocardium) were quantified using ImageJ (NIH, Bethesda, MD, USA) by blinded observer. Percentage values for AAR and infarcted myocardium were corrected to mg independently for each slice. Absolute AAR and infarct size were determined as the mg:mg ratio of AAR:LV and infarcted myocardium:AAR, respectively. Animals exceeding 80% of IS were excluded assuming absence of reperfusion.

Hearts processing for histology. At the end of reperfusion, LysM-GFP mice were re-anesthetized, placed in a supine position, their ventral thoracic regions wiped with 70% alcohol and killed by cervical dislocation. Next, 10 ml of PBS with heparin (50 U per ml) was gently infused through the vena cava to avoid blood clots. Hearts were then removed and cut into 1 mm-thick transverse sections and fixed with 2% PFA in PBS for 24 h at 4 °C.

Heart slices (1 mm) designated to histopathological analysis of capillary obliteration were dehydrated through an ethanol series, cleared in xylene, embedded in paraffin wax and consequently sectioned (4 μm) for staining with haematoxylin and eosin. All immunohistochemical procedures were performed with an automated autostainer (Autostainer Plus, Dako) at the CNIC Histology Unit. Images were digitally scanned (Nanozoomer-RS C110730, Hamamatsu) and examined with image analysis software (Tissuemorph, Visiopharm) by blinded observers. Once the lesion was identified, 10–12 images (× 20) were taken at random, and capillary obliteration was scored from 0 to 2, with 0 indicating the absence of capillary obliteration and 2 indicating presence of obstruction in all capillaries.

Confocal microscopy. Sections designated for immunofluorescence staining and confocal microscopy were post-fixed overnight and placed in 30% sucrose for 24 h and included in O.C.T. (Tissue-Tek). Serial 4 μm coronal sections were cut on a freezing microtome (Leica CM1950) and stored in cryoprotective solution. Sections designated for evaluation of neutrophil infiltration of the injured area were washed in PBS for 15 min and incubated with DAPI (1:1,000) at room temperature for 5 min, washed in PBS twice and mounted in Mowiol mounting medium. Images of full short-axis heart sections were acquired with an inverted confocal laser imaging system (Zeiss LSM7004 4-Laser) and reconstructed with Zeiss ZEN reprocessing software. Presence of Lysm-GFP + cells analysis was performed with ImageJ (NIH) by blinded observers. Values of total GFP + surface were normalized to LV section surface. A second set of sections were stained with Dylight-650-conjugated anti-1A8 Ly6G and DAPI for quantification of specific neutrophil identification and temporal infiltration analysis. Eight independent 40 × were evaluated from injured myocardium from each animal, and presence of myeloid derived cells (LysM +), neutrophils (*LysM* + *Ly6G* +) and monocytes (*LysM* + *Ly6G*neg) were identified and analysed using ImageJ by blinded observers. Four animals were stained for basal quantification. Some sections were stained with anti-laminin to stain cell membranes (1:150) and anti-α-actinin to visualize sarcomeres in cardiac fibres (1:200) for detailed illustration of neutrophil infiltration in the injured myocardium. Images were post-processed and edited using the Imaris software (Bitplane AG, Switzerland) as indicated below.

Neutrophil–platelet interactions staining in infarcted mouse heart was adapted from Sreeramkumar *et al.*[8]. Briefly, OCT-embedded heart slices were cut into 50 μm sections, washed in PBS for 15 min and incubated for 20 min at room temperature in blocking buffer (PBS containing 10% BSA and 2% goat serum). For detailed visualization and characterization of the injured zone, cell membranes were stained with anti-laminin (1:150) and platelets were stained with PE-conjugated anti-*CD41* (1:200). Primary and secondary antibodies were diluted 1:200 in blocking buffer, and incubations were conducted for 1 h at room temperature. Nonspecific staining was assessed by omission of primary antibody. Samples were counterstained with DAPI and mounted in Mowiol. Images were acquired with a laser-scanning confocal imaging system (Leica SP8 or SP5) at the CNIC Microscopy Unit and post-processed with Leica Las AF and Imaris software (Bitplane AG, Switzerland). Independent vessels (7–9) were evaluated for each animal, and intravascular neutrophil and neutrophil–platelet interactions were scored manually.

Neutrophil purification and *Adrb1* expression. *Adrb1* expression in circulating neutrophils was examined in blood drawn from wild-type or *Adrb1*KO mice 20 min after injection of heparin (50 μl of 50 U per ml). Whole blood was filtered and pooled, and polymorphonuclear leukocytes were purified by gradient-centrifugation (800*g*, 20 min, 4 °C) in 65% Percoll Plus in Hanks balanced salt solution (HBSS). Cells were washed in PBS and residual erythrocytes were lysed using hypotonic buffer. Neutrophils were washed and resuspended in HBSS. Before RNA isolation, neutrophil identity was confirmed by flow cytometry (anti-1A8 Ly6G) and viability evaluated.

Total RNA from whole hearts, BM and purified neutrophils samples was isolated with the Qiagen RNeasy Plus Mini Kit. RNA (1–2 μg) was reverse transcribed using Ready-to-go RT–PCR Beads (27-9259-01, GE Healthcare). PCR was performed with 40 cycles of 95 °C for 12 s and 60 °C for 1 min. All PCR reactions were done in triplicate. Primers for Hprt and *Adrb1* were as follows: mHprt_fw-5′-GAGGAGTCCTGTTGATGTTGCCAG-3′, mHprt_rv-5′-GGCTGG CCTATAGGCTCATAGTGC-3′; m*Adrb1*_fw-5′-GTGGGTAACGTGCTG GTGAT-3′, m*Adrb1*_rv-5′-GAAGTCCAGAGCTCGCAGAA-3′. Amplicons generated in the qPCR were loaded on to an agarose gel to confirm single PCR products.

Migration transwell assay. The ability of leukocytes to migrate towards chemokine (C-X-C motif) ligand 1 (CXCL1) was assessed using a modification of the method of Villablanca *et al.*[55]. Briefly, wild-type or *Adrb1*KO mice were heparinized (50 μl of 50 U per ml, IP) and 20 min later blood was collected and filtered, and residual erythrocytes were lysed with hypotonic buffer. PBS-washed leukocytes of the same genotype were pooled and resuspended in RPMI containing 10% FBS and the appropriate treatment: saline (vehicle control), 10 μM epinephrine (positive control), 10 μM metoprolol-tartrate, or a combination of epinephrine and metoprolol. Transwell inserts (6.5 mm, 5.0 μm pore size (3421; Corning Costar Corporation)) were pretreated with 50 μl RPMI for 20 min and placed in 24-well-plates before seeding cells (100 μl; $\sim 1 \times 10^5$; > 90% viability). Lower compartments (wells) were filled with 600 μl DMEM medium containing 0.04 ng per μl CXCL1 to induce directional movement. Spontaneous migration was assessed in wells lacking CXCL1. After incubation at 37 °C for 1.5 h, cells in the lower compartment were collected and neutrophils (Ly6G + cells) were evaluated by flow cytometry. Each independent experiment was conducted with leukocytes pooled from nine animals, and each of the five conditions was run with four replicates. Mean spontaneous migration was subtracted from the migration value of each well, and neutrophil migration was expressed as a percentage of the total number of neutrophils seeded in the upper chamber at the start of the experiment. For comparison between experiments and genotypes, migration was normalized to the mean control (vehicle) value.

Neutrophil oxidative burst assay. Blood from wild-type or *Adrb1*KO mice was collected in heparinized tubes and distributed in 100 μl aliquots, erythrocytes were lysed with hypotonic buffer. After centrifugation leucocytes were first washed and then re-suspended in high glucose phenol red free DMEM. Cells were then incubated for 50 min with or without metoprolol-tartrate 100 μM at 37 °C. As previously described[30,31], dihydrorhodamine 123 (DHR 123, 1 μM), which converts to the fluorescent product rhodamine 123 (Rho 123) upon oxidation was then added to the medium and cells were stimulated with the *chemotactic FPR activator-peptide,* w-peptide 1 μM (WKYMVM, 1799 Tocris). After 20 min incubation at 37 °C the reaction was stopped in ice and cells were washed in cold HBSS containing DAPI 0.1 μg per ml (D8417, Sigma). Mean fluorescent intensity for Rho 123 was evaluated for neutrophils (*Ly6G* + cells) alive (DAPIneg) by flow cytometry.

Model of thioglycolate-induced peritonitis. To assess the ability of metoprolol to inhibit neutrophil recruitment, we used a well-established thioglycolate-induced peritonitis model (see Fig. 3). Wild-type mice were intraperitoneally injected with 1 ml of thioglycolate and immediately randomized to receive a single 50 μl i.v. injection of vehicle or metoprolol-tartrate (10 mM). Sixteen hours later, 100 μl of blood from each animal was collected into EDTA tubes for later haematological analysis in a haematocytometer (Pentra 80). Next, animals were killed, 2 ml PBS was injected intraperitoneally and distributed manually for 30 s to detach infiltrated circulatory cells. Next, another 8 ml PBS was injected to facilitate collection of 6 ml peritoneal exudate. Exudates were gently centrifuged, and cells were washed twice with PBS and incubated for 1 h with anti-GR1 (1:200) and PE-conjugated anti-CD115 (1:200). After washing with PBS, cells were incubated for 30 min with anti-rat 647 to detect GR1. Cell nuclei were stained with DAPI. All samples were analysed by flow cytometry for exactly 30 s of constant flow. Neutrophil recruitment efficiencies are presented as neutrophils per ml of exudate for each independent animal.

To evaluate the role of ADRB1 in different compartments, we performed the same experiments in *Adrb1*KO mice and generated cohorts of chimeric mice by transplantation with BM cells from wild-type and *Adrb1*KO donors. Four weeks after BM transplantation, chimerism was evaluated by flow cytometry as the percentage of donated cells. Animals with chimerism below 85% were discarded; those with chimerism above 85% underwent the thioglycolate-induced peritonitis

protocol followed by randomization to receive either i.v. vehicle or metoprolol (10 mM). To compare between the different chimeric groups, the mean value for each metoprolol-treated group was normalized to the mean for the vehicle-treated group.

Bone marrow transplant. BM transplants protocols were adapted from Casanova *et al.*[28]. Recipient mice from *Adrb1*KO or wild-type genotypes (DsRed + or DsRed- as appropriate) were lethally irradiated (13 Gy in two doses) before reconstitution with donor BM. Donor BM was collected from mice of the appropriate genotype by flushing both tibiae and femurs into PBS containing 2 mM EDTA (PEB buffer). Contaminating erythrocytes were lysed with hypotonic buffer. Engraftment in recipient animals was assessed by flow cytometry 3–4 weeks after transplantation. Animals bled for engraftment evaluations were rested for 1 week before any other procedure.

Flow cytometry. Neutrophil purity for *in vitro* migration assay and *Adrb1* expression analysis was evaluated by incubating cells with Dylight-650-conjugated anti-1A8 *Ly6G* and with DAPI to assess viability. Mouse primary blood leukocytes from peritonitis experiments were incubated with anti-Gr1 conjugated with AF-647 and with PE-conjugated anti-CD115 and DAPI. Neutrophils were gated on the basis of Gr1-positive and CD115-negative staining in a FACS Canto-3L flow cytometre equipped with DIVA software (BD Biosciences). Doublet discrimination and viability (negative to DAPI) was assessed for every sample. Data were analysed with FlowJo (Ashland) software by blinded observer. All experiments were conducted at the CNIC-Cellomics Unit.

Intravital microscopy. IVM of the cremaster muscle was performed after intrascrotal injection of TNFα (0.5 mg R&D Systems)[8], followed immediately by injection of a single i.v. bolus of metoprolol (10 mM) or vehicle, and neutrophil behaviour was evaluated 3 h after stimulus. In some experiments metoprolol was injected 3 h after treatment with TNF-α and images immediately acquired for analysis (see Fig. 4). The IVM system was built by 3i (Intelligent Imaging Innovations, Denver, CO, USA) on an Axio Examiner Z.1 workstation (Zeiss, Oberkochen, Germany) mounted on a 3-Dimensional Motorized Stage (Sutter Instrument, Novato, CA, USA). This set up allows precise computer-controlled lateral movement between XY positions and a Z focusing drive for confocal acquisition. The microscope is equipped with a CoolLED pE widefield fluorescence LED light source system (CoolLED Ltd. UK) and a quad pass filter cube with a Semrock Di01-R405/488/561/635 dichroic and a FF01-446/523/600/677 emitter. We used a plan-Apochromat ×40 W NA1.0 ∞/0 objective (Zeiss). Images were collected with a CoolSnap HQ2 camera (6.45 × 6.45-μm pixels, 1,392 × 1,040 pixel format; Photometrics, Tucson, AZ, USA). For confocal high-speed IVM, we used laser stacks for 488, 561 and 640 nm beams coupled with a confocal scanner (Yokogawa CSUX-A1; Yokogawa, Japan); images were acquired at 0.5 μm Z-intervals. Image acquisition was coordinated and offline data analysis facilitated with SlideBook software (Intelligent Imaging Innovations), run on a Dell Precision T7500 computer (Dell Inc., Round Rock, TX, USA). For three-dimensional analysis we used the 3D surface view function to determine the position of the *CD62L* + clusters relative to the cell body and the lumen. Six to ten venules per mouse were analysed 210 to 300 min after TNF-α treatment by acquisition of fluorescence (Cy3/561 channels for phycoerythirn, FITC/488 channels for FITC and Cy5/640 channels for allophycocianin) and bright-field images with 2 × 2 for 2 min. For double staining with PE- and FITC-conjugated antibodies, acquisition was facilitated in single (FITC) and quad (PE) filters in order to avoid bleed-through of fluorescent signals between channels. For *in vivo* labelling of neutrophils and platelets surface molecules, fluorescently labelled antibodies were injected intravenously (anti-*CD62L*-FITC, anti-*Ly6G*-APC and anti-*CD41*-PE; 0.5–1.25 μg per mouse). Images were post-processed and edited using the Imaris software (Bitplane AG, Switzerland) as indicated below.

Analysis of blood cell interactions. Platelets in the inflamed cremaster muscle were visualized as CD41-labelled cells and quantified as reported[8]. Briefly, we defined the uropod of adherent neutrophils as the domain staining positive for CD62L, and the leading edge as the CD62L-negative pole forming multiple protrusions and showing guided movement. Six to ten venules per mouse were recorded, and platelet interactions with neutrophils were counted and analysed manually at the two distinct domains of the polarized neutrophil with the help of Slidebook software.

Analysis of tracking of crawling neutrophils. Time-lapse movies of crawling neutrophils were analysed with ImageJ, which includes the Manual Tracking and the Chemotaxis and Migration Tool plugins. For each movie we first adjusted channel intensities and converted them into RGB format. Movies were rotated so that the vessels and the blood flow were positioned horizontally and oriented left-right. When necessary, the Background subtraction and Image stabilization pre-stablished plugins were applied to eliminate noise and reduce tissue twitching, respectively. Both plugins were set up with xy calibration values, which depend on the camera and microscope parameters, to convert pixels into linear measures, as well as the time interval value between movie frames (3 s). Each polarized neutrophil (identified by a clear polarized morphology or uropod staining) was tracked manually for 1 min using the Manual Tracking Plugin, which generated a data set with the respective xy track coordinates. We then used the Chemotaxis and Migration Tool to plot and the velocity (μm per s), accumulated distance (μm), euclidean distance (μm) and directionality of the tracks obtained. The Euclidean distance is the length of the straight-line segment connecting the initial and finishing points, whereas the accumulated distance is the total length of the path covered by the cell. Directionality measures how straight the cell track is, and is calculated as the ratio of euclidean distance to accumulated distance.

Analysis of 3D reconstructions of polarized neutrophils. We measured the 3D features of intravascular neutrophils using Imaris Software (Bitplane, Oxford, UK). From the parameters provided by the ImarisCell module, we selected prolate ellipticity by obtaining the lengths of the three semi-axes, which correspond with the Ellipsoid axis parameters. A prolate ellipsoid (cigar-like shape) is one for which the polar radius is greater than the equatorial radius. For 3D cell reconstructions, we used the ImarisCell module to define the cell body. We then segmented a region of interest to enclose an individual cell within this region, so that the subsequent reconstruction fitted the real cell structure. Afterwards, the respective source channel from which the cells had to be computed was selected. For reconstruction analysis, we chose the *Ly6G*-APC channel as it is a membrane-bound protein that yields a strong signal and allows a good rendering of the actual cell morphology. ImarisCell module determines the cell threshold by calculating voxel (3D pixel) intensities from the enclosed cell and comparing them with the background intensity in the enclosed sub-region. To obtain the height-to-length ratios, we visually established the cell orientation with respect to the vessel wall surface. Sections of each polarized neutrophil were analysed to manually measure the height of the cell and maximum length (from the top view) with respect to the vessel wall. For this purpose, we used Imaris Section View, which shows the coordinates in the three display areas (xy top view, zy lateral view and xz front view), and the Extended Crosshairs of the Section View, which in turn allows selection of the z-stack planes to visualize the entire cell (not just one plane or section) in the three views. A snapshot of these three views from a single cell was taken and imported into ImageJ, where height and maximum length were measured from the different views after setting the capture scale.

Human blood sampling. Functional tests were performed in blood samples from 20 volunteers (36 ± 6 years, 15 men). Exclusion criteria were as follows: any antiplatelet, anticoagulant or anti-inflammatory drug taken within the 2 previous weeks; abnormal platelet or leukocyte count; or any history of abnormal bleeding, thrombosis, or active inflammatory disease. Written consent was obtained from all volunteers. Blood samples were collected into polypropylene tubes containing sodium citrate from an antecubital vein with a 21-gauge needle, discarding the first 2 ml to avoid platelet activation. Blood was collected between 8:00 and 10:00 after overnight fasting. Samples were processed immediately. ACS patients were recruited at our cath-lab (both genders, age <80) from among those referred for coronary angiogram and subsequent percutaneous coronary intervention. Exclusion criteria were as follows: active treatment with β-blockers; any situation which might make it imprudent to administer an i.v.-β-blocker; asthma or chronic obstructive lung disease; bradycardio (HR <55 b.p.m.); heart failure or valvular heart disease; atrial fibrillation requiring antiarrhythmic therapy; renal failure with creatinine ≥2 mg per ml; liver disease with bilirubin ≥2 mg per ml; acute illness of any malignancy; pregnancy or nursing; body mass index ≥27 kg per m^2; previous severe adverse reaction to β-blockers; concomitant use of other antithrombotic drugs such as anticoagulants, dypiridamol, ticlopidine or cilostazol; treatment before the intervention with GP IIb/IIIa inhibitors, or need for nonsteroid anti-inflammatory drugs. Written informed consent was obtained from all patients enrolled. Blood samples were collected from a femoral artery catheter into polypropylene tubes containing sodium citrate, discarding the first 2 ml. Samples were processed immediately.

Human neutrophil–platelet interactions evaluation. Human citrated blood was diluted 1:5 in HEPES-Tyrode's* (5 mM hydroxyethylpiperazineethane-sulfonic acid (HEPES), 137 mM NaCl, 2.7 mM $NaHCO_3$, 0.36 mM NaH_2PO_4, 2 mM NaH_2PO_4, 2 mM $CaCl_2$, 5 mM glucose, bovine albumin 0.2%. pH = 7.4) and incubated with 0, 2 or 5 μM metoprolol for 10 min. Then, 5 ml of diluted blood was incubated with 5 μM epinephrine for 10 min. Unstimulated and epinephrine-stimulated samples were stained with PC5-conjugated anti-*CD14* anti *CD45*-FITC and anti-*CD61* PC7 for 20 min at room temperature in the dark. Erythrocytes were lysed for 10 min using Versalyse solution. Appropriate mouse isotype controls were used for each antibody. Flow cytometry analysis was performed with a Gallios cytometer (Beckman Coulter, Miami, FL, USA). Leukocytes were by *CD45*-FITC staining. Neutrophils identification was adapted from refs 34,35 and performed by morphological parameters (side scatter) and negative staining for *CD14*-PC5 but positive staining for *CD45*-FITC. Neutrophil–platelet conjugates were identified as bivariate histogram particles negative for *CD14*-PC5 and positive to *CD61*-PC7 (refs 36,37). The acquisition process was stopped after collection of 5,000 monocytes. Data are expressed as the percentage of neutrophil–platelet aggregates.

All experiments were conducted at the Hospital Universitario Clínico San Carlos, Madrid.

Human platelet function evaluation. Platelet aggregation was assessed using light transmittance aggregometry in PRP by the turbidimetric method in a four-channel aggregometer (Chrono-Log 490 Model, Chrono-Log Corp., Havertown, PA, USA) according to standard protocols. The PRP was obtained from citrated blood at centrifuge (800 r.p.m.) for 10 min and platelet-poor plasma was obtained after a second centrifugation (2,500 r.p.m.) for 10 min. PRP will be adjusted to 250,000 per µl with autologous plasma. PRP was incubated with metoprolol 2 and 5 µM or saline buffer for 15 min and then stimulated using epinephrine (5 µM). Light transmission was adjusted to 0% with PRP and to 100% with platelet-poor plasma for each measurement. Curves were recorded during 5 min and platelet aggregation was determined as the maximal percent change in light transmittance.

Platelet function was determined by assessing platelet activation as surface expression of activated GP IIb/IIIa (Becton Dickinson) and P-Selectin using flow cytometry. Whole blood from healthy donors were drawn into trisodium citrate tubes diluted with Hepes-tyrodes-buffer (0.2% BSA) to a final volume of 1:8:1 (blood: Hepes-tyrodes:citrate). Diluted blood was incubated with metoprolol 2 and 5 µM or saline for 15 min. Following activation with epinephrine (5 µM) samples were incubated for 20 min with polyclonal *PAC1*-FITC conjugated or PE-conjugated anti-*CD62P*. Appropriate isotype controls were used in each case. Platelet activation was expressed as the percentage of platelets positive for antibody binding. Platelets were gated on the basis of light scatter and *CD61* antibody expression. Activated platelets were defined as the percentage of expressing the activated confirmation of *PAC1* binding and P-selectin (*CD62P*). Data were expressed as the percentage of platelets positive for antibody binding. All experiments were conducted at the Hospital Universitario Clínico San Carlos, Madrid.

Statistics. Data are represented as mean ± s.e. of the mean (s.e.m.), and analysed using Prism software (Graph pad, Inc.) and Stata (Stata 12.0; StataCorp LP, College Station, TX, USA). Comparisons between two groups were performed by using the unpaired two-tailed Student's *t*-test or the nonparametric Wilcoxon–Mann–Whitney test as appropriate. Comparisons between more than two groups were performed by using the one-way ANOVA. The *P*-value was adjusted with the Holm Sidak's multiple comparison test. Multiple linear regression analysis was used to study the influence of metoprolol on MVO, adjusted for factors potentially affecting MVO such as sex, age, ischaemia duration, diabetes, use of thrombectomy or glycoprotein IIb/IIIa inhibitors. Test for linear trend after one-way ANOVA was used to study the relationship between LVEF at 6 months and MVO quartiles at 1 week. Power calculations were applied to obtain statistically significant at *P* values below 0.05 significant. $^{*}P<0.05$, $^{**}P<0.01$, $^{***}P<0.001$.

Study approval. All studies in patients and volunteers were approved by the ethics committee of Hospital Clínico San Carlos, Madrid. Written informed consent was received from all participants before inclusion in the study.

Data availability. The data that support the conclusions of this study are available from the corresponding author on reasonable request.

References

1. Ibanez, B., Heusch, G., Ovize, M. & Van de Werf, F. Evolving therapies for myocardial ischemia/reperfusion injury. *J. Am. Coll. Cardiol.* **65,** 1454–1471 (2015).
2. Hausenloy, D. J. & Yellon, D. M. Myocardial ischemia-reperfusion injury: a neglected therapeutic target. *J. Clin. Invest.* **123,** 92–100 (2013).
3. Vinten-Johansen, J. Involvement of neutrophils in the pathogenesis of lethal myocardial reperfusion injury. *Cardiovasc. Res.* **61,** 481–497 (2004).
4. Kolaczkowska, E. & Kubes, P. Neutrophil recruitment and function in health and inflammation. *Nat. Rev. Immunol.* **13,** 159–175 (2013).
5. Fernandez-Jimenez, R. *et al.* Pathophysiology underlying the bimodal edema phenomenon after myocardial ischemia/reperfusion. *J. Am. Coll. Cardiol.* **66,** 816–828 (2015).
6. Huebener, P. *et al.* The HMGB1/RAGE axis triggers neutrophil-mediated injury amplification following necrosis. *J. Clin. Invest.* **125,** 539–550 (2015).
7. Li, J. *et al.* Neutrophil AKT2 regulates heterotypic cell–cell interactions during vascular inflammation. *J. Clin. Invest.* **124,** 1483–1496 (2014).
8. Sreeramkumar, V. *et al.* Neutrophils scan for activated platelets to initiate inflammation. *Science* **346,** 1234–1238 (2014).
9. Ibanez, B. *et al.* Effect of early metoprolol on infarct size in ST-segment-elevation myocardial infarction patients undergoing primary percutaneous coronary intervention: the effect of metoprolol in cardioprotection during an acute myocardial infarction (METOCARD-CNIC) trial. *Circulation* **128,** 1495–1503 (2013).
10. Pizarro, G. *et al.* Long-term benefit of early pre-reperfusion metoprolol administration in patients with acute myocardial infarction: results from the METOCARD-CNIC trial (effect of metoprolol in cardioprotection during an acute myocardial infarction). *J. Am. Coll. Cardiol.* **63,** 2356–2362 (2014).
11. Antoniucci, D. Block the ischemia and reperfusion damage: an old adjunctive drug for a new reperfusion strategy. *J. Am. Coll. Cardiol.* **63,** 2363–2364 (2014).
12. Marino, F. & Cosentino, M. Adrenergic modulation of immune cells: an update. *Amino Acids* **45,** 55–71 (2013).
13. Flierl, M. A. *et al.* Phagocyte-derived catecholamines enhance acute inflammatory injury. *Nature* **449,** 721–725 (2007).
14. Zieziulewicz, T. J., Mondal, T. K., Gao, D. & Lawrence, D. A. Stress-induced effects, which inhibit host defenses, alter leukocyte trafficking. *Cell Stress Chaperones* **18,** 279–291 (2013).
15. Kim, M. H. *et al.* Catecholamine stress alters neutrophil trafficking and impairs wound healing by beta2-adrenergic receptor-mediated upregulation of IL-6. *J. Invest. Dermatol.* **134,** 809–817 (2014).
16. Scanzano, A. *et al.* Adrenergic modulation of migration, CD11b and CD18 expression, ROS and interleukin-8 production by human polymorphonuclear leukocytes. *Inflamm. Res.* **64,** 127–135 (2015).
17. Horn, N. A. *et al.* Epinephrine enhances platelet-neutrophil adhesion in whole blood in vitro. *Anesth. analg.* **100,** 520–526 (2005).
18. Ibanez, B. *et al.* Study design for the "effect of METOprolol in CARDioproteCtioN during an acute myocardial InfarCtion" (METOCARD-CNIC): a randomized, controlled parallel-group, observer-blinded clinical trial of early pre-reperfusion metoprolol administration in ST-segment elevation myocardial infarction. *Am. Heart J.* **164,** 473–480 e475 (2012).
19. Eitel, I. *et al.* Comprehensive prognosis assessment by CMR imaging after ST-segment elevation myocardial infarction. *J. Am. Coll. Cardiol.* **64,** 1217–1226 (2014).
20. Barron, H. V., Cannon, C. P., Murphy, S. A., Braunwald, E. & Gibson, C. M. Association between white blood cell count, epicardial blood flow, myocardial perfusion, and clinical outcomes in the setting of acute myocardial infarction: a thrombolysis in myocardial infarction 10 substudy. *Circulation* **102,** 2329–2334 (2000).
21. O'Donoghue, M. *et al.* Association between baseline neutrophil count, clopidogrel therapy, and clinical and angiographic outcomes in patients with ST-elevation myocardial infarction receiving fibrinolytic therapy. *Eur. Heart J.* **29,** 984–991 (2008).
22. Palmerini, T. *et al.* Impact of leukocyte count on mortality and bleeding in patients with myocardial infarction undergoing primary percutaneous coronary interventions: analysis from the Harmonizing Outcome with Revascularization and Stent in Acute Myocardial Infarction trial. *Circulation* **123,** 2829–2837 (2011).
23. Chen, Y. *et al.* Cocaine and catecholamines enhance inflammatory cell retention in the coronary circulation of mice by upregulation of adhesion molecules. *Am. j. physiol. Heart circ. physiol.* **288,** H2323–H2331 (2005).
24. Dhabhar, F. S., Malarkey, W. B., Neri, E. & McEwen, B. S. Stress-induced redistribution of immune cells—from barracks to boulevards to battlefields: a tale of three hormones—Curt Richter Award winner. *Psychoneuroendocrinology* **37,** 1345–1368 (2012).
25. Epelman, S., Liu, P. P. & Mann, D. L. Role of innate and adaptive immune mechanisms in cardiac injury and repair. *Nat. rev. Immunol.* **15,** 117–129 (2015).
26. Jordan, J. E., Zhao, Z. Q. & Vinten-Johansen, J. The role of neutrophils in myocardial ischemia-reperfusion injury. *Cardiovasc. Res.* **43,** 860–878 (1999).
27. Looney, M. R. & Matthay, M. A. Neutrophil sandwiches injure the microcirculation. *Nat. Med.* **15,** 364–366 (2009).
28. Casanova-Acebes, M. *et al.* Rhythmic modulation of the hematopoietic niche through neutrophil clearance. *Cell* **153,** 1025–1035 (2013).
29. Lefer, D. J. Do neutrophils contribute to myocardial reperfusion injury? *Basic Res. Cardiol.* **97,** 263–267 (2002).
30. Seo, J. K. *et al.* A peptide with unique receptor specificity: stimulation of phosphoinositide hydrolysis and induction of superoxide generation in human neutrophils. *J. Immunol.* **158,** 1895–1901 (1997).
31. Chen, Y. & Junger, W. G. Measurement of oxidative burst in neutrophils. *Methods Mol. Biol.* **844,** 115–124 (2012).
32. Grisanti, L. A. *et al.* Pro-inflammatory responses in human monocytes are beta1-adrenergic receptor subtype dependent. *Mol. immunol.* **47,** 1244–1254 (2010).
33. Swirski, F. K. & Nahrendorf, M. Leukocyte behavior in atherosclerosis, myocardial infarction, and heart failure. *Science* **339,** 161–166 (2013).
34. Botto, N. *et al.* An increased platelet–leukocytes interaction at the culprit site of coronary artery occlusion in acute myocardial infarction: a pathogenic role for 'no-reflow' phenomenon? *Int. J. cardiol.* **117,** 123–130 (2007).
35. Xiao, Z. & Theroux, P. Clopidogrel inhibits platelet-leukocyte interactions and thrombin receptor agonist peptide-induced platelet activation in patients with an acute coronary syndrome. *J. Am. Coll. Cardiol.* **43,** 1982–1988 (2004).
36. van Velzen, J. F., Laros-van Gorkom, B. A., Pop, G. A. & van Heerde, W. L. Multicolor flow cytometry for evaluation of platelet surface antigens and activation markers. *Thromb. Res.* **130,** 92–98 (2012).

37. Giacomazzi, A., Degan, M., Calabria, S., Meneguzzi, A. & Minuz, P. Antiplatelet agents inhibit the generation of platelet-derived microparticles. *Front. Pharmacol.* **7,** 314 (2016).
38. Ndrepepa, G. & Kastrati, A. Intravenous beta-blockers in primary percutaneous coronary intervention: new hope for an old therapy. *Circulation* **128,** 1487–1489 (2013).
39. Mateos, A. *et al.* Efficacy and safety of out-of-hospital intravenous metoprolol administration in anterior ST-segment elevation acute myocardial infarction: insights from the METOCARD-CNIC trial. *Ann. Emerg. Med.* **65,** 318–324 (2015).
40. Ibanez, B. *et al.* Early metoprolol administration before coronary reperfusion results in increased myocardial salvage: analysis of ischemic myocardium at risk using cardiac magnetic resonance. *Circulation* **115,** 2909–2916 (2007).
41. Ibanez, B. *et al.* The cardioprotection granted by metoprolol is restricted to its administration prior to coronary reperfusion. *Int. J. Cardiol.* **147,** 428–432 (2011).
42. Eltzschig, H. K. & Eckle, T. Ischemia and reperfusion--from mechanism to translation. *Nat. Med.* **17,** 1391–1401 (2011).
43. Phillipson, M. & Kubes, P. The neutrophil in vascular inflammation. *Nat. Med.* **17,** 1381–1390 (2011).
44. Beril Gok, H. *et al.* Metoprolol treatment decreases tissue myeloperoxidase activity after spinal cord injury in rats. *J. Clin. Neurosci.* **14,** 138–142 (2007).
45. Ibrahim-Zada, I., Rhee, P., Gomez, C. T., Weller, J. & Friese, R. S. Inhibition of sepsis-induced inflammatory response by beta1-adrenergic antagonists. *J. Trauma Acute Care Surg.* **76,** 320–327 discussion 327-328 (2014).
46. Dunzendorfer, S. & Wiedermann, C. J. Modulation of neutrophil migration and superoxide anion release by metoprolol. *J. Mol. Cell Cardiol.* **32,** 915–924 (2000).
47. Jaboureck-Bouttier, R. *et al.* Effects of two antihypertensive agents, labetalol and metoprolol, on the production of reactive oxygen species by normal polymorphonuclear leukocytes in vitro. *Hypertens. Pregnancy* **18,** 239–247 (1999).
48. Srivastava, K. C. Influence of some beta blockers (pindolol, atenolol, timolol and metoprolol) on aggregation and arachidonic acid metabolism in human platelets. *Prostaglandins Leukot. Med.* **29,** 79–84 (1987).
49. Celik, T. *et al.* Effects of nebivolol on platelet activation in hypertensive patients: a comparative study with metoprolol. *Int. J. Cardiol.* **116,** 206–211 (2007).
50. Investigators, A.A. *et al.* Pexelizumab for acute ST-elevation myocardial infarction in patients undergoing primary percutaneous coronary intervention: a randomized controlled trial. *JAMA* **297,** 43–51 (2007).
51. Granger, C. B. *et al.* Pexelizumab, an anti-C5 complement antibody, as adjunctive therapy to primary percutaneous coronary intervention in acute myocardial infarction: the COMplement inhibition in Myocardial infarction treated with Angioplasty (COMMA) trial. *Circulation* **108,** 1184–1190 (2003).
52. Faxon, D. P. *et al.* The effect of blockade of the CD11/CD18 integrin receptor on infarct size in patients with acute myocardial infarction treated with direct angioplasty: the results of the HALT-MI study. *J. Am. Coll. Cardiol.* **40,** 1199–1204 (2002).
53. Faust, N., Varas, F., Kelly, L. M., Heck, S. & Graf, T. Insertion of enhanced green fluorescent protein into the lysozyme gene creates mice with green fluorescent granulocytes and macrophages. *Blood* **96,** 719–726 (2000).
54. Garcia-Prieto, J. *et al.* beta3 adrenergic receptor selective stimulation during ischemia/reperfusion improves cardiac function in translational models through inhibition of mPTP opening in cardiomyocytes. *Basic Res. Cardiol.* **109,** 422 (2014).
55. Villablanca, E. J. *et al.* Tumor-mediated liver X receptor-alpha activation inhibits CC chemokine receptor-7 expression on dendritic cells and dampens antitumor responses. *Nat. Med.* **16,** 98–105 (2010).

Acknowledgements

We are grateful to all the METOCARD-CNIC trial investigators and to Noemi Escalera for coordinating the clinical work and Maite D. Rodriguez for handling human samples (CNIC). Angel Macías and Barulio-Pérez-Asenjo (CNIC) performed the MRI studies. Noelia A-González (CNIC) supplied the LysM-GFP+ mice. R.P. Khaton, J. Mateos and V. Zorita provided technical support and animal care. M. Casanova-Acebes gave advice on neutrophil isolation. J.M. Adrover for IVM technical advice. R. Doohan, A. Guijarro and A. Molina-Iracheta provided technical support in histology. A.M. Santos-Beneit helped with microscopy image analysis and movie editing. We also thank the CNIC Animal, Cellomics and Microscopy units for support. Simon Bartlett provided English editing. We are grateful to Eeva I. Soininen and Ana I. Castillo for their inconditional support and management of the grants supporting this work. This work was supported by a competitive grant from the Institute of Health Carlos III and the European Regional Development Fund (ERDF/FEDER) (PI10/02268, PI13/01979 & RD12/0042/0054). R. F.-J. was the recipient of non-overlapping grants from the Institute of Health Carlos III and ERDF/FEDER (Rio Hortega fellowship) and the Fundación Jesús Serra, the Fundación Interhospitalaria de Investigación Cardiovascular (FIC) and the CNIC (FICNIC fellowship). A.H. is funded by MINECO and ERDF/FEDER (SAF2015-65607-R) and Fundació La Marató-TV3 (120/C/2015-20153032). The CNIC is supported by the Spanish Ministry of Economy and Competitiveness (MINECO) and the Pro-CNIC Foundation, and is a Severo Ochoa Center of Excellence (MINECO award SEV-2015-0505). Borja Ibanez is the 2010 Princess of Girona awardee in Science.

Author contributions

B.I. is responsible for the design of the entire study, assisted by J.G.-P. Experimental myocardial IR, peritonitis experiments, neutrophil migration assays and bone marrow transplants were done by J.G-P., M.G., R.V.-G. and A.P.-G. Interpreted by B.I. Genotyping and transcripts expression evaluation were done by M.G., R.V.-G. and D.S.-R. Histological processing and evaluations were done by M.G., R.V.-G., R.B.-M. and J.G.-P. MVO evaluation in MRI studies from the METOCARD-CNIC trial were analysed by I.G.-L., R.F.-J., J.M.G.-R. and G.P. METOCARD-CNIC trial PIs: B.I and V.F. Correlation studies of WBC and MVO were done by J.M.G.-R. and J.G.-P. Interpreted by B.I. Intravital microscopy experiments and analysis were done by G.C., V.S. and A.S.dV. Interpreted by A.H. Human neutrophil–platelet interaction and platelet function experiments were done by E.B. and analysed by J.G.-P. Interpreted by A.F.-O and B.I. Statistical analyses were done by J.G.-P., J.M.G.-R. and R.F.-J. Manuscript was drafted by J.G.-P, and critically revised by A.H., V.F. and B.I. B.I. and J.G.-P are responsible for the final version of the manuscript, which was approved by all authors.

Additional information

Supplementary Information accompanies this paper at http://www.nature.com/naturecommunications

Competing financial interests: The authors declare no competing interests.

Reprints and permission information is available online at http://npg.nature.com/reprintsandpermissions/

How to cite this article: García-Prieto, J. *et al.* Neutrophil stunning by metoprolol reduces infarct size. *Nat. Commun.* **8**, 14780 doi: 10.1038/ncomms14780 (2017).

Publisher's note: Springer Nature remains neutral with regard to jurisdictional claims in published maps and institutional affiliations.

This work is licensed under a Creative Commons Attribution 4.0 International License. The images or other third party material in this article are included in the article's Creative Commons license, unless indicated otherwise in the credit line; if the material is not included under the Creative Commons license, users will need to obtain permission from the license holder to reproduce the material. To view a copy of this license, visit http://creativecommons.org/licenses/by/4.0/

© The Author(s) 2017

RESEARCH ARTICLE SUMMARY

HEART MITOCHONDRIA

Imbalanced OPA1 processing and mitochondrial fragmentation cause heart failure in mice

Timothy Wai, Jaime García-Prieto, Michael J. Baker, Carsten Merkwirth, Paule Benit, Pierre Rustin, Francisco Javier Rupérez, Coral Barbas, Borja Ibañez,* Thomas Langer*

INTRODUCTION: Mitochondria are essential organelles whose form and function are inextricably linked. Balanced fusion and fission events shape mitochondria to meet metabolic demands and to ensure removal of damaged organelles. A fragmentation of the mitochondrial network occurs in response to cellular stress and is observed in a wide variety of disease conditions, including heart failure, neurodegenerative disorders, cancer, and obesity. However, the physiological relevance of stress-induced mitochondrial fragmentation remains unclear.

RATIONALE: Proteolytic processing of the dynamin-like guanosine triphosphatase (GTPase) OPA1 in the inner membrane of mitochondria is emerging as a critical regulatory step to balance mitochondrial fusion and fission. Two mitochondrial proteases, OMA1 and the AAA protease YME1L, cleave OPA1 from long (L-OPA1) to short (S-OPA1) forms. L-OPA1 is required for mitochondrial fusion, but S-OPA1 is not, although accumulation of S-OPA1 in excess accelerates fission. In cultured mammalian cells, stress conditions activate OMA1, which cleaves L-OPA1 and inhibits mitochondrial fusion resulting in mitochondrial fragmentation. In this study, we generated conditional mouse models for both YME1L and OMA1 and examined the role of OPA1 processing and mitochondrial fragmentation in the heart, a metabolically demanding organ that depends critically on mitochondrial functions.

RESULTS: Deletion of *Yme1l* in cardiomyocytes did not grossly affect mitochondrial respiration but induced the proteolytic cleavage of OPA1 by the stress-activated peptidase OMA1 and drove fragmentation of mitochondria in vivo. These mice suffered from dilated cardiomyopathy characterized by well-established features of heart failure that include necrotic cell death, fibrosis and ventricular remodelling, and a metabolic switch away from fatty acid oxidation and toward glucose use. We discovered that additional deletion of *Oma1* in cardiomyocytes prevented OPA1 processing altogether and restored normal mitochondrial morphology and cardiac health. On the other hand, mice lacking YME1L in both skeletal muscle and cardiomyocytes exhibited normal cardiac function and life span despite mitochondrial fragmentation in cardiomyocytes. Imbalanced OPA1 processing in skeletal muscle, which is an insulin signaling tissue, induced systemic glucose intolerance and prevented cardiac glucose overload and cardiomyopathy. We observed a similar effect on cardiac metabolism upon feeding mice lacking *Yme1l* in cardiomyocytes a high-fat diet, which preserved heart function despite mitochondrial fragmentation.

ON OUR WEB SITE

Read the full article at http://dx.doi.org/10.1126/science.aad0116

CONCLUSION: Our work highlights the importance of balanced fusion and fission of mitochondria for cardiac function and unravels an intriguing link between mitochondrial dynamics and cardiac metabolism in the adult heart in vivo. Mitochondrial fusion mediated by L-OPA1 preserves cardiac function, whereas its stress-induced processing by OMA1 and mitochondrial fragmentation triggers dilated cardiomyopathy and heart failure. In contrast to previous genetic models of the mitochondrial fusion machinery, mice lacking *Yme1l* in cardiomyocytes do not show pleiotropic respiratory deficiencies and thus provide a tool to directly assess the physiological importance of mitochondrial dynamics. Preventing mitochondrial fragmentation by deleting *Oma1* protects against cell death and heart failure. The identification of OMA1 as a critical regulator of mitochondrial morphology and cardiomyocyte survival holds promise for translational applications in cardiovascular medicine. Mitochondrial fragmentation induces a metabolic switch from fatty acid to glucose utilization in the heart. It turns out that reversing this switch and restoring normal cardiac metabolism is sufficient to preserve heart function despite mitochondrial fragmentation. These findings raise the intriguing possibility that the switch in fuel usage that occurs in the failing adult heart may, in fact, be maladaptive and could contribute to the pathogenesis of heart failure. ■

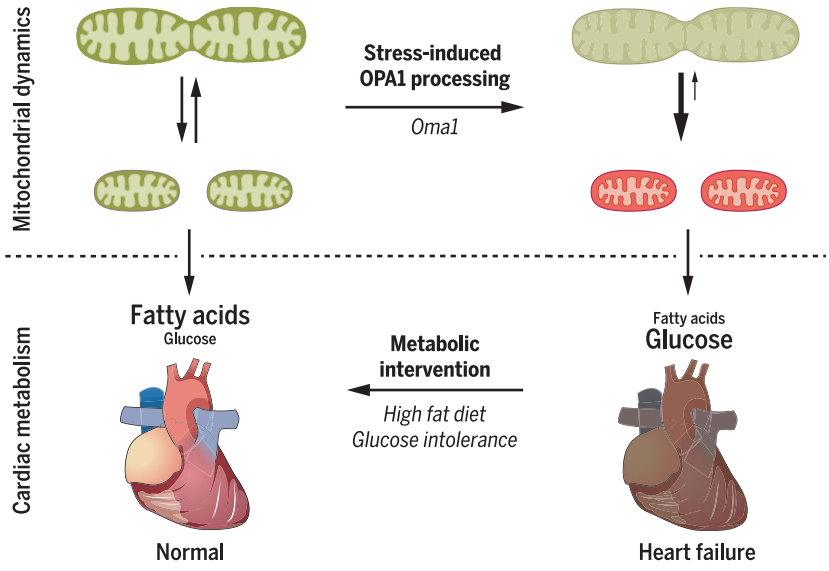

Critical role of balanced mitochondrial fusion and fission for cardiac metabolism and heart function. Induced processing of the dynamin-like GTPase OPA1 in the inner membrane by the stress-activated peptidase OMA1 leads to mitochondrial fragmentation, cardiomyopathy and heart failure, which is characterized by a switch in fuel utilization. Heart function can be preserved by reversing this metabolic switch without suppressing mitochondrial fragmentation.

The list of author affiliations is available in the full article online.
*Corresponding author. E-mail: thomas.langer@uni-koeln.de (T.L.); bibanez@cnic.es (B.I.)
Cite this article as T. Wai *et al.*, *Science* **350**, aad0116 (2015).
DOI: 10.1126/science.aad0116

Downloaded from www.sciencemag.org on December 4, 2015

RESEARCH ARTICLE

HEART MITOCHONDRIA

Imbalanced OPA1 processing and mitochondrial fragmentation cause heart failure in mice

Timothy Wai,[1,2]* Jaime García-Prieto,[3]* Michael J. Baker,[1] Carsten Merkwirth,[1] Paule Benit,[4,5] Pierre Rustin,[4,5] Francisco Javier Rupérez,[6] Coral Barbas,[6] Borja Ibañez,[3,7]† Thomas Langer[1,2,8,9]†

Mitochondrial morphology is shaped by fusion and division of their membranes. Here, we found that adult myocardial function depends on balanced mitochondrial fusion and fission, maintained by processing of the dynamin-like guanosine triphosphatase OPA1 by the mitochondrial peptidases YME1L and OMA1. Cardiac-specific ablation of *Yme1l* in mice activated OMA1 and accelerated OPA1 proteolysis, which triggered mitochondrial fragmentation and altered cardiac metabolism. This caused dilated cardiomyopathy and heart failure. Cardiac function and mitochondrial morphology were rescued by *Oma1* deletion, which prevented OPA1 cleavage. Feeding mice a high-fat diet or ablating *Yme1l* in skeletal muscle restored cardiac metabolism and preserved heart function without suppressing mitochondrial fragmentation. Thus, unprocessed OPA1 is sufficient to maintain heart function, OMA1 is a critical regulator of cardiomyocyte survival, and mitochondrial morphology and cardiac metabolism are intimately linked.

The dynamic behavior of mitochondria preserves mitochondrial integrity and distribution and allows mitochondrial shape and function to be adapted to altered physiological demands (*1*, *2*). Disturbed mitochondrial dynamics is associated with a number of neurodegenerative disorders and cardiac hypertrophy in mice (*3*, *4*). Dynamin-like guanosine triphosphatases (GTPases) mediate the fusion and fission of mitochondrial membranes. Mitofusins 1 and 2 (MFN1 and MFN2) orchestrate outer mitochondrial membrane fusion, whereas OPA1 is required for inner mitochondrial membrane fusion. Fission, on the other hand, is executed by dynamin-related protein 1 (DRP1), a cytosolic protein that is recruited to the mitochondrial surface in response to various physiological cues. This complex machinery, including DRP1-specific receptor proteins and cytoskeletal components, assembles at contact sites between the mitochondria and the endoplasmic reticulum, which mark mitochondrial division sites (*5*, *6*).

Fusion and fission of mitochondrial membranes occur in a coordinated manner. Balanced cycles of fusion and fission determine the shape, size, and number of mitochondria, which leads to a large variability in the morphology of mitochondria in different cell types. Although mitochondria form interconnected, tubular networks in cultured fibroblasts, they appear as distinct entities in tissues, such as heart and skeletal muscle, that are characterized by low fusion and fission rates (*7*). Moreover, coordinated mitochondrial dynamics is critical for the bioenergetic function of mitochondria and is closely linked to metabolism. Changes in mitochondrial ultrastructure and dynamics occur in response to altered metabolic demands (*8*–*11*), and components involved in mitochondrial fusion are central regulators of cellular metabolism (*12*). Coordinated fusion and fission events are crucial for mitochondrial quality-control. Fusion contributes to mitochondrial maintenance, whereas excessive fission causes mitochondrial fragmentation, which allows removal of irreversibly damaged mitochondria by mitophagy and is associated with cell death (*13*, *14*). Fragmentation of the mitochondrial network is observed in a wide variety of diseases.

The dynamin-like GTPase OPA1 mediates mitochondrial fusion and orchestrates mitochondrial cristae morphogenesis and resistance to apoptosis in response to physiological demands (*15*–*17*). The processing of OPA1 is emerging as a central regulatory step coordinating fusion and fission of mitochondria (*18*, *19*). Two peptidases in the inner membrane, OMA1 and the *i*-AAA protease YME1L, convert long OPA1 forms (L-OPA1) into short forms (S-OPA1) (*20*–*23*). The balanced accumulation of both forms maintains normal mitochondrial morphology: Fusion depends on L-OPA1 only, whereas S-OPA1 is associated with mitochondrial fission (Fig. 1A) (*24*–*26*). Cellular stress, mitochondrial dysfunction, or genetic interventions (such as deletion of *Yme1l*) can activate OMA1, which results in the increased conversion of L-OPA1 into S-OPA1 and mitochondrial fragmentation (*25*, *27*–*30*). Loss of *Yme1l* in cultured fibroblasts does not impair fusion but triggers mitochondrial fragmentation (*22*, *25*, *31*), which can be suppressed by deletion of *Oma1* (*22*, *25*, *31*). Thus, although OPA1 processing is dispensable for mitochondrial fusion per se, an increased oxidative phosphorylation promotes cleavage of OPA1 by YME1L (*10*). It thus appears that different stimuli modulate OPA1 processing by YME1L or OMA1, which allows the coordination of mitochondrial fusion and division under various physiological conditions.

In agreement with its role for stress-induced OPA1 processing, ablation of *Oma1* in mice causes impaired thermogenesis and diet-induced obesity and protects against ischemic kidney injury (*29*, *32*). Here, we generated tissue-specific mouse models for the OPA1-processing peptidases YME1L and OMA1 and examined the role of OPA1 processing in myocardial function.

Results

YME1L is essential for embryonic development

To study the importance of balanced mitochondrial dynamics (Fig. 1A), we generated conditional mouse models of the OPA1-processing peptidases *Yme1l* and *Oma1* (fig. S1, A to D, and table S1). We used a mouse line expressing Cre recombinase under the control of the β-actin promoter to delete *Yme1l* or *Oma1* by Cre/loxP-mediated recombination in all tissues. As expected (*29*), $Oma1^{-/-}$ mice were born at the expected Mendelian ratio (fig. S1E). $Yme1l^{+/-}$ mice were viable and exhibited no obvious phenotypes, but heterozygous intercrosses did not yield viable null offspring (Fig. 1B). We observed a generalized developmental delay in $Yme1l^{-/-}$ embryos isolated from embryonic day 8.5 (E8.5) to E12.5 (Fig. 1C). Hearts from $Yme1l^{-/-}$ embryos isolated at E9.5 and E10.5 failed to beat properly, and we did not recover any null embryos after E13.5. Thus, YME1L is essential for embryogenesis.

Cardiomyocyte-specific deletion of Yme1l *causes dilated cardiomyopathy*

We next examined the requirement of YME1L for the function of the heart, a metabolically demanding organ sensitive to disruption of mitochondrial shape (*7*, *33*). We crossed $Yme1l^{LoxP/LoxP}$ mice to mice expressing Cre recombinase specifically in cardiomyocytes (Myh6-Cre; cYKO) (*34*). cYKO mice were viable but had a significantly shortened life span (median life span: 46 weeks) (Fig. 1, D and E) punctuated by weight loss before their demise (Fig. 1F), which suggested that YME1L is required for normal heart function.

[1]Institute for Genetics, University of Cologne, 50674 Cologne, Germany. [2]Max-Planck-Institute for Biology of Aging, Cologne, Germany. [3]Myocardial Pathophysiology Area, Centro Nacional de Investigaciones Cardiovasculares Carlos III (CNIC), Madrid, Spain. [4]INSERM UMR 1141, Hôpital Robert Debré, Paris, France. [5]Université Paris 7, Faculté de Médecine Denis Diderot, Paris, France. [6]Centre for Metabolomics and Bioanalysis (CEMBIO), Faculty of Pharmacy, Universidad San Pablo CEU, Campus Monteprincipe, Boadilla del Monte, 28668 Madrid, Spain. [7]Department of Cardiology, Instituto de Investigación Sanitaria (IIS), Fundación Jiménez Díaz Hospital, Madrid, Spain. [8]Cologne Excellence Cluster on Cellular Stress Responses in Aging-Associated Diseases (CECAD), University of Cologne, Cologne, Germany. [9]Center for Molecular Medicine (CMMC), University of Cologne, Cologne, Germany.
*These authors contributed equally to this work.
†Corresponding author. E-mail: thomas.langer@uni-koeln.de (T.L.); bibanez@cnic.es (B.I.)

We examined heart function from an early age up to 40 weeks of age in cYKO mice (Fig. 2A). Longitudinal echocardiographic (echo) analyses (fig. S2A) revealed progressive cardiac dysfunction (table S2), which became apparent at 20 weeks and was characterized by hallmarks of dilated cardiomyopathy (DCM): a reduced percentage of LVEF (% LVEF) (Fig. 2B and fig. S2A), a dilated left ventricular chamber (Fig. 2C), and a preserved left ventricular mass (fig. S2B). We observed myocardial fibrosis (Fig. 2D), increased serum levels of cardiac troponin T (Fig. 2E), and evidence of ongoing necrotic cell death (Fig. 2, F and G) in cYKO mice.

The failing adult heart is commonly characterized by an altered metabolism where glucose use is increased and β oxidation is decreased (*35*, *36*). We monitored in vivo cardiac uptake of ^{18}fluorodeoxyglucose ([^{18}F]FDG) in cYKO mice by hybrid positron emission tomography–computed tomography (PET-CT). The loss of YME1L in cardiomyocytes caused an increase in in vivo cardiac glucose uptake (Fig. 2, H and I) and in vitro glycolysis rates (fig. S2C). Gas chromatography–mass spectrometry analyses revealed increased endogenous glucose levels and decreased lactate levels in cYKO hearts, whereas the levels of citric acid cycle intermediates were not altered (fig. S2D) nor were the levels and use of pyruvate (fig. S2E). However, we observed a global reduction of total cardiac acylcarnitines (fig. S2F), which indicated reduced β oxidation in YME1L-deficient cardiomyocytes. Thus, loss of YME1L in cardiomyocyte mitochondria can induce a metabolic shift from lipid utilization to carbohydrate utilization that is typically observed in the failing heart (*37*). In conclusion, cYKO mice develop DCM, which progresses to heart failure and middle-aged death.

Loss of YME1L impairs mitochondrial morphology in cardiomyocytes

To define the molecular basis of DCM in cYKO mice, we first analyzed mitochondrial respiration. Ex vivo cardiac respiration measurements revealed no differences between resting hearts isolated from cYKO mice and controls (Fig. 3A). Specific activities of mitochondrial complexes II, III,

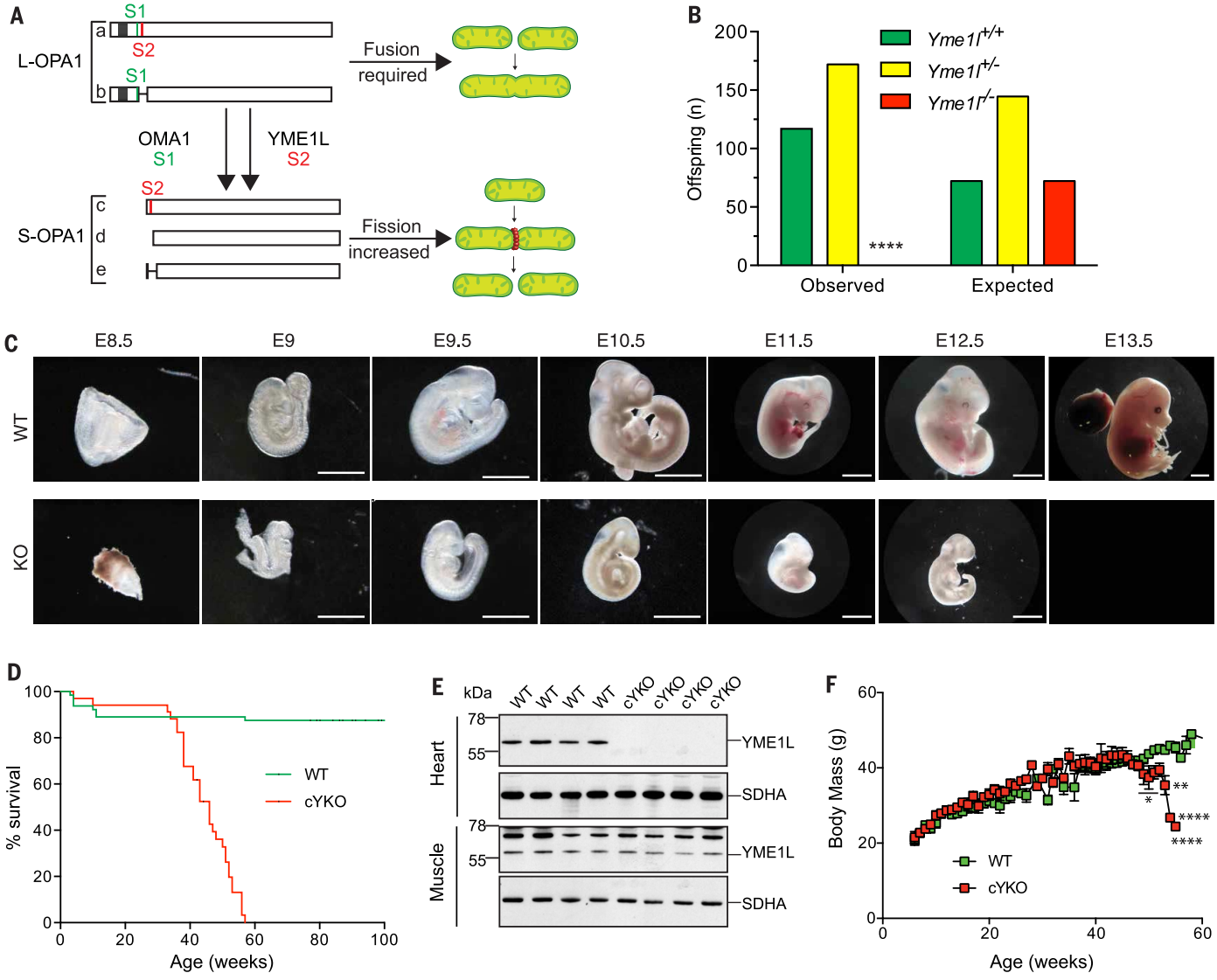

Fig. 1. YME1L is required in the developing embryo and the adult heart. (**A**) The mitochondrial proteases OMA1 and YME1L cleave L-OPA1 (a and b) at S1 and S2, respectively, to yield S-OPA1 forms (c, d, and e). (**B**) No viable *Yme1l*$^{-/-}$ mice were recovered from intercrosses of *Yme1l*$^{+/-}$ mice (0 out of 289 offspring). Chi-squared test, ****P < 0.0001. (**C**) Postimplantation developmental delay of *Yme1l*$^{-/-}$ embryos scaled relative to WT. Scale bar, 2 mm. (**D**) Life span of cardiomyocyte-specific cYKO mice (Myh6-Cre red; median of 46 weeks, n = 69) is reduced relative to WT littermates (green; n = 74). Log-rank (Mantel-Cox) test, ****P < 0.0001. (**E**) Immunoblots of tissues isolated from 18-week-old WT and cYKO mice. Antibodies directed against succinate dehydrogenase subunit A (SDHA) were used to control for gel loading. (**F**) Mean body weight (g) of cYKO males (red; n = 30) declines relative to WT (green; n = 30). Multiple t test, *P < 0.05, ****P < 0.0001. Data are means ± SEM.

and IV were increased, although we observed only moderately impaired adenosine 5′-triphosphate (ATP) synthesis by complex V in cYKO hearts (Fig. 3B) and no significant differences in the assembly of respiratory chain complexes and supercomplexes (fig. S3A). Respiratory deficiencies thus appeared unlikely to be the major cause for DCM in cYKO mice.

We next examined the morphology of mitochondria and performed transmission electron microscopy (TEM) of cYKO hearts (Fig. 3C). Smaller mitochondria with normal architecture of cristae accumulated in the absence of YME1L, which indicated impaired mitochondrial dynamics (Fig. 3, C and D). Similar results were seen in primary adult cardiomyocytes isolated from 8-week-old (before DCM development) and 40-week-old cYKO hearts (Fig. 3, E and F, and fig. S3B). Consistent with our TEM data, we observed distorted mitochondrial morphology in *Yme1l*$^{-/-}$ cardiomyocytes, as seen previously in noncardiac cell types lacking YME1L (*20*, *22*, *25*). Loss of YME1L in cardiomyocytes abolished formation of S-OPA1 form d and led to the accumulation of S-OPA1 forms c and e, which are generated by OMA1 (Fig. 3, G and H). Moreover, the mitochondrial lipid transfer protein PRELID1, normally degraded by YME1L, accumulated (Fig. 3G) (*38*). Notably, *Yme1l* is specifically deleted in cardiomyocytes and was not lost in cardiac fibroblasts isolated from cYKO mice. However, in vitro deletion of *Yme1l* in adult cardiac fibroblasts did recapitulate fragmentation of the mitochondrial network (fig. S3, C and D) and impaired OPA1 processing (fig. S3E) as observed in *Yme1l*$^{-/-}$ cardiomyocytes. Thus, YME1L deficiency in cardiomyocytes induces OPA1 processing and mitochondrial fragmentation, which raises the possibility that disturbed mitochondrial morphology could cause heart failure in cYKO mice.

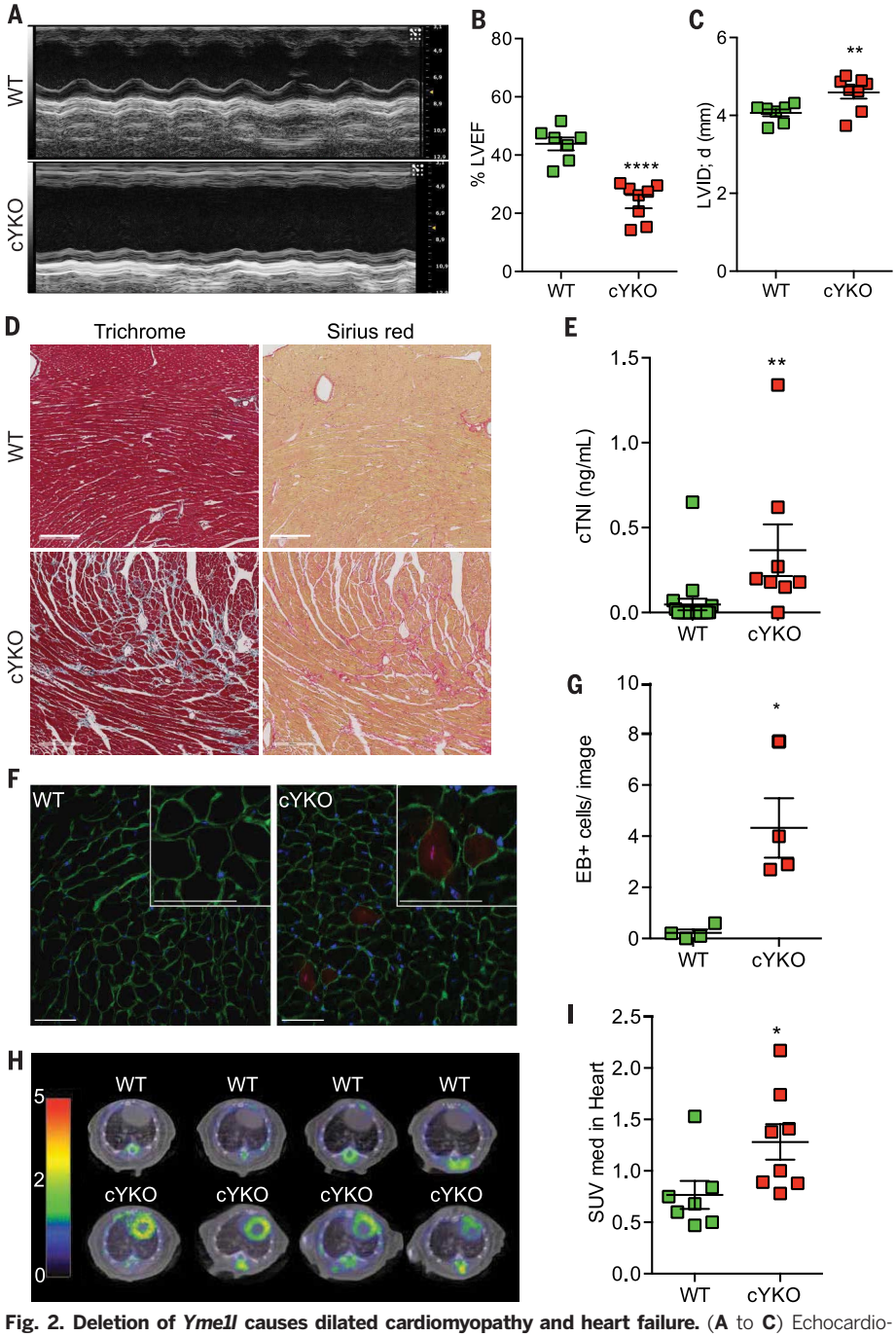

Fig. 2. Deletion of *Yme1l* causes dilated cardiomyopathy and heart failure. (**A** to **C**) Echocardiographic evaluation of cardiac function (by M-mode) of randomized 40-week-old WT (n = 8) and cYKO (n = 8) males reveals DCM characterized by (B) reduced LVEF (****P < 0.0001) and (C) increased left ventricular internal dimension (LVID) [d (mm), **P = 0.0154]. (**D**) Cardiac fibrosis in cYKO mice monitored by trichrome and sirius red staining of heart sections [40 weeks old (40w), n = 3; scale bar, 200 μm]. (**E**) Increased serum levels of cardiac troponin (cTNI ng/ml) in 30-week-old cYKO mice (n = 8) relative to WT (n = 19). Mann-Whitney test, **P = 0.0027. (**F** and **G**) Cardiomyocyte necrosis analysis of 20-week-old cYKO (n = 4) and WT (n = 4) hearts stained with Evans Blue (EB red), wheat germ agglutinin (green), and DAPI (blue). Individual t test, *P = 0.0286; scale bar, 50 μm. (**H**) PET-CT of 40-week-old cYKO (n = 8) and WT (n = 7) animals after [^{18}F]FDG injections. Representative images of four cYKO and four WT thoracic scans are shown. (**I**) Average standardized uptake value (SUV) in WT (n = 7) and cYKO hearts (n = 8); unpaired t test, *P = 0.0140. In graphs, data are means ± SEM.

Deletion of Oma1 *restores mitochondrial morphology and myocardial function in the absence of YME1L*

The accumulation of OPA1 forms c and e in cardiomyocytes lacking YME1L indicated activation of OMA1, as previously observed in YME1L-deficient mouse embryonic fibroblasts (MEFs) in vitro (*25*). Because additional deletion of *Oma1* in *Yme1l*$^{-/-}$ MEFs restores tubular mitochondria and apoptotic resistance (*25*), we reasoned that ablation of *Oma1* may preserve the mitochondrial network in cardiomyocytes lacking YME1L. To examine the role of disturbed mitochondrial morphology in DCM and heart failure in cYKO mice, we generated double-knockout mice lacking both YME1L and OMA1 specifically in cardiomyocytes (cDKO; *Myh6-Cre*$^{tg/wt}$*Yme1l*$^{LoxP/LoxP}$ *Oma1*$^{LoxP/LoxP}$) and monitored heart function (Fig. 4A). In contrast to cYKO mice, cDKO mice showed normal cardiac function and normal exercise tolerance in treadmill tests (Fig. 4, B to D). Myocardial fibrosis present in cYKO mice (Fig. 2E) was absent in cDKO hearts (Fig. 4E). Moreover, TEM analysis of cDKO hearts revealed that mitochondrial fragmentation was largely suppressed (Fig. 4, F and G). Similarly, mitochondrial morphology was restored in primary adult cardiomyocytes isolated from cDKO mice (Fig. 4, H and I). L-OPA1 processing was prevented in these cells, whereas other YME1L substrates such as PRELID1 continued to accumulate to

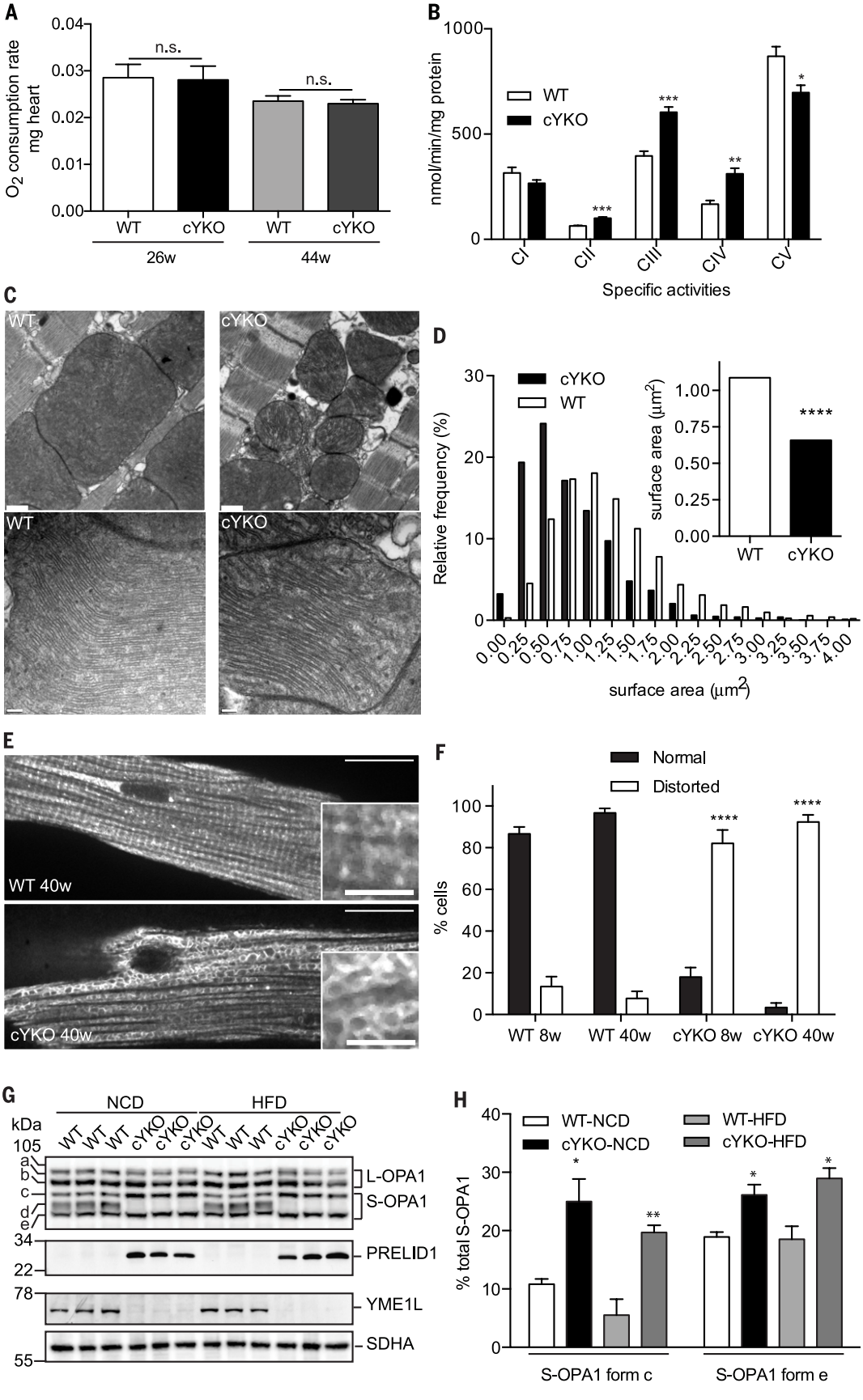

Fig. 3. Stress-induced OPA1 processing in cardiomyocytes perturbs mitochondrial morphology. (**A**) Ex vivo respiration measured in resting hearts (n = 3 to 5) from 26- and 44-week-old WT (white or pale gray) and cYKO (black or dark gray) mice. Linear oxygen uptake rates are presented as nmol O_2/min per mg (weight, heart weight). Differences were not significant. (**B**) Respiratory chain activity measurements of complex I to V (CI to CV) in 44-week-old hearts of WT (white) and cYKO (black) mice. Individual unpaired t tests (n = 3 to 5); CI (P = 0.1442), CII (***P = 0.0003), CIII (***P = 0.0003), CIV (**P = 0.0020), and CV (*P = 0.0172). (**C**) TEM of 20-week-old WT and cYKO hearts (thick scale bar, 500 nm; thin scale bar, 100 nm). (**D**) Mitochondrial size was represented as median surface area, and frequency distributions of mitochondrial surface were calculated from 20-week-old WT (n = 4224) and cYKO (n = 2308) mitochondria imaged by TEM. Kruskal-Wallis test, ****P < 0.0001. Data are median values. (**E**) Indirect immunocytochemistry with antibodies directed against TOMM20 (a rabbit-specific antibody) in cardiomyocytes isolated from WT (n = 3) and cYKO (n = 3) mice (thin scale bar, 30 µm; thick scale bar, 7.5 µm). 40w, 40 weeks old. (**F**) Mitochondrial morphology in WT (8w, n = 2; 40w, n = 3) and cYKO (8w, n = 2; 40w, n = 3) cardiomyocytes (****P < 0.0001). Cells (>100) were counted. 8w, 8 weeks old. (**G**) Immunoblot analysis of cardiomyocytes isolated from 40-week-old mice fed a normal chow diet (NCD) or high-fat diet (HFD). SDHA was used as a loading control. (**H**) Quantification of OPA1 processing in hearts of WT and cYKO mice (Fig. 3F). (Pairwise t test, *P < 0.05, **P < 0.01) relative to WT-NCD controls. In graphs (B), (F), and (H), data are means ± SEM.

similar levels as in cardiomyocytes of cYKO mice (Fig. 4J).

Thus, YME1L ablation in cardiomyocytes activates OMA1 and promotes OPA1 processing and mitochondrial fragmentation, which causes DCM and heart failure.

Loss of YME1L in skeletal muscle preserves the function of YME1L-deficient hearts

The results obtained from cardiomyocyte-specific knockout mice establish an essential role of YME1L for normal cardiac function in vivo. We observed, to our surprise, the normal life span of mice lacking YME1L both in cardiomyocytes and skeletal muscle (hmYKO for heart and muscle–specific YME1L knockout; median life span 125 weeks) (Fig. 5A, fig. S5A, and table S1). hmYKO mice were obtained by crossing *Yme1l*$^{LoxP/LoxP}$

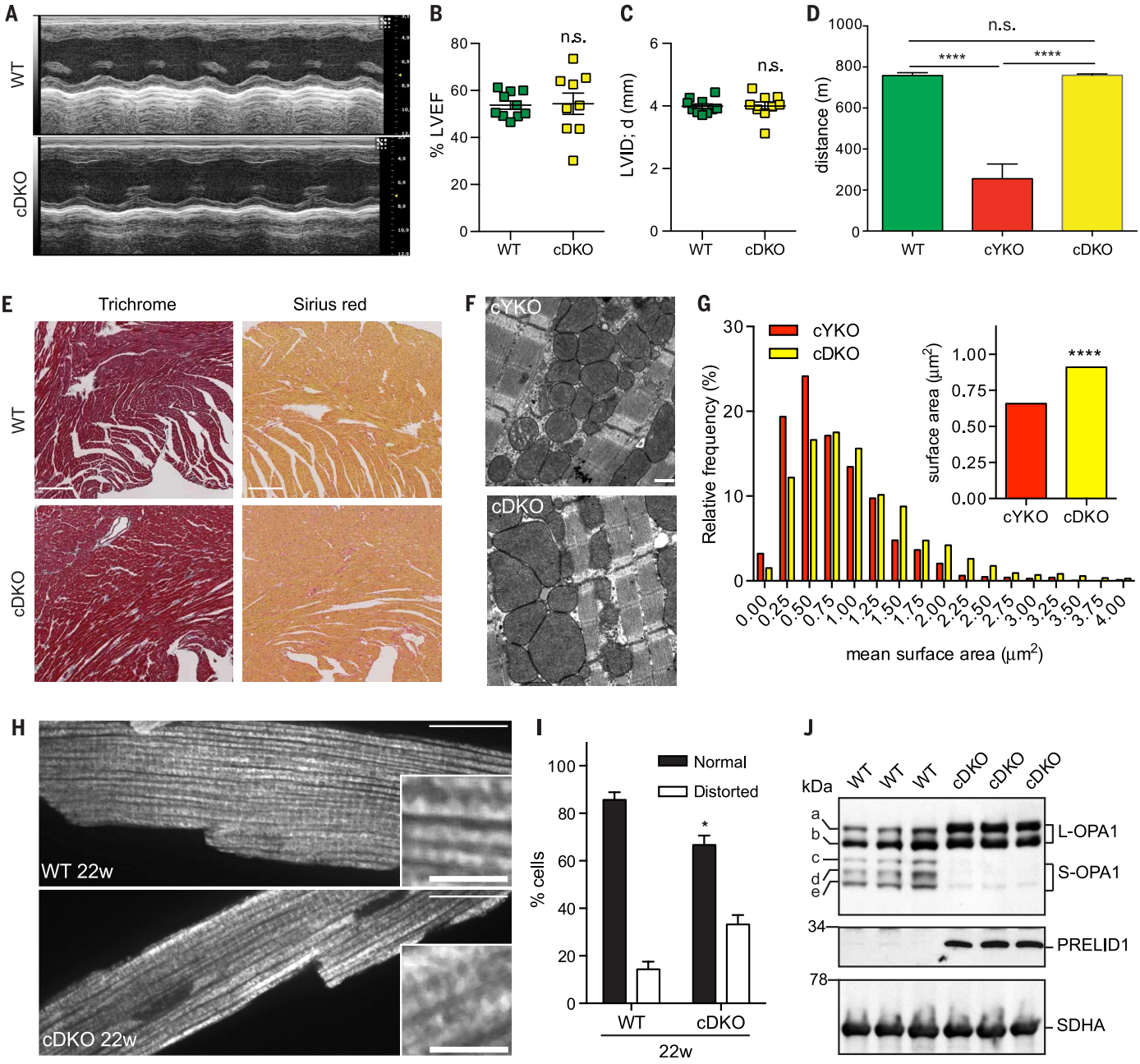

Fig. 4. *Oma1* ablation restores mitochondrial morphology and protects cYKO mice against DCM and heart failure. (**A**) Echocardiographic evaluation of cardiac function (by M-mode) of 22-week-old WT and cDKO mice. (**B** and **C**) Percentage LVEF and (C) diastolic LVID of 22-week-old WT (n = 10) and cDKO (n = 9) mice. n.s., not significant. (**D**) Treadmill endurance of 20-week-old WT (n = 10), cYKO (n = 10), and cDKO (n = 5) mice (5% incline). cYKO mice versus WT, ****P = 0.0003; cYKO versus cDKO, ****P = 0.0001. (**E**) Suppression of cardiac fibrosis in cDKO mice. Trichrome and sirius red staining of heart sections of 22-week-old WT and cDKO mice (n = 3). Scale bar, 200 μm. (**F**) TEM of 20-week-old cYKO and cDKO hearts (thick scale bar, 500 nm). (**G**) Mitochondrial size represented as median surface area and frequency distributions of mitochondrial surface calculated from 20-week-old cYKO (n = 2308) and cDKO (n = 3122) mitochondria imaged by TEM. Kruskal-Wallis test, ****P < 0.0001. Data are median values. (**H**) Indirect immunocytochemistry with TOMM20-specific antibodies in cardiomyocytes isolated from 22-week-old WT and cDKO mice (thin scale bar, 30 μm; thick scale bar, 7.5 μm). (**I**) Quantification of mitochondrial morphology from (H) (n = 3, n > 100 cells; *P = 0.0112). In (B) to (D) and (I), data are means ± SEM. (**J**) Immunoblot analysis of cardiomyocytes from 22-week-old WT (n = 3) and cDKO (n = 3) mice. SDHA was used as a loading control.

mice to mice expressing Cre recombinase under the control of the muscle creatine kinase (Ckmm) promoter, which is active in cardiomyocytes and additionally in skeletal muscle (*39*). Note that differences in life span could not be explained by differences in the efficiency of *Yme1l* deletion: mRNA (fig. S5B) and protein (fig. S5C) levels were profoundly depleted in adult hearts of both cYKO and hmYKO mice. YME1L was lost with similar efficiencies and kinetics upon Cre recombinase–mediated deletion of *Yme1l* both in postnatal hearts of cYKO and hmYKO mice (fig. S5, D to G). Unlike cYKO mice, however, myocardial activity was preserved in hmYKO mice. We observed normal heart function by echocardiography and normal cardiac uptake of [^{18}F]FDG in these mice (Fig. 5, B to D, and fig. S5, H and I).

We analyzed the morphology of mitochondria in hmYKO hearts by TEM. Smaller mitochondria accumulated in hearts of hmYKO mice as observed in cYKO mice, which indicated mitochondrial

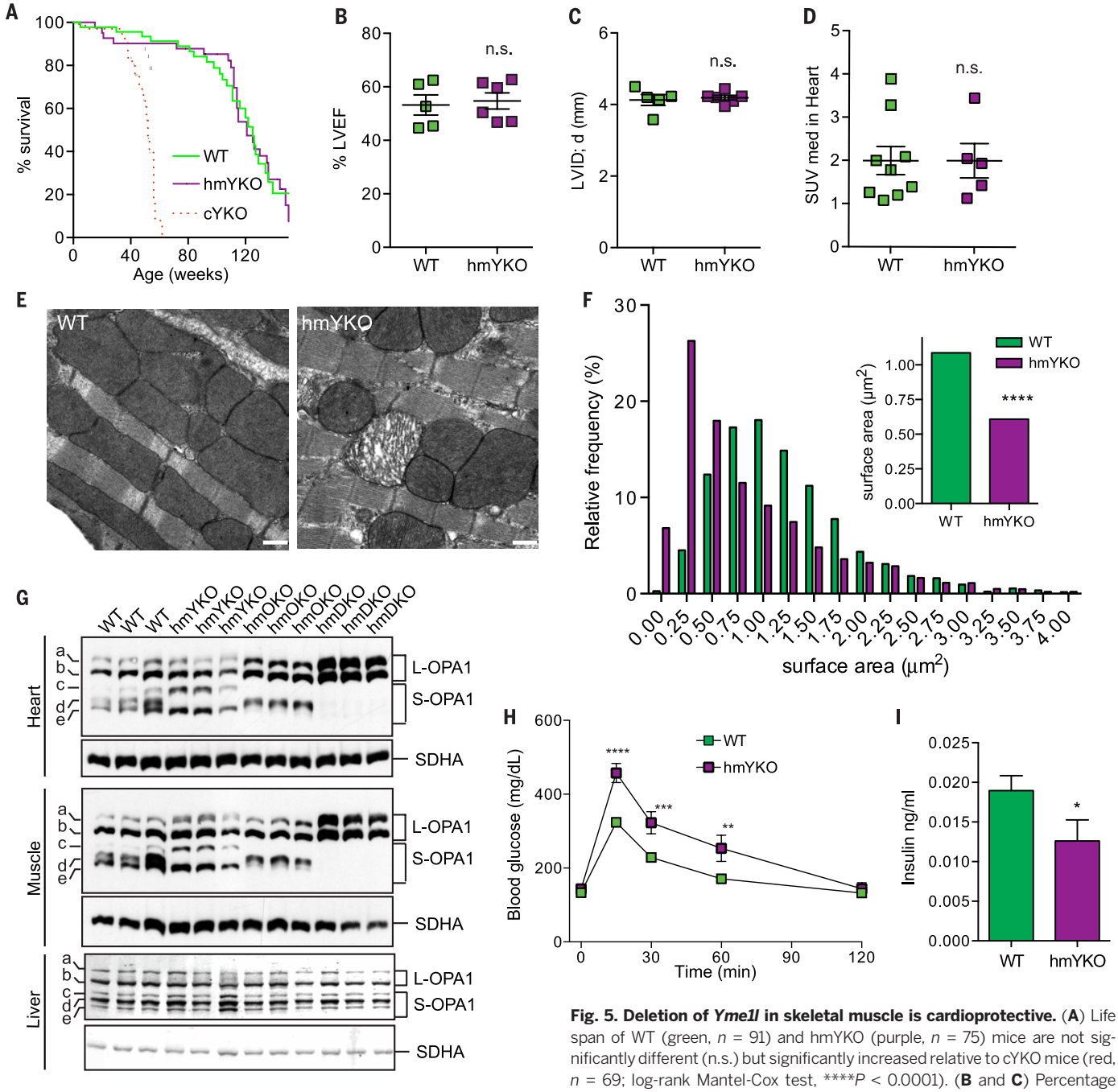

Fig. 5. Deletion of *Yme1l* in skeletal muscle is cardioprotective. (**A**) Life span of WT (green, $n = 91$) and hmYKO (purple, $n = 75$) mice are not significantly different (n.s.) but significantly increased relative to cYKO mice (red, $n = 69$; log-rank Mantel-Cox test, $^{****}P < 0.0001$). (**B** and **C**) Percentage LVEF and diastolic LVID in 46-week-old WT ($n = 5$) and hmYKO ($n = 6$) mice analyzed by echocardiography (fig. S5A). (**D**) PET-CT average standardized cardiac glucose uptake in 46-week-old WT (green, $n = 8$) and hmYKO (purple, $n = 5$) mice fed normal chow. (**E**) TEM of 20-week-old WT and hmYKO hearts (thick scale bar, 500 nm). (**F**) Mitochondrial size represented as median surface area and frequency distributions of mitochondrial surface calculated from 20-week-old WT ($n = 4224$) (Fig. 3, C and D) and hmYKO ($n = 3246$) mitochondria imaged by TEM. Kruskal-Wallis test, $^{****}P < 0.0001$. Data are median values. (**G**) Immunoblot analysis of lysates from heart skeletal muscle and liver of 18-week-old hmYKO mice ($n = 3$), hmOKO mice (Ckmm-Cre; *Oma1*$^{LoxP/LoxP}$, $n = 3$), and hmDKO mice (Ckmm-Cre; *Oma1*$^{LoxP/LoxP}$ *Yme1l*$^{LoxP/LoxP}$, $n = 3$) reveals altered OPA1 processing. (**H**) Intraperitoneal glucose tolerance tests in 18-week-old WT ($n = 18$) and hmYKO ($n = 13$) mice. Two-way ANOVA ($^{**}P < 0.01$, $^{***}P < 0.001$, $^{****}P < 0.0001$) relative to WT controls. (**I**) Fasting insulin levels in 20-week-old WT ($n = 6$) and hmYKO ($n = 7$) mice. ($^{*}P = 0.0357$). In (A), (C), (F), (H), and (I), data are means ± SEM.

fragmentation (Fig. 5, E and F). These morphological changes corresponded to defects in OPA1 processing that were similar in cardiomyocytes isolated from hmYKO and cYKO mice (Figs. 3G and 5G). In both models, deletion of *Yme1l* in cardiomyocytes prevented formation of S-OPA1 form d, whereas S-OPA1 forms c and e accumulated, which was indicative of OMA1 activation (fig. S5F). OPA1 processing was affected similarly upon loss of YME1L in skeletal muscle of hmYKO mice (Fig. 5G) but normal in skeletal muscle of cYKO mice harboring YME1L (Fig. 1E). Thus, loss of YME1L impairs OPA1 processing and induces mitochondrial fragmentation in cardiomyocytes of both cYKO and hmYKO mice. Furthermore, additional deletion of *Yme1l* in skeletal muscle maintains heart function and life span without restoring mitochondrial morphology defects in cardiomyocytes lacking YME1L.

Mitochondrial dysfunction in skeletal muscle is associated with impaired insulin signaling and glucose intolerance (*40*–*42*). Thus, possible endocrine effects owing to the loss of YME1L in skeletal muscle may cause metabolic alterations in cardiomyocytes; this preserves heart function downstream of mitochondrial deficiencies. We thus investigated systemic glucose homeostasis and performed intraperitoneal glucose tolerance tests (GTT) in both hmYKO and cYKO mice (Figs. 5H and 6A). We observed glucose intolerance in hmYKO mice but not in cYKO mice (Figs. 5H and 6A), which suggested that deletion of *Yme1l* in skeletal muscle impaired glucose homeostasis systemically. Additional ablation of *Oma1* in hmYKO mice (hmDKO; table S1) prevented OPA1 processing in both heart and skeletal muscle (Fig. 5G) and restored normal glucose tolerance (fig. S5F). Thus, stress-induced OPA1 processing by OMA1 in skeletal muscle impairs glucose homeostasis in hmYKO mice.

Deletion of *Pgc1α* in skeletal muscle significantly impairs glucose-stimulated insulin secretion, which suggests a cytokine-mediated cross-talk between skeletal muscle and pancreatic islets (*41*). In agreement with these findings, we observed lowered fasting insulin concentration in the serum of hmYKO mice (Fig. 5I), although *Yme1l* was not deleted in the pancreas of these mice. hmYKO mice had normal fasting blood glucose (fig. S5G), normal weight gains (fig. S5H), and body composition as normal lean and fat mass (fig. S5I).

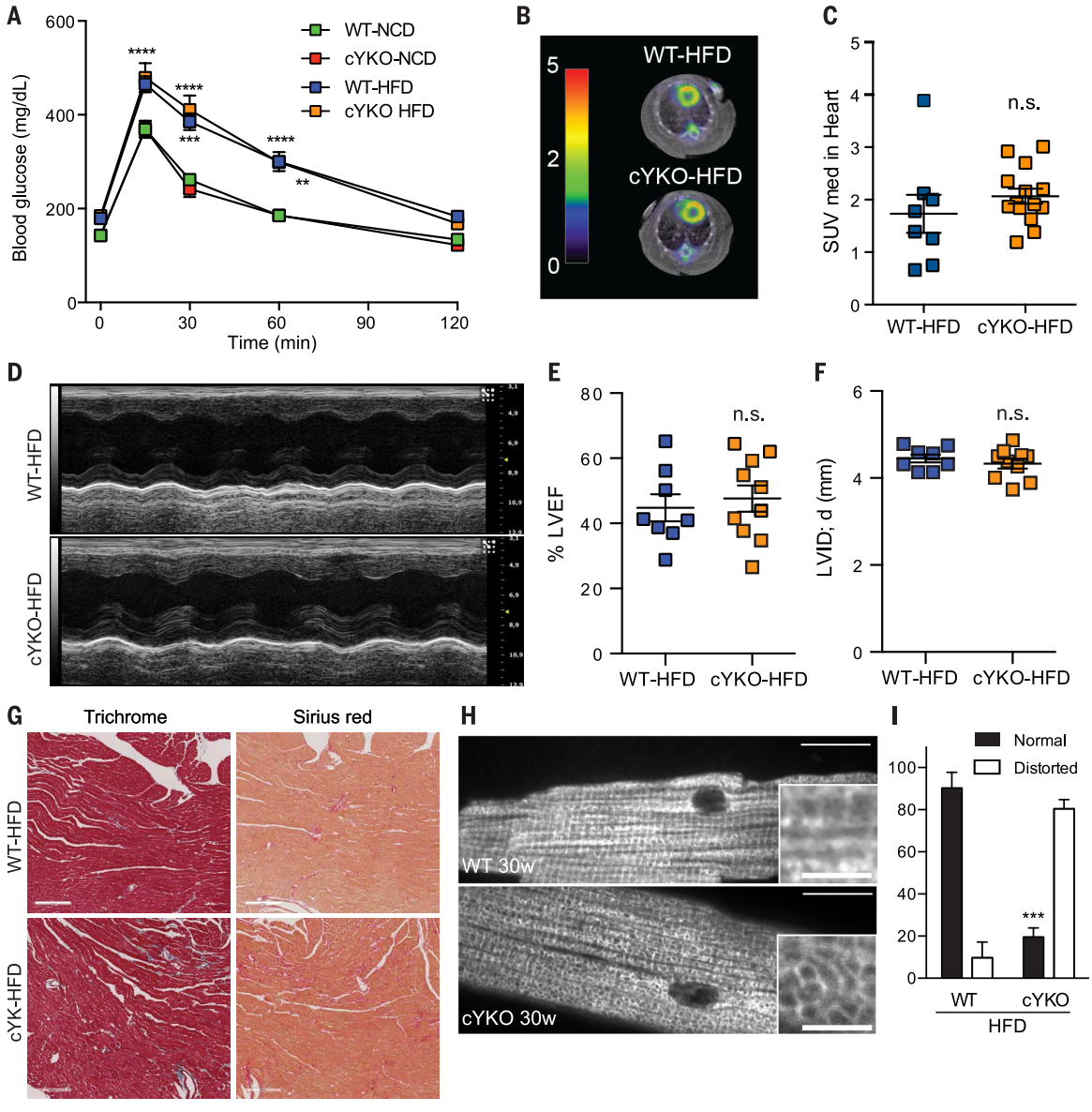

Fig. 6. Suppression of DCM and heart failure by dietary intervention. (**A**) Intraperitoneal glucose tolerance tests in WT (green, $n = 30$; blue, $n = 13$) and cYKO (orange, $n = 5$; red, $n = 14$) mice fed HFD or NCD. Two-way ANOVA (*$P < 0.05$, **$P < 0.01$, ***$P < 0.001$, ****$P < 0.0001$) relative to WT-NCD controls. (**B**) PET-CT in 30-week-old WT and cYKO mice treated with HFD starting at 9 weeks of age. Representative images of 2 cYKO and 2 WT mice are shown. (**C**) Average standardized cardiac glucose uptake in 30-week-old WT ($n = 8$; blue) and cYKO mice ($n = 14$; orange) treated with HFD starting at 9 weeks of age. (**D**) Echocardiographic M-mode images of 30-week-old WT and cYKO mice fed with HFD starting at 9 weeks of age. (**E** and **F**) Percentage LVEF and diastolic LVID of WT ($n = 14$) and cYKO ($n = 10$) mice. n.s., not significant. (**G**) Trichrome and sirius red stainings of heart sections of 40-week-old HFD-fed WT ($n = 3$) and cYKO ($n = 3$) mice. Scale bar, 200 μm. (**H**) Indirect immunocytochemistry using antibodies directed against TOMM20 in cardiomyocytes isolated from 30-week-old HFD-fed WT ($n = 3$) and cYKO ($n = 3$) mice (thin scale bar, 30 μm; thick scale bar, 7.5 μm). OPA1 processing in these cells is shown in Fig. 3G. (**I**) Quantification of mitochondrial morphology from (H) (WT, $n \geq 100$ cells; cYKO, $n = 3$; ***$P = 0.001$). In graphs, data are means ± SEM.

Thus, loss of YME1L in skeletal muscle induces systemic glucose intolerance and lowers insulin levels, which blunts increased cardiac glucose uptake and alters cardiac metabolism. Furthermore, cell nonautonomous metabolic alleviation can preserve cardiac function and prevent DCM and heart failure despite mitochondrial fragmentation in cardiomyocytes.

Feeding a high-fat diet suppresses heart failure and restores the life span of cYKO mice

The protective effect of systemic glucose intolerance on the heart suggests that deleterious effects of mitochondrial fragmentation in cardiomyocytes can be circumvented by metabolic intervention. To provide further support for this notion, we subjected wild-type (WT) and cYKO mice to a high-fat diet. This diet is commonly used to dysregulate systemic glucose homeostasis. It impairs insulin signaling in target tissues and compromises glucose-stimulated insulin secretion by pancreatic β cells triggering obesity. Mice were fed a high-fat diet beginning at 9 weeks of age, at a time when cardiac function was normal. Both WT and cYKO mice fed a high-fat diet gained weight significantly more rapidly than mice fed normal chow (fig. S6A) and exhibited reduced glucose tolerance (Fig. 6A).

To determine whether this dietary intervention could influence cardiac metabolism, we examined the cardiac uptake of [^{18}F]FDG by PET-CT and determined levels of endogenous glucose and acylcarnitine in the hearts of high fat–fed cYKO mice. In contrast to mice fed normal chow, we did not observe significant differences in cardiac glucose uptake (Fig. 6, B and C) nor in the levels of endogenous cardiac glucose or acylcarnitine between high fat–fed WT and cYKO mice (fig. S2, D and F). The adjustment of the levels of these cardiac metabolites was accompanied by restoration of cardiac function in cYKO mice (Fig. 6, D to F, and fig. S5B): left ventricular ejection fraction (LVEF) and left ventricular chamber diameter values were indistinguishable from those of high fat–fed littermate controls. Treatment with the high-fat diet also prevented cardiac fibrosis (Fig. 6G) and suppressed differences in exercise tolerance previously observed between WT and cYKO mice fed normal chow (fig. S6, C and D).

Similar to normally fed cYKO mice (Fig. 3, F and G), cardiomyocytes isolated from high fat–fed cYKO mice still contained distorted mitochondria (Fig. 6, H and I), because the high-fat diet had not rescued the proteolytic activity of YME1L or OMA1-dependent, stress-induced processing of OPA1 (Fig. 3G, H). High-fat feeding did not markedly alter oxygen consumption or the activity of respiratory complexes in cYKO mice (fig. S6, E and F). Thus, the consequences of mitochondrial defects in cYKO mice can be metabolically circumvented to suppress cardiomyopathy.

Discussion

In these experiments, we observed the deleterious effects of stress-induced OPA1 processing and mitochondrial fragmentation on myocardial function, which revealed an unexpected functional link between systemic glucose homeostasis, cardiac metabolism, and mitochondrial dynamics in vivo.

Uncleaved, fusion-active L-OPA1 is sufficient to maintain cardiac activity. Mice lacking both YME1L and OMA1 in cardiomyocytes exhibited normal heart function, which demonstrates that proteolytic cleavage of OPA1 by YME1L and OMA1 is dispensable. The previously described, essential role of OPA1 for normal cardiac functioning can thus be attributed to the loss of L-OPA1 (*43*, *44*). L-OPA1 is sufficient to mediate mitochondrial fusion, which serves a prosurvival function (*24*–*26*). Mitochondrial fusion protects against mitophagy (*4*, *45*) and is thought to serve a repair function by allowing content mixing and by preventing the accumulation of mitochondrial damage in cultured cells (*46*). Although mitochondrial fusion occurs infrequently in adult cardiomyocytes (*7*), it is required for cardiomyocyte differentiation and cardiac development (*7*, *47*–*51*).

Whereas L-OPA1 is sufficient to preserve cardiac function, accumulation of S-OPA1 and unopposed fission is deleterious for the heart. Our results establish cardiomyocyte-specific YME1L-deficient mice as a model for DCM and heart failure, which culminates in middle-aged death (Fig. 7). The loss of YME1L activates OMA1 and triggers stress-induced OPA1 processing, which unbalances fusion and fission of mitochondria and impairs mitochondrial morphology in cardiomyocytes. In the absence of YME1L, we observed the accumulation of smaller mitochondria in the heart and mitochondrial fragmentation in cardiomyocytes and cardiac fibroblasts in vitro. Mitochondrial fragmentation is caused by the loss of L-OPA1 forms mediating fusion and the concomitant accumulation of S-OPA1 forms c and e that are generated by OMA1 and are associated with fission (*21*, *23*–*26*). Deletion of *Oma1* restores normal mitochondrial morphology in cardiomyocytes lacking YME1L and myocardial activity in vivo, which demonstrates that accelerated OPA1 processing and mitochondrial fragmentation cause heart failure (Fig. 7). Consistent with a deleterious effect of unopposed fission in the heart (*7*), pharmacological inhibition of mitochondrial fission protects against ischemia and reperfusion injury (*52*). Notably, germline deletion of *Oma1* does not impair embryogenesis and is not able to suppress postimplantation embryonic lethality of *Yme1l*$^{-/-}$ embryos (fig. S1F), which indicates that stress-induced OPA1 processing is not deleterious for prenatal organogenesis in these mice.

How does stress-induced OPA1 processing and mitochondrial fragmentation affect cardiac function? Mitochondria are vital for the beating heart, and defects in mitochondrial respiration cause cardiac dysfunction (*36*, *53*, *54*). However, we observed only a minor impairment of respiratory activities and ATP synthesis and no accumulation of lactate in YME1L-deficient hearts, unlike other animal models of mitochondrial cardiomyopathy (*7*, *36*, *51*, *54*). Whereas severe and lethal cardiomyopathies manifest not long after birth in most of these models, cardiac ablation of YME1L causes DCM and death at ~1 year of age.

Unrestrained autophagy can also cause cardiomyocyte loss and heart failure (*55*), which raises the possibility that stress-induced OPA1 processing and the accumulation of S-OPA1 affects the autophagic disposal of mitochondria. The analysis of heart-specific DRP1 knockout mice indeed pointed to a major role of DRP1 and fission for mitochondrial quality-control and autophagy in the heart (*56*–*58*). However, autophagic marker proteins such as p62/SQSTM1 or microtubule-associated

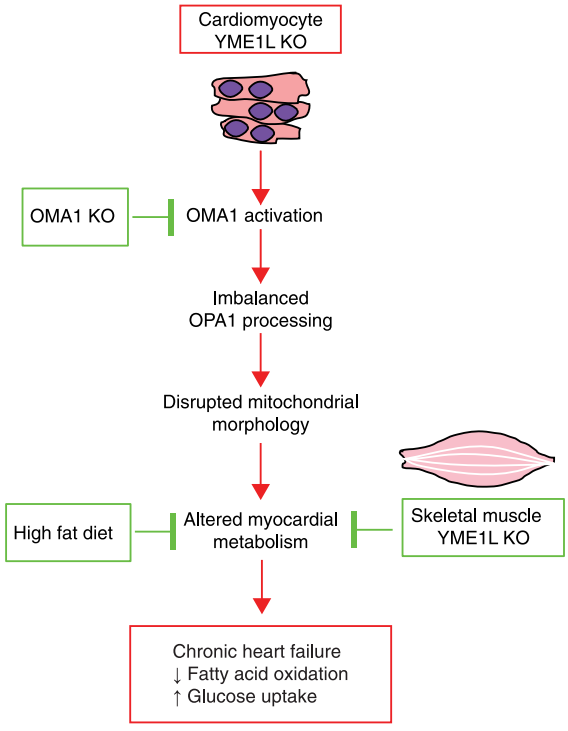

Fig. 7. Unbalanced mitochondrial dynamics in cardiomyocytes upon loss of YME1L causes DCM and heart failure. Unregulated OPA1 processing by OMA1 causes metabolic alterations triggering DCM and heart failure in cardiomyocyte-specific *Yme1l*$^{-/-}$ mice. Heart function is preserved upon restoration of mitochondrial morphology by *Oma1* ablation or without suppressing mitochondrial morphology defects by metabolic intervention bypassing deleterious effects of disturbed mitochondrial dynamics on cardiac metabolism.

protein 1 light chain 3 did not accumulate in YME1L-deficient heart nor were myocardial amino acid levels altered (fig. S7, A and B). Thus, increased autophagy is unlikely to cause the loss of cardiomyocytes in this model. In contrast, our results suggest that stress-induced OPA1 processing by OMA1 promotes cardiomyocyte death in the absence of YME1L (fig. S7, C and D). We observed increased serum levels of cardiac troponin, fibrotic remodeling, and necrotic cell death, as well as the dysregulation of genes functionally linked to cell death in YME1L-deficient hearts (fig. S7, C and D). These results identify OMA1 as a critical regulator of cardiomyocyte survival in vivo, consistent with an antiapoptotic effect of OMA1 in cultured cells (*21*, *25*, *29*). Note that cardiac mitochondria form normal cristae in the absence of YME1L. Thus, cristae remodeling and facilitated cytochrome c release does not drive cell death in these mice, which instead is triggered by the loss of L-OPA1 and the impairment of mitochondrial fusion. In light of these observations, it is conceivable that the recently reported, protective effect of OPA1 overexpression in various mouse models for mitochondrial disease (*59*, *60*) can be attributed to L-OPA1 alone, which drives fusion and can support cell survival independent of cristae morphogenesis.

Similar to previous models for the failing heart (*36*, *61*), the cardiomyocyte-specific loss of YME1L and disturbed mitochondrial dynamics provoked a downstream metabolic shift from lipid to glucose metabolism in the myocardium. We observed reduced levels of acylcarnitine and increased glucose uptake that indicated reinforced myocardial glucose utilization, which is known to be associated with heart failure when combined with disturbed fatty acid metabolism (*37*). These alterations occur in the absence of overt respiratory deficiencies, which were previously observed to enhance cardiac glucose metabolism (*36*, *61*), which highlights the regulatory role of mitochondrial dynamics in cardiac metabolism. Increasing evidence indeed supports a close link between energy metabolism and mitochondrial fusion and fission in various tissues, including the central nervous system and brown adipose tissue, and suggests an association between mitochondrial fission, lipid metabolism, and energy expenditure (*62*–*64*).

Our experiments provide strong evidence that alterations in metabolism cause heart failure in cYKO mice. Additional deletion of *Yme1l* in skeletal muscle preserved cardiac function and normal life span of mice lacking YME1L in cardiomyocytes without restoring defects in mitochondrial morphology (Fig. 7). This is likely due to an endocrine effect by the skeletal muscle on glucose uptake in the heart. Dysfunction of mitochondria in skeletal muscle was previously reported to affect systemic glucose metabolism by impairing insulin secretion by pancreatic β cells and glucose uptake in target tissues (*41*). Similarly, we observed lowered fasting-insulin concentrations, systemic glucose intolerance, and normalized heart glucose uptake in mice upon additional deletion of *Yme1l* in skeletal muscle. Loss of YME1L appears to impair insulin signaling via its effect on mitochondrial dynamics and stress-induced OPA1 processing by OMA1, because we observed normal systemic glucose homeostasis in mice lacking both OMA1 and YME1L in skeletal muscle. These results highlight the physiological importance of tissue cross-talk that must be taken into consideration when analyzing tissue-specific models for mitochondrial disease.

Further support for a critical role of disturbed cardiomyocyte metabolism for heart failure came from the observation that feeding a high-fat diet preserved normal cardiac function of cardiomyocyte-specific YME1L knockout mice (Fig. 7). Similar to ablation of *Yme1l* in skeletal muscle, this metabolic intervention did not circumvent the primary mitochondrial defects in cardiomyocytes because the catalytic activity of YME1L, OMA1 activation, mitochondrial morphology, and respiratory chain profiles were unaffected by diet. However, it did blunt downstream metabolic disruptions and normalized cardiac glucose uptake in cardiomyocyte-specific YME1L knockout mice, which suppressed cell death and preserved cardiac function. Remarkably, feeding of cardiomyocyte-specific YME1L knockout mice with a high-fat diet prevents cardiomyopathy at least at early stages despite normal weight gain of the mice. Echocardiographic analyses of failing cYKO hearts demonstrate that these mice have reduced contractile function but normal left ventricular mass, which suggests that YME1L ablation does not result in a concentric hypertrophic response, and thus cardiac dysfunction can be improved by metabolic intervention. In this sense, some forms of DCM in humans can be treated by pharmacological means (*65*). Consistent with previous reports (*37*), high-fat feeding of WT mice did not incite contractile dysfunction (table S2). In contrast, feeding mice manifesting cardiomyopathy associated with ventricular hypertrophy a high-fat diet exacerbates myocardial dysfunction (*66*, *67*). It is thus an intriguing possibility that this metabolic intervention is beneficial exclusively in the context of DCM. Our results reveal an intimate relation between alterations in mitochondrial morphology and metabolism in the heart, which may underlie myocardial disease in humans. Metabolic interventions can preserve cardiac function even if mitochondrial morphology is disturbed, which opens potential avenues for therapeutic interventions in myocardial disease.

Methods

Echocardiography and PET-CT

Echocardiography and functional examination in mice was performed as previously described (*68*). All PET-CT studies were performed with a small-animal PET-CT device. Briefly, animals were fasted overnight, and anatomic thorax CT scanning was performed 1 hour after [^{18}F]FDG injections, followed by metabolic PET static acquisition for 15 min. Image analysis was performed in prefused and prereconstructed images with Osirix (Aycam Medical Systems, LLC); we selected myocardium of the whole left ventricle and calculated mean myocardial standardized uptake value (SUV med) for each animal. See supplemental methods for full methods description.

Incline treadmill

Treadmill experiments were conducted using a TSE treadmill and up to six randomized mice assessed simultaneously. Low-intensity incline (5%) experiments began at 0.05 m/s and increasing to 0.1 m/s for 60 s, 0.1 m/s for 600 s, then increasing to 0.28 m/s for 3100 s by 172-s increments. Blinded determination of exercise exhaustion was assessed and plotted as a function of total distance (m).

Histology and immunochemistry

Paraffin-embedded sections (4 μm) were subjected to hematoxylin and eosin, picrosirius red, or Masson's trichrome staining. Images were acquired using a Leica SCN400 automated slide scanner at 40×.

Generation of primary cardiomyocytes and cardiac fibroblasts

Adult cardiomyocytes were isolated by retrograde Langerdorff perfusion with an enzymatic digestion buffer containing trypsin and Liberase (Roche Applied Science) (*68*). Primary cardiac fibroblasts obtained during cardiomyocyte isolations were immortalized using a plasmid encoding SV40 large T antigen and deleted for *Yme1l* in vitro. See supplemental methods for full methods description.

Transmission electron microscopy (TM)

Left ventricle samples of hearts perfused with paraformaldehyde [2% (w/v) in phosphate-buffered saline (PBS)] and glutaraldehyde [2% (w/v) in PBS] hearts were fixed for 3 days in 2% (v/v) glutaraldehyde, 2.5% (w/v) sucrose, 3 mM $CaCl_2$, and 100 mM HEPES-KOH, pH7.4, at 4°C. After washes, samples were fixed using reduced OsO_4 [1% (w/v) OsO_4, 10 mg/ml potassium ferrocyanide, 1.25% (w/v) sucrose, and 100 mM sodium cacodylate, pH 7.4] for 1 hour on ice. After washes in water, cells were incubated in 2% (w/v) uranyl acetate for 30 min. After dehydration with 50, 70, 90, and 100% ethanol, samples were embedded in epon resin. Samples were observed under a transmission electron microscope (EM902; Carl Zeiss) at an acceleration voltage of 80 kV.

Confocal fluorescence microscopy

To monitor mitochondrial morphology by immunofluorescence microscopy, primary cardiomyocytes were fixed and stained with antibodies directed against TOMM20 (rabbit-specific antibody 1:1000, Santa Cruz Biotechnology). Fluorescently coupled secondary antibody Alexa Fluor 568 (a goat antibody directed against a rabbit secondary antibody) was used at 1:1000 dilution (Invitrogen). Images were acquired using an UltraVIEW VoX spinning disc microscope (CSU-X1; Yokogawa Corporation of America). Quantification of mitochondrial morphology in primary cardiomyocytes was performed by blinded, randomized examination of z-stack images. Cardiac necrosis was assessed by Evans Blue diffusion as previously described (*57*). Paraffin-embedded cardiac sections were stained with

fluorescein isothoicyante–conjugated wheat germ agglutinin (Invitrogen, W834) for 30 min before nuclear counterstaining with 4′,6′-diamidino-2-phenylindole (DAPI). Evans Blue–positive cardiomyocytes fluorescence is in red. Images were acquired using a Leica SP8 confocal microscope at 40×.

Blood glucose and serum analyses

Intraperitoneal GTTs were carried out in mice after they were fasted for 6 hours. After determination of fasted blood glucose levels, an intraperitoneal bolus of 2 g glucose/kg body weight [20% (w/v) glucose]. Blood glucose levels were determined after 15, 30, 60, and 120 min using Contour test strips (Bayer, Germany). Serum insulin levels were measured from blood collected from 6 hours fasted mice, by enzyme-linked immunosorbent assays (ELISAs), according to the manufacturer's instructions (Mouse/Rat Insulin ELISA, Mouse Leptin ELISA;Crystal Chem Inc.). Serum levels of cardiac troponin assayed by auto-analyzer Dimension RxL Max HM (Siemens).

Oxygen consumption measurements

Oxygen consumption of WT and cYKO hearts, fed normal chow diet (NCD) or high-fat diet (HFD), was measured using a fluorescence-based micro-optode that consisted of an optic fiber equipped with an oxygen-sensitive fluorescent terminal sensor (FireSting O_2; Bionef, Paris, France) as described previously (*69*). Hearts were perfused in buffer (10 mM KH_2PO_4, 300 mM mannitol, 10 mM KCl, 5 mM $MgCl_2$, 5 mM bovine serum albumin, pH 7.4), dissected, weighted, and assayed at rest, precisely 3 min after mice were killed by cervical dislocation. Oxygen uptake rates (nmol O_2/min) were adjusted relative to wet heart weight.

Respiratory chain measurements

Activity of respiratory chain complexes and citrate synthase was spectrophotometrically assayed as previously described (*70*).

Statistical analysis

Statistical analyses were performed using Prism (GraphPad Software Inc., San Diego, CA). All values are expressed as means ± SEM. Statistical significance was assessed by using a two-tailed unpaired Student's *t* test or the Mann-Whitney test for two-group comparisons. Two-way analysis of variance (ANOVA) with Bonferroni post hoc tests (corrected *P* values are given for comparison between genotypes at specific time points) were used to evaluate multiple pairwise comparisons of groups. Life span survival curves were compared by using a log-rank Mantel-Cox test. Differences were considered statistically significant at a value of $P < 0.05$. $^{*}P < 0.05$, $^{**}P < 0.01$, $^{***}P < 0.001$, $^{****}P < 0.0001$.

REFERENCES AND NOTES

1. J. R. Friedman, J. Nunnari, Mitochondrial form and function. *Nature* **505**, 335–343 (2014). doi: 10.1038/nature12985; pmid: 24429632
2. P. Mishra, D. C. Chan, Mitochondrial dynamics and inheritance during cell division, development and disease. *Nat. Rev. Mol. Cell Biol.* **15**, 634–646 (2014). doi: 10.1038/nrm3877; pmid: 25237825
3. F. Burté, V. Carelli, P. F. Chinnery, P. Yu-Wai-Man, Disturbed mitochondrial dynamics and neurodegenerative disorders. *Nat. Rev. Neurol.* **11**, 11–24 (2015). doi: 10.1038/nrneurol.2014.228; pmid: 25486875
4. G. W. Dorn 2nd, R. N. Kitsis, The mitochondrial dynamism-mitophagy-cell death interactome: Multiple roles performed by members of a mitochondrial molecular ensemble. *Circ. Res.* **116**, 167–182 (2015). doi: 10.1161/CIRCRESAHA.116.303554; pmid: 25323859
5. J. R. Friedman *et al*., ER tubules mark sites of mitochondrial division. *Science* **334**, 358–362 (2011). doi: 10.1126/science.1207385; pmid: 21885730
6. F. Korobova, V. Ramabhadran, H. N. Higgs, An actin-dependent step in mitochondrial fission mediated by the ER-associated formin INF2. *Science* **339**, 464–467 (2013). doi: 10.1126/science.1228360; pmid: 23349293
7. Y. Chen, Y. Liu, G. W. Dorn 2nd, Mitochondrial fusion is essential for organelle function and cardiac homeostasis. *Circ. Res.* **109**, 1327–1331 (2011). doi: 10.1161/CIRCRESAHA.111.258723; pmid: 22052916
8. L. C. Gomes, L. Scorrano, Mitochondrial elongation during autophagy: A stereotypical response to survive in difficult times. *Autophagy* **7**, 1251–1253 (2011). doi: 10.4161/auto.7.10.16771; pmid: 21743300
9. D. A. Patten *et al*., OPA1-dependent cristae modulation is essential for cellular adaptation to metabolic demand. *EMBO J.* **33**, 2676–2691 (2014). doi: 10.15252/embj.201488349; pmid: 25298396
10. P. Mishra, V. Carelli, G. Manfredi, D. C. Chan, Proteolytic cleavage of Opa1 stimulates mitochondrial inner membrane fusion and couples fusion to oxidative phosphorylation. *Cell Metab.* **19**, 630–641 (2014). doi: 10.1016/j.cmet.2014.03.011; pmid: 24703695
11. C. R. Hackenbrock, Ultrastructural bases for metabolically linked mechanical activity in mitochondria. I. Reversible ultrastructural changes with change in metabolic steady state in isolated liver mitochondria. *J. Cell Biol.* **30**, 269–297 (1966). doi: 10.1083/jcb.30.2.269; pmid: 5968972
12. D. Sebastián *et al*., Mitofusin 2 (Mfn2) links mitochondrial and endoplasmic reticulum function with insulin signaling and is essential for normal glucose homeostasis. *Proc. Natl. Acad. Sci. U.S.A.* **109**, 5523–5528 (2012). doi: 10.1073/pnas.1108220109; pmid: 22427360
13. R. J. Youle, A. M. van der Bliek, Mitochondrial fission, fusion, and stress. *Science* **337**, 1062–1065 (2012). doi: 10.1126/science.1219855; pmid: 22936770
14. G. Twig *et al*., Fission and selective fusion govern mitochondrial segregation and elimination by autophagy. *EMBO J.* **27**, 433–446 (2008). pmid: 18200046
15. A. Olichon *et al*., Loss of OPA1 perturbates the mitochondrial inner membrane structure and integrity, leading to cytochrome *c* release and apoptosis. *J. Biol. Chem.* **278**, 7743–7746 (2003). doi: 10.1074/jbc.C200677200; pmid: 12509422
16. S. Cipolat, O. Martins de Brito, B. Dal Zilio, L. Scorrano, OPA1 requires mitofusin 1 to promote mitochondrial fusion. *Proc. Natl. Acad. Sci. U.S.A.* **101**, 15927–15932 (2004). doi: 10.1073/pnas.0407043101; pmid: 15509649
17. C. Frezza *et al*., OPA1 controls apoptotic cristae remodeling independently from mitochondrial fusion. *Cell* **126**, 177–189 (2006). doi: 10.1016/j.cell.2006.06.025; pmid: 16839885
18. P. M. Quirós, T. Langer, C. López-Otín, New roles for mitochondrial proteases in health, ageing and disease. *Nat. Rev. Mol. Cell Biol.* **16**, 345–359 (2015). doi: 10.1038/nrm3984; pmid: 25970558
19. M. Roy, P. H. Reddy, M. Iijima, H. Sesaki, Mitochondrial division and fusion in metabolism. *Curr. Opin. Cell Biol.* **33**, 111–118 (2015). doi: 10.1016/j.ceb.2015.02.001; pmid: 25703628
20. L. Griparic, T. Kanazawa, A. M. van der Bliek, Regulation of the mitochondrial dynamin-like protein Opa1 by proteolytic cleavage. *J. Cell Biol.* **178**, 757–764 (2007). doi: 10.1083/jcb.200704112; pmid: 17709430
21. B. Head, L. Griparic, M. Amiri, S. Gandre-Babbe, A. M. van der Bliek, Inducible proteolytic inactivation of OPA1 mediated by the OMA1 protease in mammalian cells. *J. Cell Biol.* **187**, 959–966 (2009). doi: 10.1083/jcb.200906083; pmid: 20038677
22. Z. Song, H. Chen, M. Fiket, C. Alexander, D. C. Chan, OPA1 processing controls mitochondrial fusion and is regulated by mRNA splicing, membrane potential, and Yme1L. *J. Cell Biol.* **178**, 749–755 (2007). doi: 10.1083/jcb.200704110; pmid: 17709429
23. S. Ehses *et al*., Regulation of OPA1 processing and mitochondrial fusion by m-AAA protease isoenzymes and OMA1. *J. Cell Biol.* **187**, 1023–1036 (2009). doi: 10.1083/jcb.200906084; pmid: 20038678
24. D. Tondera *et al*., SLP-2 is required for stress-induced mitochondrial hyperfusion. *EMBO J.* **28**, 1589–1600 (2009). doi: 10.1038/emboj.2009.89; pmid: 19360003
25. R. Anand *et al*., The *i*-AAA protease YME1L and OMA1 cleave OPA1 to balance mitochondrial fusion and fission. *J. Cell Biol.* **204**, 919–929 (2014). doi: 10.1083/jcb.201308006; pmid: 24616225
26. N. Ishihara, Y. Fujita, T. Oka, K. Mihara, Regulation of mitochondrial morphology through proteolytic cleavage of OPA1. *EMBO J.* **25**, 2966–2977 (2006). doi: 10.1038/sj.emboj.7601184; pmid: 16778770
27. M. J. Baker *et al*., Stress-induced OMA1 activation and autocatalytic turnover regulate OPA1-dependent mitochondrial dynamics. *EMBO J.* **33**, 578–593 (2014). doi: 10.1002/embj.201386474; pmid: 24550258
28. K. Zhang, H. Li, Z. Song, Membrane depolarization activates the mitochondrial protease OMA1 by stimulating self-cleavage. *EMBO Rep.* **15**, 576–585 (2014). doi: 10.1002/embr.201338240; pmid: 24719224
29. P. M. Quirós *et al*., Loss of mitochondrial protease OMA1 alters processing of the GTPase OPA1 and causes obesity and defective thermogenesis in mice. *EMBO J.* **31**, 2117–2133 (2012). doi: 10.1038/emboj.2012.70; pmid: 22433842
30. X. Jiang, H. Jiang, Z. Shen, X. Wang, Activation of mitochondrial protease OMA1 by Bax and Bak promotes cytochrome c release during apoptosis. *Proc. Natl. Acad. Sci. U.S.A.* **111**, 14782–14787 (2014). doi: 10.1073/pnas.1417253111; pmid: 25275009
31. Y. Ruan *et al*., Loss of Yme1L perturbates mitochondrial dynamics. *Cell Death Dis.* **4**, e896 (2013). doi: 10.1038/cddis.2013.414; pmid: 24176854
32. X. Xiao *et al*., OMA1 mediates OPA1 proteolysis and mitochondrial fragmentation in experimental models of ischemic kidney injury. *Am. J. Physiol. Renal Physiol.* **306**, F1318–F1326 (2014). doi: 10.1152/ajprenal.00036.2014; pmid: 24671334
33. K. N. Papanicolaou *et al*., Mitofusins 1 and 2 are essential for postnatal metabolic remodeling in heart. *Circ. Res.* **111**, 1012–1026 (2012). doi: 10.1161/CIRCRESAHA.112.274142; pmid: 22904094
34. R. Agah *et al*., Gene recombination in postmitotic cells. Targeted expression of Cre recombinase provokes cardiac-restricted, site-specific rearrangement in adult ventricular muscle in vivo. *J. Clin. Invest.* **100**, 169–179 (1997). doi: 10.1172/JCI119509; pmid: 9202069
35. S. C. Kolwicz Jr., R. Tian, Glucose metabolism and cardiac hypertrophy. *Cardiovasc. Res.* **90**, 194–201 (2011). doi: 10.1093/cvr/cvr071; pmid: 21502371
36. A. Hansson *et al*., A switch in metabolism precedes increased mitochondrial biogenesis in respiratory chain-deficient mouse hearts. *Proc. Natl. Acad. Sci. U.S.A.* **101**, 3136–3141 (2004). doi: 10.1073/pnas.0308710100; pmid: 14978272
37. J. Yan *et al*., Increased glucose uptake and oxidation in mouse hearts prevent high fatty acid oxidation but cause cardiac dysfunction in diet-induced obesity. *Circulation* **119**, 2818–2828 (2009). doi: 10.1161/CIRCULATIONAHA.108.832915; pmid: 19451348
38. C. Potting *et al*., TRIAP1/PRELI complexes prevent apoptosis by mediating intramitochondrial transport of phosphatidic acid. *Cell Metab.* **18**, 287–295 (2013). doi: 10.1016/j.cmet.2013.07.008; pmid: 23931759
39. J. C. Brüning *et al*., A muscle-specific insulin receptor knockout exhibits features of the metabolic syndrome of NIDDM without altering glucose tolerance. *Mol. Cell* **2**, 559–569 (1998). doi: 10.1016/S1097-2765(00)80155-0; pmid: 9844629
40. K. T. Chambers *et al*., Chronic inhibition of pyruvate dehydrogenase in heart triggers an adaptive metabolic response. *J. Biol. Chem.* **286**, 11155–11162 (2011). doi: 10.1074/jbc.M110.217349; pmid: 21321124
41. C. Handschin *et al*., Abnormal glucose homeostasis in skeletal muscle-specific PGC-1alpha knockout mice reveals skeletal muscle-pancreatic beta cell crosstalk. *J. Clin. Invest.* **117**, 3463–3474 (2007). doi: 10.1172/JCI31785; pmid: 17932564
42. E. Jing *et al*., Sirtuin-3 (Sirt3) regulates skeletal muscle metabolism and insulin signaling via altered mitochondrial oxidation and reactive oxygen species production. *Proc. Natl. Acad. Sci. U.S.A.* **108**, 14608–14613 (2011). doi: 10.1073/pnas.1111308108; pmid: 21873205
43. L. Chen *et al*., OPA1 mutation and late-onset cardiomyopathy: Mitochondrial dysfunction and mtDNA instability. *J. Am. Heart Assoc.* **1**, e003012 (2012). doi: 10.1161/JAHA.112.003012; pmid: 23316298

44. J. Piquereau *et al*., Down-regulation of OPA1 alters mouse mitochondrial morphology, PTP function, and cardiac adaptation to pressure overload. *Cardiovasc. Res.* **94**, 408–417 (2012). doi: 10.1093/cvr/cvs117; pmid: 22406748
45. L. C. Gomes, G. Di Benedetto, L. Scorrano, During autophagy mitochondria elongate, are spared from degradation and sustain cell viability. *Nat. Cell Biol.* **13**, 589–598 (2011). doi: 10.1038/ncb2220; pmid: 21478857
46. H. Chen, A. Chomyn, D. C. Chan, Disruption of fusion results in mitochondrial heterogeneity and dysfunction. *J. Biol. Chem.* **280**, 26185–26192 (2005). doi: 10.1074/jbc.M503062200; pmid: 15899901
47. K. N. Papanicolaou *et al*., Mitofusin-2 maintains mitochondrial structure and contributes to stress-induced permeability transition in cardiac myocytes. *Mol. Cell. Biol.* **31**, 1309–1328 (2011). doi: 10.1128/MCB.00911-10; pmid: 21245373
48. Y. Chen *et al*., Mitofusin 2-containing mitochondrial-reticular microdomains direct rapid cardiomyocyte bioenergetic responses via interorganelle Ca(2+) crosstalk. *Circ. Res.* **111**, 863–875 (2012). doi: 10.1161/CIRCRESAHA.112.266585; pmid: 22777004
49. G. W. Dorn 2nd, M. Song, K. Walsh, Functional implications of mitofusin 2-mediated mitochondrial-SR tethering. *J. Mol. Cell. Cardiol.* **78**, 123–128 (2015). doi: 10.1016/j.yjmcc.2014.09.015; pmid: 25252175
50. A. Kasahara, S. Cipolat, Y. Chen, G. W. Dorn 2nd, L. Scorrano, Mitochondrial fusion directs cardiomyocyte differentiation via calcineurin and Notch signaling. *Science* **342**, 734–737 (2013). doi: 10.1126/science.1241359; pmid: 24091702
51. A. Mourier *et al*., Mitofusin 2 is required to maintain mitochondrial coenzyme Q levels. *J. Cell Biol.* **208**, 429–442 (2015). doi: 10.1083/jcb.201411100; pmid: 25688136
52. S. B. Ong *et al*., Inhibiting mitochondrial fission protects the heart against ischemia/reperfusion injury. *Circulation* **121**, 2012–2022 (2010). doi: 10.1161/CIRCULATIONAHA.109.906610; pmid: 20421521
53. C. B. Park *et al*., MTERF3 is a negative regulator of mammalian mtDNA transcription. *Cell* **130**, 273–285 (2007). doi: 10.1016/j.cell.2007.05.046; pmid: 17662942
54. B. Ruzzenente *et al*., LRPPRC is necessary for polyadenylation and coordination of translation of mitochondrial mRNAs. *EMBO J.* **31**, 443–456 (2012). doi: 10.1038/emboj.2011.392; pmid: 22045337
55. C. Riehle *et al*., Insulin receptor substrate signaling suppresses neonatal autophagy in the heart. *J. Clin. Invest.* **123**, 5319–5333 (2013). doi: 10.1172/JCI71171; pmid: 24177427
56. Y. Kageyama *et al*., Parkin-independent mitophagy requires Drp1 and maintains the integrity of mammalian heart and brain. *EMBO J.* **33**, 2798–2813 (2014). doi: 10.15252/embj.201488658; pmid: 25349190
57. M. Song, K. Mihara, Y. Chen, L. Scorrano, G. W. Dorn 2nd, Mitochondrial fission and fusion factors reciprocally orchestrate mitophagic culling in mouse hearts and cultured fibroblasts. *Cell Metab.* **21**, 273–285 (2015). doi: 10.1016/j.cmet.2014.12.011; pmid: 25600785
58. Y. Ikeda *et al*., Endogenous Drp1 mediates mitochondrial autophagy and protects the heart against energy stress. *Circ. Res.* **116**, 264–278 (2015). doi: 10.1161/CIRCRESAHA.116.303356; pmid: 25332205
59. G. Civiletto *et al*., Opa1 overexpression ameliorates the phenotype of two mitochondrial disease mouse models. *Cell Metab.* **21**, 845–854 (2015). doi: 10.1016/j.cmet.2015.04.016; pmid: 26039449
60. T. Varanita *et al*., The OPA1-dependent mitochondrial cristae remodeling pathway controls atrophic, apoptotic, and ischemic tissue damage. *Cell Metab.* **21**, 834–844 (2015). doi: 10.1016/j.cmet.2015.05.007; pmid: 26039448
61. J. M. Huss, D. P. Kelly, Mitochondrial energy metabolism in heart failure: A question of balance. *J. Clin. Invest.* **115**, 547–555 (2005). doi: 10.1172/JCI24405; pmid: 15765136
62. C. M. Nasrallah, T. L. Horvath, Mitochondrial dynamics in the central regulation of metabolism. *Nat. Rev. Endocrinol.* **10**, 650–658 (2014). doi: 10.1038/nrendo.2014.160; pmid: 25200564
63. M. O. Dietrich, Z. W. Liu, T. L. Horvath, Mitochondrial dynamics controlled by mitofusins regulate Agrp neuronal activity and diet-induced obesity. *Cell* **155**, 188–199 (2013). doi: 10.1016/j.cell.2013.09.004; pmid: 24074868
64. J. D. Wikstrom *et al*., Hormone-induced mitochondrial fission is utilized by brown adipocytes as an amplification pathway for energy expenditure. *EMBO J.* **33**, 418–436 (2014). doi: 10.1002/embj.201385014; pmid: 24431221
65. B. D. Lowes *et al*., Myocardial gene expression in dilated cardiomyopathy treated with beta-blocking agents. *N. Engl. J. Med.* **346**, 1357–1365 (2002). doi: 10.1056/NEJMoa012630; pmid: 11986409
66. S. Sankaralingam *et al*., Lowering body weight in obese mice with diastolic heart failure improves cardiac insulin sensitivity and function: Implications for the obesity paradox. *Diabetes* **64**, 1643–1657 (2015). doi: 10.2337/db14-1050; pmid: 25524917
67. Z. Sun *et al*., Diet-induced lethality due to deletion of the Hdac3 gene in heart and skeletal muscle. *J. Biol. Chem.* **286**, 33301–33309 (2011). doi: 10.1074/jbc.M111.277707; pmid: 21808063
68. J. García-Prieto *et al*., β3 Adrenergic receptor selective stimulation during ischemia/reperfusion improves cardiac function in translational models through inhibition of mPTP opening in cardiomyocytes. *Basic Res. Cardiol.* **109**, 422 (2014). doi: 10.1007/s00395-014-0422-0; pmid: 24951958
69. R. El-Khoury *et al*., Alternative oxidase expression in the mouse enables bypassing cytochrome *c* oxidase blockade and limits mitochondrial ROS overproduction. *PLOS Genet.* **9**, e1003182 (2013). doi: 10.1371/journal.pgen.1003182; pmid: 23300486
70. P. Bénit *et al*., Three spectrophotometric assays for the measurement of the five respiratory chain complexes in minuscule biological samples. *Clin. Chim. Acta* **374**, 81–86 (2006). doi: 10.1016/j.cca.2006.05.034; pmid: 16828729

ACKNOWLEDGMENTS

We thank K. Lemke, H. Bank, E. Barth, V. Zorita, and M. Gómez for technical assistance; A. Polykratis and C. Uthoff-Hachenberg for genetic engineering assistance; A. Pun-García and R. Villena-Gutierrez for cardiomyocyte isolations; A. V. Alonso López, L. Flores Ruiz, and J. Jimenez-Borreguero for echocardiography evaluation; I. Bilbao, C. Velasco, and J. Ruiz-Cabello for PET-CT evaluation; A. Ferrarini and D. Dudzik for help in metabolomics; G. Rapl for single-cell sorting of cardiac fibroblasts; P. Frommolt for microarray quality control; and J. Brüning for discussion. This work was supported by a fellowship of the Human Frontiers Science Program to T.W., by grants of the Deutsche Forschungsgemeinschaft and the European Research Council to T.L., and by a grant from the Spanish Ministry of Economy and Competitiveness (MINECO) through the Carlos III Institute of Health—Fondo de Investigación Sanitaria and European Regional Development Fund (ERDF/FEDER) funds (PI13/01979) and Networks for Cooperative Research in Health (RETIC) (RD12/0042/0054) to B.I. The CNIC is supported by the Ministry of Economy and Competitiveness and the Pro-CNIC Foundation. B.I. is Princess of Girona awardee in science. F.J.R. and C.B. acknowledge MINECO CTQ 2014-55279-R. The authors declare no competing or financial interests. The mice used in this study are available under a materials transfer agreement from the authors. The data are included in the main manuscript and the supplementary materials. Author contributions: M.J.B. generated the floxed *Oma1* mouse, T.W. generated the floxed *Yme1l* mouse, hmYKO mice, hmOKO mice, hmDKO mice, cYKO mice, and cDKO mice. C.M. designed targeting constructs. P.B. and P.R. performed oxygen consumption measurements, F.J. R. and C.B. performed the acylcarnitine profiling, and T.W. and J.G.-P. performed all other experiments. T.W., J.G.-P., B.I., and T.L. drafted the manuscript.

SUPPLEMENTARY MATERIALS

www.sciencemag.org/content/350/6265/aad0116/suppl/DC1
Additional Materials and Methods
Figs. S1 to S7
Tables S1 and S2
References (*71*, *72*)

13 July 2015; accepted 2 October 2015
10.1126/science.aad0116

Basic Res Cardiol (2014) 109:422
DOI 10.1007/s00395-014-0422-0

ORIGINAL CONTRIBUTION

β_3 adrenergic receptor selective stimulation during ischemia/reperfusion improves cardiac function in translational models through inhibition of mPTP opening in cardiomyocytes

Jaime García-Prieto · Jose Manuel García-Ruiz · David Sanz-Rosa · Andrés Pun · Ana García-Alvarez · Sean M. Davidson · Leticia Fernández-Friera · Mario Nuno-Ayala · Rodrigo Fernández-Jiménez · Juan A. Bernal · José Luis Izquierdo-Garcia · Jesús Jimenez-Borreguero · Gonzalo Pizarro · Jesús Ruiz-Cabello · Carlos Macaya · Valentín Fuster · Derek M. Yellon · Borja Ibanez

Received: 28 March 2014 / Revised: 10 June 2014 / Accepted: 11 June 2014
© Springer-Verlag Berlin Heidelberg 2014

Abstract Selective stimulation of β_3 adrenergic-receptor (β3AR) has been shown to reduce infarct size in a mouse model of myocardial ischemia/reperfusion. However, its functional long-term effect and the cardioprotective mechanisms at the level of cardiomyocytes have not been elucidated, and the impact of β3AR stimulation has not been evaluated in a more translational large animal model. This study aimed at evaluating pre-perfusion administration of BRL37344 both in small and large animal models of myocardial ischemia/reperfusion. Pre-reperfusion administration of the β3AR agonist BRL37344 (5 μg/kg) reduced infarct size at 2-and 24-h reperfusion in wild-type mice. Long-term (12-weeks) left ventricular (LV) function assessed by echocardiography and cardiac magnetic resonance (CMR) was significantly improved in β3AR agonist-treated mice. Incubation with β3AR agonist (BRL37344, 7 μmol/L) significantly reduced cell death in isolated adult mouse cardiomyocytes during hypoxia/reoxygenation and decreased susceptibility to deleterious opening of the mitochondrial permeability transition pore (mPTP), via a mechanism dependent on the Akt-NO signaling pathway. Pre-reperfusion BRL37344 administration had no effect on infarct size in cyclophilin-D KO mice, further implicating mPTP in the mechanism of protection. Large-white pigs underwent percutaneous coronary ischemia/reperfusion and 3-T CMR at 7 and 45 days post-infarction. Pre-perfusion administration of BRL37344 (5 μg/kg) decreased

J. García-Prieto, J. M. García-Ruiz, and D. Sanz-Rosa contributed equally.

Electronic supplementary material The online version of this article (doi:10.1007/s00395-014-0422-0) contains supplementary material, which is available to authorized users.

J. García-Prieto · J. M. García-Ruiz · D. Sanz-Rosa · A. Pun · A. García-Alvarez · L. Fernández-Friera · M. Nuno-Ayala · R. Fernández-Jiménez · J. Jimenez-Borreguero · G. Pizarro · V. Fuster · B. Ibanez (✉)
Imaging, Epidemiology and Atherothrombosis Department, Centro Nacional de Investigaciones Cardiovasculares Carlos III (CNIC), Melchor Fernández Almagro 3, 28029 Madrid, Spain
e-mail: bibanez@cnic.es

J. M. García-Ruiz
Hospital Universitario Central de Asturias, Oviedo, Spain

A. García-Alvarez
Hospital Clinic, Barcelona, Spain

S. M. Davidson · D. M. Yellon
Hatter Cardiovascular Institute, University College London, London, UK

L. Fernández-Friera
Hospital Universitario Monteprincipe, Madrid, Spain

J. A. Bernal
Cardiovascular Development and Repair Department, CNIC, Madrid, Spain

J. L. Izquierdo-Garcia · J. Ruiz-Cabello
Advanced Imaging Unit, CNIC, Madrid, Ciber de Enfermedades Respiratorias and Universidad Complutense, Madrid, Spain

G. Pizarro
Hospital Universitario Quirón, Madrid, Spain

C. Macaya · B. Ibanez
Cardiovascular Institute, Hospital Clínico San Carlos, Madrid, Spain

V. Fuster
Zena and Michael A. Wiener CVI, Mount Sinai School of Medicine, New York, NY, USA

Published online: 21 June 2014

infarct size and improved long-term LV contractile function. A single-dose administration of β3AR agonist before reperfusion decreased infarct size and resulted in a consistent and long-term improvement in cardiac function, both in small and large animal models of myocardial ischemia/reperfusion. This protection appears to be executed through inhibition of mPTP opening in cardiomyocytes.

Keywords β_3 adrenergic receptor · Magnetic resonance imaging · Myocardial infarction · Beta-adrenergic receptor blocker · Ischemia/reperfusion · Mitochondrial permeability transition pore

Introduction

Acute myocardial infarction (AMI) is a leading cause of mortality and morbidity worldwide. Early coronary reperfusion has been established as the best therapeutic strategy to limit infarct size and improve prognosis; however, reperfusion itself induces additional damage to the myocardium, known as ischemia/reperfusion injury (IRI) [20, 42, 49].

Evidence gathered over the past 40 years indicates that myocardial injury can be attenuated by manipulation of the response to IRI. In 1971 Braunwald et al. [38] demonstrated that the severity of myocardial necrosis due to coronary occlusion could be attenuated by appropriate interventions during ischemia. Since then, multiple strategies and interventions have been proposed as capable of limiting infarct size by reducing IRI in different animal models [5]. Despite these promising preclinical studies, attempts to translate them to the clinic have not been successful [23, 29, 47, 49] partly because of the lack of studies confirming results obtained in small animals in clinically relevant large animal models [10, 26]. The possibility of reducing the extent of cell death during an AMI is of great importance, since infarct size is the main determinant of post-infarction mortality [13]. Consequently, there is a clear need to develop therapies for reducing infarct size that go beyond early reperfusion.

The β_3 adrenergic-receptor (β3AR) is a G-protein-coupled receptor preferentially expressed in adipose tissue. The identification of β3AR expression in the myocardium [22] prompted suggestions that it might be a therapeutic target in cardiovascular diseases, and β3AR-selective stimulation has been consistently beneficial in animal models of heart failure [12, 39]. More recently, β3AR agonists have been shown to reduce infarct size in mice undergoing regional myocardial ischemia/reperfusion [3]. However, it remains unknown whether β3AR stimulation during AMI results in long-term benefits on cardiac function and, more importantly, if this strategy is cardioprotective in a more clinically relevant large-animal model [28, 32]. Confirmation of an infarct-limiting effect and long-term benefits from this new therapeutic strategy would have a significant translational impact.

The fate of cardiomyocytes upon IRI is critically dependent on mitochondria [21, 30, 31, 49]. Irreversible and pathological opening of the mitochondrial permeability transition pore (mPTP) at the onset of reperfusion is well established as a major determinant of cardiomyocyte cell death [19, 30, 31]. A key regulator of mPTP opening is mitochondrial cyclophilin-D (CypD) and its pharmacological inhibition with cyclosporin-A (CsA) has been shown to reduce infarct size both in animal models and in clinics [4, 8, 18, 41, 48]. The effect of β3AR modulators on cardiomyocyte mPTP opening remains to be established.

The aims of this study were (1) to analyze the effect of pre-reperfusion β3AR agonist therapy on infarct size and long-term myocardial performance in a mouse model of IRI, (2) to study the cardioprotective mechanisms involved in β3AR stimulation at the cardiomyocyte level, and (3) to confirm the beneficial effect of β3AR agonist therapy in a large preclinical animal model of AMI.

Materials and methods

Study design

Two sets of mice were subjected to temporal left anterior descending (LAD) coronary artery occlusion and randomized to receive a single bolus of the β3AR agonist BRL37344 or vehicle before reperfusion. In the first set, late IRI was evaluated by quantification of infarct size at 24 h reperfusion. In a second set, serial left ventricular (LV) function was assessed by echocardiography and high field (7-T) cardiac magnetic resonance (CMR) at short- (1 and 4 weeks) and long-term (12 weeks) follow-up. To confirm β3AR agonism implication, FVB/N β3AR-knockout (KO) mice were subjected to the same myocardial IRI procedure and infarct size evaluated at 24 h of reperfusion.

To study whether the protective effect of pre-reperfusion β3AR stimulation derives from a direct effect on cardiomyocytes, isolated adult mouse cardiomyocytes were subjected to simulated ischemia/reperfusion (hypoxia/reoxygenation; H/R), and cell viability evaluated in the presence or absence of BRL37344. The role of nitric oxide (NO) production as an intracellular signaling mediator was tested by co-incubation with BRL37344 and the nitric oxide synthase (NOS) inhibitor L-NAME. In addition, the H/R procedure was applied to adult cardiomyocytes from mice lacking endothelial-NOS (eNOS-KO). NO signaling

pathway activation was evaluated by western blot in isolated cardiomyocytes subjected to H/R. Susceptibility to mPTP opening during β3AR stimulation was evaluated in isolated cardiomyocytes in the presence of BRL37344, saline, or the CypD inhibitor cyclosporine-A (CsA). The implication of mPTP opening in β3AR-agonist-mediated cardioprotection was tested in vivo in CypD-KO mice subjected to the myocardial IRI procedure and randomized to receive BRL37344 or vehicle before 2 h if reperfusion.

The translational impact of β3AR-agonist-mediated cardioprotection was tested in a pig model of AMI by 60 min of percutaneous angioplasty followed by reperfusion [33, 35] and randomized to receive either BRL37344 or vehicle at the onset reperfusion. Infarct size was evaluated by 3-T CMR at 7 days post-infarction, and LV function was evaluated, also by CMR, at long-term follow-up.

Mouse model of myocardial ischemia/reperfusion injury (IRI)

Male 8- to 12-week-old mice were subjected to 45 min of left anterior descending (LAD) coronary artery occlusion followed by reperfusion. For infarct size evaluation, reperfusion was maintained for 2 or 24 h; for assessment of long-term left ventricular (LV) function, reperfusion was maintained for 12 weeks. For the LAD procedure, mice were intra-peritoneal anesthetized with ketamine (60 mg/kg), xylacine (20 mg/kg), and atropine (9 mg/kg). Once deeply asleep, and under direct visualization of the trachea, animals were orally intubated using a blunted 22G cannula and mechanically ventilated throughout the entire procedure (SAR-830. CWE Inc.). Temperature was controlled (BAT-12, Physitemp Instruments) and kept constant at 37 °C with a heated operating table (V500VStat, Peco Services) to prevent hypothermic cardioprotection [2]. As previously described by Gomez et al. [24], a nylon 8/0 monofilament suture was passed beneath the LAD approximately 2 mm below the tip of the left atrium appendage. After stabilization for 5 min, regional ischemia was induced by tightening a simple snare to stop coronary blood flow. A short segment of PE-10 tubing was placed between the tissue and the suture to minimize damage and allow for complete reperfusion after the ischemic period. Successful LAD occlusion was confirmed by ST-segment elevation on ECG (MP36R, Biopac Systems Inc.) and the appearance of myocardial pallor. During ischemia, the thorax was covered with parafilm to prevent dehydration. Anesthetic mixture was injected intra-peritoneally when needed. Five minutes before the onset of reperfusion, mice were randomized to receive a single bolus injection (50 μL, with an insulin syringe) of the β3AR agonist BRL37344 (5 μg/kg) or saline into the femoral vein. The BRL37344 dose was selected on the basis of dose–response studies performed before the initiation of the IRI procedure (data not shown). The thoraxes of animals designated for infarct-size evaluation at 24 h reperfusion were closed with a 6/0 silk thread, and animals were recovered with 100 % O_2 and analgesized with buprenorphine (S.C., 0.1 mg/kg) until the end of the procedure. Animals designated to early IRI evaluation (2 h reperfusion) were maintained completely asleep and under mechanical ventilation until the end of the procedure.

Infarct size quantification

Mice reperfused for 24 h were briefly re-anesthetized at the end of the reperfusion period, and were then intubated and the LAD re-occluded by ligating the suture in the same position as the original infarction. Animals were then killed and 1 mL of 1 % (w/v) Evans Blue dye infused i.v. to delineate the Area at Risk (AAR: myocardium lacking blood flow, i.e. negative to blue dye staining). The heart was then excised, the left ventricle (LV) was isolated and cut into seven 1-mm-thick transverse slices, and pictures were taken from both sides. In order to differentiate infarcted from viable tissue, slices were incubated in triphenyltetrazolium chloride (TTC, 1 % (w/v) diluted in PBS) at 37 °C for 15 min. The slices were then re-photographed and weighed. Regions negative for Evans Blue staining (AAR) and negative for TTC (infarcted myocardium) were calculated by a blinded observer using the computer-assisted planimetry function in ImageJ 6.0 (NIH, Bethesda, MD). Infarct size for each slice was calculated as the average percentage of infarcted myocardium from both sides of each section. Following a previously described method [9], percentile values for AAR and IS were corrected to mg independently for each slice. Finally, absolute infarct size was determined as the ratio $\sum$mg of IS/$\sum$mg of AAR. This methodology takes into account individual AAR variability [11]. The full set of LV images is shown in supplemental Fig. 2.

Echocardiography functional examination in mice

Echocardiographic evaluations to determine cardiac volume and LV contractility were performed by an experienced observer blinded to the study allocation in mice at 1, 4 and 12 weeks post-infarction. Mice were anesthetized by inhalation of isoflurane/oxygen and examined with a 30-MHz transthoracic echocardiography probe and a Vevo 2100 ultrasound system (VisualSonics, Toronto, Canada). From short-axis and long-axis B-mode views, end-systolic and end-diastolic LV volumes and LV ejection fraction (LVEF) were calculated using the area-length method [16]. LV regional function was evaluated in a 13-segment model

(basal, middle and apical segments of the septum, anterior, lateral, postero-inferior walls and the apex) and scored as follows: normal (0), hypo/akinesis (1), dyskinesis/aneurysm (2). A segmental LV wall motion score was defined as the sum of the individual segment scores in each animal.

High field CMR protocol in mice

Myocardial volumes and function were assessed by CMR 12 weeks post-AMI. Mice were anesthetized by inhalation of isoflurane/oxygen (5 %/95 %) and examined with a 7-T field preclinical CMR system (BioSpec 70/20 USR, Bruker BioSpin) with a maximum gradient of 750 mT/m. A volume resonator (72 mm inner diameter) operating in quadrature mode was used for excitation and a four-element phased array surface mouse heart coil (Rapid Biomedical) was used for signal reception. After standard cardiac localizers, cine images were acquired using fast low-angle shot (Intragate-FLASH) sequences in 6–7 short-axis planes to cover the whole LV with a field of view (FOV) of 2.7 × 3 cm, a 1-mm slice thickness without gaps, TE 2.4 ms, TR 8 ms, cardiac phases 10, and matrix of 256 × 256 pixels. Cine images were reconstructed using retrospective ECG-gating performed with IntraGate, which is included in the CMR Paravision Bruker software. ECG and breathing rhythm were monitored with a CMR-compatible system for small animals (Model 1025, S.A. Instruments, Inc., New York, USA).

Isolation of adult mouse cardiomyocytes

The protocol for mouse adult cardiomyocyte isolation was adapted from several studies [36, 44, 50]. Briefly, 10- to 12-week-old C57BL/6J WT or eNOS-KO mice were heparinized (50 USP units) and anesthetized with a mixture of ketamine (140 mg/kg), xylazine (33 mg/kg), and atropine (9 mg/kg). Once pedal pinch reflexes were completely inhibited, animals were placed in a supine position, ventral thoracic regions were wiped with 70 % alcohol, and animals were euthanized. The heart was quickly removed, cannulated through the ascending aorta, and mounted on a modified Langendorff perfusion apparatus. The heart was then retrogradely perfused (3 mL/min) for 5 min at room temperature (RT) with pre-filtered Ca^{2+}-free Perfusion-Buffer [NaCl (113 mmol/L); KCl (4.7 mmol/L); KH_2PO_4 (0.6 mmol/L); Na_2HPO_4 (0.6 mmol/L); $MgSO_4{\cdot}7H_2O$ (1.2 mmol/L); $NaHCO_3$ (12 mmol/L); $KHCO_3$ (10 mmol/L); Phenol Red (0.032 mmol/L); HEPES-Na salt (0.922 mmol/L); taurine (30 mmol/L); glucose (5.5 mmol/L); 2,3-butanedione-monoxime (10 mmol/L), pH 7.4]. Enzymatic digestion was performed with digestion-buffer [perfusion-buffer with Liberase™ (0.2 mg/mL), Trypsin 2.5 % (5.5 mmol/L); DNase (5×10^{-3} U/mL) and $CaCl_2$ (12.5 μmol/L)] for 20 min at 37 °C. At the end of enzymatic digestion, both ventricles were isolated and gently disaggregated in 5 mL of Digestion Buffer. The resulting cell suspension was filtered through a 100-μm sterile mesh (SEFAR-Nitex) and transferred for enzymatic inactivation to a tube with 10 mL of stopping-buffer-1 [perfusion-buffer supplemented with fetal bovine serum (FBS, 10 % v/v) and $CaCl_2$ (12.5 μmol/L)]. After gravity sedimentation for 20 min, cardiomyocytes were resuspended in stopping-buffer-2 containing lower FBS (5 % v/v) for another 20 min. Cardiomyocyte Ca^{2+}-reintroduction was performed in stopping-buffer-2 with five progressively increased $CaCl_2$ concentrations (62 μmol/L, 112 μmol/L, 212 μmol/L, 500 μmol/L and 1 mmol/L). Cells were resuspended and allowed to decant for 10 min in each step, contributing to the purification of the cardiomyocyte suspension. The homogeneous suspension of rod-shaped cardiomyocytes was then resuspended in M199 supplemented with Earle's salts and L-glutamine, penicillin–streptomycin (1 %), insulin–transferin–selenium-A (0.1×), bovine serum albumin (BSA, 2 g/L), blebbistatin (25 μmol/L) and FBS (5 %). Cells were plated in single drops onto 22-mm^2 glass coverslips precoated with 200 μL of mouse laminin (10 mg/mL) in phosphate-buffered saline (PBS) for 1 h.

Hypoxia/reoxygenation in adult mouse cardiomyocytes

Prior to being subjected to induced hypoxia/reoxygenation, plated isolated adult mouse cardiomyocytes were washed and stabilized for 30 min at 37 °C with normoxic-buffer (NB) [NaCl (113 mmol/L); KCl (4.7 mmol/L); KH_2PO_4 (0.6 mmol/L); Na_2HPO_4 (0.6 mmol/L); $MgSO_4{\cdot}7H_2O$ (1.2 mmol/L); $NaHCO_3$ (12 mmol/L); $KHCO_3$ (10 mmol/L); HEPES-Na Salt (0.922 mmol/L); Glucose (10 mmol/L); $CaCl_2$ (1 mmol/L) and pH 7.4]. Hoechst 33342 (H42, 1 μg/mL) was added for cell recognition, and propidium iodide (PI, 1 μg/mL) was added to evaluate cell viability. Simulated ischemia was induced at 1 % O_2 by placing cells in a H35 Hypoxystation chamber (Don Whitley Scientific Limited, UK) in ischemic-buffer (IB), in which glucose and HEPES were replaced with lactate-Na (10 mmol/L) and PIPES (10 mmol/L), at pH 6.8 for 30 min (IB was pre-equilibrated at 1 % O_2 for 2 h prior to use). After the hypoxia incubation, IB was replaced with NB for 1 h to simulate reperfusion. Duplicate wells were randomized to receive (1) control: NaCl (0.9 %), (2) insulin as positive control (2 nmol/L), (3) BRL37344 (7 μmol/L), or (4) NG-nitro-L-arginine methyl ester (L-NAME (10 μmol/L). Fluorescent images were acquired with a Nikon Time-lapse confocal microscope after 15, 30, 45 and 60 min of reoxygenation. An average of 350 rod-shaped cells/well from 6 independent experiments was analyzed by a blinded

observer using ImageJ 6.0 (NIH, Bethesda, MD, USA). Cell death, indicated by internalization of red fluorescence (Red, PI positive) was expressed as a percentage of the total number of cardiomyocytes at each point (Blue, H42 positive) and normalized to saline treatment.

Western blot

For protein isolation, cardiomyocytes were maintained in suspension in 1 mL of IB for 30 min at 1 % O_2 in a H35 Hypoxystation chamber (Don Whitley Scientific Limited, UK) followed by 15 min of simulated reoxygention in NB in the CO_2 incubator. Cardiomyocytes were spun down and proteins isolated in RIPA lysis buffer (150 mmol/L NaCl, 1.0 % IGEPAL, 0.5 % sodium deoxycholate, 0.1 % SDS, 50 mmol/L Tris, pH 8.0) supplemented with protease/phosphatase inhibitors. After quantification (Pierce BCA Protein Assay Kit) 30 μg of protein was loaded on 10 and 7 % SDS polyacrylamide gels. After electrophoresis, proteins were transferred to a polyvinylidene fluoride (PVDF) membrane. Primary antibodies specific for total Akt and phospho-Akt (Ser473) (Cell Signaling Technology, USA) were incubated with the PVDF membranes overnight in Tris Buffered Saline containing 0.1 % Tween and 5 % bovine serum albumin. After HRP-secondary antibody incubation blots were developed by chemiluminescence using Luminata Forte substrate (Millipore, USA). Densitometry of bands was analyzed with ImageJ 6.0 (NIH, Bethesda, MD, USA). The ratio between the phospho-specific and total protein densitometry signals was calculated.

Induction and detection of mPTP opening

To determine the effect of beta-3-adrenoceptor stimulation on the susceptibility to mPTP opening, we used a well-characterized model that simulates the deleterious effect of mitochondrial reactive oxygen species (ROS) production upon reperfusion [6, 15, 17]. Maintained confocal laser-stimulation of the fluorescent mitotraker tetramethyl-rhodamine methyl ester (TMRM) produces ROS within the mitochondria, which results in mPTP opening as indicated by mitochondrial membrane depolarization [51]. Susceptibility to mPTP opening was defined as the time taken to induce mitochondrial membrane depolarization, visualized as dequenching of TMRM fluorescence upon its translocation to the cytoplasm. Isolated adult cardiomyocytes, freshly plated on laminin-precoated (10 mg/mL) coverslips, were loaded with TMRM (3 μmol/L) in Hank's buffered saline solution (1.2 mmol/L $CaCl_2$, 15 min at 37 °C). Before induction and detection of mPTP opening, cardiomyocytes were randomly assigned to the following treatment groups and loaded for 10 min with (1) vehicle control: DMSO (0.02 %) + NaCl (0.9 %); (2) CsA positive control (0.4 μmol/L); (3) BRL37344 (7 μmol/L); (4) Both treatments in combination (CsA + BRL37344). An average of 200 rod-shaped cells was analyzed per group in 9 different experiments. Cells were monitored with a Leica confocal microscope (SP5), and images were acquired at 2.63-s intervals with simultaneous excitation at 543 nm. The gain was adjusted to achieve maximum signal intensity without saturation. All time values were normalized against the mean time for cardiomyocytes maintained in vehicle.

Pig model of AMI

A re-perfused anterior wall AMI was experimentally induced in 3-month-old castrated male Large-white pigs bred at the CNIC's farm. The protocol for AMI induction is detailed elsewhere [33, 35]. In brief, anesthesia was induced by intramuscular injection of ketamine (15 mg/kg), xylazine (2 mg/kg), and midazolam (0.5 mg/kg). buprenorphine (0.03 mg/kg) was used as an analgesic during the intervention. All animals were intubated and mechanically ventilated with oxygen (fraction of inspired O_2, 28 %) and anesthesia was maintained by intravenous administration of midazolam (0.2 mg/kg/h). A continuous infusion of amiodarone (300 mg, 150 mg/h) was maintained during the procedure in all pigs as prophylaxis for malignant ventricular arrhythmias. The LAD immediately distal to the origin of the first diagonal branch was occluded for 60 min with an angioplasty balloon inserted via the percutaneous femoral route. Animals were allocated 1:1 by a restricted randomization (Efron's biased coin randomization) to receive the β3AR agonist (BRL37344, 5 μg/kg) or vehicle via marginal vein of the ear 5 min before reperfusion. The treatment (BRL37344 or vehicle) was prepared in non-labeled syringes before the AMI induction and administered by operators blinded to the randomization. After balloon deflation, a coronary angiogram was obtained to confirm appropriate coronary reperfusion. Animals were recovered thereafter and cared by dedicated veterinarians and technicians at the CNIC Comparative Medicine Unit.

CMR protocol in pigs

Cardiac magnetic resonance studies were performed 7 and 45 days after AMI to assess infarct size and LV performance. Pigs were anesthetized by intramuscular injection of ketamine, xylacine and midazolam as described above, and anesthesia was maintained by continuous intravenous infusion of midazolam. All studies were performed using a Philips 3-T Achieva Tx whole body scanner (Philips Medical Systems, Best, The Netherlands) equipped with a 32-element cardiac phased-array surface coil. Images were acquired with the use of ECG gating by operators blinded

to the study arm. Segmented cine steady-state free precession (SSFP) was performed to acquire 11–13 contiguous short-axis slices covering the heart from the base to the apex to evaluate global and regional LV motion (FOV of 280 × 280 mm; slice thickness of 8 mm without gap; TR 2.8 ms; TE 1.4 ms, flip angle 45; cardiac phases 25; voxel size 1.8 × 1.8 mm; 3 NEX). Edema imaging (for AAR quantification) was performed with a T2-weighted, triple inversion-recovery fast spin-echo (T2W-STIR) sequence (FOV of 280 × 280; 11–13 short-axis slices with thickness of 8 mm and no gap; TR 2–3 heartbeats; TE 80 ms; voxel size 1.4 × 1.4 mm; STIR delay 210 ms; trigger delay longest; echo-train length 16; 2 NEX). A coil sensitivity correction algorithm for all T2W images was implemented in the scan acquisition. Finally, late gadolinium enhancement imaging was performed 15 min after the administration of 0.2 mmol/kg gadopentate dimeglumine using an inversion-recovery fast gradient-echo sequence to

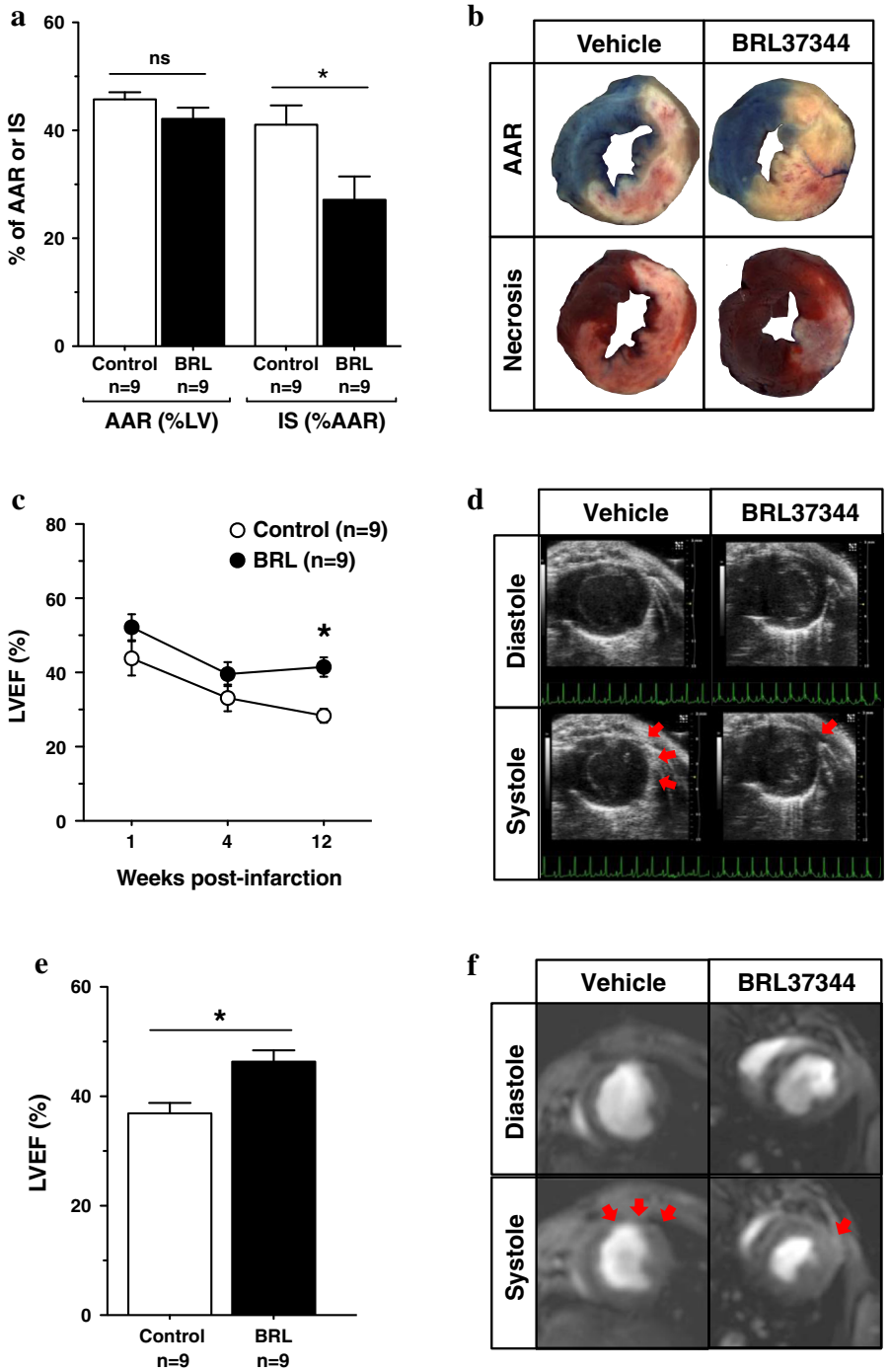

Fig. 1 Long-term cardioprotective effect in mice subjected to ischemia/reperfusion after pre-reperfusion administration of the β3AR agonist BRL37344. **a** AAR (%LV) and IS (%AAR) in C57BL/6J WT mice subjected to myocardial IRI and treated with the β3AR agonist BRL37344 (BRL, 5 μg/kg) or vehicle before reperfusion. **b** Representative histological images of 1-mm-thick transverse ventricular slices of mice treated with BRL37344 or vehicle. *Upper images* show the AAR (negative for Evans Blue staining). *Lower images* show the extent of necrosis (*paler area*) in the same sections after incubation in TTC. **c** LVEF evaluated by serial echocardiography at 1, 4 and 12 weeks post-infarction in mice treated with BRL37344 or vehicle before reperfusion. **d** Representative short-axis echocardiography images at mid-ventricular level, illustrating left-ventricular contractility defects (*red arrows*). **e** LVEF evaluated by serial CMR at 12 weeks post-infarction in mice treated with BRL37344 or vehicle before reperfusion. **f** Representative short-axis CMR images at mid-ventricular level, illustrating LV contractility defects (*red arrows*). LV motion videos obtained by echocardiography and CMR are available in Supplemental material online. Data are presented as mean ± SEM. $*p < 0.05$

determine MI size (FOV of 280 × 280 mm; 11–13 short-axis slices with a thickness of 8 mm and no gap; TR 5.6 ms; TE 2.8 ms; voxel size 1.6 × 1.6 mm; time interval optimized to null normal myocardium; trigger delay longest; bandwidth, 304 Hz per pixel; 2 NEX).

CMR data analysis

All CMR images were analyzed using dedicated software (QMass MR v.7.6, Medis, Leiden, The Netherlands). Images were analyzed by two experienced observers with vast experience in CMR analysis and blinded to the study allocation. The analysis protocol has been detailed elsewhere [34]. In brief, LV cardiac borders were traced in each cine image to obtain LV end-diastolic volume (LVEDV), end-systolic volume (LVESV) and LVEF. LV volumes normalized to the body surface area were calculated with Brody's formula [37]. The left ventricle was divided into 16 segments based on the American Heart Association (AHA) segmented model. Fractional wall systolic thickening was quantified from endocardial and epicardial tracings using a centerline analysis and expressed as the mean of the segmental thickenings. A wall systolic thickening index was calculated in each animal as the number of segments of LV with fractional wall systolic thickening higher than 30 % [40]. The area of myocardium AAR was defined as the extent of the LV demonstrating high signal intensity on T2W-STIR images [1]. Infarct size (necrosis) was quantified from the extent of abnormal delayed gadolinium enhancement. AAR and necrosis were identified as hyperintense regions, defined as >50 % of the peak myocardial signal intensity (full width half maximum) with manual adjustment when needed. If present, a central hypointense core within the area of increased signal was included in the T2W-STIR or late gadolinium enhancement analysis. As described above, infarct size was expressed as a percentage of the AAR. In addition, three short-axis slices (basal, mid-cavity and apical) from the SSFP sequence of each animal were selected for deformation analysis using CMR-based feature tracking [45]. Circumferential strain was assessed with ad hoc software (2D Cardiac Performance Analysis MR, TomTec Imaging System, Germany). Endocardial borders were manually drawn in all analyzed slices and then the automatic computation was triggered. Finally, the global circumferential strain (GCS) in each animal was calculated as the median of all segmental circumferential strains.

All animal studies conducted at the CNIC were approved by the local ethics committee, and all animal procedures conformed to EU Directive 2010/63EU and Recommendation 2007/526/EC regarding the protection of animals used for experimental and other scientific purposes, enforced in Spanish law under Real Decreto 1201/2005. Procedures carried out at the Hatter Cardiovascular Institute (UCL) were conducted in accordance with the UK National Institute of Health Guidelines for the Care and Use of Laboratory Animals. Authors had full access to and take full responsibility for the integrity of the data. All authors have read and agree to the manuscript as written.

Drugs

Reagents were purchased from Sigma-Aldrich Co. LLC., Thermo Fisher Scientific Inc., and Tocris Bioscience.

Statistical analysis

The distribution of continuous variables was analyzed with graphical methods. For normally distributed variables, results are expressed as mean (SD) and compared either by

Table 1 Echocardiography-derived parameters from the mouse model of myocardial IRI

Follow-up post-I/R	Vehicle ($n = 9$)	BRL37344 ($n = 11$)	p value
1-week echo			
HR (bpm)	457 (58)	456 (54)	0.956
LVEDV (μL)	53.3 (13.2)	51.5 (15.7)	0.787
LVESV (μL)	30.9 (14.6)	24.9 (11.3)	0.312
LVEF (%)	44.2 (13.8)	52.7 (11.3)	0.148
SV (μL)	22.4 (6.3)	26.6 (8.8)	0.244
CO (mL/min)	10.2 (2.8)	12.0 (4.0)	0.264
SWMS	2.0 [2.5]	2.0 [2.0]	0.583
4-week echo			
HR (bpm)	506 (55)	474 (46)	0.171
LVEDV (μL)	66.9 (19.4)	54.7 (9.4)	0.111
LVESV (μL)	45.9 (18.4)	33.4 (8.8)	0.090
LVEF (%)	33.0 (10.7)	39.6 (10.7)	0.188
SV (μL)	21.0 (5.4)	21.2 (4.8)	0.920
CO (mL/min)	10.5 (2.3)	10.1 (2.4)	0.686
SWMS	3.0 [2.0]	2.0 [2.0]	0.073
12-week echo			
HR (bpm)	487 (40)	505 (52)	0.417
LVEDV (μL)	75.4 (22.4)	61.2 (12.4)	0.089
LVESV (μL)	54.4 (18.5)	35.9 (10.7)	**0.012**
LVEF (%)	28.4 (5.7)	41.7 (8.5)	**0.001**
SV (μL)	20.9 (5.1)	25.3 (6.2)	0.108
CO (mL/min)	10.2 (2.6)	12.7 (3.4)	0.080
SWMS	3.0 [0.5]	1.0 [1.0]	**0.005**

Bold values indicate statistical significance according to the pre-specified threshold of significance ($p < 0.05$). For a more detailed information, the actual p values are provided

Values are expressed as mean (SD) or median [IQR] as appropriate

CO cardiac output, *HR* heart rate, *I/R* ischemia/reperfusion, *LVEDV* LV end-diastolic volume, *LVEF* LV ejection fraction, *LVESV* LV end-systolic volume, *SV* stroke volume, *SWMS* segmental LV wall motion score

Student's unpaired *t* test (with Welch's correction when appropriate) or one-way ANOVA. When repeated measurements were performed, two-way repeated-measures ANOVA were applied followed by Bonferroni correction for post hoc analysis. Non-normal data are reported as median (IQR) and compared by Mann–Whitney *U* test. Differences were considered statistically significant at p value <0.05 (two-tailed).

Results

Pre-reperfusion administration with β3AR agonist reduces infarct size and improves long-term cardiac function in mice

Administration of the β3AR agonist BRL37344 before reperfusion induced a significant reduction in infarct size

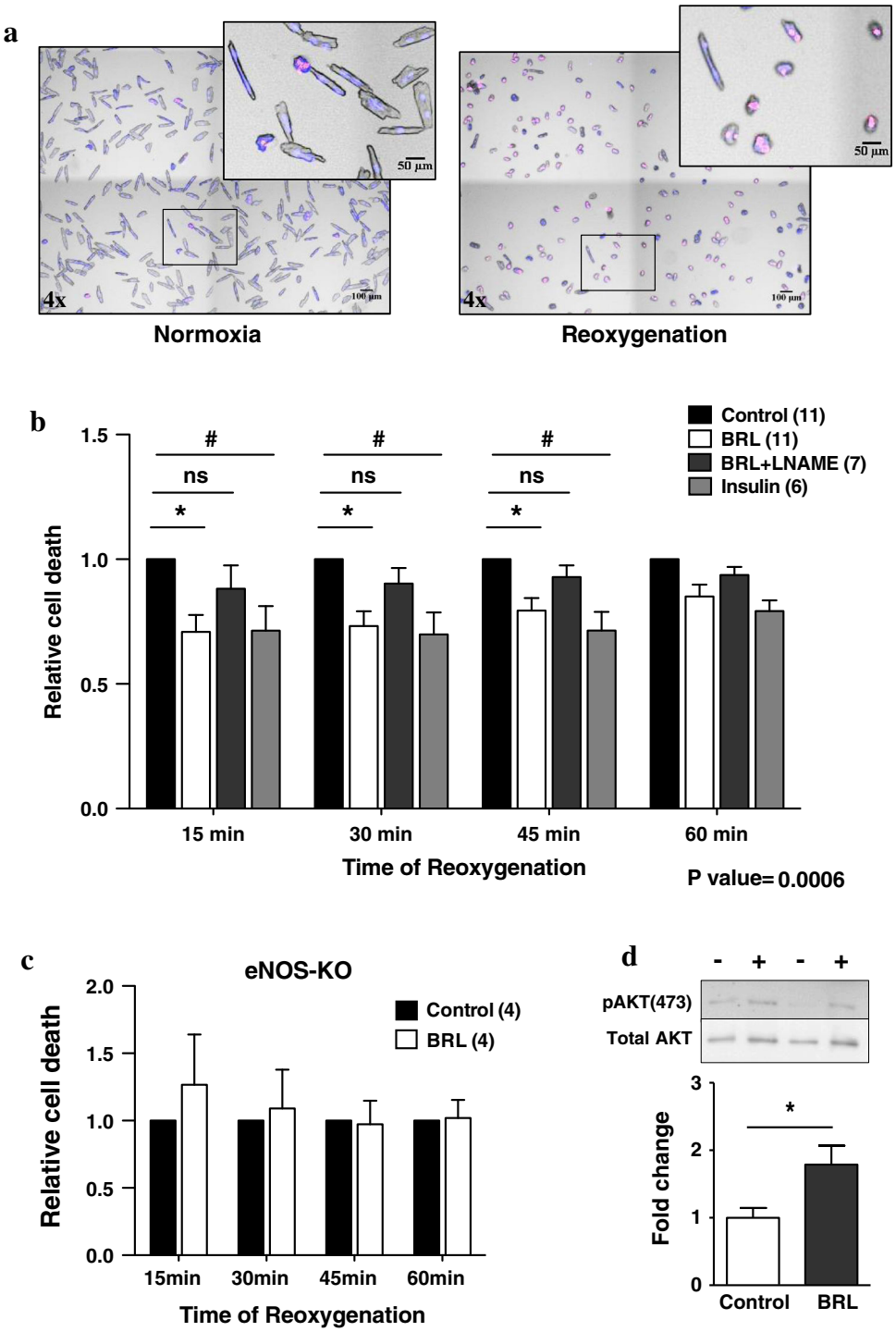

Fig. 2 β_3 adrenergic receptor stimulation protects isolated cardiomyocytes against hypoxia/reoxygenation through NO-dependent signaling. Isolated adult mouse cardiomyocytes were subjected to 30-min hypoxia followed by reoxygenation in the presence of vehicle (0.9 % NaCl), BRL37344 (BRL, 7 µM), L-NAME (10 µM) or insulin (2 nM; positive control). **a** Representative fluorescent microscopical images of isolated cardiomyocytes before H/R during (1) normoxia: showing PI-negative rod-shaped fresh cardiomyocytes and (2) reoxygenation: showing a high % of PI-positive hypercontracted rounded cells. **b** BRL37344 (BRL) treatment significantly reduces cell death while co-incubation with L-NAME abrogates the protective effect, detected as the % of PI-positive cells. Data are mean ± SEM of % PI scores in images taken at 15 min intervals up to 1 h. Groups were compared by two-way repeated measures ANOVA with the Bonferroni correction for post hoc analysis. **c** Percentage of cell death in adult cardiomyocytes isolated from eNOS-KO mice and subjected to H/R with or without pretreatment with BRL37344. The protective effect of BRL37344 is abrogated in the absence of eNOS. **d** Phospho-serine 473 AKT [pAKT(473)] levels detected after 15 min of reoxygenation in untreated and BRL37344-treated WT cardiomyocytes. Data are presented as mean ± SEM. $^*p < 0.05$

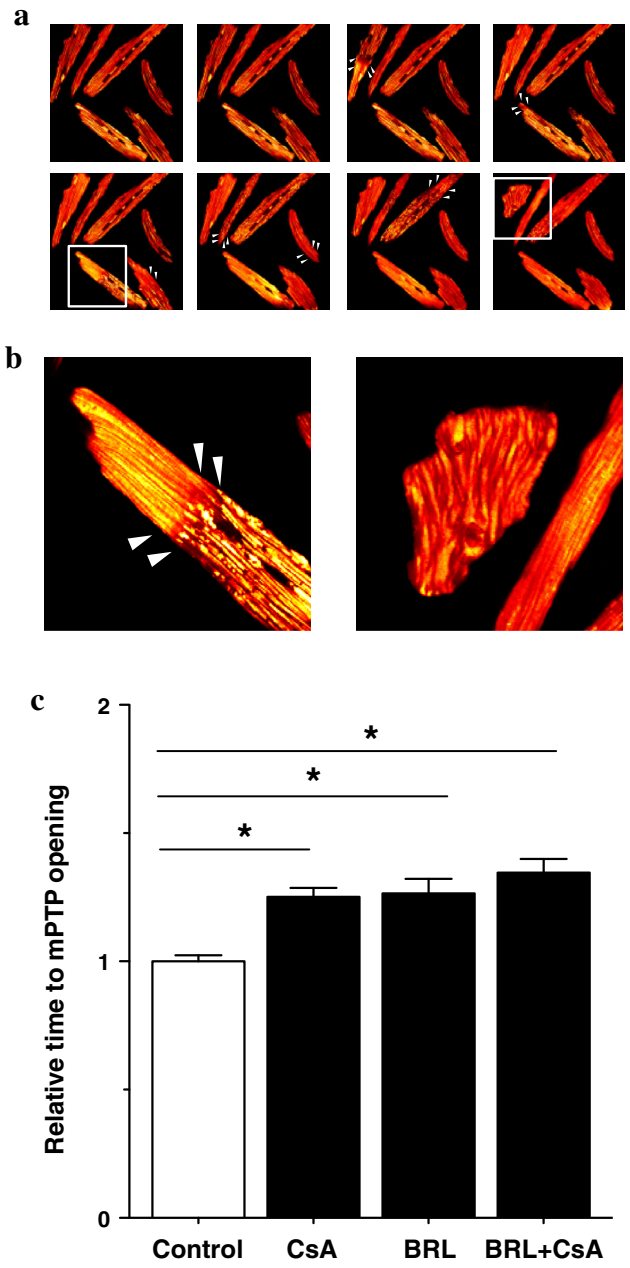

◀**Fig. 3** β_3 adrenergic receptor stimulation delays mPTP opening in TMRM-preloaded adult cardiomyocytes subjected to laser-mediated oxidative stress. **a** Time-lapse confocal images showing progressive loss of mitochondrial membrane potential after induction of oxidative stress by sustained confocal laser scanning. *Arrows* indicate sites of incipient mPTP opening and consequent dequenching of the dye in the cytoplasm. **b** Detailed view of mitochondrial membrane depolarization: mPTP opening triggers rapid TMRM release from mitochondria, resulting in locally increased fluorescence intensity due to dye dequenching. mPTP opening proceeds in a wave across the cell in a polarized manner and of the phenomenon of cardiomyocyte hypercontractility, caused by mitochondrial membrane depolarization after sustained exposure to oxidative stress. **c** Normalized mean values of the time to mPTP opening in cardiomyocytes after addition of vehicle (DMSO, 0.02 %), cyclosporine-A (positive control; CsA, 0.4 μM), BRL37344 (BRL, 7 μM) and BRL + CsA. *n* independent experiments, with 150–200 cells analyzed per treatment. Data are presented as mean ± SEM. $*p < 0.05$

(27.1 (13.0) % of area at risk (AAR) in β3AR-treated mice vs. 41.1 (10.7) % with vehicle; $p = 0.025$) (Fig. 1a). AAR was similar in both groups. Consistent with the reduced infarct size, pre-reperfusion BRL37344 led to a long-term improvement in LV contractile function, as assessed by echocardiography at sequential follow-up evaluations (Fig. 1c; Table 1). Similarly, CMR evaluation revealed that LV ejection fraction (LVEF) was significantly higher in BRL37344-treated mice than controls after 12 weeks (46.5 (6.3) vs. 37.7 (6.0) %; $p = 0.004$; Fig 1e; Table 1). The cardioprotection afforded by BRL37344 administration was absent in β3AR-KO mice: (31.5 (9.5) % of AAR vs. 24.1 (6.7) %; $p = 0.112$; Supplemental Fig 1). Echocardiographic and CMR videos are available in the supplemental material online.

Selective β3AR stimulation with BRL37344 increases survival of isolated adult cardiomyocytes undergoing hypoxia/reoxygenation (H/R)

Isolated adult cardiomyocytes from WT mice were subjected to simulated ischemia/reperfusion in the presence of BRL37344 or saline. Analysis of PI exclusion showed significant reduction of cell death in the presence of BRL37344. Co-incubation with the NOS inhibitor L-NAME abrogated the cardioprotection shown by BRL37344 (Fig. 2a). When we repeated the procedure in eNOS-KO cardiomyocytes no differences were found between BRL37344-treated and non-treated cells. These results confirm the key role of NO in the protection exerted by β3AR-selective stimulation (Fig. 2c). Due to the importance of Akt in cardioprotection [27], we assessed the activation of AKT by western blot. Densitometric analysis showed a significant increase of Akt phosphorylation at serine 473 in BRL37344-treated cells (Fig. 2d).

The cardioprotective effect of β3AR-selective stimulation involves mPTP

To determine whether selective β3AR stimulation has a direct pharmacological effect on mPTP, TMRM-preloaded adult cardiomyocytes were incubated with BRL37344, saline, or CsA, alone or in combination, and subjected to oxidative-stress-induced mPTP opening. BRL37344 treatment delayed the time to mPTP opening by 1.26 (0.67)-fold compared with vehicle values ($p < 0.001$; Fig. 3c). Interestingly, combined treatment with BRL37344 and

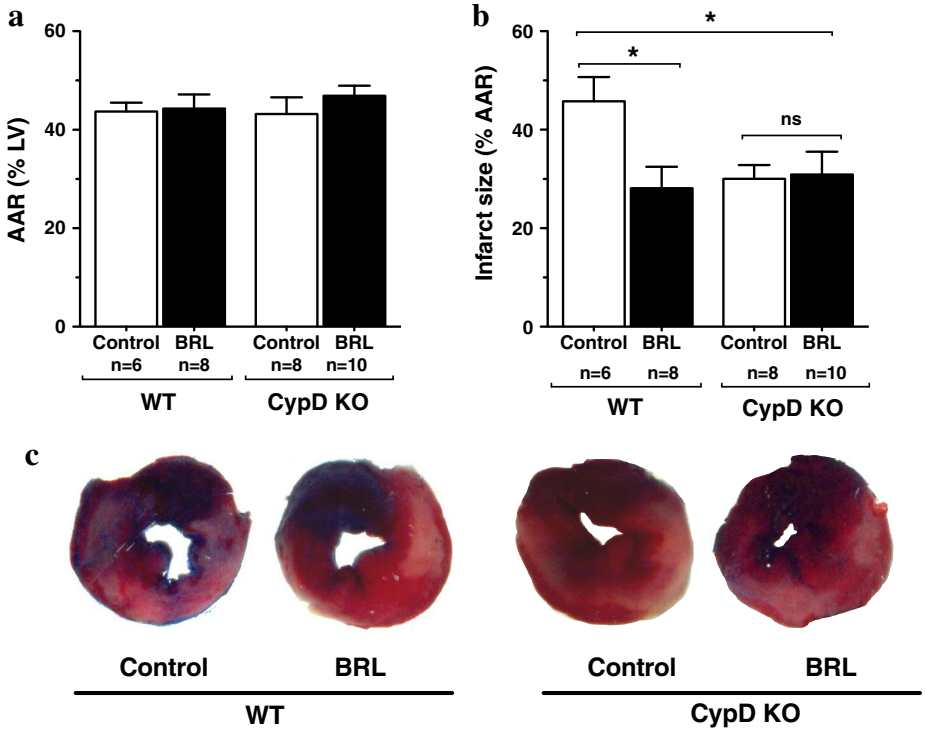

Fig. 4 Pre-reperfusion administration of BRL37344 does not provide an additional cardioprotective effect in CypD KO mice. **a** AAR (%LV) in WT and CypD KO mice treated with vehicle or BRL37344 (BRL, 5 μg/kg) (p = ns). **b** Infarct size (% of AAR) at 2 h reperfusion. Data presented as mean ± SEM. **c** Representative histological images of heart slices after staining to delineate the AAR (negative for Evans Blue) and infarcted area (*paler* region on TTC staining) for all groups. *$p < 0.05$

CsA did not further delay mPTP opening compared with each treatment independently.

To confirm the implication of mPTP in β3AR-mediated cardioprotection in vivo, we tested the effect of pre-reperfusion BRL37344 on early IRI in WT and CypD KO mice. In WT mice, β3AR stimulation significantly reduced infarct size at 2 h reperfusion (28.1 (12.3) % of AAR vs. 45.8 (12.1) % in vehicle-treated mice; $p = 0.020$; Fig. 4b). Consistent with the in vitro cardiomyocyte experiments, β3AR stimulation did not reduce infarct size in animals lacking mitochondrial CypD (30.9 (14.7) % vs. 30.0 (7.9) % of AAR in BRL37344- and vehicle-treated CypD KO mice, respectively; $p = 0.884$; Fig. 4b).

Pre-reperfusion β3AR agonist administration reduces infarct size and improves long-term cardiac function in a swine model of myocardial I/R

Acute myocardial infarction was induced in Large-white pigs (40.1 (6.2) kg) by percutaneous angioplasty (60 min balloon-mediated LAD coronary occlusion) followed by reperfusion. No pigs died during AMI induction, but seven died within the first week after infarction and, therefore, did not undergo day-7 CMR (3 allocated to BRL37344 and 4 to vehicle). Two pigs (one per treatment group) died suddenly before completing the day 45 CMR. Final numbers of animals are noted in the figures.

Pre-reperfusion administration of BRL37344 provoked a transient increase in heart rate compared with vehicle (10.0 (9.5) vs. −1.2 (2.3) change from baseline bpm; $p = 0.013$); heart rate returned to baseline after 10 min. Conversely, pre-reperfusion BRL37344 had no significant effect on mean blood pressure (−0.13 (7.4) vs. −0.83 (2.8) mmHg; $p = 0.78$). Full data in Supplemental Table 1.

On day 7 CMR, infarct size was significantly smaller in the β3AR-agonist-treated group (80.0 (21.4) % of AAR, vs. 93.5 (16.8) % in vehicle-treated pigs; $p = 0.044$; Fig. 5a). Consistent with this, BRL37344-treated pigs had improved LV contractile performance on day 45 CMR: pigs receiving BRL37344 showed a better regional myocardial contractile function than pigs treated with vehicle, as evidenced by higher fractional systolic thickening (45.4 (5.8) % vs. 36.4 (9.0) %; $p = 0.032$; Table 2) and systolic thickening index (11.0 (1.0) vs. 9.0 (2.0) segments; $p = 0.026$; Fig. 5c). BRL37344-treated pigs also showed a trend on day 45 CMR toward a higher LVEF (41.4 (6.3) % vs. 37.0 (4.6) %; $p = 0.119$; Fig. 5b). Finally, myocardial deformation analyses showed that pigs receiving the β3AR agonist had a better global circumferential strain (−20.1 (1.7) vs. −17.0 (2.8) %; $p = 0.018$; Fig. 5e). Full CMR is presented in Table 2.

Discussion

This study presents the first evidence for long-term benefits from pre-reperfusion IV administration of a β3AR-selective agonist in AMI. In a mouse model, these

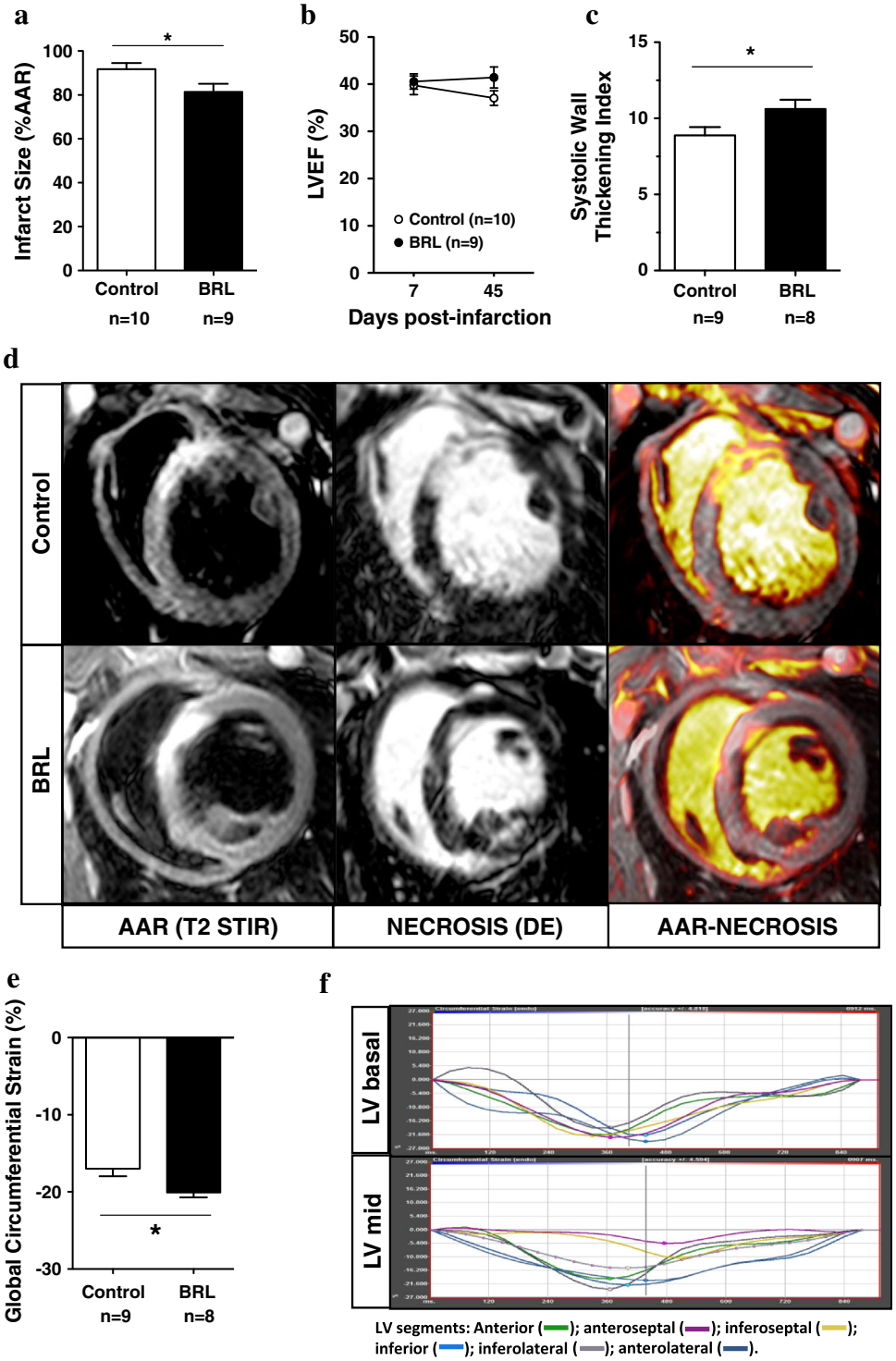

Fig. 5 Pre-reperfusion treatment of the β3AR agonist BRL37344 reduces infarct size and exerts a long-term beneficial effect in a pig model of AMI. **a** Infarct size (%AAR) assessed by CMR at 7 days post-infarction in large-white pigs. BRL stands for BRL37344 (5 μg/kg). **b** Evolution of LVEF in vehicle- and BRL37344-treated pigs, assessed by CMR at 7 and 45 days post-infarction; LVEF tends to improve in BRL37344-treated pigs while it tends to worsen in vehicle-treated pigs. **c** LV systolic wall thickening index assessed by CMR at long-term follow-up. **d** Representative short-axis CMR images at the same level of the LV, showing the extent of area at risk (AAR: hyper-intense area in T2-weighted CMR sequence), myocardial necrosis [delayed enhancement (DE) after gadolinium injection], and the merged view of both in one animal receiving pre-reperfusion BRL37344 and in another receiving vehicle. **e** Global circumferential strain assessed by CMR-based feature tracking. **f** Representative segmental circumferential strain images evaluated by CMR-based feature tracking in a pig receiving pre-reperfusion β3AR agonist treatment. Data are presented as mean ± SEM. $^{*}p < 0.05$

beneficial effects are evident both at very early (2 h reperfusion) and late (24 h reperfusion) stages of IRI and in isolated cardiomyocytes. Analysis with CMR shows that β3AR agonism with BRL37344 limits infarct size and improves cardiac function several weeks post AMI in mice and pigs. This cardioprotective effect is mediated by a delay in mPTP opening dependent on the Akt-NO signaling pathway. To our knowledge, this is the first demonstration of reduced IRI and associated long-term functional benefits after a single i.v. administration of a β3AR agonist in a clinically relevant large animal model of AMI.

Table 2 CMR-derived parameters from the large animal (pig) model of AMI

	Vehicle	BRL37344	*p* value
7-day CMR	$n = 10$	$n = 9$	
LVEDV (mL/m^2)	129.1 (18.2)	120.9 (18.4)	0.344
LVESV (mL/m^2)	78.0 (15.3)	72.4 (15.6)	0.440
LVEF (%)	39.8 (6.3)	40.6 (4.8)	0.766
AAR (% LV)	28.2 (5.2)	29.0 (4.2)	0.718
Infarct size (% AAR)	93.5 [16.8]	80.0 [21.4]	0.044
45-day CMR	$n = 9$	$n = 8$	
LVEDV (mL/m^2)	147.6 (26.6)	139.3 (20.4)	0.487
LVESV (mL/m^2)	93.3 (19.8)	82.3 (19.3)	0.269
LVEF (%)	37.0 (4.6)	41.4 (6.3)	0.119
SWT (%)	36.4 (9.0)	45.4 (5.8)	0.032
SWT index	9.0 [2.0]	11.0 [1.0]	0.026
GCS (%)	−17.0 (2.8)	−20.1 (1.7)	0.018

Values are expressed as mean (SD) or median [IQR] as appropriate

AAR area at risk, *GCS* global circumferential strain, *LVEDV* LV end-diastolic volume, *LVESV* LV end-systolic volume, *SWT* systolic wall thickening

β3AR agonist administration before reperfusion reduces infarct size, resulting in a long-term beneficial effect

β3AR-selective stimulation has recently been proposed as a new therapy for several myocardial diseases [3, 12, 39]. Aragon et al. [3] recently demonstrated a reduction in infarct size (evaluated 24 h after IRI) when a β3AR agonist was administered before reperfusion but reported no improvement in cardiac function after β3AR agonist treatment in mice assessed by echocardiography at short-term follow-up (1 week), raising doubts about whether evidence of cardioprotection from histological evaluation translates to functional benefits. Our present data confirm the beneficial pre-reperfusion β3AR agonist administration effect when evaluated at early stages (2 h reperfusion), suggesting that the cardioprotection afforded by this therapy takes place within the first minutes of reperfusion. Similar to Aragon's results, our data show that LV function 1 week after AMI did not differ significantly between β3AR-agonist- and vehicle-treated animals. However, the longer follow-up period in our study allowed us to demonstrate a clear association of the infarct-limiting effects of pre-reperfusion β3AR-agonist treatment with improved cardiac function shown by both echocardiography and CMR. The most likely reason for the late appearance of improved cardiac function is that at early stages the salvaged myocardium is in a stunned, non-contractile, state and that full contractile recovery is, therefore, seen only after longer follow-up. This interpretation is supported by the gradual recovery of segmental LV wall motion scores after 1-week follow-up in β3AR-agonist-treated mice (Table 1). These results thus highlight the importance of long-term follow-up for evaluation of the functional benefits of a cardioprotective intervention.

It is noteworthy that infarcts in β3AR KO mice appear to be smaller than those in wild-type mice. A similar effect is apparent in previous works by other groups [3]. In this regard, it should be noted that the β3AR KO mice used here were in the FVB/N genetic background, which has been reported to confer innate cardioprotection against IRI [25]. Another potential explanation for this effect could be that the absence of β3AR results in a redistribution of the other two types of βAR. If βAR redistribution would result in an upregulation of β2AR, this might explain the spontaneous protection of these mice, since signaling via β2AR during IRI has been shown to reduce infarct size [7], and its upregulation by gene therapy results in an incremental protective cardiac phenotype [43]. However, this alternative protective scenario in β3AR KO mice is speculative since the actual redistribution of β1AR and β2AR in the absence of β3AR has not been studied in the heart.

Cardiomyocyte β3AR-Akt-eNOS-NO-mPTP signaling pathway is implicated in the cardioprotection afforded by β3AR-selective stimulation

Previous studies into the protective effect of β3AR-selective stimulation in cardiac diseases [3, 14, 39] did not address whether the mechanism involves an action in cardiomyocytes [28]. In our analysis, β3AR-selective stimulation significantly increased the viability of isolated adult cardiomyocytes in response to hypoxia/reoxygenation, indicating that the cardioprotection associated with β3AR-agonist stimulation occurs in the early phases of IRI through an effect at the cardiomyocyte level. We further demonstrate that serine 473 phosphorylation of Akt and NO-dependent signaling are both critical mediators of this protection.

Moreover, BRL37344 significantly delays the opening of the mPTP, which plays a central role in cardiomyocyte death upon IRI [4, 18]. Interestingly, the co-incubation of cardiomyocytes with BRL37344 and a known inhibitor of mPTP opening, CsA, did not significantly increase the delay in mPTP opening, suggesting that the two agents act on the same cardioprotective pathway. Finally, we have documented that β3AR stimulation had no additional infarct-limiting effect in CypD-KO mice [4], which have been shown to be protected against IRI [4, 6], again suggesting action on the same pathway. Although CypD KO mice are strongly protected against IRI, further reductions in infarct size in these animals can be obtained with

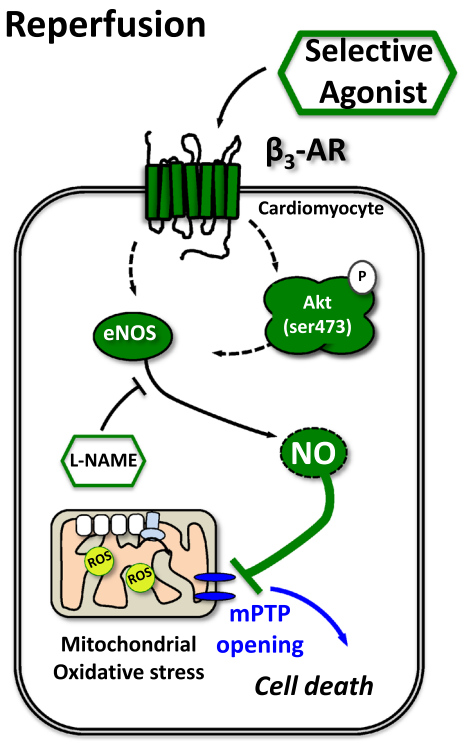

Fig. 6 Schematic mechanism through β3AR stimulation and the increase of cell viability by the inhibition of the opening of the mPTP. Following ischemia, reperfusion triggers accumulation reactive oxygen species (ROS). Excessive accumulation of ROS induces mitochondrial collapse, subsequent opening of the mPTP and the ultimate cell death. Here we report that a β_3 selective agonist BRL37344 (BRL) exerts an Akt-eNOS-NO dependent effect on the cardiomyocytes which is translated into a delay in the opening of the mPTP and thus an increase in cell survival. Inhibition of bioavailability of NO with L-NAME abrogates the effect of BRL. *eNOS* endothelial nitric oxide synthase, *NO* nitric oxide, *Akt-P* Akt phosphorylation at ser473 during reperfusion

protective strategies affecting targets other than the mPTP [6]. Altogether, these data indicate that the protection exerted by β3AR selective stimulation involves the mPTP.

Pre-reperfusion β3AR agonist administration provides cardioprotection in a preclinical large animal model of AMI

A key finding of the present study is that pre-reperfusion β3AR-agonist administration reduces infarct size and improves long-term cardiac function in a more translational large animal (pig) model of AMI. Several novel therapies have demonstrated beneficial effects in preclinical studies but subsequently failed in the clinical arena. This poor translation between preclinical findings and clinical studies is in part due to the absence of randomized studies showing robust beneficial outcomes in large-animal models [46]. The pig model was selected because of its anatomical and physiological similarities to humans. To mimic a potential clinical scenario, we administered BRL37344 before coronary reperfusion and quantified infarct size by CMR, assessing the myocardial AAR to better define the protective effect of the intervention.

Taken together, our results show that a single i.v. administration of a β3AR agonist before reperfusion provides a powerful and highly translational cardioprotective therapy for AMI, and this beneficial effect is translated into long-term improvement in cardiac contractile function. In addition, we show that β3AR selective stimulation during IRI is associated with an increase in Akt phosphorylation and bioavailability of NO and ultimately in inhibition of lethal mitochondrial collapse upon restoration of blood flow (see Fig. 6).

Acknowledgments We thank Dr. S. Mendez-Ferrer (CNIC) for supplying the β3AR knockout mice. We thank Rachel Dongworth, Rupa Parvin Khaton, and Virginia Zorita for the help and technical support. We also thank Ana V. Alonso for her outstanding technical support in mouse echocardiography and Gonzalo J. López and Angel Macías for theirs in swine CMR evaluations. We are grateful to the animal facilities at the CNIC and the UCL and to CNIC's farm for their superb support with the animal care. Antonio M. Santos-Beneit provided advice in microscopy and image analysis. Simon Bartlett provided English editing.

CMR images were analyzed using dedicated software (QMass MR v.7) with support through a scientific collaboration with Medis medical imaging systems BV. Regional CMR analysis was conducted with TomTec 2D CPA MR Quantification Software with full support through scientific collaboration with Tomtec.

This work was supported by an award from the Fondo de Investigación Sanitaria to BI a (FIS 10/02268) and by the competitive grant "CNIC translational 01/2009", also to BI.

D.S-R is supported by a CNIC-Postdoctoral Fellowship; JM.G-R and A.G-A were supported by CNIC-Cardiojoven Fellowships. The "Red de Investigación Cardiovascular (RIC)" of the Spanish Ministry of Health supports B.I (RD 12/0042/0054) and A.G-A. The "Centro Nacional de Investigaciones Cardiovasculares Carlos III (CNIC)" is supported by the Spanish Ministry of Economy and Competitiveness, and the Pro-CNIC Foundation.

Conflict of interest None.

References

1. Aletras AH, Tilak GS, Natanzon A, Hsu LY, Gonzalez FM, Hoyt RF Jr, Arai AE (2006) Retrospective determination of the area at risk for reperfused acute myocardial infarction with t2-weighted cardiac magnetic resonance imaging: histopathological and displacement encoding with stimulated echoes (dense) functional validations. Circulation 113:1865–1870. doi:10.1161/CIRCULATIONAHA.105.576025
2. Alzaga AG, Cerdan M, Varon J (2006) Therapeutic hypothermia. Resuscitation 70:369–380. doi:10.1016/j.resuscitation.2006.01.017
3. Aragon JP, Condit ME, Bhushan S, Predmore BL, Patel SS, Grinsfelder DB, Gundewar S, Jha S, Calvert JW, Barouch LA, Lavu M, Wright HM, Lefer DJ (2011) Beta3-adrenoreceptor stimulation ameliorates myocardial ischemia–reperfusion injury via endothelial nitric oxide synthase and neuronal nitric oxide

synthase activation. J Am Coll Cardiol 58:2683–2691. doi:10.1016/j.jacc.2011.09.033
4. Baines CP, Kaiser RA, Purcell NH, Blair NS, Osinska H, Hambleton MA, Brunskill EW, Sayen MR, Gottlieb RA, Dorn GW, Robbins J, Molkentin JD (2005) Loss of cyclophilin d reveals a critical role for mitochondrial permeability transition in cell death. Nature 434:658–662. doi:10.1038/nature03434
5. Bell R, Beeuwkes R, Botker HE, Davidson S, Downey J, Garcia-Dorado D, Hausenloy DJ, Heusch G, Ibanez B, Kitakaze M, Lecour S, Mentzer R, Miura T, Opie L, Ovize M, Ruiz-Meana M, Schulz R, Shannon R, Walker M, Vinten-Johansen J, Yellon D (2012) Trials, tribulations and speculation! Report from the 7th biennial hatter cardiovascular institute workshop. Basic Res Cardiol 107:300. doi:10.1007/s00395-012-0300-6
6. Bell RM, Kunuthur SP, Hendry C, Bruce-Hickman D, Davidson S, Yellon DM (2013) Matrix metalloproteinase inhibition protects cypd knockout mice independently of risk/mptp signalling: a parallel pathway to protection. Basic Res Cardiol 108:331. doi:10.1007/s00395-013-0331-7
7. Bhushan S, Kondo K, Predmore BL, Zlatopolsky M, King AL, Pearce C, Huang H, Tao YX, Condit ME, Lefer DJ (2012) Selective beta2-adrenoreceptor stimulation attenuates myocardial cell death and preserves cardiac function after ischemia–reperfusion injury. Arterioscler Thromb Vasc Biol 32:1865–1874. doi:10.1161/ATVBAHA.112.251769
8. Boengler K, Hilfiker-Kleiner D, Heusch G, Schulz R (2010) Inhibition of permeability transition pore opening by mitochondrial stat3 and its role in myocardial ischemia/reperfusion. Basic Res Cardiol 105:771–785. doi:10.1007/s00395-010-0124-1
9. Bohl S, Medway DJ, Schulz-Menger J, Schneider JE, Neubauer S, Lygate CA (2009) Refined approach for quantification of in vivo ischemia–reperfusion injury in the mouse heart. Am J Physiol Heart Circ Physiol 297:H2054–2058. doi:10.1152/ajpheart.00836.2009
10. Bolli R, Becker L, Gross G, Mentzer R Jr, Balshaw D, Lathrop DA (2004) Myocardial protection at a crossroads: the need for translation into clinical therapy. Circ Res 95:125–134. doi:10.1161/01.RES.0000137171.97172.d7
11. Botker HE, Kaltoft AK, Pedersen SF, Kim WY (2012) Measuring myocardial salvage. Cardiovasc Res 94:266–275. doi:10.1093/cvr/cvs081
12. Bundgaard H, Liu CC, Garcia A, Hamilton EJ, Huang Y, Chia KK, Hunyor SN, Figtree GA, Rasmussen HH (2010) Beta(3) adrenergic stimulation of the cardiac na+–k+ pump by reversal of an inhibitory oxidative modification. Circulation 122:2699–2708. doi:10.1161/CIRCULATIONAHA.110.964619
13. Burns RJ, Gibbons RJ, Yi Q, Roberts RS, Miller TD, Schaer GL, Anderson JL, Yusuf S (2002) The relationships of left ventricular ejection fraction, end-systolic volume index and infarct size to six-month mortality after hospital discharge following myocardial infarction treated by thrombolysis. J Am Coll Cardiol 39:30–36. doi:10.1016/S0735-1097(01)01711-9
14. Calvert JW, Condit ME, Aragon JP, Nicholson CK, Moody BF, Hood RL, Sindler AL, Gundewar S, Seals DR, Barouch LA, Lefer DJ (2011) Exercise protects against myocardial ischemia–reperfusion injury via stimulation of beta(3)-adrenergic receptors and increased nitric oxide signaling: Role of nitrite and nitrosothiols. Circ Res 108:1448–1458. doi:10.1161/CIRCRESAHA.111.241117
15. Crompton M (1999) The mitochondrial permeability transition pore and its role in cell death. Biochem J 341(Pt 2):233–249. doi:10.1042/0264-6021:3410233
16. Cruz-Adalia A, Jimenez-Borreguero LJ, Ramirez-Huesca M, Chico-Calero I, Barreiro O, Lopez-Conesa E, Fresno M, Sanchez-Madrid F, Martin P (2010) Cd69 limits the severity of cardiomyopathy after autoimmune myocarditis. Circulation 122:1396–1404. doi:10.1161/CIRCULATIONAHA.110.952820
17. Davidson SM, Hausenloy D, Duchen MR, Yellon DM (2006) Signalling via the reperfusion injury signalling kinase (risk) pathway links closure of the mitochondrial permeability transition pore to cardioprotection. Int J Biochem Cell Biol 38:414–419. doi:10.1016/j.biocel.2005.09.017
18. Davidson SM, Yellon DM, Murphy MP, Duchen MR (2012) Slow calcium waves and redox changes precede mitochondrial permeability transition pore opening in the intact heart during hypoxia and reoxygenation. Cardiovasc Res 93:445–453. doi:10.1093/cvr/cvr349
19. Duchen MR, McGuinness O, Brown LA, Crompton M (1993) On the involvement of a cyclosporin a sensitive mitochondrial pore in myocardial reperfusion injury. Cardiovasc Res 27:1790–1794. doi:10.1093/cvr/27.10.1790
20. Eltzschig HK, Eckle T (2011) Ischemia and reperfusion—from mechanism to translation. Nat Med 17:1391–1401. doi:10.1038/nm.2507
21. Frohlich GM, Meier P, White SK, Yellon DM, Hausenloy DJ (2013) Myocardial reperfusion injury: looking beyond primary pci. Eur Heart J 34:1714–1722. doi:10.1093/eurheartj/eht090
22. Gauthier C, Tavernier G, Charpentier F, Langin D, Le Marec H (1996) Functional beta3-adrenoceptor in the human heart. J Clin Invest 98:556–562. doi:10.1172/JCI118823
23. Gerczuk PZ, Kloner RA (2012) An update on cardioprotection: a review of the latest adjunctive therapies to limit myocardial infarction size in clinical trials. J Am Coll Cardiol 59:969–978. doi:10.1016/j.jacc.2011.07.054
24. Gomez L, Chavanis N, Argaud L, Chalabreysse L, Gateau-Roesch O, Ninet J, Ovize M (2005) Fas-independent mitochondrial damage triggers cardiomyocyte death after ischemia–reperfusion. Am J Physiol Heart Circ Physiol 289:H2153–2158. doi:10.1152/ajpheart.00165.2005
25. Guo Y, Flaherty MP, Wu WJ, Tan W, Zhu X, Li Q, Bolli R (2012) Genetic background, gender, age, body temperature, and arterial blood ph have a major impact on myocardial infarct size in the mouse and need to be carefully measured and/or taken into account: results of a comprehensive analysis of determinants of infarct size in 1,074 mice. Basic Res Cardiol 107:288. doi:10.1007/s00395-012-0288-y
26. Hausenloy DJ, Baxter G, Bell R, Botker HE, Davidson SM, Downey J, Heusch G, Kitakaze M, Lecour S, Mentzer R, Mocanu MM, Ovize M, Schulz R, Shannon R, Walker M, Walkinshaw G, Yellon DM (2010) Translating novel strategies for cardioprotection: the hatter workshop recommendations. Basic Res Cardiol 105:677–686. doi:10.1007/s00395-010-0121-4
27. Hausenloy DJ, Yellon DM (2006) Survival kinases in ischemic preconditioning and postconditioning. Cardiovasc Res 70:240–253. doi:10.1016/j.cardiores.2006.01.017
28. Heusch G (2011) Beta3-adrenoceptor activation just says no to myocardial reperfusion injury. J Am Coll Cardiol 58:2692–2694. doi:10.1016/j.jacc.2011.09.034
29. Heusch G (2013) Cardioprotection: chances and challenges of its translation to the clinic. Lancet 381:166–175. doi:10.1016/S0140-6736(12)60916-7
30. Heusch G, Boengler K, Schulz R (2008) Cardioprotection: nitric oxide, protein kinases, and mitochondria. Circulation 118:1915–1919. doi:10.1161/CIRCULATIONAHA.108.805242
31. Heusch G, Boengler K, Schulz R (2010) Inhibition of mitochondrial permeability transition pore opening: the holy grail of cardioprotection. Basic Res Cardiol 105:151–154. doi:10.1007/s00395-009-0080-9
32. Heusch G, Skyschally A, Schulz R (2011) The in situ pig heart with regional ischemia/reperfusion—ready for translation. J Mol Cell Cardiol 50:951–963. doi:10.1016/j.yjmcc.2011.02.016

33. Ibanez B, Cimmino G, Prat-Gonzalez S, Vilahur G, Hutter R, Garcia MJ, Fuster V, Sanz J, Badimon L, Badimon JJ (2011) The cardioprotection granted by metoprolol is restricted to its administration prior to coronary reperfusion. Int J Cardiol 147:428–432. doi:10.1016/j.ijcard.2009.09.551
34. Ibanez B, Fuster V, Macaya C, Sanchez-Brunete V, Pizarro G, Lopez-Romero P, Mateos A, Jimenez-Borreguero J, Fernandez-Ortiz A, Sanz G, Fernandez-Friera L, Corral E, Barreiro MV, Ruiz-Mateos B, Goicolea J, Hernandez-Antolin R, Acebal C, Garcia-Rubira JC, Albarran A, Zamorano JL, Casado I, Valenciano J, Fernandez-Vazquez F, de la Torre JM, Perez de Prado A, Iglesias-Vazquez JA, Martinez-Tenorio P, Iniguez A (2012) Study design for the "effect of metoprolol in cardioprotection during an acute myocardial infarction" (metocard-cnic): A randomized, controlled parallel-group, observer-blinded clinical trial of early pre-reperfusion metoprolol administration in st-segment elevation myocardial infarction. Am Heart J 164(473–480):e475. doi:10.1016/j.ahj.2012.07.020
35. Ibanez B, Prat-Gonzalez S, Speidl WS, Vilahur G, Pinero A, Cimmino G, Garcia MJ, Fuster V, Sanz J, Badimon JJ (2007) Early metoprolol administration before coronary reperfusion results in increased myocardial salvage: Analysis of ischemic myocardium at risk using cardiac magnetic resonance. Circulation 115:2909–2916. doi:10.1161/CIRCULATIONAHA.106.679639
36. Ibarra C, Vicencio JM, Estrada M, Lin Y, Rocco P, Rebellato P, Munoz JP, Garcia-Prieto J, Quest AF, Chiong M, Davidson SM, Bulatovic I, Grinnemo KH, Larsson O, Szabadkai G, Uhlen P, Jaimovich E, Lavandero S (2013) Local control of nuclear calcium signaling in cardiac myocytes by perinuclear microdomains of sarcolemmal insulin-like growth factor 1 receptors. Circ Res 112:236–245. doi:10.1161/CIRCRESAHA.112.273839
37. Kelley KW, Curtis SE, Marzan GT, Karara HM, Anderson CR (1973) Body surface area of female swine. J Anim Sci 36:927–930
38. Maroko PR, Kjekshus JK, Sobel BE, Watanabe T, Covell JW, Ross J Jr, Braunwald E (1971) Factors influencing infarct size following experimental coronary artery occlusions. Circulation 43:67–82. doi:10.1161/01.CIR.43.1.67
39. Niu X, Watts VL, Cingolani OH, Sivakumaran V, Leyton-Mange JS, Ellis CL, Miller KL, Vandegaer K, Bedja D, Gabrielson KL, Paolocci N, Kass DA, Barouch LA (2012) Cardioprotective effect of beta-3 adrenergic receptor agonism: role of neuronal nitric oxide synthase. J Am Coll Cardiol 59:1979–1987. doi:10.1016/j.jacc.2011.12.046
40. Nowosielski M, Schocke M, Mayr A, Pedarnig K, Klug G, Kohler A, Bartel T, Muller S, Trieb T, Pachinger O, Metzler B (2009) Comparison of wall thickening and ejection fraction by cardiovascular magnetic resonance and echocardiography in acute myocardial infarction. J Cardiovasc Magn Reson 11:22. doi:10.1186/1532-429X-11-22
41. Piot C, Croisille P, Staat P, Thibault H, Rioufol G, Mewton N, Elbelghiti R, Cung TT, Bonnefoy E, Angoulvant D, Macia C, Raczka F, Sportouch C, Gahide G, Finet G, Andre-Fouet X, Revel D, Kirkorian G, Monassier JP, Derumeaux G, Ovize M (2008) Effect of cyclosporine on reperfusion injury in acute myocardial infarction. N Engl J Med 359:473–481. doi:10.1056/NEJMoa071142
42. Piper HM, Garcia-Dorado D, Ovize M (1998) A fresh look at reperfusion injury. Cardiovasc Res 38:291–300. doi:10.1016/S0008-6363(98)00033-9
43. Rengo G, Zincarelli C, Femminella GD, Liccardo D, Pagano G, de Lucia C, Altobelli GG, Cimini V, Ruggiero D, Perrone-Filardi P, Gao E, Ferrara N, Lymperopoulos A, Koch WJ, Leosco D (2012) Myocardial beta(2)-adrenoceptor gene delivery promotes coordinated cardiac adaptive remodelling and angiogenesis in heart failure. Br J Pharmacol 166:2348–2361. doi:10.1111/j.1476-5381.2012.01954.x
44. Sambrano GR, Fraser I, Han H, Ni Y, O'Connell T, Yan Z, Stull JT (2002) Navigating the signalling network in mouse cardiac myocytes. Nature 420:712–714. doi:10.1038/nature01306
45. Schuster A, Kutty S, Padiyath A, Parish V, Gribben P, Danford DA, Makowski MR, Bigalke B, Beerbaum P, Nagel E (2011) Cardiovascular magnetic resonance myocardial feature tracking detects quantitative wall motion during dobutamine stress. J Cardiovasc Magn Reson 13:58. doi:10.1186/1532-429X-13-58
46. Schwartz Longacre L, Kloner RA, Arai AE, Baines CP, Bolli R, Braunwald E, Downey J, Gibbons RJ, Gottlieb RA, Heusch G, Jennings RB, Lefer DJ, Mentzer RM, Murphy E, Ovize M, Ping P, Przyklenk K, Sack MN, Vander Heide RS, Vinten-Johansen J, Yellon DM (2011) New horizons in cardioprotection: recommendations from the 2010 national heart, lung, and blood institute workshop. Circulation 124:1172–1179. doi:10.1161/CIRCULATIONAHA.111.032698
47. Sharma V, Bell RM, Yellon DM (2012) Targeting reperfusion injury in acute myocardial infarction: a review of reperfusion injury pharmacotherapy. Expert Opin Pharmacother 13:1153–1175. doi:10.1517/14656566.2012.685163
48. Skyschally A, Schulz R, Heusch G (2010) Cyclosporine a at reperfusion reduces infarct size in pigs. Cardiovasc Drugs Ther 24:85–87. doi:10.1007/s10557-010-6219-y
49. Yellon DM, Hausenloy DJ (2007) Myocardial reperfusion injury. N Engl J Med 357:1121–1135. doi:10.1056/NEJMra071667
50. Zhou YY, Wang SQ, Zhu WZ, Chruscinski A, Kobilka BK, Ziman B, Wang S, Lakatta EG, Cheng H, Xiao RP (2000) Culture and adenoviral infection of adult mouse cardiac myocytes: methods for cellular genetic physiology. Am J Physiol Heart Circ Physiol 279:H429–H436
51. Zorov DB, Filburn CR, Klotz LO, Zweier JL, Sollott SJ (2000) Reactive oxygen species (ros)-induced ros release: a new phenomenon accompanying induction of the mitochondrial permeability transition in cardiac myocytes. J Exp Med 192:1001–1014. doi:10.1084/jem.192.7.1001

Effect of Early Metoprolol on Infarct Size in ST-Segment–Elevation Myocardial Infarction Patients Undergoing Primary Percutaneous Coronary Intervention

The Effect of Metoprolol in Cardioprotection During an Acute Myocardial Infarction (METOCARD-CNIC) Trial

Borja Ibanez, MD, PhD; Carlos Macaya, MD, PhD; Vicente Sánchez-Brunete, MD; Gonzalo Pizarro, MD; Leticia Fernández-Friera, MD, PhD; Alonso Mateos, MD; Antonio Fernández-Ortiz, MD, PhD; José M. García-Ruiz, MD; Ana García-Álvarez, MD, PhD; Andrés Iñiguez, MD, PhD; Jesús Jiménez-Borreguero, MD; Pedro López-Romero, PhD; Rodrigo Fernández-Jiménez, MD; Javier Goicolea, MD, PhD; Borja Ruiz-Mateos, MD; Teresa Bastante, MD; Mercedes Arias, MD, PhD; José A. Iglesias-Vázquez, MD; Maite D. Rodriguez, RN; Noemí Escalera, BPT; Carlos Acebal, MD; José A. Cabrera, MD, PhD; Juan Valenciano, MD; Armando Pérez de Prado, MD, PhD; María J. Fernández-Campos, MD; Isabel Casado, MD; Juan C. García-Rubira, MD, PhD; Jaime García-Prieto, BSc; David Sanz-Rosa, PhD; Carlos Cuellas, MD, PhD; Rosana Hernández-Antolín, MD, PhD; Agustín Albarrán, MD, PhD; Felipe Fernández-Vázquez, MD, PhD; José M. de la Torre-Hernández, MD, PhD; Stuart Pocock, PhD; Ginés Sanz, MD, PhD; Valentin Fuster, MD, PhD

Downloaded from http://circ.ahajournals.org/ by guest on October 24, 2017

Background—The effect of β-blockers on infarct size when used in conjunction with primary percutaneous coronary intervention is unknown. We hypothesize that metoprolol reduces infarct size when administered early (intravenously before reperfusion).

Methods and Results—Patients with Killip class II or less anterior ST-segment–elevation myocardial infarction (STEMI) undergoing percutaneous coronary intervention within 6 hours of symptoms onset were randomized to receive intravenous metoprolol (n=131) or not (control, n=139) before reperfusion. All patients without contraindications received oral metoprolol within 24 hours. The predefined primary end point was infarct size on magnetic resonance imaging performed 5 to 7 days after STEMI. Magnetic resonance imaging was performed in 220 patients (81%). Mean±SD infarct size by magnetic resonance imaging was smaller after intravenous metoprolol compared with control (25.6±15.3 versus 32.0±22.2 g; adjusted difference, −6.52; 95% confidence interval, −11.39 to −1.78; P=0.012). In patients with pre–percutaneous coronary intervention Thrombolysis in Myocardial Infarction grade 0 to 1 flow, the adjusted treatment difference in infarct size was −8.13 (95% confidence interval, −13.10 to −3.16; P=0.0024). Infarct size estimated by peak and area under the curve creatine kinase release was measured in all study populations and was significantly reduced by intravenous metoprolol. Left ventricular ejection fraction was higher in the intravenous metoprolol group (adjusted difference, 2.67%; 95% confidence interval, 0.09–5.21; P=0.045). The composite of death, malignant ventricular arrhythmia, cardiogenic shock, atrioventricular block, and reinfarction at 24 hours in the intravenous metoprolol and control groups was 7.1% and 12.3%, respectively (P=0.21).

Conclusions—In patients with anterior Killip class II or less ST-segment–elevation myocardial infarction undergoing primary percutaneous coronary intervention, early intravenous metoprolol before reperfusion reduced infarct size and increased left ventricular ejection fraction with no excess of adverse events during the first 24 hours after STEMI.

Received May 7, 2013; accepted August 5, 2013.

From Centro Nacional de Investigaciones Cardiovasculares Carlos III, Madrid, Spain (B.I., G.P., L.F.-F., A.M., A.F.-O., J.M.G.-R., A.G.-A., J.J.B., P.L.-R., R.F.-J., M.D.R., N.E., J.G.-P., D.S.-R., S.P., G.S., V.F.); Hospital Clínico San Carlos-IdISSC, Madrid, Spain (B.I., C.M., A.F.-O., R.F.-J., B.R.-M., C.A., J.C.G.-R., R.H.-A.); Servicio de Urgencia Médica de Madrid (SUMMA 112), Madrid, Spain (V.S.-B., A.M., J.V., M.J.F.-C.); Hospital Universitario Quirón, Madrid, Spain (G.P., J.A.C.); Complejo Hospitalario Universitario de Vigo-Meixoeiro, Pontevedra, Spain (A.I., M.A.); Hospital Universitario de la Princesa, Madrid, Spain (J.J.-B., T.B.); Hospital Universitario Puerta de Hierro, Madrid, Spain (J.G.); Servicio de Emergencia Medica 061 de Galicia-Sur, Galicia, Spain (J.A.I.-V.); Hospital Universitario León, León, Spain (A.P.d.P., C.C., F.F.-V.); Servicio de Atención Médica Urgente (SAMUR)–Protección Civil, Madrid, Spain (I.C.); Hospital Universitario Doce de Octubre, Madrid, Spain (A.A.); Hospital Universitario Marqués de Valdecilla, Santander, Spain (J.M.d.l.T.-H.); London School of Hygiene & Tropical Medicine, London, UK (S.P.); and the Zena and Michael A. Wiener CVI, Mount Sinai School of Medicine, New York, NY (V.F.).

Correspondence to Borja Ibanez, MD, PhD, FESC, Centro Nacional de Investigaciones Cardiovasculares Carlos III (CNIC), Melchor Fernández Almagro, 3, 28029, Madrid, Spain. E-mail bibanez@cnic.es

© 2013 American Heart Association, Inc.

Circulation **is available at http://circ.ahajournals.org** **DOI: 10.1161/CIRCULATIONAHA.113.003653**

Clinical Trial Registration—URL: http://www.clinicaltrials.gov. Unique identifier: NCT01311700. EUDRACT number: 2010-019939-35. **(*Circulation*. 2013;128:1495-1503.)**

Key Words: adrenergic beta-antagonist ■ infarction ■ magnetic resonance imaging ■ metoprolol ■ myocardial infarction ■ percutaneous coronary intervention ■ reperfusion injury

Downloaded from http://circ.ahajournals.org/ by guest on October 24, 2017

Timely reperfusion by primary percutaneous coronary intervention (PCI) is the best therapeutic strategy for ST-segment–elevation myocardial infarction (STEMI),[1,2] and its widespread use has significantly reduced mortality.[3] However, STEMI survivors are at high risk of recurrent cardiovascular events such as congestive heart failure, arrhythmia, and sudden death. A major determinant of postinfarction mortality and morbidity is the extent of myocardial necrosis after STEMI[4]; therefore, strategies to limit infarct size (cardioprotection during STEMI) are important. Several mechanical and pharmacological interventions have been proposed as potential cardioprotective therapies,[5] but their use in clinical practice has been limited.

Editorial see p 1487
Clinical Perspective on p 1503

The potential of β-blockers to limit myocardial necrosis was proposed long ago,[6] but their cardioprotective capacity during STEMI has been disputed.[7] Most analyses of the infarct-limiting effects of β-blockers were done in the prereperfusion era and yielded conflicting results.[8–11] Data on the cardioprotective effect of β-blockers during thrombolytic reperfusion are scarce, with just 1 randomized[12] and 1 nonrandomized[13] study, with contradictory results. In the era of primary PCI as the treatment of choice for STEMI, no randomized trials aiming to test the infarct-limiting effect of β-blockers have been published.

Data from large-animal models of acute myocardial infarction show that the β1-selective blocker metoprolol is able to markedly reduce infarct size but only when administered intravenously before reperfusion.[14,15] Current clinical guidelines for STEMI recommend the initiation of oral β-blockers within 24 hours after infarction for patients with no contraindications[1,2]; very early intravenous β-blockade, although permitted, is not mandatory.

We aimed to determine whether early pre-reperfusion intravenous β-blocker administration reduces infarct size in STEMI patients treated by primary PCI by performing a multicenter, randomized, controlled, clinical trial.

Methods

The design of the study has previously been published.[16] The Effect of Metoprolol in Cardioprotection During an Acute Myocardial Infarction (METOCARD-CNIC) trial was a multicenter, randomized, parallel-group, single-blinded (to outcome evaluators) clinical trial in STEMI patients comparing pre-reperfusion intravenous metoprolol and no pre-reperfusion metoprolol (control). The primary hypothesis of the trial was that anterior STEMI patients receiving early intravenous metoprolol before reperfusion would have a reduced infarct size compared with control subjects. All patients received oral metoprolol within 24 hours after reperfusion, as recommended by current clinical guidelines.[1,2]

The study was approved by the ethics committees and institutional review boards at each participating center. All eligible patients gave written informed consent.

Patient Selection and Randomization

Patients eligible for enrollment were 18 to 80 years of age and showed symptoms consistent with STEMI for >30 minutes and ST elevation ≥2 mm in ≥2 contiguous leads in V_1 through V_5 with an anticipated time of symptom onset to reperfusion of ≤6 hours. To ensure that all patients underwent reperfusion within 6 hours from symptom onset, the inclusion criterion was ≤4.5 hours from symptom onset to randomization.[16] Exclusion criteria were Killip class III to IV acute myocardial infarction, systolic blood pressure persistently <120 mm Hg, PR interval >240 milliseconds (or type II–III atrioventricular block), heart rate persistently <60 bpm, or active treatment with any β-blocker agent.

To avoid a potential selection bias, randomization was done after informed consent was signed by the patient.

Patients randomized to intravenous metoprolol received up to three 5-mg boluses of metoprolol tartrate 2 minutes apart.[17] Patients were identified and randomized either out of hospital by the participating emergency medical services or on arrival at any of the 7 participating hospitals (in 4 regions across Spain). Patients randomized to the intravenous metoprolol group in the out-of-hospital setting received intravenous metoprolol during transfer to the PCI center.

Apart from intravenous metoprolol, patients were treated according to clinical guidelines. Thrombus aspiration and use of glycoprotein IIb/IIIa during PCI were recommended. All patients except those who developed contraindications received oral metoprolol tartrate during hospitalization. The first oral dose was scheduled for 12 to 24 hours after infarction, in line with clinical guidelines.[1,2]

Randomization was stratified by time from symptom onset to enrollment (<1.5 versus ≥1.5 hours), diabetes mellitus status, sex, and age (<60 versus ≥60 years). Patients were randomized 1:1 by telephone with a block size of 4 within strata. The randomization center was located at the SUMMA112 emergency medical services headquarters and was run around the clock by trained nurses.

Magnetic resonance imaging (MRI) was scheduled for 5 to 7 days after infarction. Patients on long-term β-blocker treatment, with a history of previous acute myocardial infarction, or with no final diagnosis of acute myocardial infarction (no enzymatic evidence of infarction) were excluded from the primary analysis according to the protocol and thus did not undergo MRI.[16]

End Points

The primary end point was infarct size by MRI (extent of myocardial necrosis quantified by delayed gadolinium enhancement). Prespecified efficacy secondary end points were the extent of myocardial salvage on MRI, infarct size quantified by MRI in the subgroup of patients with a pre-PCI Thrombolysis in Myocardial Infarction (TIMI) grade 0 to 1 flow, and infarct size estimated by peak and area under the curve (AUC; 72 hours) release of creatine kinase (CK). The major prespecified safety secondary end point was the incidence of major adverse cardiac events, defined as a composite of death, malignant ventricular arrhythmias, advanced atrioventricular block, cardiogenic shock, and reinfarction during the first 24 hours after STEMI.

MRI and angiography were evaluated at independent core laboratories; end-point events were adjudicated by an independent clinical events committee. All were blinded to treatment group.

MRI Performance and Analysis

A detailed description of the MRI protocol and methods for analysis is reported elsewhere.[16] Analyses were undertaken by the core laboratory at Centro Nacional de Investigaciones Cardiovasculares Carlos III (CNIC). Data were quantified with dedicated software (QMass MR 7.5; Medis, Leiden, the Netherlands). Left ventricular (LV)

volume, LV mass, LV ejection fraction (LVEF), and the extent of edema and necrosis were determined. Myocardial necrosis (grams of LV tissue) was defined by the extent of abnormal delayed gadolinium enhancement, whereas myocardium at risk (grams of LV tissue) was defined by the extent of edema (high signal intensity on T2-weighted short T1 inversion-recovery images).[18,19] Myocardial salvage was defined as the difference between myocardium at risk and myocardial necrosis normalized to myocardium at risk.[18,19]

Statistical Methods

The study was powered for detect a relative reduction in infarct size of 20% in patients receiving intravenous metoprolol. This required 220 evaluable patients to provide 90% power (2-sided α=0.05). Sample size calculation was based on a previous MRI-based study reporting mean infarct size and dispersion in anterior STEMI patients.[20] To compensate for ≈20% patients not undergoing MRI,[16] we planned to recruit ≈275 patients. All randomized patients, including those not undergoing MRI, were analyzed for clinical end points.

All efficacy analyses were performed according to the intention-to-treat principle. For quantitative variables, data are expressed as mean±SD and compared by parametric methods. Nonnormal data are reported as medians with first and third quartiles and were compared by nonparametric methods (Wilcoxon rank-sum test). For categorical data, percentages were compared by use of exact methods. Because the variance of peak and AUC CK release data tends to be proportional to the mean, a square-root transformation was used.

MRI data were analyzed by linear regression models, with treatment effect estimates (and 95% confidence intervals [CIs]) presented both without and with adjustment for the 4 stratification variables.

To confirm that the analysis based on MRI-quantified infarct size was not influenced by selection bias, a sensitivity analysis was performed comparing the estimated difference between treatments for peak and AUC CK release between the overall study population and the subset undergoing MRI. All analyses were conducted with the R 2.14.1 statistical language.

Results

Study Population

Between November 2010 and October 2012, 270 patients were randomized to receive intravenous metoprolol pre-reperfusion (n=139) or no metoprolol pre-reperfusion (n=131, control subjects). One hundred forty-seven patients (55%) were randomized out of hospital during ambulance transfer to the PCI center. Four patients (2 in each group) withdrew consent. Twenty-four patients (9%) were not scheduled for MRI because of erroneous recruitment criteria (n=14) or no enzymatic evidence of infarction (n=10). Of patients scheduled for MRI, 22 (9%) did not undergo MRI because of poor clinical status (n=7), claustrophobia (n=12), or technical problems with the magnet (n=3). Patients with poor clinical status not undergoing MRI included 4 patients in the intravenous metoprolol group (2 patients with refractory heart failure, 1 patient with cardiac rupture, and 1 patient with massive hemoptysis) compared with 3 patients in the control group (2 patients with refractory heart failure and 1 patient with aortic dissection). Thus, 220 patients (106 receiving intravenous metoprolol and 114 control subjects) had MRI data available for primary analysis. A CONSORT (Consolidated Standards of Reporting Trials) flow diagram is shown in Figure 1. Baseline characteristics of the study population are presented in Table 1.

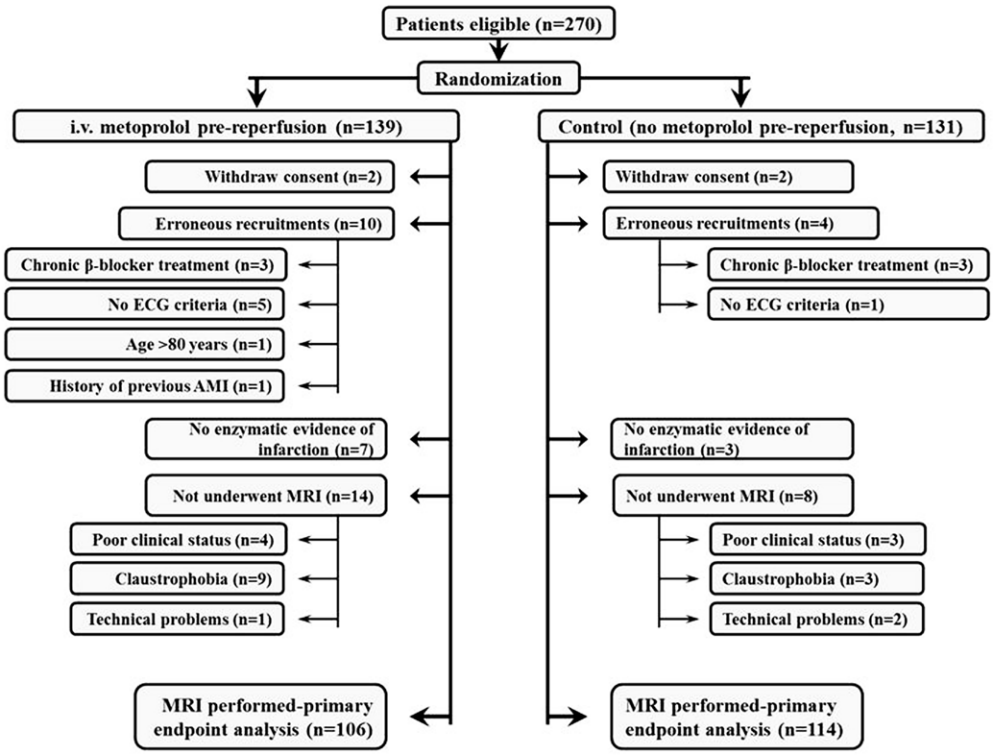

Figure 1. Diagram of patients flow in the Effect of Metoprolol in Cardioprotection During an Acute Myocardial Infarction (METOCARDCNIC) trial. Patients with no ECG criteria exclusions included the following. Three patients (all 3 allocated to intravenous metoprolol pre-reperfusion) who had no ST-segment elevation ≥2 mm. These patients had no enzymatic evidence of infarction and had a final diagnosis of unspecific chest pain. Two patients (1 in each study group) had ST-segment elevation only in leads II, III, and aVF. One patient (allocated to intravenous metoprolol pre-reperfusion) had junction rhythm. AMI indicates acute myocardial infarction; and MRI, magnetic resonance imaging.

Downloaded from http://circ.ahajournals.org/ by guest on October 24, 2017

Table 1. Baseline Characteristics of the Patients*

	All Patients (n=270)		Patients Undergoing MRI (n=220)	
	Intravenous Metoprolol (n=139)	Control (n=131)	Intravenous Metoprolol (n=106)	Control (n=114)
Age, y	58.7±12.7	58.2±10.8	58.4±12.4	58.7±10.6
Male sex, n (%)	119 (85.6)	114 (87)	92 (86.8)	99 (86.8)
Body mass index, kg/m^2	27.6±3.7	27.9±3.9	27.5±3.5	27.8±3.9
Hypertension, n (%)	54 (40.3)	54 (42.2)	38 (36.5)	48 (42.1)
Smoking, n (%)				
Current smoker	71 (53)	69 (53.9)	56 (53.8)	59 (51.8)
Ex-smoker (0–10 y before)	14 (10.4)	14 (10.9)	12 (11.5)	12 (10.5)
Dyslipidemia, n (%)	53 (39.8)	51 (40.2)	43 (41.3)	47 (41.2)
Diabetes mellitus, n (%)	31 (23.3)	24 (18.8)	21 (20.2)	22 (19.3)
Ischemia duration, min†	197±61	187±66	198±62	187±67
Killip class at recruitment, n (%)				
I	128 (92.1)	114 (87.0)	98 (92.5)	100 (87.7)
II	11 (7.9)	17 (13.0)	8 (7.5)	13 (11.4)
Infarct artery lesion location, n (%)				
Proximal LAD	37 (26.6)	38 (29.0)	29 (27.4)	34 (29.8)
Mid LAD	76 (54.7)	71 (54.2)	62 (58.5)	67 (58.8)
Distal LAD	11 (7.9)	11 (8.4)	11 (10.4)	9 (7.9)
Diagonal	3 (2.2)	1 (0.8)	2 (1.9)	1 (0.9)
Left main	1 (0.7)	1 (0.8)	0 (0)	0 (0)
Other	11 (7.9)	9 (6.9)	2 (1.9)	3 (2.6)
TIMI grade 0–1 flow before PCI, n (%)	104 (76.5)	101 (77.1)	86 (81.1)	92 (80.7)
Successful PCI, n (%)‡	128 (94.1)	125 (95.4)	106 (100)	111 (97.4)
SBP at recruitment, mm Hg	143±19	142±19	142±18	142±19
HR at recruitment, bpm	82±14	82±14	82±13	82±14
SBP after intravenous metoprolol, mm Hg	129±20	NA	128±18	NA
HR after intravenous metoprolol, bpm	69±12	NA	68±12	NA
Treatment at the time of PCI, n (%)				
Heparin	123 (95.3)	119 (96)	102 (96.2)	108 (96.4)
Aspirin	127 (98.4)	121 (97.6)	105 (99.1)	109 (97.3)
Thienopyridine	126 (97.7)	121 (97.6)	104 (98.1)	110 (98.2)
Thrombus aspiration	108 (82.4)	100 (80.6)	91 (85.8)	92 (82.1)
GP IIb/IIIa during PCI	92 (70.2)	99 (79.8)	76 (71.7)	90 (80.4)

There were no significant differences in any of the baseline characteristics. GP indicates glycoprotein; HR, heart rate; LAD, left anterior descending coronary artery; MRI, magnetic resonance imaging; NA, not applicable; PCI, percutaneous coronary intervention; SBP, systolic blood pressure; and TIMI, Thrombolysis in Myocardial Infarction.

*Plus-minus values are mean±SD.

†Ischemia duration means time from symptom onset to reperfusion.

‡Successful PCI was defined as TIMI grade 2 to 3 flow after PCI.

Metoprolol Administration

Of the 139 patients allocated to pre-reperfusion intravenous metoprolol, 138 (99%) received at least one 5-mg metoprolol intravenous bolus (82% received 2 boluses and 67% received 3 boluses). The same pattern was found for the subset randomized in the out-of-hospital environment. Intravenous metoprolol was administered at a median of 10 minutes (quartiles 1 and 3, 7 and 19 minutes) after STEMI diagnosis. Oral metoprolol was initiated within 24 hours after STEMI in 96% and 92% of patients in the intravenous metoprolol and control groups, with mean±SD initiation times of 15.7±10.6 and 15.9±8.7 hours after reperfusion, respectively.

Two patients allocated to the control group erroneously received pre-reperfusion intravenous metoprolol. These patients were included in the control group for the intention-to-treat analyses and in the intravenous metoprolol group for the safety analysis of major adverse cardiac events. Similarly, 1 patient allocated to intravenous metoprolol did not receive any owing to a vagal reaction and was included in the intravenous metoprolol group for primary analysis and in the control group for the analysis of major adverse cardiac events.

Downloaded from http://circ.ahajournals.org/ by guest on October 24, 2017

Table 2. Magnetic Resonance Imaging Data (5 to 7 Days After Infarction)

	Patients Undergoing MRI (n=220)					
	Intravenous Metoprolol (n=106)	Control (n=114)	Unadjusted		Adjusting for Stratification Variables	
	Mean (SD)	Mean (SD)	Difference (95% CI)	*P* Value	Difference (95% CI)	*P* Value
LVEDV, mL	169.0 (33.0)	172.6 (39.4)	−3.64 (−13.14 to 5.84)	0.46	−4.37 (−13.22 to 4.41)	0.33
LVESV, mL	91.9 (26.7)	99.6 (34.8)	−7.70 (−15.92 to 0.41)	0.063	−7.85 (−15.70 to −0.09)	0.047
LV mass, g	108.8 (24.7)	112.5 (26.3)	−3.72 (−10.29 to 2.84)	0.28	−4.08 (−10.06 to 1.89)	0.2
Myocardium at risk, g	37.6 (17.1)	40.9 (20.0)	−3.30 (−8.19 to 1.44)	0.19	−3.44 (−8.29 to 1.26)	0.16
Infarcted myocardium, g*	25.6 (15.3)	32.0 (22.2)	−6.43 (−11.46 to −1.67)	0.013	−6.52 (−11.39 to −1.78)	0.012
Infarcted myocardium, % LV	21.2 (11.5)	25.1 (13.9)	−3.85 (−7.28 to −0.51)	0.029	−3.77 (−7.17 to −0.46)	0.032
Salvage index: (MAR–IM)/MAR, %†	34.9 (22.3)	27.7 (23.7)	7.17 (0.80 to 13.30)	0.028	7.20 (0.78 to 13.48)	0.024
LVEF, %	46.1 (9.3)	43.4 (10.4)	2.74 (0.13 to 5.35)	0.039	2.67 (0.09 to 5.21)	0.045
Infarcted myocardium in pre-PCI TIMI grade 0–1 flow, g‡	26.7 (15.0)	34.4 (20.0)	−7.72 (−12.82 to −2.85)	0.004	−8.13 (−13.10 to −3.16)	0.002
Infarcted myocardium in pre-PCI TIMI grade 0–1 flow, % LV	21.9 (11.1)	26.7 (13.0)	−4.77 (−8.21 to −1.25)	0.011	−4.91 (−8.40 to −1.35)	0.0078

CI indicates confidence interval; IM, infarcted myocardium; LVEDV, left ventricular end-diastolic volume; LVEF, left ventricular ejection fraction; LVESV, left ventricular end-systolic volume; MAR, myocardium at risk; MRI, magnetic resonance imaging; PCI, percutaneous coronary intervention; and TIMI, Thrombolysis in Myocardial Infarction.

*Primary end point.

†Prespecified secondary end point.

‡Prespecified secondary end point in 178 patients (86 receiving intravenous metoprolol and 92 control subjects).

Effect on Infarct Size

MRI data are presented in Table 2. Mean±SD infarct size in the intravenous metoprolol group (primary end point) was 25.6±15.3 versus 32.0±22.2 g in the control group (adjusted treatment effect, −6.52; 95% CI, −11.39 to −1.78; *P*=0.012). Myocardial salvage (see Methods) in the intravenous metoprolol group was 34.9±22.3% versus 27.7±23.7% in the control group (adjusted treatment effect, 7.20%; 95% CI, 0.78–13.48; *P*=0.024). Infarct size in the subset of patients with a pre-PCI TIMI grade 0 to 1 flow (prespecified secondary end point) was 26.7±15.0 g in intravenous metoprolol patients versus 34.4±20.0 in the control group (adjusted treatment effect, −8.13; 95% CI, −13.10 to −3.16; *P*=0.0024). In the subset of patients with a pre-PCI TIMI grade 2 to 3 flow (patent artery), infarct size was 20.7±16.4 g in the intravenous metoprolol group versus 22.2±28.3 g in the control group (*P*=0.6). Infarct size distributions in the 2 predefined study groups are illustrated in Figure 2.

Infarct size was also estimated in all study population by peak and AUC CK release as prespecified secondary end points. Pre-reperfusion intravenous metoprolol administration significantly reduced infarct size estimated by peak and AUC CK release. Peak CK in the intravenous metoprolol group was 2397±214 versus 3176±254 IU/L in the control group (adjusted treatment effect, −740; 95% CI, −1361 to −120; *P*=0.019). The AUC CK in the intravenous metoprolol group was 49 427±4013 versus 62 953±4634 IU/L in the control group (adjusted treatment effect, −12 825; 95% CI, −24 346 to −1305; *P*=0.029). Similar results were obtained in the subset of patients undergoing MRI. These findings are shown in Figure 3.

Pre-reperfusion administration of intravenous metoprolol significantly increased LVEF on MRI (46.1±9.3% versus 43.4±10.4%; adjusted treatment effect, 2.67; 95% CI, 0.09–5.21; *P*=0.045). In the subset of patients with a TIMI grade 0 to 1 flow before primary PCI, LVEF was 45.1±8.9% in the intravenous metoprolol group versus 41.0±9.5% in the control group (adjusted treatment effect, 4.13; 95% CI, 1.34–6.85; *P*=0.0031).

Safety Data

The prespecified safety end point was the incidence of major adverse cardiac events within 24 hours after STEMI in all patients (entire study population). Prereperfusion administration of intravenous metoprolol did not increase the incidence of major adverse cardiac events: There were 10 events (7.1%) in the prereperfusion intravenous metoprolol group and 16

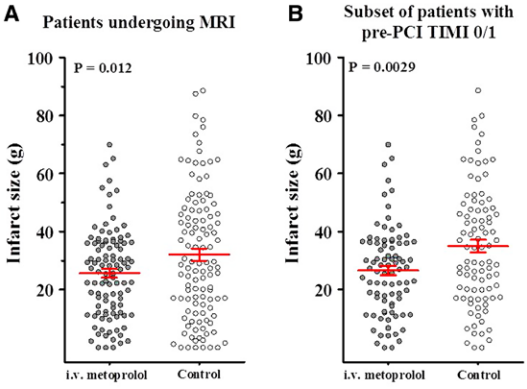

Figure 2. Effect of early pre-reperfusion intravenous metoprolol administration on infarct size evaluated by magnetic resonance imaging (MRI) 5 to 7 days after infarction. **A** and **B**, Infarct size assessed by delayed gadolinium enhancement in all patients undergoing MRI (**A**) and in the subset of patients with TIMI grade 0 to 1 flow before primary percutaneous coronary intervention (PCI) (**B**). Red lines represent mean±SEM. Circles are individual patient data. TIMI indicates Thrombolysis in Myocardial Infarction.

Downloaded from http://circ.ahajournals.org/ by guest on October 24, 2017

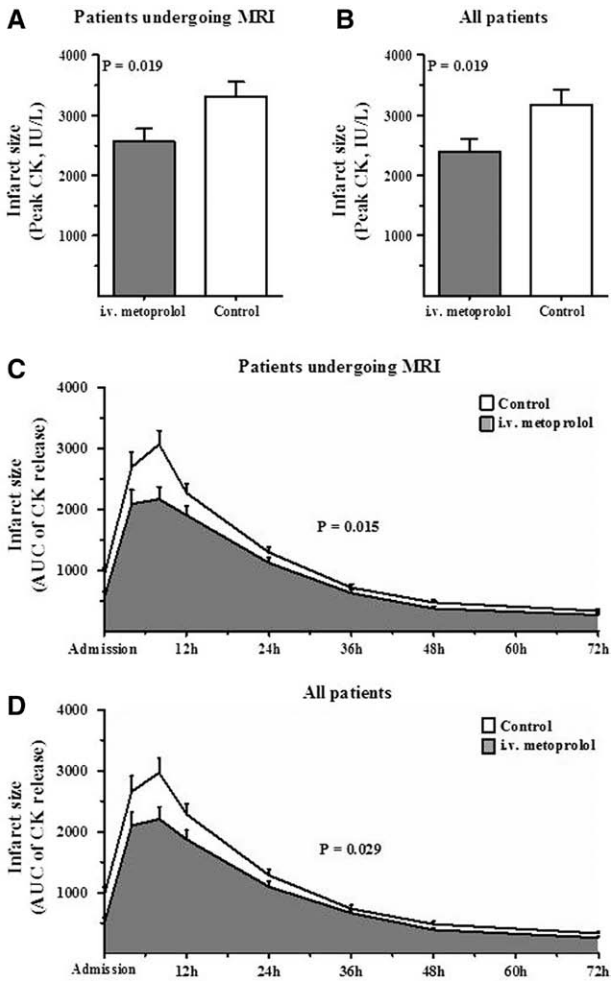

Figure 3. Effect of early pre-reperfusion intravenous metoprolol administration on infarct size estimated by peak and area under the curve (AUC) creatine kinase (CK) release. **A** and **B**, Back-transformed mean±SEM of peak CK release in patients undergoing magnetic resonance imaging (MRI; **A**) and in the entire study population (**B**). Nontransformed median of peak CK release in patients undergoing MRI was 2600 IU/L (quartiles 1 and 3, 1306 and 4272 IU/L) in the intravenous metoprolol group vs 3700 IU/L (quartiles 1 and 3, 1311 and 5626 IU/L) in the control group (P=0.040). Nontransformed median of peak CK release in the entire study population was 2217 IU/L (quartiles 1 and 3, 877 and 4151 IU/L) in the intravenous metoprolol group vs 3558 IU/L (quartiles 1 and 3, 1118 and 5593 IU/L) in the control group (P=0.011). **C** and **D**, AUC CK release in patients undergoing MRI (**C**) and in the entire study population (**D**). Data are presented as back-transformed mean±SEM for each time point of serum CK determination. Nontransformed median AUC CK release in patients undergoing MRI was 49 984 IU/L (quartiles 1 and 3, 28 279 and 76 748 IU/L) in the intravenous metoprolol group vs 65 966 IU/L (quartiles 1 and 3, 28 837 and 109 329 IU/L) in the control group (P=0.042). Nontransformed median AUC CK release in the entire study population was 47 030 IU/L (quartiles 1 and 3, 23 869 and 78 453 IU/L) in the intravenous metoprolol group vs 63 656 IU/L (quartiles 1 and 3, 27 988 and 108 686 IU/L) in the control group (P=0.025).

events (12.3%) in the control group (P=0.21). Adverse cardiac events are presented in Table 3.

Table 3. Adverse Cardiac Events

	Intravenous Metoprolol (n=140), n (%)	Control (n=130), n (%)
MACE at 24 h	10 (7.1)	16 (12.3)
Death	0 (0)	1 (0.8)
Malignant ventricular arrhythmia	5 (3.6)	10 (7.7)
Advanced AV block	1 (0.7)	2 (1.5)
Cardiogenic shock	6 (4.3)	7 (5.4)
Reinfarction	0 (0)	0 (0)
Death during admission	3 (2.1)	3 (2.3)
Killip class III or greater during admission	11 (7.9)	9 (6.9)
Reinfarction during admission	1 (0.7)*	0 (0)

AV indicates atrioventricular; and MACE, major adverse cardiac events (composite of death, malignant ventricular arrhythmias [ventricular fibrillation/sustained ventricular tachycardia], advanced AV block, cardiogenic shock, and reinfarction).

*Periprocedural infarction during percutaneous coronary intervention to a nonculprit coronary artery 4 days after index ST-segment–elevation myocardial infarction.

Discussion

This study shows that early administration of intravenous metoprolol before reperfusion reduces infarct size and increases LVEF in anterior STEMI patients undergoing primary PCI. It also appears safe and does not increase the incidence of cardiac events during admission.

Our objective was to determine whether intravenous metoprolol reduced infarct size in STEMI patients treated according to current clinical guidelines,[1,2] including glycoprotein IIb/IIIa and thrombus aspiration, 2 widely applied interventions with potential infarct-limiting effects.[21,22]

Infarct size was evaluated by 3 different methods: total myocardial necrosis by MRI (the gold standard), relative myocardial necrosis by MRI (normalized to myocardium at risk), and biomarker (CK) release. All 3 methodologies provided evidence of a significant and consistent reduction in infarct size resulting from pre-reperfusion intravenous metoprolol administration. LVEF 1 week after STEMI was significantly increased by intravenous metoprolol, as evaluated by highly accurate MRI technology. Because reduced LVEF is a strong predictor of postinfarction mortality, this finding adds to the clinical value of pre-reperfusion intravenous metoprolol administration.

β-Blockers are a first-line treatment in secondary prevention after acute myocardial infarction with a clear reduction in mortality.[23] Current guidelines recommend oral β-blockade within 24 hours after STEMI[1,2] but with no emphasis on early intravenous initiation before reperfusion. Previous studies of β-blocker effects on infarct size had inconclusive results[7] but were conducted before reperfusion became the standard treatment for STEMI. Recent studies in large animals indicate that metoprolol can reduce infarct size[14] if administered before reperfusion[15] and may reduce reperfusion injury.[24] We therefore hypothesized that the conflicting findings on the cardioprotective capacity of β-blockers in STEMI reflect the facts that very few clinical studies have been performed in the reperfusion era and that no studies testing the ability of β-blockers to reduce infarct size have been done in the era of primary PCI as the treatment of choice for STEMI. Van de Werf et al[12]

Downloaded from http://circ.ahajournals.org/ by guest on October 24, 2017

randomized STEMI patients undergoing thrombolysis to receive prethrombolysis atenolol or placebo. Contrasting with our results, they found no reduction in infarct size by intravenous β-blocker administration. The reason for this disparity is unknown; however, a possible explanation is that ischemia/reperfusion injury differs between patients treated by thrombolysis and primary PCI and that cardioprotective strategies in patients treated by PCI (abrupt coronary opening) do not work in patients treated by thrombolysis (gradual coronary opening). Another potential explanation is that not all β-blockers have the same cardioprotective effect. In this regard, the nonrandomized TEAHAT (Thrombolysis Early in Acute Heart Attack) study found a significant infarct size reduction in STEMI patients undergoing thrombolysis and receiving early intravenous metoprolol.[13] It is also likely to be significant that, in contrast to our trial, only 33% of STEMIs in the Van de Werf et al[12] study were of anterior location and that reperfusion was never achieved in 25% of the study population. Finally, infarct size in our study was evaluated by MRI and was estimated by biomarker release by van de Werf et al.

In the era of primary PCI, a few retrospective studies[25–27] and 1 small randomized trial[28] have evaluated the effect of pre-PCI β-blocker administration on clinical events. Despite none of these studies being designed to detect differences in infarct size, the clinical benefits observed by prereperfusion β-blockade in all of them are in agreement with our results.

It is our hypothesis that metoprolol reduces infarct size by ameliorating reperfusion injury.[24] For that reason, a prespecified secondary end point was infarct size in the subgroup of patients with a pre-PCI occluded artery. Infarct size in the subgroup of patients with pre-PCI TIMI grade 0 of 1 flow was reduced to a larger extent than in the entire study population (Table 2), supporting our hypothesis. In agreement with this idea, infarct size was not reduced in the subgroup of patients with pre-PCI TIMI grade 2 to 3 flow; however, the small number of patients with an open artery precludes a definite statement.

The results of the Clopidogrel and Metoprolol in Myocardial Infarction Trial (COMMIT) trial[29] are the main reason why clinical practice guidelines do not emphasize early intravenous β-blocker initiation in STEMI.[1] In this trial, STEMI patients undergoing thrombolysis were randomized to early intravenous followed by oral metoprolol or matching placebo. The COMMIT trial did not report data on infarct size but showed significantly reduced rates of reinfarction and ventricular fibrillation in response to early intravenous metoprolol; however, this benefit came at the cost of excess cardiogenic shock, resulting in a net neutral effect on mortality.[29] Although patients in COMMIT presented late (mean time from symptom onset to thrombolysis, 10.3 hours), mortality was lower in Killip class I and II patients receiving intravenous metoprolol. Conversely, total mortality was increased by intravenous metoprolol in Killip class III patients.[29] In addition, metoprolol increased mortality in patients with systolic blood pressure <120 mm Hg. These results reinforce the contraindications for intravenous β-blocker therapy in patients with overt heart failure, and these patients have been systematically excluded from other β-blocker trials. In contrast to the COMMIT trial, we randomized patients presenting early (within 6 hours of STEMI onset), used PCI as the reperfusion strategy, and excluded patients with Killip class III or greater at first medical contact. In METOCARD-CNIC, the number of patients who progressed to Killip class grade III to IV during admission was similar in both treatment groups (7.9% for intravenous metoprolol versus 6.9% for control). Patients with Killip class III to IV STEMI potentially have larger infarctions. Given that we excluded these types of patients (for safety reasons), we might have underestimated infarct size in our population and potentially diluted the benefits of this cardioprotective strategy.

A possible limitation of our trial is that 19% of the recruited patients population did not undergo MRI for primary end-point evaluation. This attrition rate was as we projected[16] and is similar to those in other STEMI trials using MRI.[21,30] Moreover, we analyzed infarct size by peak and AUC CK release in the entire study population to see if the loss of recruited patients introduced a selection bias, and this proved compatible with the MRI findings. A significant reduction in infarct size was observed in patients allocated to intravenous metoprolol before reperfusion in the entire population. Another limitation is that 22 patients scheduled for MRI were withdrawn from the imaging study for various reasons. However, this rate of withdrawal from scheduled MRI is compatible with previous experience[16] and is lower than in other trials performing MRI early after STEMI.[21,30,31]

As shown in Figure 1, there was a significant difference in the proportion of no MRI performance between groups (higher in the intravenous metoprolol group). This was observed despite the fact that the evaluation of the qualifying criteria for MRI performance was done blinded to treatment allocation or other variables that might influence the outcome. In this regard, a sensitivity analysis showed that the estimated difference between treatments for CK release in all study population and in the subset of patients undergoing MRI was similar, ruling out a selection bias.

METOCARD-CNIC was a prospective, randomized, open, blinded end-point (PROBE) trial. Evaluators of all outcomes were nonetheless blinded to treatment allocation. Although evidence suggests that PROBE trials yield results similar to double-blinded trials,[32] we cannot completely rule out an influence of this design on the study results.

Infarct size is a major determinant of postinfarction mortality, so limiting the extent of myocardial necrosis in STEMI is a major therapeutic target.[33] Huge resources have been dedicated to exploring novel therapies that might reduce infarct size but so far with little success.[34] Here, we show that an inexpensive medication already approved for STEMI treatment (intravenous metoprolol) can significantly reduce infarct size simply by being administered before reperfusion. Further evidence is needed to assess potential longer-term clinical benefits in a larger clinical trial.

Acknowledgments

We are indebted to the unpaid commitment of the nurses and supervising physicians at the SUMMA112 "SCU." All coinvestigators in the different emergency medical services (SUMMA112, 061 Galicia, SAMUR) and hospitals have been capital for the rigorous conduct of this trial. A full list of researchers is available at https://metocard.cnic.es/. MRIs were analyzed with dedicated software (QMass MR version 7.5) partially supported by a scientific collaboration with

Downloaded from http://circ.ahajournals.org/ by guest on October 24, 2017

Medis Medical Imaging Systems BV. Simon Bartlett (CNIC) provided English editing.

Sources of Funding

The METOCARD-CNIC trial was a noncommercial trial; the main sponsor was the CNIC through competitive CNIC translational grant 01-2009. We also had an independent research grant from the Spanish National Ministry of Health and Social Policy (EC10-042), a Mutua Madrileña Foundation grant (AP8695-2011), and a master research agreement between Philips Healthcare and CNIC. Dr Ibanez is recipient of the ISCIII grant "Fondo de Investigación Sanitaria PI10/02268," which relates to the topic of this study.

Disclosures

None.

References

1. O'Gara PT, Kushner FG, Ascheim DD, Casey DE Jr, Chung MK, de Lemos JA, Ettinger SM, Fang JC, Fesmire FM, Franklin BA, Granger CB, Krumholz HM, Linderbaum JA, Morrow DA, Newby LK, Ornato JP, Ou N, Radford MJ, Tamis-Holland JE, Tommaso CL, Tracy CM, Woo YJ, Zhao DX, Anderson JL, Jacobs AK, Halperin JL, Albert NM, Brindis RG, Creager MA, DeMets D, Guyton RA, Hochman JS, Kovacs RJ, Kushner FG, Ohman EM, Stevenson WG, Yancy CW; American College of Cardiology Foundation/American Heart Association Task Force on Practice Guidelines. 2013 ACCF/AHA guideline for the management of ST-elevation myocardial infarction: a report of the American College of Cardiology Foundation/American Heart Association Task Force on Practice Guidelines. *Circulation*. 2013;127:e362–e425.
2. Steg PG, James SK, Atar D, Badano LP, Blomstrom-Lundqvist C, Borger MA, Di Mario C, Dickstein K, Ducrocq G, Fernandez-Aviles F, Gershlick AH, Giannuzzi P, Halvorsen S, Huber K, Juni P, Kastrati A, Knuuti J, Lenzen MJ, Mahaffey KW, Valgimigli M, van 't Hof A, Widimsky P, Zahger D. ESC guidelines for the management of acute myocardial infarction in patients presenting with ST-segment elevation. *Eur Heart J*. 2012;33:2569–2619.
3. Krumholz HM, Wang Y, Chen J, Drye EE, Spertus JA, Ross JS, Curtis JP, Nallamothu BK, Lichtman JH, Havranek EP, Masoudi FA, Radford MJ, Han LF, Rapp MT, Straube BM, Normand SL. Reduction in acute myocardial infarction mortality in the United States: risk-standardized mortality rates from 1995-2006. *JAMA*. 2009;302:767–773.
4. Larose E, Rodés-Cabau J, Pibarot P, Rinfret S, Proulx G, Nguyen CM, Déry JP, Gleeton O, Roy L, Noël B, Barbeau G, Rouleau J, Boudreault JR, Amyot M, De Larochellière R, Bertrand OF. Predicting late myocardial recovery and outcomes in the early hours of ST-segment elevation myocardial infarction traditional measures compared with microvascular obstruction, salvaged myocardium, and necrosis characteristics by cardiovascular magnetic resonance. *J Am Coll Cardiol*. 2010;55:2459–2469.
5. Heusch G. Cardioprotection: chances and challenges of its translation to the clinic. *Lancet*. 2013;381:166–175.
6. Sommers HM, Jennings RB. Ventricular fibrillation and myocardial necrosis after transient ischemia: effect of treatment with oxygen, procainamide, reserpine, and propranolol. *Arch Intern Med*. 1972;129:780–789.
7. Hearse DJ, Yellon DM, Downey JM. Can beta blockers limit myocardial infarct size? *Eur Heart J*. 1986;7:925–930.
8. Metoprolol in Acute Myocardial Infarction (MIAMI): a randomised placebo-controlled international trial: the MIAMI Trial Research Group. *Eur Heart J*. 1985;6:199–226.
9. Yusuf S, Sleight P, Rossi P, Ramsdale D, Peto R, Furze L, Sterry H, Pearson M, Motwani R, Parish S, Gray R, Bennett D, Bray C. Reduction in infarct size, arrhythmias and chest pain by early intravenous beta blockade in suspected acute myocardial infarction. *Circulation*. 1983;67(pt 2):I32–I41.
10. Reduction of infarct size with the early use of timolol in acute myocardial infarction. *N Engl J Med*. 1984;310:9–15.
11. Rude RE, Buja LM, Willerson JT. Propranolol in acute myocardial infarction: the MILIS experience. *Am J Cardiol*. 1986;57:38F–42F.
12. Van de Werf F, Janssens L, Brzostek T, Mortelmans L, Wackers FJ, Willems GM, Heidbuchel H, Lesaffre E, Scheys I, Collen D. Short-term effects of early intravenous treatment with a beta-adrenergic blocking agent or a specific bradycardiac agent in patients with acute myocardial infarction receiving thrombolytic therapy. *J Am Coll Cardiol*. 1993;22:407–416.
13. Risenfors M, Herlitz J, Berg CH, Dellborg M, Gustavsson G, Gottfridsson C, Lomsky M, Swedberg K, Hjalmarsson A. Early treatment with thrombolysis and beta-blockade in suspected acute myocardial infarction: results from the TEAHAT Study. *J Intern Med Suppl*. 1991;734:35–42.
14. Ibanez B, Prat-González S, Speidl WS, Vilahur G, Pinero A, Cimmino G, García MJ, Fuster V, Sanz J, Badimon JJ. Early metoprolol administration before coronary reperfusion results in increased myocardial salvage: analysis of ischemic myocardium at risk using cardiac magnetic resonance. *Circulation*. 2007;115:2909–2916.
15. Ibanez B, Cimmino G, Prat-González S, Vilahur G, Hutter R, García MJ, Fuster V, Sanz J, Badimon L, Badimon JJ. The cardioprotection granted by metoprolol is restricted to its administration prior to coronary reperfusion. *Int J Cardiol*. 2011;147:428–432.
16. Ibanez B, Fuster V, Macaya C, Sánchez-Brunete V, Pizarro G, López-Romero P, Mateos A, Jiménez-Borreguero J, Fernández-Ortiz A, Sanz G, Fernández-Friera L, Corral E, Barreiro MV, Ruiz-Mateos B, Goicolea J, Hernández-Antolín R, Acebal C, García-Rubira JC, Albarrán A, Zamorano JL, Casado I, Valenciano J, Fernández-Vázquez F, de la Torre JM, Pérez de Prado A, Iglesias-Vázquez JA, Martínez-Tenorio P, Iñiguez A. Study design for the "effect of METOprolol in CARDioproteCtioN during an acute myocardial InfarCtion" (METOCARD-CNIC): a randomized, controlled parallel-group, observer-blinded clinical trial of early pre-reperfusion metoprolol administration in ST-segment elevation myocardial infarction. *Am Heart J*. 2012;164:473–480.e5.
17. Roberts R, Rogers WJ, Mueller HS, Lambrew CT, Diver DJ, Smith HC, Willerson JT, Knatterud GL, Forman S, Passamani E. Immediate versus deferred beta-blockade following thrombolytic therapy in patients with acute myocardial infarction: results of the Thrombolysis in Myocardial Infarction (TIMI) II-B Study. *Circulation*. 1991;83:422–437.
18. Friedrich MG, Abdel-Aty H, Taylor A, Schulz-Menger J, Messroghli D, Dietz R. The salvaged area at risk in reperfused acute myocardial infarction as visualized by cardiovascular magnetic resonance. *J Am Coll Cardiol*. 2008;51:1581–1587.
19. Lønborg J, Vejlstrup N, Kelbæk H, Bøtker HE, Kim WY, Mathiasen AB, Jørgensen E, Helqvist S, Saunamäki K, Clemmensen P, Holmvang L, Thuesen L, Krusell LR, Jensen JS, Køber L, Treiman M, Holst JJ, Engstrøm T. Exenatide reduces reperfusion injury in patients with ST-segment elevation myocardial infarction. *Eur Heart J*. 2012;33:1491–1499.
20. Wu E, Ortiz JT, Tejedor P, Lee DC, Bucciarelli-Ducci C, Kansal P, Carr JC, Holly TA, Lloyd-Jones D, Klocke FJ, Bonow RO. Infarct size by contrast enhanced cardiac magnetic resonance is a stronger predictor of outcomes than left ventricular ejection fraction or end-systolic volume index: prospective cohort study. *Heart*. 2008;94:730–736.
21. Stone GW, Maehara A, Witzenbichler B, Godlewski J, Parise H, Dambrink JH, Ochala A, Carlton TW, Cristea E, Wolff SD, Brener SJ, Chowdhary S, El-Omar M, Neunteufl T, Metzger DC, Karwoski T, Dizon JM, Mehran R, Gibson CM; INFUSE-AMI Investigators. Intracoronary abciximab and aspiration thrombectomy in patients with large anterior myocardial infarction: the INFUSE-AMI randomized trial. *JAMA*. 2012;307:1817–1826.
22. Svilaas T, Vlaar PJ, van der Horst IC, Diercks GF, de Smet BJ, van den Heuvel AF, Anthonio RL, Jessurun GA, Tan ES, Suurmeijer AJ, Zijlstra F. Thrombus aspiration during primary percutaneous coronary intervention. *N Engl J Med*. 2008;358:557–567.
23. Freemantle N, Cleland J, Young P, Mason J, Harrison J. beta Blockade after myocardial infarction: systematic review and meta regression analysis. *BMJ*. 1999;318:1730–1737.
24. Ibanez B, Cimmino G, Badimon JJ. Myocardial reperfusion injury [letter]. *N Engl J Med*. 2007;357:2409.
25. Harjai KJ, Stone GW, Boura J, Grines L, Garcia E, Brodie B, Cox D, O'Neill WW, Grines C. Effects of prior beta-blocker therapy on clinical outcomes after primary coronary angioplasty for acute myocardial infarction. *Am J Cardiol*. 2003;91:655–660.
26. Halkin A, Grines CL, Cox DA, Garcia E, Mehran R, Tcheng JE, Griffin JJ, Guagliumi G, Brodie B, Turco M, Rutherford BD, Aymong E, Lansky AJ, Stone GW. Impact of intravenous beta-blockade before primary angioplasty on survival in patients undergoing mechanical reperfusion therapy for acute myocardial infarction. *J Am Coll Cardiol*. 2004;43:1780–1787.
27. Valle JA, Zhang M, Dixon S, Aronow HD, Share D, Naoum JB, Gurm HS. Impact of pre-procedural beta blockade on inpatient mortality in patients undergoing primary percutaneous coronary intervention for ST elevation myocardial infarction. *Am J Cardiol*. 2013;111:1714–1720.
28. Hanada K, Higuma T, Nishizaki F, Sukekawa T, Yokota T, Yamada M, Saito S, Kushibiki M, Oikawa K, Abe N, Tomita H, Osanai T, Okumura K. Randomized study on the efficacy and safety of landiolol, an ultra-short-acting β1-adrenergic blocker, in patients with acute myocardial

Downloaded from http://circ.ahajournals.org/ by guest on October 24, 2017

infarction undergoing primary percutaneous coronary intervention. *Circ J*. 2012;76:439–445.
29. Chen ZM, Pan HC, Chen YP, Peto R, Collins R, Jiang LX, Xie JX, Liu LS; COMMIT (Clopidogrel and Metoprolol in Myocardial Infarction Trial) Collaborative Group. Early intravenous then oral metoprolol in 45,852 patients with acute myocardial infarction: randomised placebo-controlled trial. *Lancet*. 2005;366:1622–1632.
30. Atar D, Petzelbauer P, Schwitter J, Huber K, Rensing B, Kasprzak JD, Butter C, Grip L, Hansen PR, Süselbeck T, Clemmensen PM, Marin-Galiano M, Geudelin B, Buser PT; F.I.R.E. Investigators. Effect of intravenous FX06 as an adjunct to primary percutaneous coronary intervention for acute ST-segment elevation myocardial infarction results of the F.I.R.E. (Efficacy of FX06 in the Prevention of Myocardial Reperfusion Injury) trial. *J Am Coll Cardiol*. 2009;53:720–729.
31. Desmet W, Bogaert J, Dubois C, Sinnaeve P, Adriaenssens T, Pappas C, Ganame J, Dymarkowski S, Janssens S, Belmans A, Van de Werf F. High-dose intracoronary adenosine for myocardial salvage in patients with acute ST-segment elevation myocardial infarction. *Eur Heart J*. 2011;32:867–877.
32. Smith DH, Neutel JM, Lacourcière Y, Kempthorne-Rawson J. Prospective, randomized, open-label, blinded-endpoint (PROBE) designed trials yield the same results as double-blind, placebo-controlled trials with respect to ABPM measurements. *J Hypertens*. 2003;21:1291–1298.
33. Bell R, Beeuwkes R, Bøtker HE, Davidson S, Downey J, Garcia-Dorado D, Hausenloy DJ, Heusch G, Ibanez B, Kitakaze M, Lecour S, Mentzer R, Miura T, Opie L, Ovize M, Ruiz-Meana M, Schulz R, Shannon R, Walker M, Vinten-Johansen J, Yellon D. Trials, tribulations and speculation! Report from the 7th Biennial Hatter Cardiovascular Institute Workshop. *Basic Res Cardiol*. 2012;107:300.
34. Prasad A, Stone GW, Holmes DR, Gersh B. Reperfusion injury, microvascular dysfunction, and cardioprotection: the "dark side" of reperfusion. *Circulation*. 2009;120:2105–2112.

CLINICAL PERSPECTIVE

The capacity of β-blockers to reduce infarct size was evaluated extensively in the prereperfusion era with controversial results. In the context of reperfusion as the treatment of choice for ST-segment–elevation myocardial infarction (STEMI), this has been poorly investigated. Experimental data suggest that the β-blocker metoprolol is able to reduce infarct size only when administered intravenously before reperfusion. Here, we present the results of the Effect of Metoprolol in Cardioprotection During an Acute Myocardial Infarction (METOCARD-CNIC) trial, the first randomized, clinical trial prospectively evaluating the effect of early intravenous β-blockade on infarct size in conjunction with primary angioplasty. A total of 270 patients with anterior STEMI (Killip class II or less) revascularized within 6 hours after symptom onset were randomized to receive intravenous metoprolol or not before reperfusion. All patients received oral metoprolol according to clinical guidelines (first dose, 12–24 hours after infarction). Infarct size, evaluated by magnetic resonance imaging and creatine kinase release, was significantly reduced in the intravenous metoprolol group with no excess side effects. Left ventricular ejection fraction was higher in the intravenous metoprolol group. This cardioprotective effect appeared to be restricted to patients with a preangioplasty Thrombolysis in Myocardial Infarction grade 0 to 1 flow. Here, we show that an inexpensive medication already approved in the context of STEMI can significantly reduce infarct size just by administering it intravenously before reperfusion in patients with no contraindications. Given the important role of final infarct size as a main determinant of long-term mortality in STEMI survivors, the possibility of applying inexpensive strategies available to a wide proportion of STEMI patients is of clinical value.

Downloaded from http://circ.ahajournals.org/ by guest on October 24, 2017

Journal of the American College of Cardiology
© 2014 by the American College of Cardiology Foundation
Published by Elsevier Inc.

Vol. 63, No. 22, 2014
ISSN 0735-1097/$36.00
http://dx.doi.org/10.1016/j.jacc.2014.03.014

CLINICAL RESEARCH | Acute Coronary Syndrome

Long-Term Benefit of Early Pre-Reperfusion Metoprolol Administration in Patients With Acute Myocardial Infarction

Results From the METOCARD-CNIC Trial (Effect of Metoprolol in Cardioprotection During an Acute Myocardial Infarction)

Gonzalo Pizarro, MD,*† Leticia Fernández-Friera, MD, PhD,*‡ Valentin Fuster, MD, PhD,*§ Rodrigo Fernández-Jiménez, MD,*‖ José M. García-Ruiz, MD,*¶ Ana García-Álvarez, MD, PhD,*# Alonso Mateos, MD,** María V. Barreiro, MD,†† Noemí Escalera, BPT,* Maite D. Rodriguez, RN,* Antonio de Miguel, MD,‡‡ Inés García-Lunar, MD,*†§§ Juan J. Parra-Fuertes, MD,‖‖ Javier Sánchez-González, PhD,*¶¶ Luis Pardillos, MD,** Beatriz Nieto, MD,‡‡ Adriana Jiménez, MD,## Raquel Abejón, RN,** Teresa Bastante, MD,*** Vicente Martínez de Vega, MD,† José A. Cabrera, MD, PhD,† Beatriz López-Melgar, MD,*‖‖ Gabriela Guzman, MD, PhD,*††† Jaime García-Prieto, BSc,* Jesús G. Mirelis, MD, PhD,*§§ José Luis Zamorano, MD, PhD,‖ Agustín Albarrán, MD, PhD,‖‖ Javier Goicolea, MD, PhD,§§ Javier Escaned, MD, PhD,*‖ Stuart Pocock, PhD,*‡‡‡ Andrés Iñiguez, MD, PhD,‡‡ Antonio Fernández-Ortiz, MD, PhD,*‖ Vicente Sánchez-Brunete, MD,** Carlos Macaya, MD, PhD,‖ Borja Ibanez, MD, PhD*‖

Madrid, Oviedo, Barcelona, Galicia, Pontevedra, and León, Spain; New York, New York; and London, United Kingdom

Objectives The goal of this trial was to study the long-term effects of intravenous (IV) metoprolol administration before reperfusion on left ventricular (LV) function and clinical events.

Background Early IV metoprolol during ST-segment elevation myocardial infarction (STEMI) has been shown to reduce infarct size when used in conjunction with primary percutaneous coronary intervention (pPCI).

Methods The METOCARD-CNIC (Effect of Metoprolol in Cardioprotection During an Acute Myocardial Infarction) trial recruited 270 patients with Killip class ≤II anterior STEMI presenting early after symptom onset (<6 h) and randomized them to pre-reperfusion IV metoprolol or control group. Long-term magnetic resonance imaging (MRI) was performed on 202 patients (101 per group) 6 months after STEMI. Patients had a minimal 12-month clinical follow-up.

Results Left ventricular ejection fraction (LVEF) at the 6 months MRI was higher after IV metoprolol (48.7 ± 9.9% vs. 45.0 ± 11.7% in control subjects; adjusted treatment effect 3.49%; 95% confidence interval [CI]: 0.44% to 6.55%; p = 0.025). The occurrence of severely depressed LVEF (≤35%) at 6 months was significantly lower in patients treated with IV metoprolol (11% vs. 27%, p = 0.006). The proportion of patients fulfilling Class I indications for an implantable cardioverter-defibrillator (ICD) was significantly lower in the IV metoprolol group (7% vs. 20%, p = 0.012). At a median follow-up of 2 years, occurrence of the pre-specified composite of death, heart failure admission, reinfarction, and malignant arrhythmias was 10.8% in the IV metoprolol group versus 18.3% in the control group, adjusted hazard ratio (HR): 0.55; 95% CI: 0.26 to 1.04; p = 0.065. Heart failure admission was significantly lower in the IV metoprolol group (HR: 0.32; 95% CI: 0.015 to 0.95; p = 0.046).

Conclusions In patients with anterior Killip class ≤II STEMI undergoing pPCI, early IV metoprolol before reperfusion resulted in higher long-term LVEF, reduced incidence of severe LV systolic dysfunction and ICD indications, and fewer heart failure admissions. (Effect of METOprolol in CARDioproteCtioN During an Acute Myocardial InfarCtion. The METOCARD-CNIC Trial; NCT01311700) (J Am Coll Cardiol 2014;63:2356–62) © 2014 by the American College of Cardiology Foundation

Downloaded From: https://content.onlinejacc.org/ on 06/11/2014

ST-segment elevation myocardial infarction (STEMI) is a major contributor to mortality and morbidity worldwide (1–3). Beyond the high mortality rate in the acute phase, STEMI survivors are at high risk of recurrent events such as congestive heart failure, arrhythmia, or sudden death. Post-infarction patients with severely depressed left ventricular ejection fraction (LVEF) are at the highest risk of long-term adverse outcomes. Pharmacological and nonpharmacological (implantable cardioverter-defibrillator [ICD]) interventions have greatly reduced long-term mortality rates in these patients (4,5). However, the implementation of such strategies represents a huge economic burden that precludes its universal application. There is, therefore, a need for additional low-cost therapies to prevent severe post-infarction left ventricular (LV) dysfunction.

See page 2363

The size of the infarct after a STEMI has been revealed as the main determinant of adverse post-infarction outcomes (6). Therapies able to reduce infarct size are therefore urgently sought under the hypothesis that smaller infarctions will result in better long-term heart performance and that this will translate into fewer adverse clinical events (7,8).

Early intervention with intravenous (IV) metoprolol before reperfusion (METOCARD-CNIC [Effect of Metoprolol in Cardioprotection During an Acute Myocardial Infarction] trial) was recently shown to significantly reduce infarct size as evaluated by magnetic resonance imaging (MRI) 1 week post-infarction (9). Here, we present the prespecified evaluation on long-term LVEF (primary MRI measurement) and the effect on clinical endpoints of the METOCARD-CNIC trial.

Methods

Study population. The design of the study has been previously published (10). METOCARD-CNIC was a multicenter randomized clinical trial in which STEMI patients undergoing primary percutaneous coronary intervention (pPCI) were randomized to receive IV metoprolol or control group (no metoprolol) before reperfusion. Between November 2010 and October 2012, 270 patients were randomized to IV metoprolol pre-reperfusion (n = 139) or control group (n = 131). Inclusion criteria were patient age 18 to 80 years, Killip class ≤II anterior STEMI, and anticipated symptom onset-to-reperfusion time ≤6 h. Exclusion criteria were systolic blood pressure persistently <120 mm Hg, atrioventricular block, heart rate <60 beats/min, prior infarction, or active treatment with β-blockers. Patients randomized to IV metoprolol received up to 3 5-mg boluses of metoprolol tartrate. Fifty-five percent of the study group was recruited and treated during ambulance transfer to the hospital. Apart from IV metoprolol pre-reperfusion (or control group), all patients received state-of-the-art treatment according to clinical guidelines, including long-term oral treatment with β-blockers (first dose within 24 h after admission) in all patients with no contraindication. All patients were treated by local physicians who were blinded to treatment allocation and were responsible for all clinical actions.

Abbreviations and Acronyms

CI = confidence interval
HR = hazard ratio
ICD = implantable cardioverter-defibrillator
IV = intravenous
LV = left ventricular
LVEF = left ventricular ejection fraction
MACE = major adverse cardiac event(s)
MRI = magnetic resonance imaging
pPCI = primary percutaneous coronary intervention
STEMI = ST-segment elevation myocardial infarction

The primary readout of the trial (infarct size evaluated by MRI performed 1 week post-infarction) was available in 220 patients. The results of the 1-week MRI have been reported (9): administration of pre-reperfusion IV metoprolol resulted in significantly smaller (by 20%) infarcts and with no excessive side effects.

The study was approved by the ethics committees and institutional review boards at each participating center, and all eligible patients gave written informed consent.

Long-term MRI data. The protocol included a follow-up MRI 6 months after infarction in all patients except for those who showed no evidence of infarction on baseline MRI (no detectable gadolinium delayed enhancement). The detailed MRI protocol and methods for analysis have been reported (10). Analyses were undertaken by the Centro Nacional de Investigaciones Cardiovasculares Carlos III (CNIC) imaging core laboratory by expert researchers blinded to treatment arm. Data were quantified using

From the *Centro Nacional de Investigaciones Cardiovasculares Carlos III (CNIC), Madrid, Spain; †Hospital Universitario Quirón-Universidad Europea de Madrid, Madrid, Spain; ‡Hospital Montepríncipe, Madrid, Spain; §The Zena and Michael A. Wiener Cardiovascular Institute, Mount Sinai School of Medicine, New York, New York; ‖Hospital Clínico San Carlos, Madrid, Spain; ¶Hospital Universitario Central de Asturias, Oviedo, Spain; #Hospital Clinic, Barcelona, Spain; **Servicio de Urgencia Médica de Madrid (SUMMA 112), Madrid, Spain; ††Servicio de Emergencia Medica 061 de Galicia, Galicia, Spain; ‡‡Complejo Hospitalario Universitario de Vigo-Meixoeiro, Pontevedra, Spain; §§Hospital Universitario Puerta de Hierro, Madrid, Spain; ‖‖Hospital Universitario Doce de Octubre, Madrid, Spain; ¶¶Philips Healthcare, Madrid, Spain; ##Hospital Universitario León, León, Spain; ***Hospital de la Princesa, Madrid, Spain; †††Hospital Universitario La Paz, Madrid, Spain; and the ‡‡‡London School of Hygiene & Tropical Medicine, London, United Kingdom. The main sponsor of the METOCARD-CNIC trial was the Centro Nacional de Investigaciones Cardiovasculares Carlos III (CNIC), through the competitive grant "CNIC translational 01-2009." Other sponsors were the Spanish Ministry of Health and Social Policy (EC10-042), the Mutua Madrileña Foundation (AP8695-2011), and a Master Research Agreement (MRA) between Philips Healthcare and the CNIC. Dr. Ibanez is a recipient of the ISCIII grants "Fondo de Investigación Sanitaria" PI10/02268 and PI13/01979 that relate to the topic of this work. The magnetic resonance images were analyzed with dedicated software (QMass MR version 7.5), partially supported by a scientific collaboration with Medis Medical Imaging Systems BV. Dr. Pizarro, Dr. Fernández-Friera, Ms. Escalera, Mr. García-Prieto, Dr. Mirelis, Dr. Goicolea, and Dr. Ibanez are members of the Spanish "Red de Investigación Cardiovascular" (RIC; Program 4: HISPANICVS). Dr. Sánchez-González is an employee of Philips Healthcare. All other authors have reported that they have no relationships relevant to the contents of this paper to disclose. Drs. Pizarro and Fernández-Friera contributed equally to this work.

Manuscript received February 19, 2014; revised manuscript received March 6, 2014, accepted March 6, 2014.

Downloaded From: https://content.onlinejacc.org/ on 06/11/2014

dedicated software (QMass MR version 7.5, Medis, Leiden, the Netherlands). At 6-month MRI follow-up, LV volume, LV mass, LVEF, and the extent of myocardial necrosis (grams of LV tissue on delayed gadolinium enhancement images) were determined.

A post-hoc comparison was performed of the between-group frequencies of long-term LV reduced ejection fraction according to established cutoffs for clinical relevance (30%, 35%, and 40%) (4).

Evaluation of the indication for ICD implantation. Given the clinical, social, and economic implications of post-infarction ICD implantation, we performed a post-hoc analysis of the rate of ICD indication between study groups. ICD indication was defined according to Class I recommendations in current clinical guidelines (4,5): chronic LVEF ≤30% or chronic LVEF 30% to 35% in patients in New York Heart Association functional class II or III.

Clinical endpoints. The pre-specified clinical endpoint was the composite of death, readmission because of heart failure, reinfarction, and malignant ventricular arrhythmias (10). Clinical follow-up was performed by telephone interview and access to hospital reports. Once a potential event was detected, an independent clinical events committee blinded to the treatment arm reviewed the primary source data and adjudicated the event according to the pre-established protocol.

Statistical methods. The distribution of the continuous variables was analyzed using graphical methods. For quantitative variables, data are expressed as mean ± SD and compared by parametric methods. For categorical data, percents were compared using exact methods. MRI data were analyzed between treatment groups by linear regression models. LVEF was categorized by cutoffs of clinical significance, as described in the preceding text. To evaluate between-group trends, an ordinal regression was performed, and the proportional odds assumption was then checked. The survival distributions during follow-up of patients with and without IV metoprolol treatment were estimated by the Kaplan-Meier method, followed by the Cox proportional hazards regression model. The proportional hazards assumption was confirmed by inspection of Schoenfeld residuals. Finally, as a pre-specified outcome, the treatment effect on the incidence of 1-year follow-up major adverse cardiac events (MACE) was evaluated by logistic regression. Treatment effect estimates of all regression models (and 95% confidence intervals [CIs]) are presented both without and with adjustment for the 4 stratification variables used in the randomization: time from symptom onset to enrollment (<1.5 h vs. ≥1.5 h), diabetes mellitus status, sex, and age (<60 years vs. ≥60 years).

Differences were considered statistically significant at a p value <0.05 (2-tailed).

All statistical tests were performed with IBM SPSS Statistics software, v.20.0 (SPSS, IBM, Armonk, New York) and Stata 12 (Stata Statistical Software: Release 12, 2011, StataCorp, College Station, Texas).

Results

Long-term MRI data. MRI was scheduled 6 months after STEMI in all 220 patients undergoing 1-week MRI except for those with no evidence of infarction in the first MRI study (3 IV metoprolol, 6 control subjects). Nine additional patients did not undergo follow-up MRI for the following causes: 1 death (control group), 1 disabling stroke (control group), 1 technical problem with the MRI (IV metoprolol group), 1 emigration (IV metoprolol group), and 5 refusals to undergo follow-up MRI (3 IV metoprolol, 2 control subjects). Thus, a total of 202 patients underwent 6-month MRI (101 IV metoprolol and 101 control subjects). Long-term medication with known beneficial effects on LV remodeling was similar in both groups of patients (Online Table 1).

MRI data are presented in Table 1. Pre-reperfusion administration of IV metoprolol resulted in a significantly higher long-term mean LVEF on 6-month MRI (48.7 ± 9.9% vs. 45.0 ± 11.7% in control patients; adjusted treatment effect 3.49; 95% CI: 0.44% to 6.55%; p = 0.025) (Fig. 1). LV end-systolic volume was significantly lower in patients treated with pre-reperfusion IV metoprolol (98.1 ± 36.0 ml vs. 112.0 ± 45.0 ml; adjusted treatment effect −13.25; 95% CI: −24.47 to −2.03; p = 0.021). The LVEF values from the 1-week study (9) correlated tightly with the 6-month values regardless of treatment group (Online Fig. 1). Long-term extension of scar tissue was 15.7 ± 10.4 g in the IV metoprolol group versus 18.6 ± 11.3

Table 1 MRI Data (6 Months After Infarction)

	IV Metoprolol Group (n = 101)	Control Group (n = 101)	Unadjusted		Adjusted for Stratification Variables	
			Difference (95% CI)	p Value	Difference (95% CI)	p Value
LVEDV, ml	187.0 ± 38.8	197.6 ± 45.7	−10.62 (−22.45 to 1.22)	0.078	−10.34 (−21.73 to −1.05)	0.075
LVESV, ml	98.2 ± 36.1	112.0 ± 45.0	−13.87 (−25.22 to −2.51)	0.017	−13.25 (−24.47 to −2.03)	0.021
LV mass, g	84.6 ± 17.4	86.8 ± 18.1	−2.20 (−7.15 to 2.75)	0.38	−2.09 (−6.81 to 2.63)	0.38
Infarcted myocardium, g	15.7 ± 10.5	18.6 ± 11.3	−2.89 (−6.02 to 0.24)	0.070	−2.58 (−5.69 to 0.53)	0.10
Infarcted myocardium, % LV	15.7 ± 9.6	18.3 ± 9.8	−2.52 (−5.29 to 0.26)	0.075	−2.30 (−5.09 to 0.49)	0.11
LVEF, %	48.7 ± 10.0	45.0 ± 11.7	3.67 (0.64 to 6.71)	0.018	3.49 (0.44 to 6.55)	0.025

Values are mean ± SD unless otherwise indicated.

CI = confidence interval; IV = intravenous; LV = left ventricle; LVEDV = left ventricular end-diastolic volume; LVEF = left ventricular ejection fraction; LVESV = left ventricular end-systolic volume; MRI = magnetic resonance imaging.

Downloaded From: https://content.onlinejacc.org/ on 06/11/2014

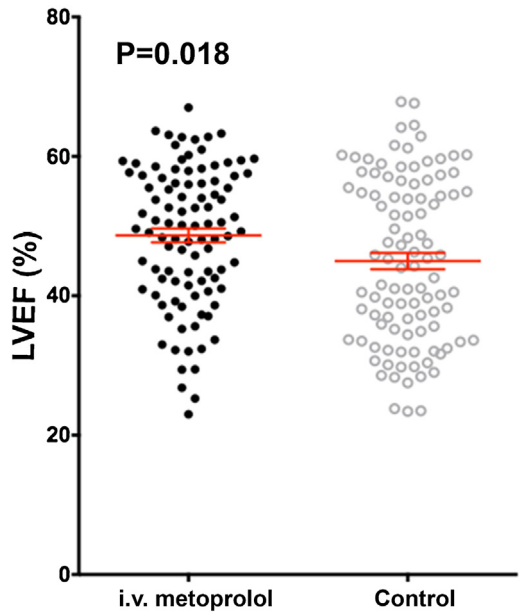

Figure 1 LVEF on MRI 6 Months After Infarction

Left ventricular ejection fraction (LVEF) in patients undergoing magnetic resonance imaging (MRI) 6 months after infarction. **Boxplots** represent mean (±SEM). **Circles** are individual patient data. i.v. = intravenous.

g in the control group (treatment effect −2.89; 95% CI: −6.02 to 0.24; p = 0.070).

LVEF depression and ICD indications according to clinical guidelines. The numbers of patients in each treatment group according to clinically relevant LVEF cut-offs are illustrated in Figure 2A. The proportion of patients with depressed LVEF at 6 months was significantly lower in the IV metoprolol group (e.g., 11% vs. 27% with LVEF ≤35%, p = 0.006), and the treatment groups also differed in the distribution of patients by LVEF category. Treatment allocation to IV metoprolol was associated with being in a higher LVEF category (common odds ratio 1.84; 95% CI: 1.11 to 3.07; p = 0.019).

The 6-month MRI data were analyzed for formal indication for ICD implantation according to current clinical guidelines (4,5) (Fig. 2B). Pre-reperfusion metoprolol administration resulted in a significant reduction of patients with ICD Class I recommendation (7% vs. 20% in the control patients, a risk difference of 12.7% [95% CI: 3.2% to 22.3%]; p = 0.012; adjusted odds ratio 0.32; 95% CI: 0.13 to 0.81; p = 0.016). The number needed to treat to avoid 1 ICD indication was 8 (95% CI: 4.5 to 31; p = 0.015).

Clinical follow-up. Median follow-up was 2 years after STEMI, with all patients but 6 lost to follow-up having a minimum of 12 months follow-up. The incidence of the pre-specified MACE endpoint (composite of death, heart failure admission, reinfarction, and malignant arrhythmia) and its individual components by treatment group are summarized in Table 2. There were fewer numerical MACE events after pre-reperfusion IV metoprolol administration: 10.8% versus 18.3% in control group (adjusted hazard ratio [HR]: 0.55; 95% CI: 0.26 to 1.04; p = 0.065). This was mainly driven by a lower rate of readmission because of heart failure (2.2% in the IV metoprolol group vs. 6.9% in the control group; HR: 0.32; 95% CI: 0.015 to 0.95; p = 0.046). Kaplan-Meier curves are shown in Figure 3.

Discussion

This pre-specified follow-up of the METOCARD-CNIC trial shows that patients receiving pre-reperfusion IV metoprolol have a significantly higher long-term mean LVEF compared with control groups and are protected

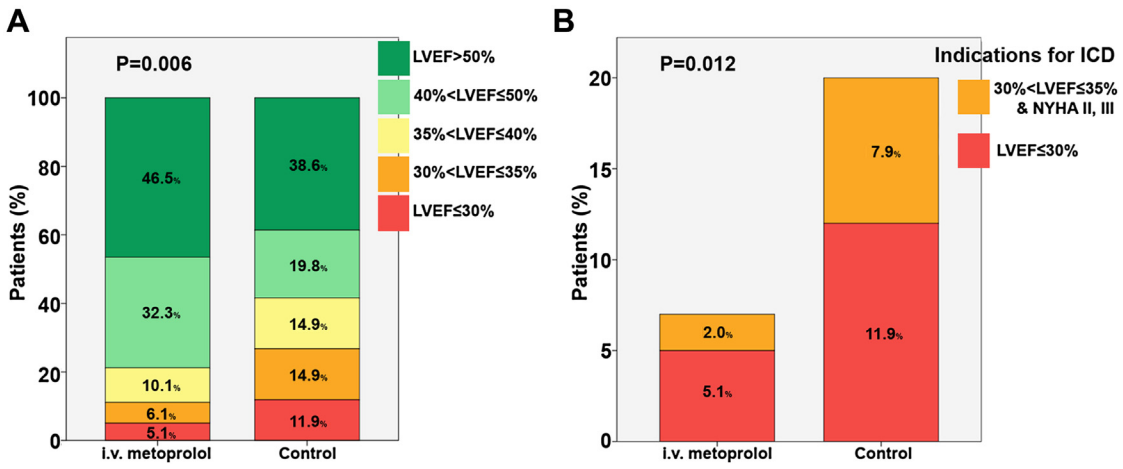

Figure 2 Follow-Up LVEF Categories and Indications for ICD According to Treatment Allocation

(A) Distribution of patients according to LVEF categories. Fisher exact test p = 0.026 and linear-by-linear association test p = 0.006. **(B)** Rate of formal indication (Class I recommendation in clinical guidelines) for ICD; see text. Fisher exact test p = 0.012. NYHA = New York Heart Association; other abbreviations as in Figure 1.

Downloaded From: https://content.onlinejacc.org/ on 06/11/2014

Table 2 Clinical Events

	IV Metoprolol	Control	p Value
MACE	15 (10.8)	24 (18.3)	0.065
Death	6 (4.3)	6 (4.6)	0.92
Cardiac death	3 (2.2)	5 (3.8)	
Noncardiac death	3 (2.2)	1 (0.8)	
Heart failure admission	3 (2.2)	9 (6.9)	0.046
ICD implantation	2 (1.4)	7 (5.3)	
Decompensation	1 (0.7)	3 (2.3)	
Re-AMI	1 (0.7)	3 (2.3)	0.15
Malignant ventricular arrhythmia	5 (3.6)	10 (7.7)	0.18

Values are n (%). MACE was the composite of all-cause death, heart failure admission (internal cardioverter defibrillator [ICD] implantation or clinical decompensation), reinfarction, and malignant ventricular arrhythmias (ventricular fibrillation/sustained ventricular tachycardia). Values were adjusted for randomization of variables.

AMI = acute myocardial infarction; IV = intravenous; MACE = major adverse cardiac event(s).

against long-term LVEF depression. These effects were accompanied by a trend towards reduced hard clinical endpoints. To the best of our knowledge, this is the first demonstration of a pharmacological cardioprotective strategy used in conjunction with pPCI resulting in sustained benefits on overall LVEF and in a significant reduction of cases of chronic severe LV systolic dysfunction.

The design of the METOCARD-CNIC trial included a 6 months MRI study for the evaluation of the effect of the therapy on long-term validated prognostic parameters. MRI is the gold standard for the evaluation of heart anatomy and function (11). In the 6 months MRI, we found that besides a higher LVEF, patients in the IV metoprolol group had significantly smaller LV end-systolic volumes, another well-established post-infarction prognostic parameter (12). We previously reported a significantly higher LVEF in the IV metoprolol group in the 1-week post-infarction MRI study (9). As presented, the LVEF values from the 1-week study correlated tightly with the follow-up values in both groups of treatment, supporting the conclusion that the long-term benefits of pre-reperfusion IV metoprolol are a consequence of the short-term beneficial effects detected at 1 week post-infarction. In order to determine whether the attrition of patients between the 1-week and 6-month MRI studies could have biased the results reported here, we evaluated the 1-week MRI LVEF in those patients who underwent the first scan, but not the 6-month follow-up (n = 18): median (first and third quartile) LVEF values were 53.0% (45.5% to 59.0%) in the IV metoprolol group versus 52.5% (46.8% to 62.0%) in the control group, excluding the possibility of selection bias introduced by patient attrition between 1-week and follow-up MRIs.

The long-term beneficial effects of pre-reperfusion IV metoprolol on LVEF were associated with a nonsignificant trend toward reduced hard clinical endpoints. The main limitation for the interpretation of this finding is that our trial was not powered to detect differences in clinical events. Other small trials testing the effect of cardioprotective strategies in STEMI have reported a significant reduction in long-term events despite being underpowered. In the CONDI (Remote Ischemic Conditioning in Primary PCI) trial, Sloth et al. (13) found that remote ischemic conditioning in STEMI seemed to improve long-term clinical outcomes. Their minimum follow-up was 3 years, whereas ours was 12 months. In fact, the survival curves in the CONDI trial showed a clear divergence after 2 years of follow-up. In a different study, Stone et al. (14) found that intracoronary abciximab in anterior STEMI resulted in a significant events reduction in the non–pre-specified time range (30 days to 12 months) post-infarction. Given the strong trend towards events reduction found in our trial, it is plausible that longer follow-up will reveal statistically significant differences. Similarly, non–pre-specified analyses of our study showed

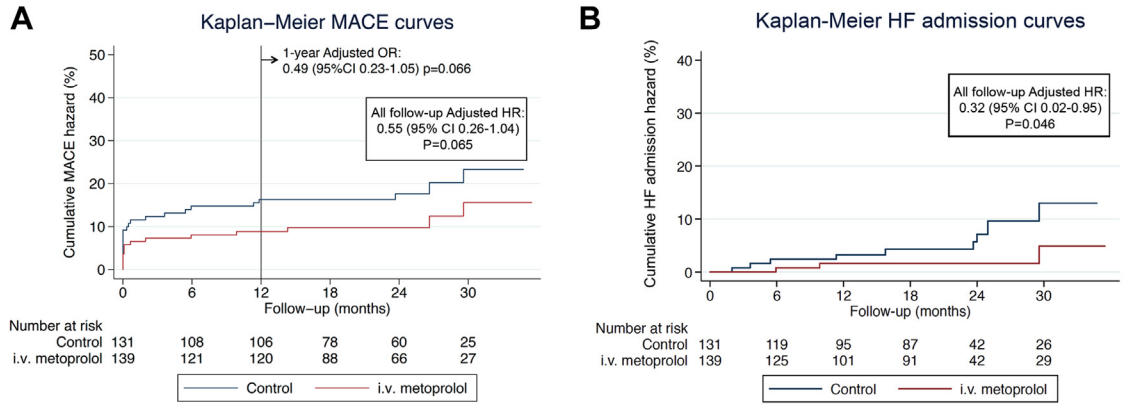

Figure 3 Follow-Up Clinical Endpoints

(A) Kaplan-Meier curves illustrating cumulative incidence of the pre-specified composite of death, admission as a result of heart failure (HF), reinfarction, or malignant ventricular arrhythmias. **(B)** Kaplan-Meier curves showing the cumulative incidence of readmission as a result of heart failure. CI = confidence interval; HR = hazard ratio; i.v. = intravenous; MACE = major adverse cardiac events.

Downloaded From: https://content.onlinejacc.org/ on 06/11/2014

statistical significance (heart failure admission HR: 0.32; p = 0.046). However, we feel that these non-powered or non–pre-specified analyses are of limited value even when statistical significance is shown. We believe that our data form a sufficient basis for a larger STEMI clinical trial of early IV metoprolol powered for clinical events reduction.

The implementation of reperfusion strategies over the past decades has significantly reduced the acute mortality associated with STEMI (15). However, a high proportion of survivors remain at high risk of future cardiovascular events throughout life, including sudden death and repetitive episodes of heart failure. Long-term post-infarction LV systolic function is a major predictor of these clinical events; indeed, LVEF remains the principal objective parameter used for the indication for post-infarction heart failure therapies (4,5). Extensive clinical research has led to chronic heart failure interventions (pharmacological and device-based) that reduce long-term mortality in STEMI survivors with low LVEF (4,5). Nonetheless, the implementation of these strategies comes at a high socioeconomic cost (16,17). The enormous economic burden for health services is the main factor preventing universal implementation of these new heart failure therapies (18,19), and most countries in development cannot afford them (20), despite having implemented reperfusion strategies for STEMI. Even in advanced economies, economic considerations prevent universal use of the most expensive therapies (ICD and cardiac resynchronization devices) (21,22). The present trial demonstrates that administration of a low-cost therapy (<2€ in Spain, <$3 in the United States) results in higher long-term LVEF. Although the observed 3.7-point absolute difference in mean LVEF could be judged as small, the much lower number of patients with severely depressed LVEF in the treatment group is more clinically relevant, and would translate into a greater socioeconomic impact. Furthermore, the number of patients with a formal indication for ICD implantation according to clinical guidelines was two-thirds less among the IV metoprolol patients. Overall, the rate of actual ICD implantation among cases with a formal indication was 33% (9 of 27, Table 2). This rate of ICD implantation is in agreement with other dedicated studies (rate between 30% and 35%) (23,24), and above what is seen in the general population (around 13%) (25).

In the first report on the METOCARD-CNIC trial, we documented an average 20% smaller infarct size in patients randomized to IV metoprolol, as evaluated by MRI 1 week after infarction (9). At 6 months, total infarct size difference between groups had been attenuated (15.6 g in the IV metoprolol group vs. 18.6 g in the control group, p = 0.07). Thus, despite the infarct size still being ≈17% smaller in the active treatment group, the natural shrinkage of scar tissue narrowed the absolute difference (26). It is also important to consider that this trial was powered to detect differences in infarct size in the acute phase (1 week after STEMI).

Beta-blockers have been shown to reduce mortality when used as secondary prevention after infarction (27), and are an established part of the pharmacological armamentarium, with a Class I indication in clinical guidelines (1,2). However, very early IV administration before reperfusion is not encouraged, mainly because of the results of the COMMIT (Efficacy and Safety of Adding Clopidogrel to Aspirin or Use of Metoprolol in Myocardial Infarction) trial, which showed no short-term net clinical benefit of early metoprolol in STEMI patients undergoing thrombolysis (28). The COMMIT trial recruited all comers with almost no restriction. By contrast, the METOCARD-CNIC trial recruited Killip class ≤II patients presenting with systolic blood pressure ≥120 mm Hg, heart rate ≥60 beats/min, and reperfused by pPCI within 6 h of infarct onset. Subgroup analyses of the COMMIT trial (28) suggested that patients fitting the inclusion criteria of the METOCARD-CNIC trial benefited from early IV metoprolol in terms of mortality reduction. In addition, the clinical benefits associated with infarct size reduction (and post-infarction LVEF improvement) are expected to occur late (months to years) after STEMI (13,29). In the COMMIT trial, clinical follow-up was <1 month. It is plausible that longer follow-up of the COMMIT trial would show additional benefit of early IV metoprolol in survivors. Thus, an important lesson from the COMMIT trial is that not all STEMI patients benefit from very early IV metoprolol, a deduction supported by the results reported here.

Study limitations. This trial was not powered to detect differences in hard clinical endpoints, and thus, the results on this outcome should be taken with caution.

Conclusions

Intravenous metoprolol administered before reperfusion results in higher long-term LVEF and a lower incidence of post-infarction severe LVEF depression in anterior STEMI patients undergoing primary PCI during the first 6 h of infarction. This low-cost therapy could have an important socioeconomic impact by reducing the number of patients requiring expensive interventions to treat post-infarction heart failure and prevent sudden death. The results of the METOCARD-CNIC trial warrant a large study powered to detect differences in hard clinical endpoints.

Acknowledgments

The authors thank Angel Macías, Gonzalo Javier López, and Braulio López-Asenjo for their work in the acquisition of the MRI studies; and Eeva Soininen and Anabel Castillo, who were principal for the logistics of the trial and overall project development. The authors also acknowledge the continuous professional support from the administration of the CNIC, as well as from the training department (Julia Redondo, Susana Negrete, Cristina Giménez), which facilitated the conductance of this project; and the coordinating center and the SUMMA112 "SCU," whose altruistic dedication were capital for the proper development of this trial. The authors thank Simon Bartlett (CNIC) for providing English editing.

Downloaded From: https://content.onlinejacc.org/ on 06/11/2014

Reprint requests and correspondence: Dr. Borja Ibanez, Epidemiology, Atherothrombosis, and Imaging Department, Centro Nacional de Investigaciones Cardiovasculares Carlos III (CNIC), Melchor Fernández Almagro, 3, 28029 Madrid, Spain. E-mail: bibanez@cnic.es.

REFERENCES

1. O'Gara PT, Kushner FG, Ascheim DD, et al. 2013 ACCF/AHA guideline for the management of ST-elevation myocardial infarction: a report of the American College of Cardiology Foundation/American Heart Association Task Force on Practice Guidelines. J Am Coll Cardiol 2013;61:e78–140.
2. Steg PG, James SK, Atar D, et al. ESC guidelines for the management of acute myocardial infarction in patients presenting with ST-segment elevation. Eur Heart J 2012;33:2569–619.
3. Roger VL, Go AS, Lloyd-Jones DM, et al. Heart disease and stroke statistics—2012 update: a report from the American Heart Association. Circulation 2012;125:e2–220.
4. Yancy CW, Jessup M, Bozkurt B, et al. 2013 ACCF/AHA guideline for the management of heart failure: a report of the American College of Cardiology Foundation/American Heart Association Task Force on Practice Guidelines. J Am Coll Cardiol 2013;62:e147–239.
5. McMurray JJ, Adamopoulos S, Anker SD, et al. ESC guidelines for the diagnosis and treatment of acute and chronic heart failure 2012: the Task Force for the Diagnosis and Treatment of Acute and Chronic Heart Failure 2012 of the European Society of Cardiology. Eur Heart J 2012;33:1787–847.
6. Larose E, Rodes-Cabau J, Pibarot P, et al. Predicting late myocardial recovery and outcomes in the early hours of ST-segment elevation myocardial infarction: traditional measures compared with microvascular obstruction, salvaged myocardium, and necrosis characteristics by cardiovascular magnetic resonance. J Am Coll Cardiol 2010;55:2459–69.
7. Heusch G. Cardioprotection: chances and challenges of its translation to the clinic. Lancet 2013;381:166–75.
8. Kloner RA. Current state of clinical translation of cardioprotective agents for acute myocardial infarction. Circ Res 2013;113:451–63.
9. Ibanez B, Macaya C, Sanchez-Brunete V, et al. Effect of early metoprolol on infarct size in ST-segment-elevation myocardial infarction patients undergoing primary percutaneous coronary intervention: the Effect of Metoprolol in Cardioprotection During an Acute Myocardial Infarction (METOCARD-CNIC) trial. Circulation 2013;128:1495–503.
10. Ibanez B, Fuster V, Macaya C, et al. Study design for the "Effect of Metoprolol in Cardioprotection During an Acute Myocardial Infarction" (METOCARD-CNIC): a randomized, controlled parallel-group, observer-blinded clinical trial of early pre-reperfusion metoprolol administration in ST-segment elevation myocardial infarction. Am Heart J 2012;164:473–480.e475.
11. Kramer CM, Budoff MJ, Fayad ZA, et al. ACCF/AHA 2007 clinical competence statement on vascular imaging with computed tomography and magnetic resonance. A report of the American College of Cardiology Foundation/American Heart Association/American College of Physicians Task Force on Clinical Competence and Training. J Am Coll Cardiol 2007;50:1097–114.
12. Burns RJ, Gibbons RJ, Yi Q, et al. The relationships of left ventricular ejection fraction, end-systolic volume index and infarct size to six-month mortality after hospital discharge following myocardial infarction treated by thrombolysis. J Am Coll Cardiol 2002;39:30–6.
13. Sloth AD, Schmidt MR, Munk K, et al. Improved long-term clinical outcomes in patients with st-elevation myocardial infarction undergoing remote ischaemic conditioning as an adjunct to primary percutaneous coronary intervention. Eur Heart J 2014;35:168–75.
14. Stone GW, Witzenbichler B, Godlewski J, et al. Intralesional abcximab and thrombus aspiration in patients with large anterior myocardial infarction: one-year results from the INFUSE-AMI trial. Circ Cardiovasc Interv 2013;6:527–34.
15. Roe MT, Messenger JC, Weintraub WS, et al. Treatments, trends, and outcomes of acute myocardial infarction and percutaneous coronary intervention. J Am Coll Cardiol 2010;56:254–63.
16. Buxton M, Caine N, Chase D, et al. A review of the evidence on the effects and costs of implantable cardioverter defibrillator therapy in different patient groups, and modelling of cost-effectiveness and cost-utility for these groups in a UK context. Health Technol Assess 2006;10:iii–iv, ix–xi, 1–164.
17. Bryant J, Brodin H, Loveman E, Clegg A. Clinical effectiveness and cost-effectiveness of implantable cardioverter defibrillators for arrhythmias: a systematic review and economic evaluation. Int J Technol Assess Health Care 2007;23:63–70.
18. Lubinski A, Bissinger A, Boersma L, et al. Determinants of geographic variations in implantation of cardiac defibrillators in the European Society of Cardiology member countries—data from the European Heart Rhythm Association White Book. Europace 2011;13:654–62.
19. Hlatky MA, Mark DB. The high cost of implantable defibrillators. Eur Heart J 2007;28:388–91.
20. Abegunde DO, Mathers CD, Adam T, Ortegon M, Strong K. The burden and costs of chronic diseases in low-income and middle-income countries. Lancet 2007;370:1929–38.
21. LaPointe NM, Al-Khatib SM, Piccini JP, et al. Extent of and reasons for nonuse of implantable cardioverter defibrillator devices in clinical practice among eligible patients with left ventricular systolic dysfunction. Circ Cardiovasc Qual Outcomes 2011;4:146–51.
22. Udell JA, Juurlink DN, Kopp A, et al. Inequitable distribution of implantable cardioverter defibrillators in Ontario. Int J Technol Assess Health Care 2007;23:354–61.
23. Hernandez AF, Fonarow GC, Liang L, et al. Sex and racial differences in the use of implantable cardioverter-defibrillators among patients hospitalized with heart failure. JAMA 2007;298:1525–32.
24. Fonarow GC, Yancy CW, Albert NM, et al. Heart failure care in the outpatient cardiology practice setting: findings from IMPROVE HF. Circ Heart Fail 2008;1:98–106.
25. Narayanan K, Reinier K, Uy-Evanado A, et al. Frequency and determinants of implantable cardioverter defibrillator deployment among primary prevention candidates with subsequent sudden cardiac arrest in the community. Circulation 2013;128:1733–8.
26. Baks T, van Geuns RJ, Biagini E, et al. Effects of primary angioplasty for acute myocardial infarction on early and late infarct size and left ventricular wall characteristics. J Am Coll Cardiol 2006;47:40–4.
27. Freemantle N, Cleland J, Young P, Mason J, Harrison J. Beta blockade after myocardial infarction: systematic review and meta regression analysis. BMJ 1999;318:1730–7.
28. Chen ZM, Pan HC, Chen YP, et al. Early intravenous then oral metoprolol in 45,852 patients with acute myocardial infarction: randomised placebo-controlled trial. Lancet 2005;366:1622–32.
29. Gibbons RJ, Valeti US, Araoz PA, Jaffe AS. The quantification of infarct size. J Am Coll Cardiol 2004;44:1533–42.

Key Words: beta-adrenergic receptors ■ heart failure ■ ICD ■ infarct size ■ LVEF ■ magnetic resonance imaging ■ metoprolol ■ myocardial infarction ■ PCI ■ STEMI.

APPENDIX

For a supplemental table and figure, please see the online version of this article.

Downloaded From: https://content.onlinejacc.org/ on 06/11/2014